THE UNIVERSITY
of EDINBURGH

Actinide Hydrocarbyl Chemistry Supported by a Small Flexible Pyrrolic Macrocycle

Markéta Sůvová

The University of Edinburgh

Submitted for the degree of Doctor of Philosophy

August 2017

Declaration

The work described in this thesis is my own, except where I have given reference to a published source or acknowledged help from a named person. This thesis has not been submitted, in whole or in part, for any degree at this or any other university. The work herein was carried out under the supervision of Professor Polly L. Arnold from September 2013 to August 2017.

Signature:

Date:

Abstract

Thorium(IV) and uranium(IV) coordination complexes have been studied for the last 60 years. They have shown interesting reactivity that is often divergent from that of transition metal complexes, and that also provides an insight into some unanticipated differences between thorium(IV) and uranium(IV). An introduction to thorium(IV) and uranium(IV) organometallic chemistry supported by carbocyclic and N-donor ligands is given in Chapter One. The reactivity of actinide alkyl, amide and alkynyl complexes towards small molecules is discussed and select examples provided. The redox chemistry of thorium and uranium is also introduced.

Chapter Two describes the alkylation and amination chemistry of uranium(IV) and thorium(IV) *trans*-calix[2]benzene[2]pyrrolide ($(L)^{2-}$) complexes, $[(L)AnCl_2]$, yielding new actinide(IV) complexes of the type $[M(L^{-2H})An(R)]$ (M = Li or K, R = Me, CH_2SiMe_3, CH_2Ph, $N(SiMe_3)_2$), where $(L)^{2-}$ undergoes further deprotonation to $(L^{-2H})^{4-}$. Additionally, the lability of the $[M(L^{-2H})An(R)]$ "ate"-complexes towards M^+ ion exchange is addressed. Further, the selective ligand reprotonation of $(L^{-2H})^{4-}$ to $(L)^{2-}$ using $HSiR'_3$ (R' = Me, ^{i}Pr) and $[Et_3NH][BPh_4]$ yielding $[(L)An(C{\equiv}CSiR'_3)_2]$ and $[(L)An(R)][BPh_4]$ respectively, is explained. The reactivity of these complexes towards amines, silanes, alkenes, tin hydrides, silicone grease, ^{t}BuNC, H_2, CO, CO_2 or CS_2 is described. Crystallographic characterisation shows that $[(L)Th(N(SiMe_3)_2)][BPh_4]$ contains an unusual example of a thorium(IV) *bis*-arene coordination mode. The reactivity of $[(L)Th(C{\equiv}CSiMe_3)_2]$ towards a number of substrates including alkenes, $[Ni(COD)_2]$, $[Pt(norbornene)_3]$, P_4, CO_2 or H_2 is also discussed. Activation of CO_2 by $[(L)Th(C{\equiv}CSiMe_3)_2]$ at 80 °C results in $(L)^{2-}$ functionalisation and abstraction to yield a new tricyclic organic molecule with the general formula LCO. The addition of $[Ni(COD)_2]$ to $[(L)Th(C{\equiv}CSiMe_3)_2]$ and PR''_3 (R'' = phenyl, cyclohexyl) yields heterobimetallic complexes $[(L)Th(C{\equiv}CSiMe_3)_2{\cdot}Ni(PR''_3)]$; these products display both *di*-pyrrolic and *bis*-arene coordination. The changes in ligand coordination mode are discussed alongside DFT computational analyses that have been carried out by collaborators. The substitution reactions of $[(L)AnCl_2]$ with $NaBH_4$ to form actinide(IV) borohydride complexes $[(L)An(BH_4)_2]$ and subsequent attempted abstractions of BH_3 from $[(L)Th(BH_4)_2]$ are presented. Conclusions are provided at the end of the chapter.

Chapter Three focusses on the oxidation chemistry of uranium(IV) within the $(L)^{2-}$ and $(L^{-2H})^{4-}$ ligand framework, prompted by the isolation of a uranium(V) complex $[Li[(L)UO_2]{\cdot}LiI]$ from the oxidation of the uranium(IV) complex $[Li(L^{-2H})U(Me)]$. Conclusions are provided at the end of the chapter.

Experimental methods and characterising data are given in Chapter Four.

Lay Summary

The aim of this work is to study the structure and reactivity of new thorium and uranium complexes, supported by a macrocyclic ligand. A number of unusual chemical transformations unique to the supporting ligand framework are presented, including the reactivity of these actinide complexes towards abundant and commercially relevant substrates, such as carbon dioxide. Additionally, the complexes described herein are shown to incorporate a second metal, including a caesium cation, the capture of which is particularly applicable to nuclear waste remediation. Furthermore, Uranium-oxo complexes have been targeted in this work. Investigating their properties is fundamentally important to the understanding of the behaviour of their highly radioactive transuranic analogues in nuclear waste.

Acknowledgements

I sincerely wish to thank my supervisor Professor Polly Arnold for her encouragement, guidance and support throughout my PhD studies. I would also like to thank Dr Stefan Minasian for his supervision during my stay at Lawrence Berkeley National Laboratory. I am grateful to The University of Edinburgh for the Principal's Career Development Scholarship, to ScotCHEM for the International Graduate School Scholarship and to The Royal Society of Chemistry for the Researcher Mobility Grant.

I wish to thank Dr Juraj Bella and Dr Lorna Murray for their invaluable help with NMR spectroscopy and Dr Gary Nichol and Dr Stephen Moggach with X-ray crystallography.

I would like to thank Professor Geoff Cloke at the University of Sussex and Dr Jessica Higgins for inspiring me to pursue a PhD in actinide chemistry.

My thanks go to all members of the Arnold and Love groups, especially to Dr Johann Hlina, Dr Joy Farnaby and Dr Catherine Weetman for giving me their time, support and friendship. Thank you, Doris, Max, Danny and Megan for our great adventures.

Finally, I wish to thank my family and James – I could not have done this without you.

List of Abbreviations

General

An	Actinide
Ar	Aryl
avg	Average
CAAC	Cyclic Alkyl Amino Carbene
COD	Cyclooctadiene
COT	Cyclooctatetraenyl
CSD	Cambridge Structural Database
Cp	Cyclopentadienyl
Cp*	Pentamethylcyclopentadienyl
Cp″	η^5-$C_5H_4SiMe_3$
Ct	Centroid
Cy	Cyclohexyl
DCM	Dichloromethane
DFT	Density Functional Theory
Dipp	2,6-di*iso*-propylphenyl
DME	1,2-Dimethoxyethane
DMTB	Dimethyl-*tert*-butylsilyl
dppf	1,1′-Ferrocenediyl-bis(diphenylphosphine)
EI	Electron Ionisation
EPR	Electron Paramagnetic Resonance
ESD	Estimated Standard Deviation
Et	Ethyl
fc	Ferrocene
FTIR	Fourier Transform Infra-Red
^{i}Pr	*Iso*-propyl
H_2L	*Trans*-calix[2]cenzene[2]pyrrolide
Ind	Indenyl
Ind*	Permethylindenyl
Ln	Lanthanide
M	Metal
Me	Methyl
MO	Molecular Orbital

MS	Mass Spectrometry
N″	$N(SiMe_3)_2$
NMR	Nuclear Magnetic Resonance
OTf	Triflate / Trifluoromethanesulfonate
Ph	Phenyl
py	Pyridine
RT	Room Temperature
SIR	Sterically-Induced Reduction
^{t}Bu	Tertiary-butyl
THF	Tetrahydrofuran
TIPS	Tri*iso*-propylsilyl
TM	Transition Metal
TMS	Trimethylsilyl
Tp*	Hydrotris(3,5-dimethylpyrazolyl)borate

NMR

$\{^{11}B\}$	Boron-11 Decoupled
br	Broad
d	Doublet
$\{^{1}H\}$	Proton Decoupled
m	Multiplet
ppm	Parts Per Million
q	Quartet
s	Singlet
t	Triplet
v	Very

List of Publications

Within the scope of this thesis:

1. M. Suvova, K. T. P. O'Brien, J. H. Farnaby, N. Kaltsoyannis, P. L. Arnold, 'Thorium(IV) and uranium(IV) trans-calix[2]benzene[2]pyrrolide alkyl and alkynyl complexes: synthesis, reactivity and electronic structure'; accepted to *Organometallics (Special Issue: Organometallic Actinide and Lanthanide Chemistry).*

Outside the scope of this thesis:

2. P. L. Arnold, B. E. Cowie, M. Suvova, M. Zegke, N. Magnani, E. Colineau, J.-C. Griveau, R. Caciuffo, J. B. Love, 'Axially symmetric U-O-Ln and U-O-U containing molecules from the control of uranyl reduction with simple f-block halides', *Angew. Chem. Int. Ed.*, 2017, **56**, 10775-10779.

3. J. A. L. Wells, M. L. Seymour, M. Suvova, P. L. Arnold, 'Dinuclear uranium complexation and manipulation using robust tetraaryloxides', *Dalton Trans*., 2016, **45**, 16026-16032. *(Themed Issue: Reactions Facilitated by Ligand Design)*

Table of Contents

Chapter One: Introduction....1

1.1 Introduction to Thorium and Uranium 1

1.2 Introduction to Organoactinide Chemistry 2

1.2.1 Metallocene Supported Organoactinide Chemistry.... 3

1.2.2 Nitrogen-Donor Supported Organoactinide Chemistry 5

1.3 Thorium(III).... 8

1.4 Uranyl(V) 10

1.5 Actinide Alkyl, Amide and Hydride Complexes: Synthesis and Reactivity.... 12

1.5.1 Cyclopentadienyl - Supported Complexes 13

1.5.2 Cyclopentadienyl and Other Ligand Sets.... 14

1.5.3 C–H Bond Activation.... 16

1.5.4 Small Molecule Activation.... 18

1.5.5 Calix[4]Tetrapyrroles.... 20

1.6 Scope of Thesis 21

1.6.1 Background 21

1.6.2 Aims.... 25

1.7 References for Chapter One 25

Chapter Two: Actinide Alkyl and Amide Complexes: Synthesis, Characterisation and Reactivity 31

2.1 Introduction.... 31

2.2 Synthesis of Actinide(IV) Halide Complexes.... 31

2.3 Synthesis of Actinide(IV) Borohydride Complexes 32

2.3.1 Introduction 32

2.3.2 Synthesis 33

2.3.3 Reactivity.... 35

2.4 Synthesis of Actinide(IV) Amide Complexes 36

2.4.1 Introduction 36
2.4.2 Synthesis of a Uranium(IV) Amide Complex 37
2.5 Synthesis of Actinide(IV) Alkyl Complexes 39
2.5.1 Introduction 39
2.5.2 Synthesis 39
2.5.3 Characterisation of Actinide(IV) Methyl Complexes 5 and 8 40
2.5.4 Characterisation of Actinide(IV) Neosilyl Complexes 6 and 9 43
2.5.5 Characterisation of Actinide(IV) Benzyl Complexes 7 and 10 45
2.5.6 Grignard Reagents 47
2.5.7 Discussion of Ligand Non-Innocence 48
2.6 Synthesis of Actinide(IV) Alkynyl Complexes 49
2.6.1 Characterisation 50
2.6.2 Discussion of Reversible Aryl Deprotonation 53
2.7 Attempted Syntheses of Thorium(IV) Imido Complexes 54
2.8 Reactivity of Actinide(IV) Alkyl and Alkynyl Complexes 56
2.8.1 Reactivity with Alkenes 56
2.8.2 Reactivity with Silanes 57
2.8.3 Reactivity with a Tin Hydride 58
2.8.4 Reactivity of 8 with Silicone Grease 59
2.8.5 Reactivity of Alkyl Complexes with Small Molecules 61
2.8.6 Reactivity of Complex 12 with $[Co_2(CO)_8]$ and $[Re_2(CO)_{10}]$ 66
2.8.7 Reactivity of Complex 12 with P_4 66
2.9 Cation Exchange Reactions 67
2.9.1 Group 1 Metal Exchange 67
2.9.2 Attempted Exchange of Group 1 Cations for *f*-Elements 68
2.10 Cationic Complexes 69
2.10.1 Synthesis 69
2.10.2 Reactivity with Small Molecules 71
2.10.3 Reactivity with Reducing Agents and Bases 71

2.11 Heterobimetallic Complexes: 12 and 13 with Group 10 72

2.11.1 Nickel Coordination to 12..... 73

2.11.2 Nickel Coordination to 12 Supported by Phosphine Donors..... 75

2.11.3 Attempted Platinum Incorporation..... 79

2.11.4 Computational Analysis and Discussion of Ancillary Ligand Rearrangement..... 80

2.12 General Trends..... 84

2.13 Summary and Conclusions for Chapter Two 85

2.14 References for Chapter Two 86

Chapter Three: Oxidation of Uranium *Trans*-Calix[2]Benzene[2]Pyrrolide Complexes.....90

3.1 Accessing Uranium-Oxo Complexes..... 90

3.2 Uranium(V)-Dioxo Complex 90

3.3 Uranium(IV)-μ-Oxo Complex 94

3.4 Synthesis of Uranium(IV)-Oxo Complexes 95

3.4.1 D_2O 95

3.4.2 Oxygen-Atom Transfer Reagents 96

3.4.3 Hydroxides..... 97

3.4.4 Air 99

3.4.5 Salt Metathesis Routes..... 99

3.5 Summary and Conclusions for Chapter Three 100

3.6 References for Chapter Three..... 101

Chapter Four: Experimental Details 102

4.1 General Procedures and Techniques 102

4.2 Preparation of Reagents..... 103

4.3 General Procedure for Gas Reactions 103

4.4 Synthetic Procedures for Chapter Two 103

4.4.1 Synthesis of [(L)UCl_2] (1)..... 103

4.4.2 Synthesis of [(L)Th(BH_4)$_2$] (2) 104
4.4.3 Synthesis of [(L)U(BH_4)$_2$] (3) 105
4.4.4 Synthesis of [K(L^{-2H})Th(N($SiMe_3$)$_2$)] (C) 105
4.4.5 Synthesis of [K(L^{-2H})U(N($SiMe_3$)$_2$)] (4) 106
4.4.6 Synthesis of [Li(L^{-2H})Th(Me)] (5) 106
4.4.7 Synthesis of [Li(L^{-2H})Th(CH_2SiMe_3)](6) 107
4.4.8 Synthesis of [K(L^{-2H})Th(CH_2Ph)] (7) 108
4.4.9 Synthesis of [Li(L^{-2H})U(Me)] (8) 108
4.4.10 Synthesis of [Li(L^{-2H})U(CH_2SiMe_3)] (9) 109
4.4.11 Synthesis of [K(L^{-2H})U(CH_2Ph)] (10) 110
4.4.12 Synthesis of [MgCl(L^{-2H})Th(CH_2Ph)] (11) 110
4.4.13 Synthesis of [(L)Th(C≡C$SiMe_3$)$_2$] (12) 111
4.4.14 Synthesis of [(L)Th(C≡CSi^iPr_3)$_2$] (13) 112
4.4.15 Synthesis of [(L)U(C≡C$SiMe_3$)$_2$] (14) 112
4.4.16 Synthesis of [(L)U(C≡CSi^iPr_3)$_2$] (15) 113
4.4.17 Attempted Syntheses of Thorium(IV) Imido Complexes from 5 113
4.4.18 Attempted Syntheses of Thorium(IV) Imido Complexes from C 114
4.4.19 Attempted 1,2-insertion into Th–C Bond of 5 114
4.4.20 Attempted [2+2+2] Cycloaddition Reactions with 12 114
4.4.21 Attempted Th^{IV} Hydride Synthesis with Silanes 114
4.4.22 Attempted Th^{IV} Hydride Synthesis with Tin Hydride 114
4.4.23 Synthesis of [(L^{-2H})U(η^2-O_2SiMe_2)(Li{THF})$_2$] (16) 115
4.4.24 Attempted Small Molecule Activation by Complexes 5-10 115
4.4.25 Attempted Small Molecule Activation by Complexes 12-15 115
4.4.26 Synthesis of [LCO] (17) 116
4.4.27 Attempted Reaction of 12 with [$Co_2(CO)_8$] or [$Re_2(CO)_{10}$] 116
4.4.28 Attempted Reaction of 12 with P_4 116
4.4.29 Synthesis of [Li(L^{-2H})Th(N")] (18) 117
4.4.30 Synthesis of [Na(L^{-2H})Th(N")] (19) 117
4.4.31 Synthesis of [Cs(L^{-2H})Th(N")] (20) 118

4.4.32 Attempted Exchange of Group 1 Cations for *f*-Elements 118
4.4.33 Synthesis of [(L)Th(CH_2Ph)][BPh_4] (21) 118
4.4.34 Synthesis of [(L)Th($N(SiMe_3)_2$)][BPh_4] (22) 119
4.4.35 Attempted Small Molecule Activation by 22 120
4.4.36 Attempted Reduction of 22 120
4.4.37 Alternative Synthesis of C 120
4.4.38 Synthesis of [(L)Th($C{\equiv}CSiMe_3)_2{\cdot}Ni$] (23) 120
4.4.39 Synthesis of [(L)Th($C{\equiv}CSiMe_3)_2{\cdot}NiPPh_3$] (24) 121
4.4.40 Synthesis of [(L)Th($C{\equiv}CSiMe_3)_2{\cdot}NiPCy_3$] (25a and 25b) 122
4.4.41 Attempted Synthesis of [(L)Th($C{\equiv}CSiMe_3)_2{\cdot}$TM(dppf)] (TM = Ni, Pt) 123
4.5 Synthetic Procedures for Chapter Three 123
4.5.1 Synthesis of [(L)U(OLi{THF}$_3$)$_2$]I (26) 123
4.5.2 Synthesis of [(L)U(O)]$_2$ (27) 123
4.5.3 Oxidation of 8 or 14 with D_2O 124
4.5.4 Attempted Oxidation of 8 or 14 with O-Atom Transfer Agents 124
4.5.5 Attempted U^{IV}-oxo syntheses from 8 with LiOD 125
4.5.6 Attempted U^{IV}-oxo syntheses from 8 or 14 with ROH (R = CPh_3, $SiMe_3$) 125
4.5.7 Oxidation of 8 or 14 in Air 125
4.5.8 Attempted synthesis of U^{V} and U^{VI} Complexes by Salt Metathesis 125
4.6 Crystallographic Details 126
4.7 References for Chapter Four 133

Chapter One: Introduction

1.1 Introduction to Thorium and Uranium

Thorium is an early actinide found in the earth's crust as ThO_2, $ThSiO_4$ and $ThPO_4$ in monazite sands and the minerals thorite (thorium silicate) and thorianite (a mixture of thorium and uranium oxides). Thorium-232 is a weak alpha-particle emitter, >99 % abundant with a half-life of 14 billion years. Its abundance in the earth's crust is comparable to that of lead or molybdenum, and is three times that of uranium.[1] In nature, uranium is most commonly found as U_3O_8 in minerals such as uraninite. The naturally occurring isotopes of uranium are uranium-234, uranium-235 and uranium-238; the latter is 99.27 % abundant with a half-life of 4.5 billion years.[2] The most fissile isotope, uranium-235, is needed for the nuclear fuel industry; natural uranium is therefore enriched to increase the proportion of uranium-235.[3] This process produces depleted uranium, where uranium-238 is >99.27 % abundant, as a by-product. Uranium-238 is a weak alpha and beta emitter. Assuming inhalation and ingestion are avoided, the radiological risks associated with handling thorium and depleted uranium are negligible.[1, 3] Depleted uranium and thorium can therefore be used safely in the synthetic laboratory, allowing for the exploration of their chemical properties and their use as models for the more radioactive transuranic elements.[4]

Thorium has an electronic configuration of [Rn] $6d^2$ $7s^2$, resulting in the stability and predominance of its +4 oxidation state. Uranium has an electronic configuration of [Rn] $5f^3$ $6d^1$ $7s^2$ allowing for a range of commonly accessible oxidation states, +3 to +6. A handful of thorium(III) complexes have been isolated to date and are discussed in Section 1.3. Rare examples of thorium(II) and uranium(II) complexes were recently reported.[5-8]

The 5*f* orbitals of the actinides become increasingly core-like across the period, however are more diffuse than the 4*f* orbitals of the lanthanides, due to the presence of a radial node in the 5*f*. This results in less shielding from 6*s* and 6*p* electrons on the 5*f* orbitals of the actinides relative to that exerted by 5*s* and 5*p* on the 4*f* orbitals of the lanthanides. The ionic radii of thorium and uranium are larger than those of transition metals and lanthanides, allowing for higher coordination numbers.[9] The ionic radii of thorium cations are larger than their uranium counterparts.[9] Although actinide cations may rely on high coordination numbers for steric stabilisation in certain cases,[10] bonding models of the actinides have shown that

bonding occurs mainly through electrostatic interactions with some covalent contribution to bonding in specific examples.[11, 12] This allows for interactions with aromatic ligand systems such as cyclopentadienyl (Cp), cyclooctatetraenyl (COT) and their analogues, resulting in unique chemical behaviour particularly in the early actinides, where π-back bonding can also occur.[13] The exact involvement of the actinide frontier orbitals in bonding remains a complex and contentious experimental and theoretical topic.[14]

1.2 Introduction to Organoactinide Chemistry

During the Manhattan Project, the difficulties associated with the air- and moisture-sensitivity of coordinatively unsaturated volatile uranium complexes such as tetraethyl uranium, intended for uranium-235 and uranium-238 separation, lead to the belief that actinide complexes displayed no applicable reactivity.[15] As a result, research into this area was limited until the first cyclopentadienyl complexes of uranium and thorium were reported by Wilkinson and Fischer,[16-18] following the discovery of ferrocene and cyclopentadienyl complexes of the lanthanides.[19] Soon after, A. Streitwieser Jr. reported the synthesis of uranocene with the uranium bound to two η^8-C_8H_8 ligands that provided significant steric saturation and stabilisation (**1B** in Scheme 1.1).[20-22] This discovery was important for the understanding of δ-bonding of actinides to aromatic ligands and was swiftly succeeded by the synthesis of the analogue thorocene (**1A** in Scheme 1.1).[23]

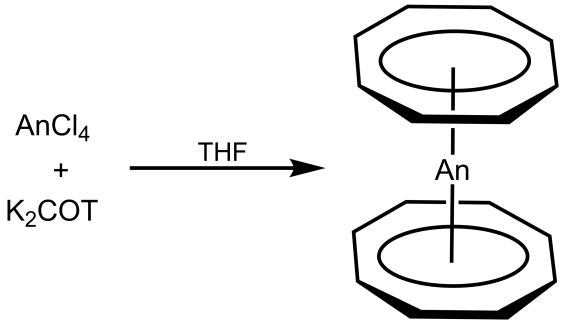

An = Th (**1A**), U (**1B**)

Scheme 1.1 Synthesis of thorocene (**1A**) and uranocene (**1B**) (COT = cyclooctatetraenyl).[20, 23]

Organoactinide chemistry has grown significantly since the initial discoveries in the field, as the actinides continue to show unique small molecule transformations and unprecedented chemistry relative to d-block metals.[24-26] Here, the design of new ligand systems continues to be important for further understanding and harnessing of actinide reactivity.

1.2.1 Metallocene Supported Organoactinide Chemistry

Cyclopentadienyl (Cp), an aromatic monoanionic carbocyclic η^5-bound ligand, and its derivatives support a range of lanthanide, actinide and transition metal (TM) chemistry.[16-19] *Mono*- or *bis*-Cp TM adducts feature extensively in organo-TM chemistry,[27, 28] due to the efficient overlap of TM d-orbitals with the molecular orbitals of Cp.[29] In *f*-element complexes, there is also significant overlap between *f*-orbitals and the hybridised molecular orbitals of Cp yielding *tris*-Cp complexes such as [Cp_3U] or [Cp_3UCl].[16] To avoid ligand redistribution reactions in solution given the larger size of the f-block metal ions,[30] functionalised derivatives of Cp such as pentamethylcyclopentadienyl (Cp*), are commonly employed to synthesise *mono*-, *bis*- and *tris*-Cp* adducts. These supporting ligand frameworks provide increased steric and electronic stabilisation to the complexes, while allowing a controlled level of reactivity at the actinide metal centre; the syntheses and reactivity studies of a range of stable species including alkyls, aryls, silyls, hydrides, alkoxides, or amides are hence possible.[31-41]

Cp*-supported complexes [$(Cp^*)_2An(R)_2$] (R = Me, CH_2Ph), discussed further in Section 1.5, have also provided insight into differences in reactivity between analogous Th^{IV} and U^{IV} systems: the activation of sp^3 hybridised C–H bonds by [$(Cp^*)_2Th(R)_2$] (R = Me, CH_2Ph) in 2,6-lutidine *N*-oxide to give [$(Cp^*)_2Th(R)(\eta^2$-(O,C)-2-CH_2-$ONC_5H_3Me)$] (R = Me (**1C**), CH_2Ph (**1D**), Scheme 1.2), does not take place with the uranium analogues of this system.[42] Further studies using 2-methylpyridine showed that [$(Cp^*)_2Th(Me)_2$] activated both sp^3 C–H and sp^2 C–H bonds, whereas [$(Cp^*)_2U(Me)_2$] was found to selectively activate sp^2 C–H bonds.[43] The exact reasons for this selectivity have remained unclear.

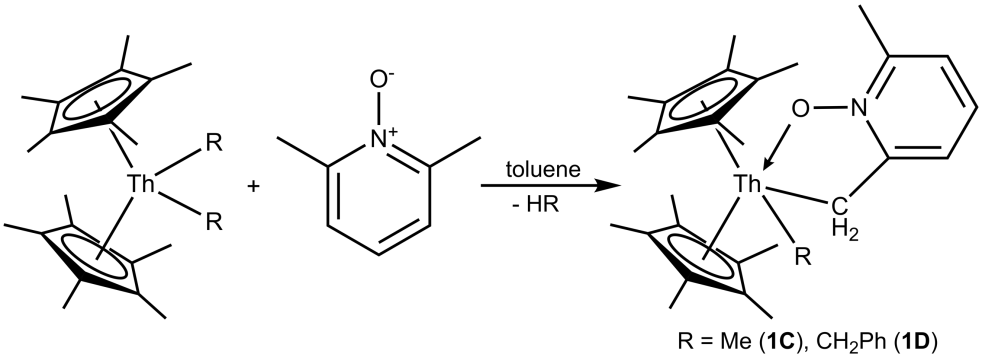

R = Me (**1C**), CH_2Ph (**1D**)

Scheme 1.2 Activation of sp^3 hybridised bonds by [$(Cp^*)_2Th(R)_2$] (R = Me, CH_2Ph) in 2,6-lutidine *N*-oxide to give[$(Cp^*)_2Th(R)(\eta^2$-(O,C)-2-CH_2-$ONC_5H_3Me)$] (R = Me (**1C**), CH_2Ph (**1D**)).[42]

Other alkyl-substituted Cp systems are also commonly used in organoactinide chemistry to tailor the reactivity and specificity of the actinide complexes. One such example is the U^{IV} complex $[(C_5Me_4SiMe_3)_2U(Me)_2]$ (**1E** in Scheme 1.3), which intra-molecularly activates a C–H bond of each silyl group upon heating, eliminating two equivalents of methane, to yield a "tuck-in" tethered complex $[(\eta^5:\eta^1\text{-}C_5Me_4SiMe_2CH_2)_2U]$ (**1F** in Scheme 1.3).[44] **1F** activates substrates such as ^{t}BuNC, CO and S_8 yielding complexes **1G**, **1H** and **1I**, respectively, shown in Scheme 1.3.[44] Upon heating, a C–C bond in **1G** is cleaved intra-molecularly to yield **1J**: a previously unobserved transformation in organometallic chemistry.[45]

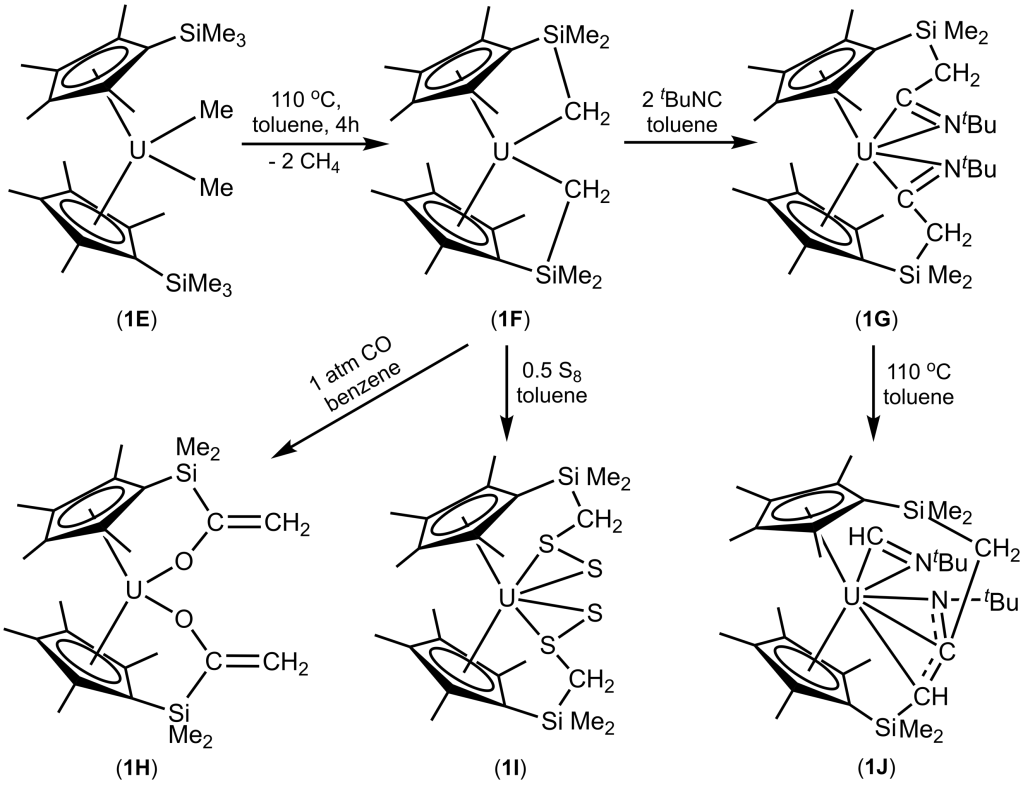

Scheme 1.3 Synthesis of "tuck-in" complex $[(\eta^5:\eta^1\text{-}C_5Me_4SiMe_2CH_2)_2U]$ (**1F**) from $[(C_5Me_4SiMe_3)_2U(Me)_2]$ (**1E**) and subsequent activation of ^{t}BuCN, CO and S_8 to give **1G**, **1H** and **1I**, respectively. A C–C bond in **1G** is cleaved intra-molecularly to yield **1J**.[44, 45]

With the aim of stabilising low-valent actinide metal centres, in 1989 Sattelberger combined both COT and Cp* ligands to synthesise the first desolvated dimeric mixed-sandwich thorium complex $[(C_8H_8)(Cp^*)ThCl]_2$ from $C_8H_8ThCl_2(THF)$ and the Grignard reagent MgClCp*(THF).[46] Several years later, the synthesis of the monomeric uranium analogue $[(C_8H_8)(Cp^*)UI]$ was reported.[47] A specific example showcasing how tailoring these ligand systems affects reactivity are the combined Cp- and COT-supported uranium(III) complexes $[(COT^{TIPS2})U(Cp^*)(THF)]$ ($COT^{TIPS2} = C_8H_6(Si^iPr_3\text{-}1,4)_2$; **1K** in Scheme 1.4) and $[(COT^{TIPS2})U(C_5Me_4H)(THF)]$ (**1M** in Scheme 1.4), which reductively couple CO to yield

bridging deltate (**1L** in Scheme 1.4) and squarate (**1N** in Scheme 1.4) complexes, respectively.[48, 49] This selectivity results from differences in steric crowding tuned by altering the Cp-ring substituents.

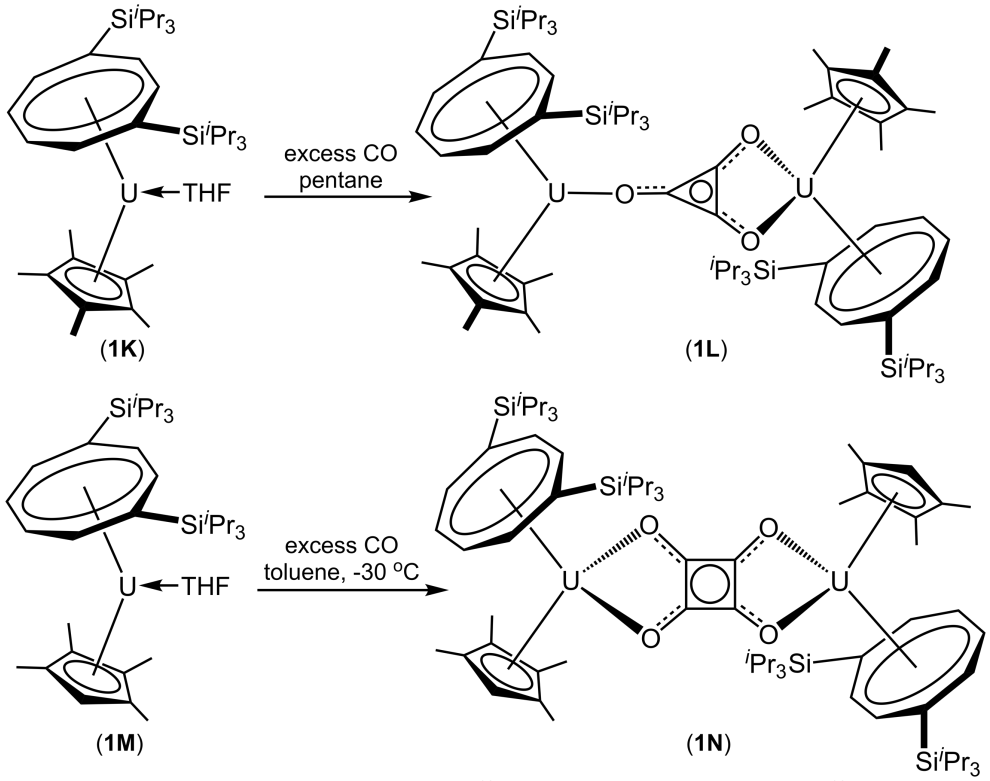

Scheme 1.4 Reductive coupling of CO by [(COT^{TIPS2})U(Cp*)(THF)] (**1K**) and [(COT^{TIPS2})U(C$_5$Me$_4$H)(THF)] (**1M**) to yield deltate (**1L**) and squarate (**1N**) complexes, respectively.[48, 49]

1.2.2 Nitrogen-Donor Supported Organoactinide Chemistry

A number of nitrogen- and oxygen-donor ligands have been used in efforts to explore new actinide chemistry and probe covalency beyond metallocene complexes. Nitrogen and oxygen are electron-rich donors, which can not only π-donate but also form bonds with the actinide metal centres that have increased ionic character, which often imparts stability to the complex. Substituents on the nitrogen donor atoms can also be altered to tune the amount of π-donation to the metal centre and hence affect reactivity.

The polydentate tripodal triamidoamine (Tren) ligand and its derivatives have been used to support a range of new actinide complexes, such as the chloride-bridged mixed U^{III}/U^{IV} complex [{U(Tren^{DMTB})}$_2$Cl] (Tren^{DMTB} = [N(CH$_2$CH$_2$NSiMe$_2$^{t}Bu)$_3$]$^{3-}$) (**1O** in Figure 1.1).[50] Liddle reported the synthesis of the first stable terminal U^V nitride [U(N)(Tren^{TIPS})][Na(12-crown-4)$_2$] (Tren^{TIPS} = [N(CH$_2$CH$_2$NSi^{i}Pr$_3$)$_3$]$^{3-}$) (**1P** in Figure 1.1), from the reaction of a U^{III}

complex [U(Tren^{TIPS})] with NaN_3 followed by the addition of two equivalents of 12-crown-4 to encapsulate the sodium counterion.[51]

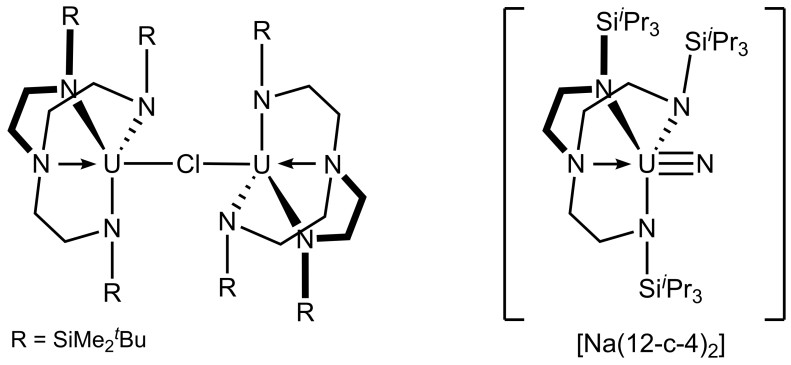

(**1O**) (**1P**)

Figure 1.1 [{U(Tren^{DMTB})}$_2$Cl] (Tren^{DMTB} = [N(CH$_2$CH$_2$NSiMe$_2$^{t}Bu)$_3$]$^{3-}$) (**1O**) and [U(N)(Tren^{TIPS})][Na(12-crown-4)$_2$] (Tren^{TIPS} = [N(CH$_2$CH$_2$NSi^{i}Pr$_3$)$_3$]$^{3-}$) (**1P**).[50, 51]

Tridentate N-donor hydrotris(3,5-dimethylpyrazolyl)borate (Tp*) ligands were first applied in organoactinide chemistry by Ball, who synthesised the Th^{IV} and U^{IV} complexes [(Tp*)AnCl$_3$(THF)] (An = Th (**1Q**), U (**1R**), Figure 1.2).[52] It was recently shown that bis-Tp* as well as mixed Cp* and Tp* ligand systems can support stable uranium(III) *mono*-alkyl complexes [(Tp*)$_2$UR] (R = CH$_2$SiMe$_3$ (**1S**), CH$_2$Ph (**1T**), Figure 1.2) and [(Tp*)(Cp*)UR] (R = CH$_2$SiMe$_3$ (**1U**), CH$_2$Ph (**1V**), Figure 1.2).[53] It has not been possible to isolate U^{III} *bis*-Cp* analogues of these complexes as a result of poor steric stabilisation of the metal centre.

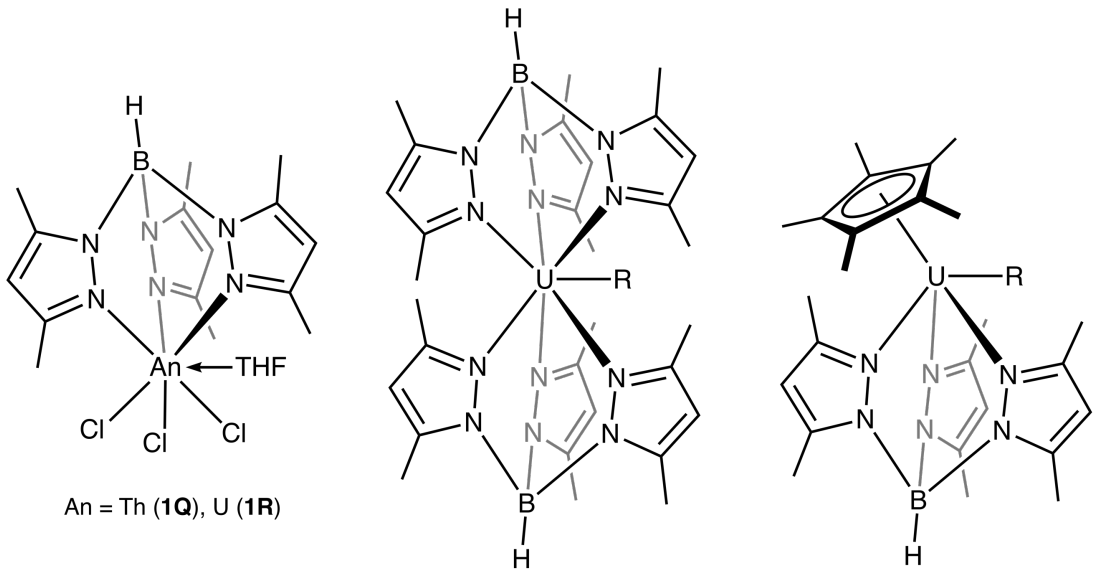

Figure 1.2 Complexes [(Tp*)AnCl$_3$(THF)] (An = Th (**1Q**), U (**1R**)),[52] [(Tp*)$_2$UR] (R = CH$_2$SiMe$_3$ (**1S**), CH$_2$Ph (**1T**)) and [(Tp*)(Cp*)UR] (R = CH$_2$SiMe$_3$ (**1U**), CH$_2$Ph (**1V**)).[53]

Love and Arnold have shown that polypyrrolic Schiff-base (Pacman) macrocycles can bind a variety of metal ions including thorium and uranium in multiple oxidation states; representative Th^{IV} tetramethyl (**1W**) and U^{VI} tetraethyl (**1X**) Pacman complexes are shown in Figure 1.3. A Np^{III} tetraethyl Pacman complexes has also been isolated and it has been predicted computationally that the tetramethyl Pacman ligand (shown on Th^{IV} in Figure 1.3) could bind plutonium, which is of relevance to the treatment of nuclear waste.[54-57] The Pacman complexes have two N_4 donor pockets that can bind up to two metals. The binding modes of these ligands are flexible, affording up to four metal-pyrrolide bonds and donation from up to four lone-pairs on the imine nitrogens. When binding Th^{IV} or U^{IV}, all eight nitrogen donors bind to the metal centre at once (Figure 1.3).[58, 59]

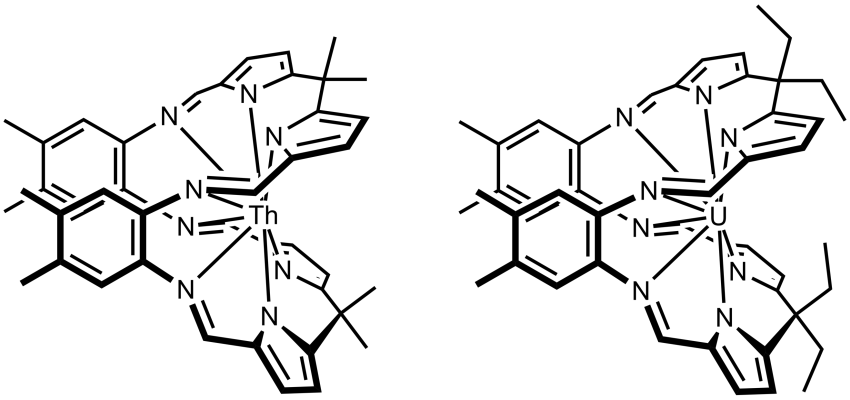

(**1W**) (**1X**)

Figure 1.3 Pacman complexes binding Th^{IV} (**1W**) and U^{IV} (**1X**).[58, 59]

It has been shown that tetramethyl Pacman can facilitate unprecedented uranyl reduction accompanied by silylation and silyl migration upon the addition of 1.5 equivalents of $[UO_2\{N(SiMe_3)_2\}_2(py)_2]$ (py = pyridine) to *mono*-uranyl tetramethyl Pacman (**1Y** in Scheme 1.5) to afford a binuclear U^{V}-dioxo complex (**1Z** in Scheme 1.5), in which one traditionally inert oxo-moiety is positioned *cis* rather than *trans*.[57]

In these polypyrrolic Pacman complexes, κ^1-coordination from the pyrrolic nitrogen atoms to the metal centre is observed. This is the most common coordination mode for pyrrolides to adopt, although the Cp-like η^5-coordination mode has also been reported.[60-67] The stability provided by the pyrrolide in its η^5 coordination mode is comparable and is sometimes greater than that achieved by the κ^1 coordination mode. It has been shown that the η^5-coordination can be promoted by blocking the α-positions on the pyrrolide rings.[68]

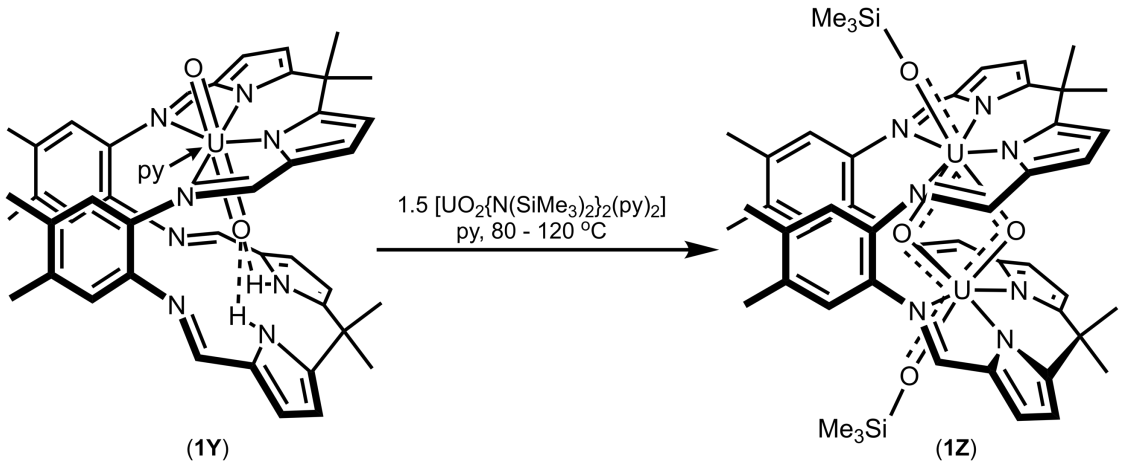

Scheme 1.5 Synthesis of a binuclear U^{V}-dioxo complex (**1Z**) from *mono*-uranyl tetramethyl Pacman (**1Y**).[57]

1.3 Thorium(III)

The reduction potential of the U^{IV}/U^{III} couple is estimated to be between -1.5 V to -2.2 V *vs* ferrocene.[69] Comparatively, the reduction potential of the Th^{IV}/Th^{III} couple is estimated to be between -3.4 V to -4.2 V *vs* ferrocene,[70-72] rendering the isolation of stable thorium(III) complexes difficult, with only a few examples of the oxidation state reported to date.[73-78] Unlike the closed-shell Th^{IV}, Th^{III} is expected to display a non-zero magnetic moment due to a [Rn]$6d^1$ or [Rn]$5f^1$ electronic configuration.

The first Th^{III} complex, $[Th(Cp)_3]$ (**1AA** in Figure 1.4), was reported in 1974 by Baumgärtner and was synthesised by the reduction of $ThCp_3Cl$ with sodium metal.[73] This complex was characterised by magnetic susceptibility measurements and displayed a magnetic moment of 0.403 μ_B at 293 K. Although the magnetic moment was lower than that expected for a $5f^1$ electronic configuration, Baumgärtner suggested that it was due to interactions with the Cp ligands. The Th^{III} complexes $[Th(Cp)_3]$ (**1AA**) and $[Th(Ind)_3]$ (**1AD** in Figure 1.4) (Ind = indenyl) were then accessed by photo-induced β-hydride elimination from the corresponding methyl, *n*-butyl and *iso*-propyl complexes.[76] The absence of hydrides was inferred from IR spectroscopic and mass spectrometric characterisation. A magnetic moment of 0.404 μ_B at 293 K was measured, which is comparable to that observed by Baumgärtner.[73]

Lappert was the first to report a crystallographically characterised thorium(III) complex $[Th(Cp^{TMS2})_3]$ (TMS = $SiMe_3$; **1AB** in Figure 1.4) in 1986.[78] The TMS groups of the modified Cp ligands provide steric protection for the Th^{III} metal centre and also act as π-acceptors for the electron density from the metal. Later EPR, thermodynamic and DFT calculations considering relativistic effects, showed that Th^{III} in **1AB** was likely to have a $6d^1$ rather than the $5f^1$ electronic configuration in the ground state.[71, 75, 79] The magnetic moment

of **1AB** was recorded as 1.91 μ_B at 300 K; the relaxation of a 5*f* electron would be too fast for observation at ambient temperature.[79] Lappert later reported the synthesis of a similar Th^{III} complex $[Th(Cp^{DMTB2})_3]$ (DMTB = $SiMe_2{}^tBu$; **1AC** in Figure 1.4) featuring larger silyl groups for increased stability and solubility.[74]

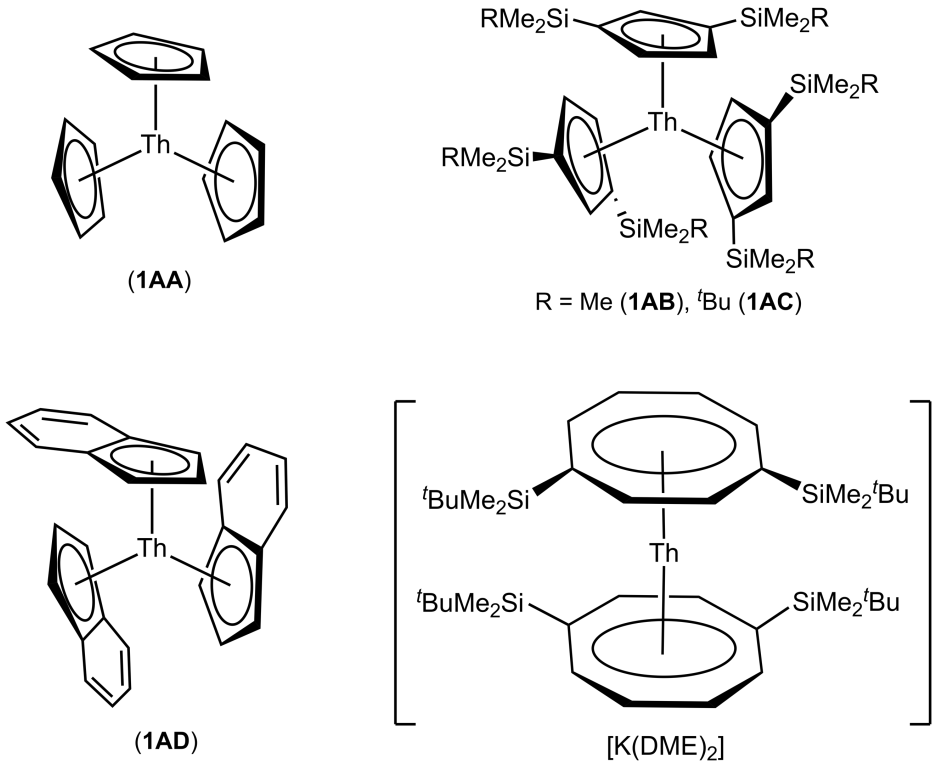

Figure 1.4 Th^{III} complexes $[Th(Cp)_3]$ (**1AA**),$[Th(Cp^{TMS2})_3]$ (**1AB**), $[Th(Cp^{DMTB2})_3]$ (**1AC**), $[Th(Ind)_3]$ (**1AD**) and $[K(DME)_2][(COT^{DMTB2})_2Th]$ (**1AE**).[71, 73-78]

An anionic Th^{III} sandwich complex $[K(DME)_2][(COT^{DMTB2})_2Th]$ (**1AE** in Figure 1.4) was reported in 1999.[77] In this complex, the thermodynamically unstable metal centre is again sterically and electronically stabilised by the bulky silyl group substituents. The magnetic moment was reported as 1.20 μ_B at 298 K and the EPR spectrum obtained at 298 K showed a sharp resonance, which is indicative of the unpaired electron in its ground state residing in the 6*d* orbital. The relaxation of a 5*f* electron would be too fast for observation at ambient temperature. Fine-structure attributed to interactions with the COT^{DMTB2} ligands was also observed at 110 K. A handful of other carbocycle-supported Th^{III} complexes have been reported since.[80]

In 2006 Gambarotta reported the ring opening, carbon-nitrogen, and carbon-oxygen bond activation *via in situ* pyrrolic macrocycle-supported Th^{III} intermediates.[81] A paramagnetic thorium complex, $[Li(DME)_3][\{\eta^5\text{-}1,3\text{-}[(\eta^5\text{-}2\text{-}C_4H_3N)(CH_3)_2C]_2C_6H_4\}ThK\text{-}(\mu\text{-}$

$Cl)_3]_n$ (**1AG** in Scheme 1.6), was then isolated from the reduction of $[Li(DME)_3][\{\eta^6\text{-}1,3\text{-}[(\eta^5\text{-}2\text{-}C_4H_3N)(CH_3)_2C]_2C_6H_4\}ThCl_3]$ (**1AF** in Scheme 1.6) with potassium metal.[82] An electron count, a paramagnetic ^1H NMR spectrum and a calculated magnetic moment of 1.23 μ_B suggested the synthesis of a Th^{III} complex. However, a broad resonance was observed in the EPR spectrum at ambient temperature; this was attributed to significant spin-orbit coupling. The resonance in the EPR spectrum sharpened significantly at 113.2 K, however fine-structure was not observed. The EPR spectrum remained inconclusive, however arene distortion from planar symmetry in the solid-state structure and DFT calculations on **1AG** indicated that the unpaired electron was mostly located on the ligand, rather than on the thorium metal centre. These data suggest that thorium is likely to be in a formal +4 oxidation state, while the ligand acts as a radical anion.[82]

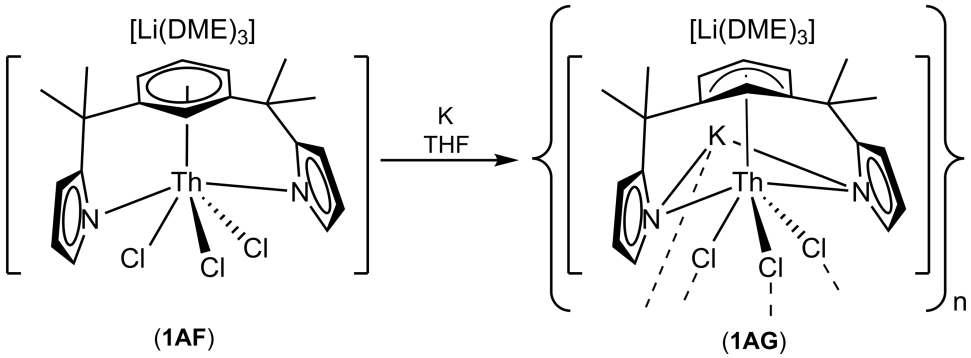

(**1AF**) (**1AG**)

Scheme 1.6 Reduction of $[\{\eta^6\text{-}1,3\text{-}[(\eta^5\text{-}2\text{-}C_4H_3N)(CH_3)_2C]_2C_6H_4\}ThCl_3][Li(DME)_3]$ (**1AF**) to give $[Li(DME)_3][\{\eta^5\text{-}1,3\text{-}[(\eta^5\text{-}2\text{-}C_4H_3N)(CH_3)_2C]_2C_6H_4\}ThK\text{-}(\mu\text{-}Cl)_3]_n$ (**1AG**).[82]

1.4 Uranyl(V)

The study of An^V (An = actinide) cations, $[AnO_2]^+$, is of significant interest due to their presence in nuclear waste and roles in its separation and long-term storage.[83] Complexes of the U^V-dioxo *mono*-cation, $[UO_2]^+$, were reputed as being difficult to isolate due to the disproportionation of $[UO_2]^+$ to uranyl(VI) $[UO_2]^{2+}$ and uranium(IV).[84] In 2003 Berthet and Ephritikhine reported the unexpected isolation of a rogue U^V complex $[UO_2(OPPh_3)_4][OTf]$ (Tf = triflate), which was shown to be stable against disproportionation, however the route to its synthesis remained unknown.[85] In 2006, a stable U^V coordination polymer, $\{[UO_2(py)_5][KI_2(py)_2]\}_n$ (**1AH** in Figure 1.5) was reproducibly synthesised *via* the oxidation of $[UI_3(THF)_4]$ with pyridine-*N*-oxide.[86] Since then, a significant number of U^V complexes have been isolated.

Most routes to $[UO_2]^+$ involve the one-electron reduction and functionalisation of $[UO_2]^{2+}$ by silicon,[4, 57, 87-93] Group 1,[88, 94, 95] Group 2,[96] main group,[95, 97, 98] transition metal,[96, 99-102] rare-earth,[100, 103, 104] or actinide complexes,[104, 105] where $[UO_2]^+$ is bound within a

polydentate ligand framework. Hayton reported an example of uranyl reductive silylation by the addition of two equivalents of Ph_3SiOTf to a uranyl β-diketonate complex $[UO_2(dbm)_2(THF)]$ (dbm = *O*C(Ph)CHC(Ph)*O*) to yield U^V complex $[U(OSiPh_3)_2(dbm)_2(OTf)]$ (**1AI** in Figure 1.5).[91]

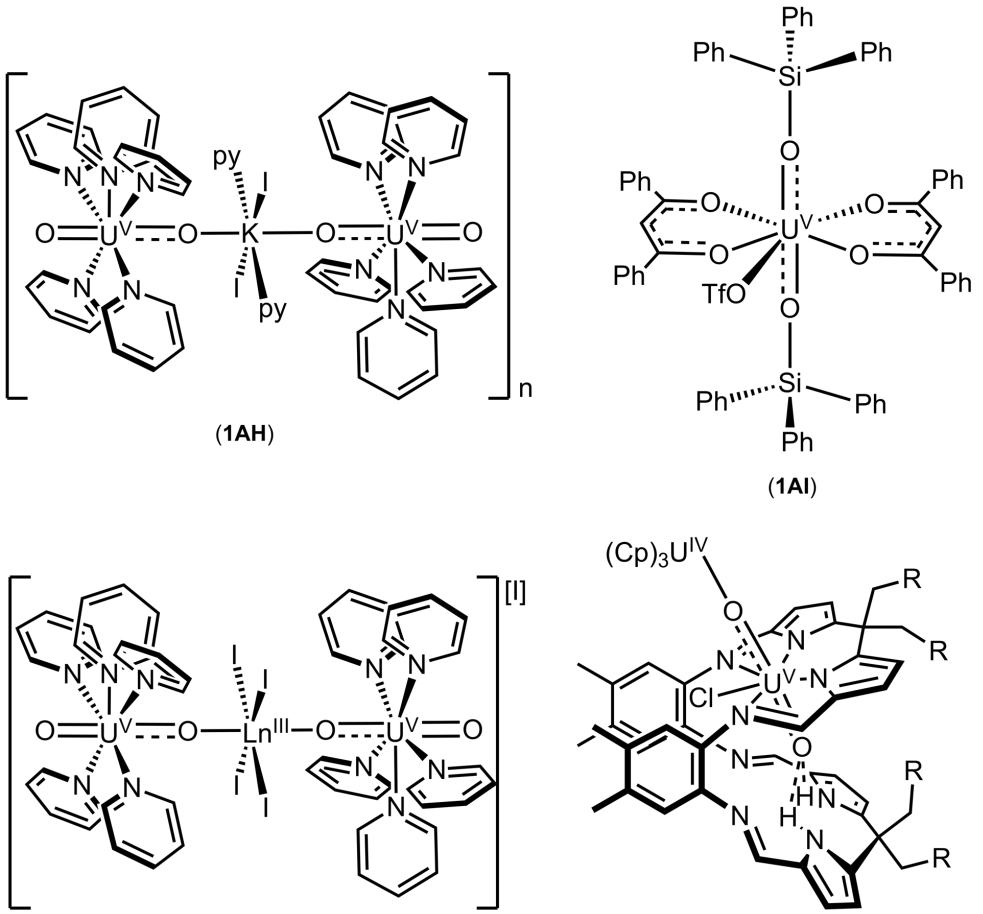

Figure 1.5 U^V complexes $\{[UO_2(py)_5][KI_2(py)_2]\}_n$ (**1AH**), $[U(OSiPh_3)_2(dbm)_2(OTf)]$ (**1AI**), $[\{UO_2(py)_5\}_2LnI_4]I$ (Ln = Sm (**1AJ**), Dy (**1AK**)), $[U(Cp)_3UO_2(THF)(L^{R4})]$ (R = Me (**1AL**), Et (**1AM**)).[86, 91, 104, 105]

Arnold and Love have explored the one-electron reductive functionalisation of uranyl extensively. Examples include the addition of $[Ln\{(N(SiMe_3)_2)\}_3]$ (Ln = Sc, Y, Ce, Sm, Eu, Gd, Dy, Er, Yb, Lu) to uranyl in a tetramethyl Pacman (L^{Me4}) framework to afford dimeric U^V-oxo Pacman complexes, $\{[UO_2Ln(py)_2(L^{Me4})]\}_2$ (**1AN-1AW** in Scheme 1.7), to which LiCl is added to yield Li-capped U^V monomers $[(py)_3LiOUOLn(py)(L^{Me4})Cl]$ (Ln = Y (**1AX**), Sm (**1AY**), Dy (**1AZ**); Scheme 1.7).[103] The addition of U^{III} complex $[U(Cp)_3]$ to uranyl in a tetramethyl Pacman (L^{Me4}) or tetraethyl Pacman (L^{Et4}) framework resulted in the formation of mixed U^{IV}/U^V complexes $[U(Cp)_3UO_2(THF)(L^{R4})]$ (R = Me (**1AL**), Et (**1AM**); Figure 1.5).[105] Most recently, reductive functionalisation of $[UO_2Cl_2(py)]$ with 1.25 equivalents of

$[SmI_2(THF)_2]$ or DyI_2 in pyridine to form axially symmetric complexes $[\{UO_2(py)_5\}_2LnI_4]I$ (Ln = Sm (**1AJ**), Dy (**1AK**), Figure 1.5) without the need for a polydentate ligand framework, was reported.[104]

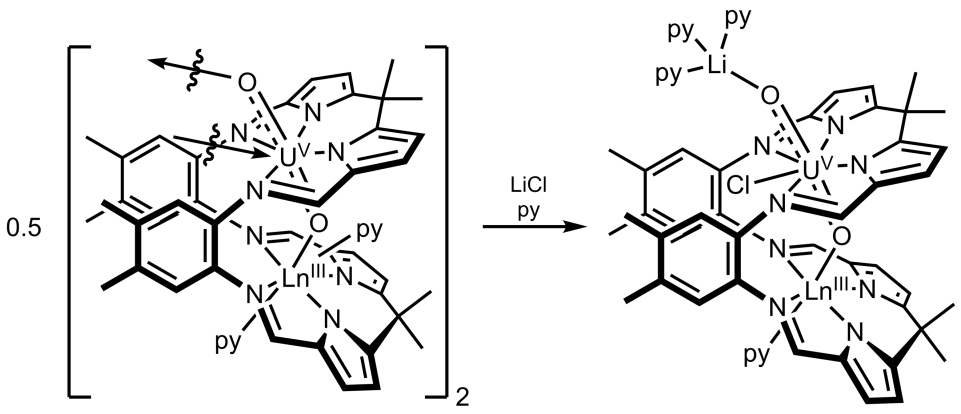

Ln = Sc (**1AN**), Y (**1AO**), Ce (**1AP**), Sm (**1AQ**), Eu (**1AR**), Gd (**1AS**), Dy (**1AT**), Er (**1AU**), Yb (**1AV**), Lu (**1AW**)

Ln = Y (**1AX**), Sm (**1AY**), Dy (**1AZ**)

Scheme 1.7 Addition of LiCl to dimeric U^V-oxo Pacman complexes, $\{[UO_2Ln(py)_2(L^{Me4})]\}_2$ (**1AN**-**1AW**), to yield a Li-capped U^V monomer $[(py)_3LiOUOLn(py)(L^{Me4})Cl]$ (Ln = Y (**1AX**), Sm (**1AY**), Dy (**1AZ**)).[103]

1.5 Actinide Alkyl, Amide and Hydride Complexes: Synthesis and Reactivity

As mentioned in Section 1.2, the few examples of homoleptic peralkyl actinide complexes are difficult to synthesise, with those containing β-hydrogens being prone to β-elimination.[106-109] $[Th(CH_2Ph)_4]$ was the first homoleptic actinide species isolated despite being light sensitive and unstable above -20 °C, however it was not structurally characterised.[49] The structure of the complex was inferred after the synthesis of its uranium analogue.[15, 108] It has been shown that homoleptic actinide peralkyl complexes can be stabilised by purposeful synthesis of "ate"-complexes.[15, 110]

A calorimetric study showed that An–N bonds are approximately 63 $kJ{\cdot}mol^{-1}$ stronger than analogous An–C bonds,[111] due to their increased ionic-character. Sattelberger then showed that actinide amide analogues of unstable actinide alkyl complexes could be readily isolated.[112] Similarly to actinide alkyl complexes, actinide amide complexes have displayed a range of interesting reactivity such as small molecule activation,[26, 113-115] or the catalysis of alcohol addition to carbodiimides.[116, 117] Silylamide ligands feature extensively in actinide chemistry due to the increased size and polarizability of the Si atom, which diffuses the ligand charge more, resulting in softer N-donors when compared with carbon analogues.[118]

1.5.1 Cyclopentadienyl - Supported Complexes

In 1972, Marks reported the first thermally stable *tris*-Cp uranium(IV) alkyl, alyl and aryl complexes of the form $[(Cp)_3U(R)]$ (R = Me, CH_2SiMe_3, C_6F_5, ^iBu, CH_2CHCH_2, ^iPr), synthesised from the salt metathesis reaction of $[(Cp)_3UCl]$ and LiR or MgClR.[33] Marks then reported the synthesis of actinide(IV) complexes of the form $[An(Cp^*)_2Cl_2]$ (An = Th (**1BA**), U (**1BB**); Scheme 1.8): here the two Cp* rings are sufficiently bulky to stabilise salt metathesis and other reactions at the actinide metal centre.[36]

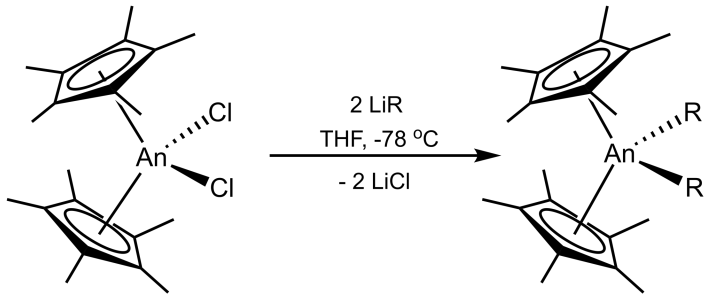

An = Th (**1BA**), U (**1BB**)

An = Th, R = Me (**1BC**), CH_2SiMe_3 (**1BD**), $N(CH_3)_2$ (**1BE**), $N(C_2H_5)_2$ (**1BF**)
An = U, R = Me (**1BG**), CH_2SiMe_3 (**1BH**), $N(CH_3)_2$ (**1BI**), $N(C_2H_5)_2$ (**1BJ**)

Scheme 1.8 Synthesis of *bis*-Cp*-supported An^{IV} dialkyl complexes of the form $[An(Cp^*)_2(R)_2]$ (An = Th, R = Me (**1BC**), CH_2SiMe_3 (**1BD**) $N(CH_3)_2$ (**1BE**), $N(C_2H_5)_2$ (**1BF**); An = U, R = Me (**1BG**), CH_2SiMe_3 (**1BH**) $N(CH_3)_2$ (**1BI**), $N(C_2H_5)_2$ (**1BJ**)) from $[An(Cp^*)_2Cl_2]$ (An = Th (**1BA**), U (**1BB**)).[36, 114]

It was found that the treatment of $[An(Cp^*)_2Cl_2]$ with LiR (R = Me, CH_2SiMe_3, $N(CH_3)_2$, $N(C_2H_5)_2$) affords a series of thermally stable *bis*-Cp* thorium and uranium dialkyl and diamide systems of the form $[An(Cp^*)_2(R)_2]$ (An = Th, R = Me (**1BC**), CH_2SiMe_3 (**1BD**) $N(CH_3)_2$ (**1BE**), $N(C_2H_5)_2$ (**1BF**); An = U, R = Me (**1BG**), CH_2SiMe_3 (**1BH**) $N(CH_3)_2$ (**1BI**), $N(C_2H_5)_2$ (**1BJ**); Scheme 1.8),[36, 114] capable of CO and CO_2 insertion and hydrogenolysis to form thermally stable actinide acyls, carboxylates (Section 1.5.4) and dihydrides.[36, 37, 119] Complexes **1BC** and **1BG** also show a range of catalytic activity, including the hydrosilylation of terminal alkynes and isonitrile coupling

Methods for the preparation of thorium hydride complexes include β-hydrogen elimination[40] and $[Th(COT)_2]$ reduction with NaH,[120] however, alkane elimination from the alkyl precursor is the most common synthetic route.[121-123] The bridging dihydride complexes $[An(Cp^*)_2(H)(\mu\text{-}H)]_2$ (An = Th (**1BK**), U (**1BL**), Scheme 1.9), synthesised from the σ-bond metathesis reaction between $[An(Cp^*)_2(Me)_2]$ and four equivalents of H_2, were the first actinide hydride complexes reported: the thorium complex was characterised by IR and neutron diffraction studies.[36, 124, 125-127].

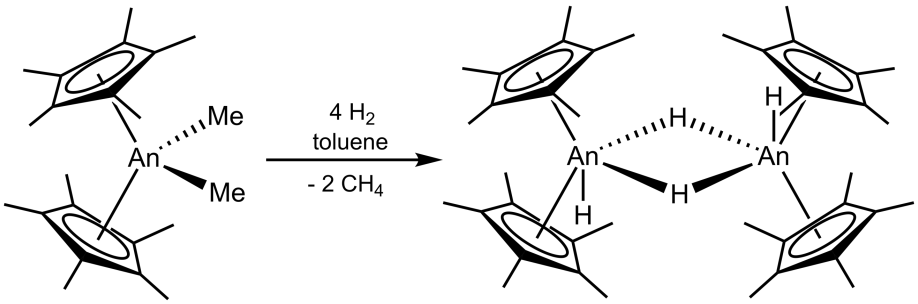

An = Th (**1BC**), U (**1BG**) An = Th (**1BK**), U (**1BL**)

Scheme 1.9 Synthesis of $[An(Cp^*)_2(H)(\mu\text{-}H)]_2$ (An = Th (**1BK**), U (**1BL**)).[36, 124]

Complexes **1BK** and **1BL** were found to effect four and six electron reductions of substrates such as PhSSPh or C_8H_8 to form new An^{IV} complexes $[An(Cp^*)_2(SPh)_2]$ (An = Th (**1BM**), U (**1BN**); Figure 1.6) and "mixed-sandwich" complexes $[\{An(Cp^*)(COT)\}_2\{\mu\text{-}C_8H_8\}]$ (An = Th (**1BO**), U (**1BP**); Figure 1.6) with two equivalents of hydrogen gas as by-products.[128]

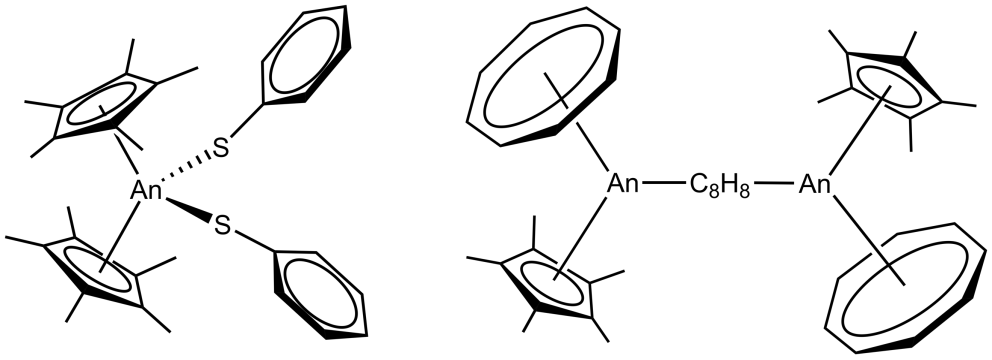

An = Th (**1BM**), U (**1BN**) An = Th (**1BO**), U (**1BP**)

Figure 1.6 An^{IV} complexes $[An(Cp^*)_2(SPh)_2]$ (An = Th (**1BM**), U (**1BN**)) and $[\{An(Cp^*)(COT)\}_2\{\mu\text{-}C_8H_8\}]$ (An = Th (**1BO**), U (**1BP**)).[128]

1.5.2 Cyclopentadienyl and Other Ligand Sets

Sattelberger and Ephritikhine reported the formation of stable alkyls, amides and hydrides from "mixed-sandwich" complexes of the form $[(C_8H_8)(Cp^*)An(R)]$ (An = Th, R = H (**1BQ**), $CH(SiMe_3)_2$ (**1BR**), $N(SiMe_3)_2$ (**1BS**); An = U, R = $CH(SiMe_3)_2$ (**1BT**), $N(SiMe_3)_2$ (**1BU**); Figure 1.7).[46, 47] Recently, the synthesis of mixed-sandwich uranium(IV) alkyl complexes of the form $[An(COT^{TIPS2})(Cp^*)(R)]$ (An = Th, R = Me (**1BV**), CH_2SiMe_3 (**1BW**), $CH(SiMe_3)_2$ (**1BX**), CH_2Ph (**1BY**); An = U, R = Me (**1BZ**), CH_2SiMe_3 (**1CA**), $CH(SiMe_3)_2$ (**1CB**), CH_2Ph (**1CC**); Figure 1.7) from the treatment of $[U(COT^{TIPS2})(Cp^*)Cl]$ with LiR, was reported. The bulky silyl groups on the COT ring provide additional steric stabilisation allowing for the isolation of smaller uranium alkyls, solubility and crystallinity.[129, 130] Addition

of H_2 to **1BV**-**1CC** results in σ-bond metathesis to yield the An^{IV} hydride complexes [An(COT^{TIPS2})(Cp*)(H)] (An = Th (**1CD**), U (**1CE**), Figure 1.7).[129, 130]

Actinide-alkyl complexes featuring nitrogen- and oxygen-donor ligands have also been reported.[131-138] Examples include diamido-ether supported U^{IV} complexes [(^{dipp}NCOCN)U(R)$_2$] (dipp = ^{i}Pr$_2$Ph; R = CH_2SiMe_3 (**1CG**), CH_2Ph (**1CH**), Figure 1.7),[131, 137] ferrocene (fc) diamide-supported U^{IV} dibenzyl complex [fc(NSiMe$_2$^{t}Bu)$_2$U(CH_2Ph)$_2$] (**1CF** in Figure 1.7),[133] or Tren^{TIPS}-supported Th^{IV} benzyl complex [(Tren^{TIPS})Th(CH_2Ph)] (**1CI** in Figure 1.7).[138] Examples of uranium(III) alkyl complexes, [(Tp*)$_2$UR] and [(Tp*)(Cp*)UR] (R = CH_2SiMe_3, CH_2Ph; **1S**-**1V** in Figure 1.2), supported by *bis*-Tp* as well as mixed Cp* and Tp* ligand systems were discussed in Section 1.2.2.[53]

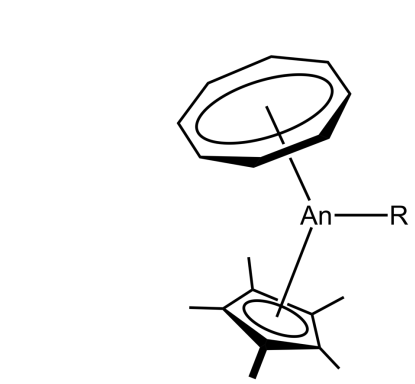

An = Th, R = H (**1BQ**), $CH(SiMe_3)_2$ (**1BR**), $N(SiMe_3)_2$ (**1BS**); An = U, R = $CH(SiMe_3)_2$ (**1BT**), $N(SiMe_3)_2$ (**1BU**)

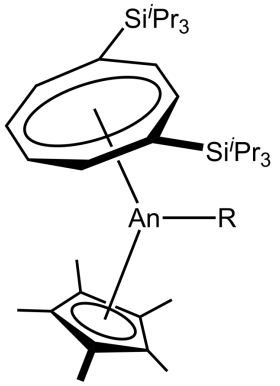

An = Th, R = Me (**1BV**), CH_2SiMe_3 (**1BW**), $CH(SiMe_3)_2$ (**1BX**), CH_2Ph (**1BY**), H (**1CD**); An = U, R = Me (**1BZ**), CH_2SiMe_3 (**1CA**), $CH(SiMe_3)_2$ (**1CB**), CH_2Ph (**1CC**), H (**1CE**)

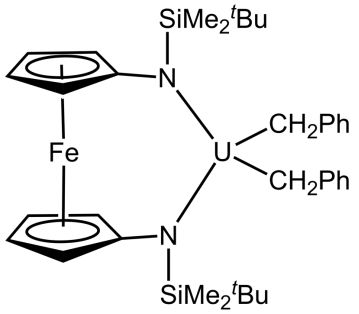

(**1CF**)

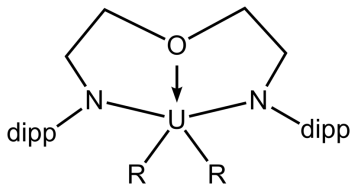

R = CH_2SiMe_3 (**1CG**), CH_2Ph (**1CH**)

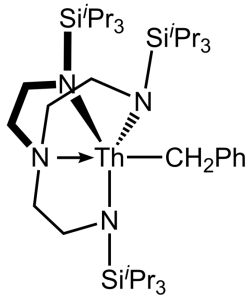

(**1CI**)

Figure 1.7 An^{IV} alkyl, amide and hydride complexes [(C_8H_8)(Cp*)An(R)] (An = Th, R = H (**1BQ**), $CH(SiMe_3)_2$ (**1BR**), $N(SiMe_3)_2$ (**1BS**); An = U, R = $CH(SiMe_3)_2$ (**1BT**), $N(SiMe_3)_2$ (**1BU**)), [An(COT^{TIPS2})(Cp*)(R)] (COT^{TIPS2} = C_8H_6(Si^{i}Pr$_3$-1,4)$_2$; An = Th, R = Me (**1BV**), CH_2SiMe_3 (**1BW**), $CH(SiMe_3)_2$ (**1BX**), CH_2Ph (**1BY**), H (**1CD**); An = U, R = Me (**1BZ**), CH_2SiMe_3 (**1CA**), $CH(SiMe_3)_2$ (**1CB**), CH_2Ph (**1CC**), H (**1CE**)), [fc(NSiMe$_2$^{t}Bu)$_2$U(CH_2Ph)$_2$] (**1CF**), [(^{dipp}NCOCN)U(R)$_2$] (dipp = ^{i}Pr$_2$Ph; R = CH_2SiMe_3 (**1CG**), CH_2Ph (**1CH**), [(Tren^{TIPS})Th(CH_2Ph)] (**1CI**).[46, 47, 129-131, 133, 137, 138]

Actinide alkyls remain rare and stabilisation of the actinide-carbon σ-bond is inherently problematic due to the preference for covalent bonding by alkyl groups; a

contrast to the preference for more ionic bond character of the actinide ions. Consequently, the An–C bond displays unprecedented reactivity, including a range of small molecule activation reactions, which have applications in catalysis. For example, actinide alkyl complexes of the form $[(Cp^*)_2An(Me)_2]$ (An = Th (**1BC**), U (**1BG**) in Scheme 1.9) have shown promise in terminal alkyne hydroamination (Scheme 1.10), where choice of actinide affects regioselectivity,[139, 140] or terminal alkyne oligomerisation and cross-oligomerisation.[141, 142]

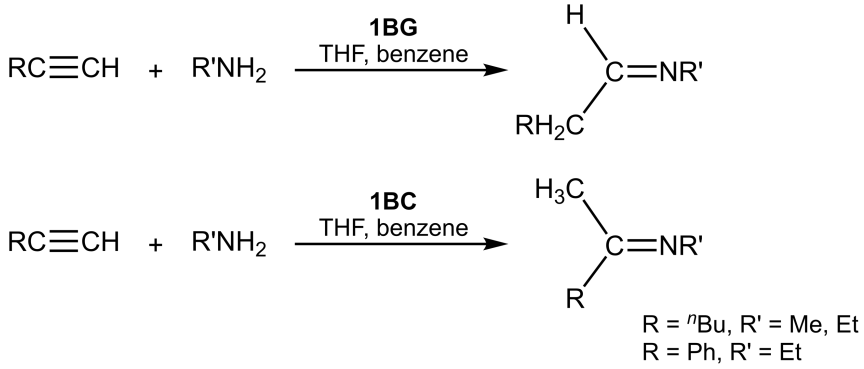

Scheme 1.10 Regioselective hydroamination of terminal alkynes using $[(Cp^*)_2An(Me)_2]$ (An = Th (**1BC**), U (**1BG**).[140]

Attempts to render these reactions commercially viable have not yet been successful. With the aim to further explore and develop this chemistry, the investigation of new ligand systems is essential. The absence of pyrrolide-supported actinide alkyl complexes in the literature has prompted this investigation into the ability of recently reported *trans*-calix[2]benzene[2]pyrrolide macrocycle-supported thorium(IV) and uranium(IV) halides to form actinide alkyls, and subsequent reactivity towards small molecules.[143]

1.5.3 C–H Bond Activation

Organometallic *f*-block alkyl complexes show exciting reactivity in C−H bond activation.[144] Examples include the uranium(III) mediated formation of both "tuck-in" and "tuck-over" products from intra- and inter-molecular pentamethylcyclopentadienyl (Cp*) C–H bond activation,[129, 145, 146] such as the formation of **1F** from **1E** in Scheme 1.3,[44] Section 1.2.1. Other examples include C–H bond activation of typically inert carbocycles, induced by steric crowding,[147] or the addition of C−H bonds across f-block metal imido and nitrido bonds.[51, 139, 148-150] These findings are important because C–H bond activation is a key step in the synthesis of a range of desirable organic products.

In spite of all the success of *d*-block hydrocarbon C−H bond activation there are no reports of an economically viable, homogeneously catalysed process.[151, 152]

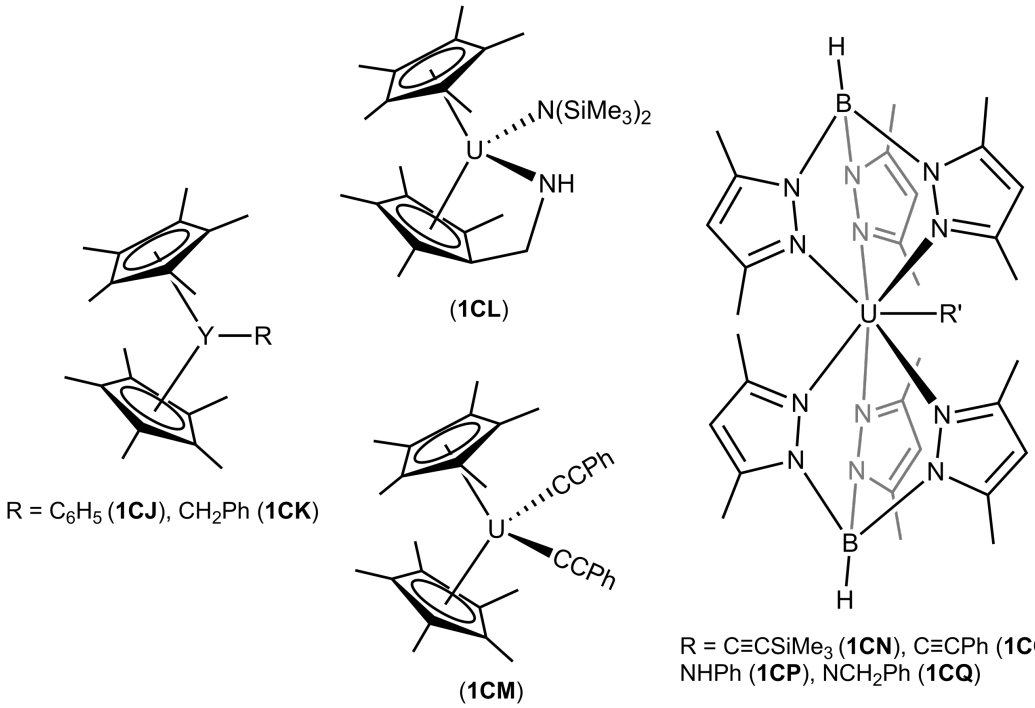

Figure 1.8 C–H bond activation products [(Cp*)$_2$Y(C$_6$H$_5$)] (**1CJ**), [(Cp*)2Y(CH2Ph)] (**1CK**), [(Cp*)U(η^5:η^1-C$_5$Me$_4$CH$_2$NH)(N(SiMe$_3$)$_2$)] (**1CL**), [(Cp*)$_2$U(C≡CPh)$_2$] (**1CM**), [(Tp*)$_2$U(R′)] (R′ = C≡CSiMe$_3$ (**1CN**), C≡CPh (**1CO**), NHPh (**1CP**), NCH$_2$Ph (**1CQ**)).[115, 147, 153, 154]

Evans showed that C–H bond activation can be induced by steric crowding when benzene or toluene is added to the complex [(Cp*)$_3$Y], resulting in sp^2 C–H bond activation and formation of an aryl complex [(Cp*)$_2$Y(C$_6$H$_5$)] (**1CJ** in Figure 1.8), or sp^3 C–H bond activation and formation of a benzyl complex [(Cp*)$_2$Y(CH$_2$Ph)] (**1CK** in Figure 1.8) and elimination of C$_5$Me$_5$H.[147] A specific example of interesting C–H bond reactivity in An^{IV} coordination complexes is the intramolecular C–H bond activation of the methyl group on Cp* by the transient terminal uranium(IV) nitride complex [Cp*$_2$U(N)(N(SiMe$_3$)$_2$)] to give [(Cp*)U(η^5:η^1-C$_5$Me$_4$CH$_2$NH)(N(SiMe$_3$)$_2$)] (**1CL** in Figure 1.8).[153] An example of intermolecular C–H bond activation is the activation of sp^3 hybridised bonds by [(Cp*)$_2$Th(R)$_2$] (R = Me (**1C**), CH$_2$Ph (**1D**), Scheme 1.2) in 2,6-lutidine *N*-oxide, mentioned in Section 1.2.1.[42]

The addition of two equivalents of HC≡CPh to the complex [(Cp*)$_2$U(Me)$_2$] (**1BG**), yielded the alkynyl complex [(Cp*)$_2$U(C≡CPh)$_2$] (**1CM** in Figure 1.8) as the σ-bond metathesis product along with methane elimination.[154] Amide and alkynyl analogues of U^{III} complexes [(Tp*)$_2$UR] (**1S-1T** in Figure 1.2) were also synthesised

by the σ-bond metathesis of C–H bonds in HR′ reagents (R′ = C≡CSiMe$_3$, C≡CPh, NHPh, NCH$_2$Ph) with the U–C bond of [(Tp*)$_2$U(CH$_2$Ph)] (**1T**) to give [(Tp*)$_2$U(R′)] (**1CN-1CQ** in Figure 1.8).[115] In the alkynyl complexes **1CN** and **1CO**, FTIR spectroscopy had shown that the C≡C bonds had been slightly weakened by coordination to U^{III}, indicating some degree of back-bonding from the uranium into the π*-orbitals of the C≡C bonds. The bond dissociation enthalpy of the U–alkynyl bond in the complex [Cp′′$_3$U(C≡CPh)] (Cp′′ = η^5-C$_5$H$_4$SiMe$_3$) is nearly twice that of U–Me in the analogous methyl complex [Cp′′$_3$U(Me)].[155] The above reactions are therefore also likely to have been driven by the strengths of the new alkynyl U–C bonds and amide U–N bonds.

1.5.4 Small Molecule Activation

Research institutions and petrochemical industries world-wide are interested in the development of new methods for the catalytic conversion of CO_2 and CO into commercially applicable products such as methanol or formic acid and fuels.[26] This process would have two major advantages: the removal of excess CO_2, a well-known greenhouse gas, from the atmosphere as well as a sustainable resolution of peak-oil crisis.[156]

Carbon monoxide has the strongest diatomic bond in nature with a bond enthalpy of 1076 kJ mol^{-1}; activation of CO is therefore difficult. The bond length in free CO is 1.128 Å and its IR stretching frequency is 2143 cm^{-1}.[157] Upon activation of CO, the stretching frequency decreases as the bond length between the atoms increases. The *d*- and *f*-orbitals of the metal interact with the frontier molecular orbitals of the CO in a way that allows for σ-donation from the gas molecule to the metal centre and π-backdonation from the metal into the antibonding orbitals of CO. This π-backdonation weakens the bond between the atoms of the diatomic molecule and depending on the extent of activation, functionalization can occur.

Some of the first examples of carbon monoxide coupling and insertion into An^{IV} metal-alkyl bonds were reported in 1978 upon the synthesis of the monomeric [Th(Cp*)$_2$(κ^2-O$_2$C$_2$(CH$_2$SiMe$_3$)$_2$)] (**1CS** in Scheme 1.11) and the dimeric [Th(Cp*)$_2$]$_2$(μ-η^1:η^1-O$_2$C$_2$Me$_2$)$_2$] (**1CR** in Scheme 1.11), from the reaction of CO with [An(Cp*)$_2$(R)$_2$] (where An = Th, U and R = Me, CH$_2$SiMe$_3$).[37] Here the migratory insertion of CO into the actinide metal-alkyl bond of [An(Cp*)$_2$(CH$_2$SiMe$_3$)Cl] to yield [An(Cp*)$_2$(OC(CH$_2$)SiMe$_3$)Cl] was also demonstrated.[37] Soon after, insertion reactions with hydride complexes were reported, where CO reacted with [Th(Cp*)$_2$(OCMe$_3$)(H)] to yield the dimeric complex [Th(Cp*)$_2$(OCMe$_3$)]$_2$(μ-η^1:η^1-O$_2$C$_2$H$_2$)] (**1CT** in Scheme 1.11).[158] It was also found that CO insertion into An–N bonds of

[$An(Cp^*)_2(NMe_2)_2$] readily occurred.[114] Other examples of CO activation include that of the "tuck-in" complex [$(\eta^5:\eta^1\text{-}C_5H_4SiMe_2CH_2)_2U$] (**1F** in Scheme 1.3) discussed in Section 1.2.1, which reacts with CO to afford complex **1H** (shown in Scheme 1.3).[44, 45]

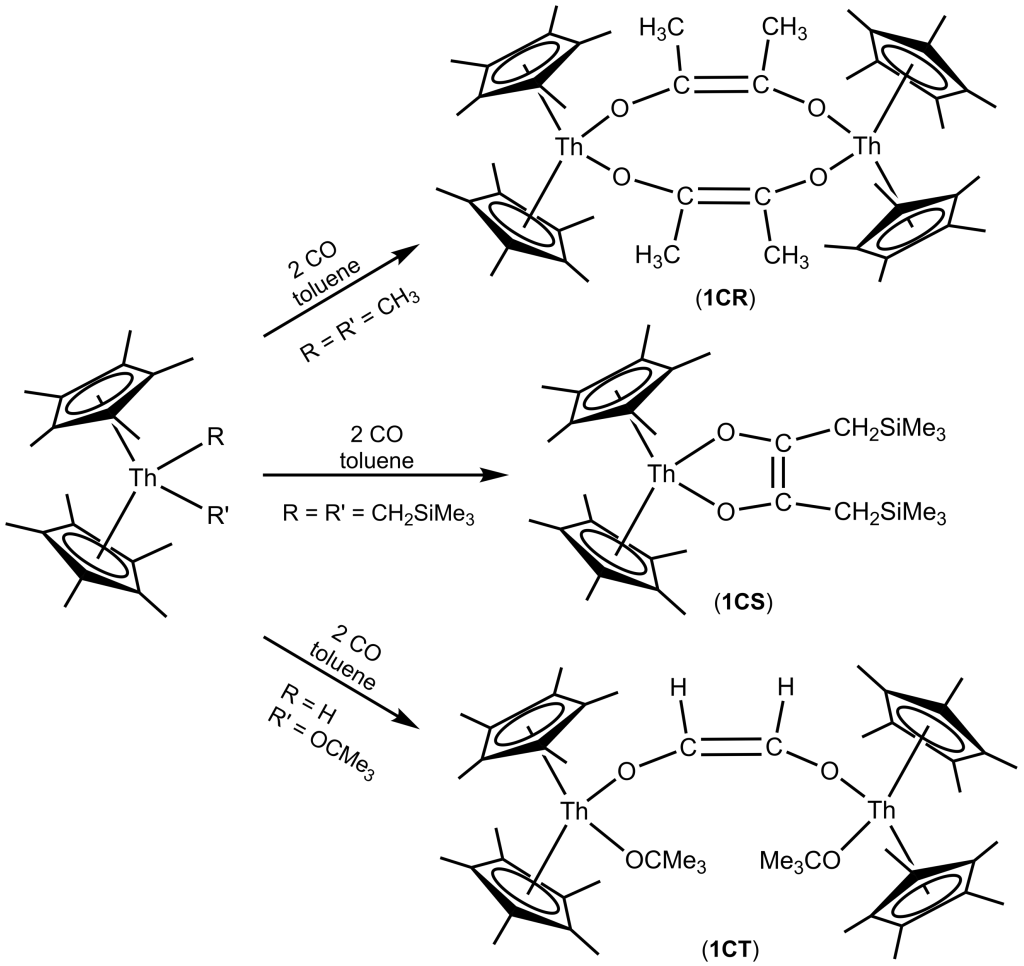

Scheme 1.11 CO coupling and insertion into Th^{IV} alkyl and hydride bonds of [$Th(Cp^*)_2(R)(R')$] to give [$Th(Cp^*)_2]_2(\mu\text{-}\eta^1:\eta^1\text{-}O_2C_2Me_2)_2$] (**1CR**), [$Th(Cp^*)_2(\kappa^2\text{-}O_2C_2(CH_2SiMe_3)_2)$] (**1CS**) or [$Th(Cp^*)_2(OCMe_3)]_2(\mu\text{-}\eta^1:\eta^1\text{-}O_2C_2H_2)$] (**1CT**).[37, 158]

Carbon dioxide can be activated chemically, photochemically, electrochemically and enzymatically. CO_2 has two sets of π-orbitals, which are orthogonal to each other and hence allow for varied bonding modes to a metal centre. The carbon to oxygen bond in CO_2 has a bond length of 1.16 Å and a bond enthalpy of 805 kJ mol^{-1}, making it easier to activate than CO.[159] Similarly to CO, carbon dioxide can act as an innocent ligand to organometallic complexes or insert into metal alkyl bonds. There is also precedent for a range of CO_2 disproportionation chemistry.[160]

The first example of CO_2 insertion into actinide metal-alkyl and actinide metal-hydride bonds was reported in 1985, where carbon dioxide was added to [$An(Cp^*)_2(Me)_2$]

(An = Th (**1BC**), U (**1BG**)) and yielded [An(Cp*)$_2$(η^2-O$_2$CMe)$_2$].[119] When CO_2 was added to [Th(Cp*)$_2$(OCH^{t}Bu$_2$)(H)] (**1CU** in Scheme 1.12), a formate insertion product [Th(Cp*)$_2$(OCH^{t}Bu$_2$)(κ^2-O$_2$CH)] (**1CV** in Scheme 1.12) was obtained.[119] The U^{IV} "mixed-sandwich" complexes [An(COT^{TIPS2})(Cp*)(R)] (**1BV**-**1CE** in Figure 1.7), discussed in Section 1.5.2, have shown analogous carbon dioxide insertion reactions yielding [U(COT^{TIPS2})(Cp*)(κ^2-O$_2$CR)] products.[129, 130] Other examples of analogous insertion chemistry have been reported with actinide alkyls and amides.[26, 115, 154, 161]

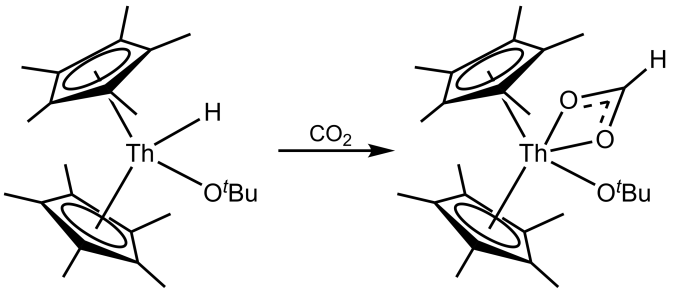

(**1CU**) (**1CV**)

Scheme 1.12 Insertion of CO_2 into the Th^{IV} hydride bond of [Th(Cp*)$_2$(OCH^{t}Bu$_2$)(H)] (**1CU**) to form [Th(Cp*)$_2$(OCH^{t}Bu$_2$)(κ^2-O$_2$CH)] (**1CV**).[119]

Despite examples of CO and CO_2 activation and functionalisation chemistry at An^{IV} metal centres, methods for the cost-effective removal of the functionalised products and regeneration of the metal complex have not yet been reported. Further research into actinide ion to ligand interactions, reactivities and periodicity within the actinide series is required.

1.5.5 Calix[4]Tetrapyrroles

Oligopyrrole and calix[4]pyrrole ligands have been shown to support interesting *f*-element chemistry, in part due to the stability gained from the macrocyclic effect.[162] In these ligand systems both η^1-pyrrolide and metallocene-like η^5-pyrrolide bonding is available. Complexes of this type facilitate the synthesis of unusual *f*-element alkyls and show small molecule activation chemistry with CO_2 and N_2.[62, 65, 163-169] Examples include the calix[4]pyrrolide samarium alkyl complexes [(Et$_8$-calix-[4]dipyrrolide-*trans*-N,N′-dimethylpyrrole)Sm(R)] (R = Me (**1CX**), CH_2SiMe_3 (**1CY**); Scheme 1.13) synthesised by salt metathesis from [(Et$_8$-calix-[4]dipyrrolide-*trans*-N,N′-dimethylpyrrole)SmCl] (**1CW** in Scheme 1.13) and LiR, which displayed the first *f*-block reductive disproportionation of CO_2 to form a carbonate complex.[165, 166]

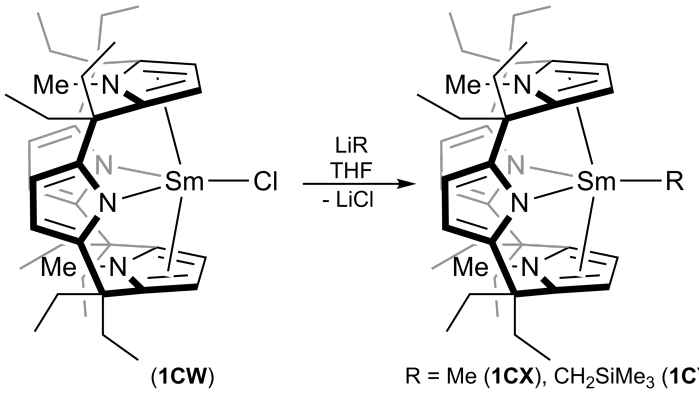

Scheme 1.13 The synthesis of pyrrolic macrocycle-supported samarium(III) alkyls **1CX** and **1CY**.[165]

Gambarotta reported the synthesis of a calix-pyrrolide-supported thorium arene complex, [{(Et_8-calix-[4]tetrapyrrole)Th}{K(DME)}(η^4-$C_{10}H_8$)][Li(DME)$_3$] (**1CZ** in Scheme 1.14), in which the arene was bent due to π-back-donation from the Th^{IV} metal centre, resulting in butadienyl-like bonding.[170] The potassium counterion was found to be η^5-coordinated to two pyrrolides and κ^1-coordinated to the remaining two pyrrolic nitrogens of the macrocycle.[170] Complex **1CZ** displayed unusual reactivity with two equivalents of neat N_3SiMe_3 to afford the Th^{IV} silylamide complex [(Et_8-calix-[4]tetrapyrrole)Th(N($SiMe_3$)$_2$)][Li(DME)$_3$] (**1DA** in Scheme 1.14), a product of N_2 elimination and silyl migration.

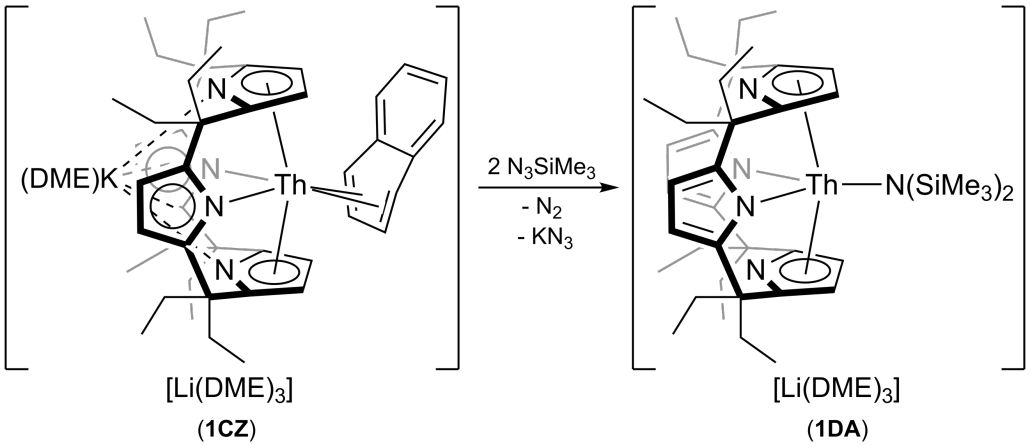

Scheme 1.14 Synthesis of [(Et_8-calix-[4]tetrapyrrole)Th(N($SiMe_3$)$_2$)][Li(DME)$_3$] (**1DA**) from [{(Et_8-calix-[4]tetrapyrrole)Th}{K(DME)}(η^4-$C_{10}H_8$)][Li(DME)$_3$] (**1CZ**).[170]

1.6 Scope of Thesis

1.6.1 Background

A *trans*-calix[2]benzene[2]pyrrole macrocyclic system (H_2L) was developed by Sessler and synthesised using $BF_3{\cdot}OEt_2$ as a catalyst, affording H_2L in 16 % yield.[171] The reaction conditions were then altered by Frey, employing Sc(OTf)$_3$ as a catalyst to afford H_2L

in 28 % yield (Scheme 1.15).[172] H_2L combines two aryl rings with two pyrrolide heterocycles connected by dimethylmethane linkers. The absence of extended conjugation in this macrocycle in comparison to porphyrins results in flexibility of the ligand and a variety of binding modes.

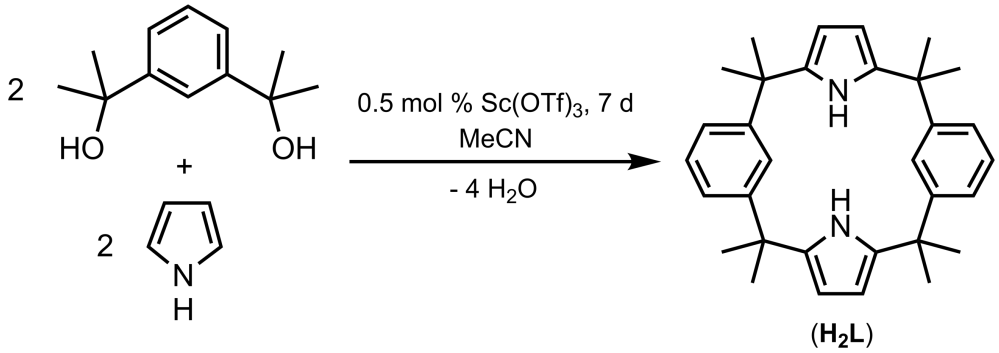

Scheme 1.15 Synthesis of the *trans*-calix[2]benzene[2]pyrrole macrocycle (H_2L).[172]

Previous work on samarium(II) and samarium(III) complexes of this ligand showed σ- or π-bonding of the ligand to the metal centre *via* either the pyrrolide or the arene.[172, 173] This work demonstrated that the samarium(II) complex [(L)Sm(THF)$_2$] (**1DB** in Scheme 1.16) and samarium(III) complex [(L)SmCl] (**1DC** in Scheme 1.16) bind κ^1 to the pyrrolic nitrogen and η^6 to the arenes. Gambarotta also synthesised a samarium(III) complex [(L^{-H})Sm(THF)]; a minor product from the reaction of [(L)SmCl] (**1DC**) with LiMe. Here the macrocycle was η^5-bound to the samarium(III) metal centre by the pyrrolides and also η^1-coordinated to one singly deprotonated aryl group.[172]

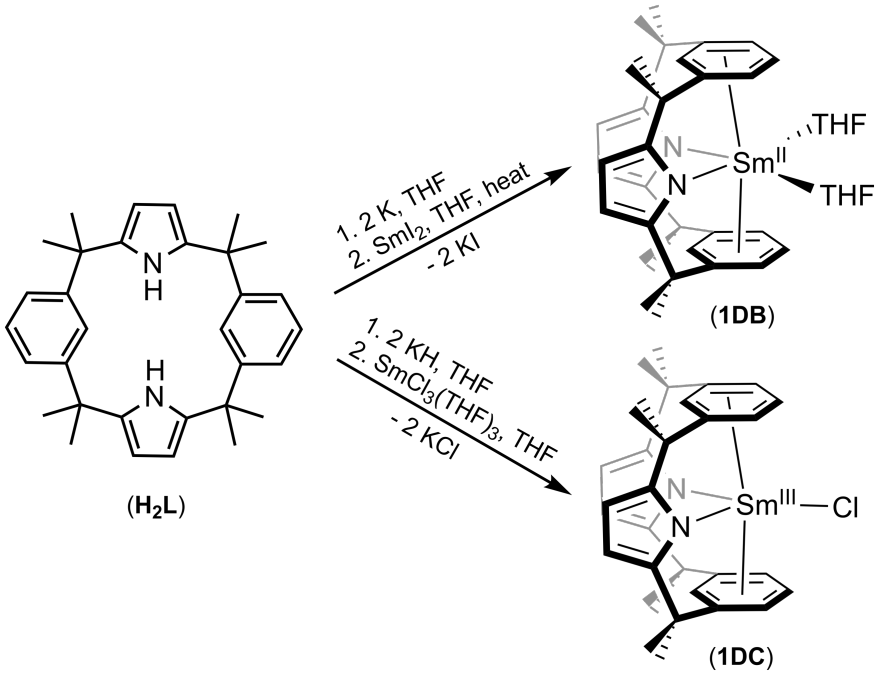

Scheme 1.16 Synthesis of [(L)Sm(THF)$_2$] (**1DB**) and [(L)SmCl] (**1DC**).[172, 173]

Based on these findings, it was hypothesised that the flexibility and range of binding modes available to the *trans*-calix[2]benzene[2]pyrrolide ligand, $(L)^{2-}$, could provide a means for the study of novel actinide reactivity beyond metallocene systems. Thorium(IV) and uranium(IV) complexes $[(L)ThCl_2]$ (**A**) and $[(L)UI_2]$ (**B**) were synthesised (Scheme 1.17),[143] and similarly to complexes **1CZ** and **1DA** show η^5-coordination of the two pyrrolide rings to the metal centres. This coordination mode is reminiscent of metallocene complexes of the form $[(Cp^*)_2AnCl_2]$. It was hypothesised that **A** and **B** will display new chemistry benefiting from the macrocyclic effect,[162] greater flexibility and multiple potential coordination sites.

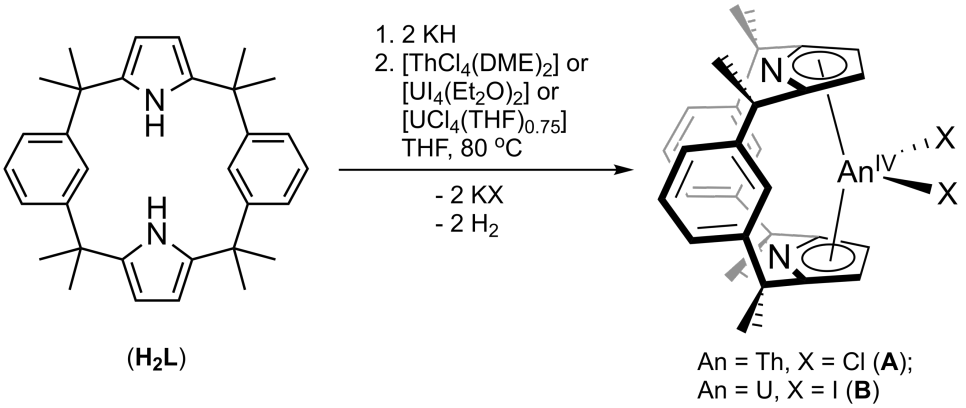

Scheme 1.17 Synthesis of An^{IV} complexes $[(L)ThCl_2]$ (**A**) and $[(L)UI_2]$ (**B**).[143]

Work carried out by colleagues during this project, showed that all U^{III} and Np^{III} complexes supported by $(L)^{2-}$ displayed η^6-coordination to the arenes and κ^1-coordination to the pyrrolic nitrogens: examples $[(L)UI(THF)]$ (**1DD**), $[(L)U(BH_4)]$ (**D**), $[(L)NpCl]$ (**1DE**) and $[(L)Np(\mu\text{-}Cl_2)NpCl_2(THF)_3]$ (**1DF**) are shown in Figure 1.9.[143, 174, 175] Computational studies have shown significant covalent character in the interactions of arenes with the electron rich U^{III} and Np^{III} centres in these complexes. It is therefore tempting to suggest an oxidation state dependence on ligand arrangement, however the exact cause of the ligand conformation change remains unknown and has been investigated in greater detail using Th^{IV} complexes in this work.

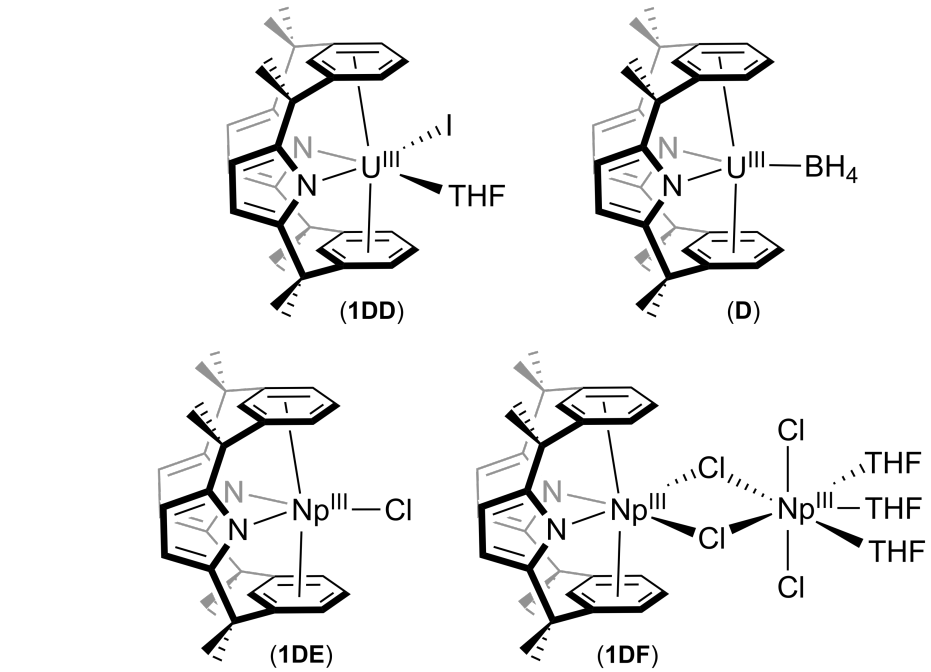

Figure 1.9 U^{III} and Np^{III} complexes [(L)UI(THF)] (**1DD**), [(L)U(BH_4)] (**D**), [(L)NpCl] (**1DE**) and [(L)Np(μ-Cl_2)$NpCl_2(THF)_3$] (**1DF**).[143, 174, 175]

Previous work in our group also showed that attempts to reduce the Th^{IV} complex [(L)$ThCl_2$] (**A**) to Th^{III} using two equivalents of potassium, resulted in the synthesis of a chloride-bridged dimeric Th^{IV} complex $[K(THF)_2(L^{-2H})Th(\mu\text{-}Cl)]_2$ (**1DG** in Figure 1.10), in which double arene deprotonation and C–H metallation of $(L)^{2-}$ to give $(L^{-2H})^{4-}$ took place.[143] The ligand remains η^5-coordinated to the pyrroles and two new Th–arene bonds form; this coordination mode is therefore described as $\eta^5{:}\eta^1{:}\eta^5{:}\eta^1$. Similarly, it was found that the addition of three equivalents of $KN(SiMe_3)_2$ to **A** results in analogous arene C–H deprotonation and the formation of a Th^{IV} amide complex $K[(L^{-2H})Th(N(SiMe_3)_2)]$ (**C** in Figure 1.10).[143]

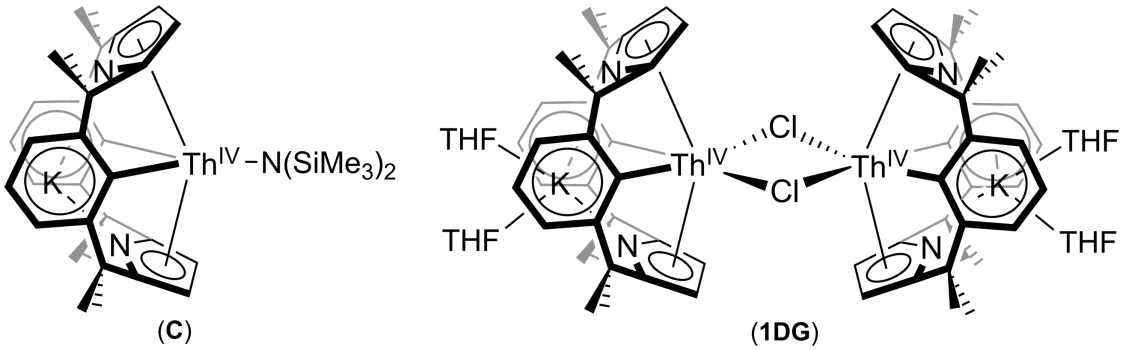

Figure 1.10 Th^{IV} complexes $K[(L^{-2H})Th(N(SiMe_3)_2)]$ (**C**) and $[K(THF)_2(L^{-2H})Th(\mu\text{-}Cl)]_2$ (**1DG**).[143]

1.6.2 Aims

This work primarily aims to probe the thorium and uranium chemistry that the *trans*-calix[2]benzene[2]pyrrolide ligand system can support. This is attempted herein by investigating:

- New actinide alkyl and borohydride chemistry supported by $(L)^{2-}$ and $(L^{-2H})^{4-}$, developing previously reported amination chemistry of this system and exploring subsequent reactivity.
- The lability of isolated $[M(L^{-2H})An(R)]$ (R = alkyl, amide) "ate"-complexes towards M^{+} ion exchange.
- The reversibility of ligand $(L)^{2-}$ deprotonation to give $(L^{-2H})^{4-}$ using $[Et_3NH][BPh_4]$ and terminal alkynes.
- Coordination modes of the macrocycle experimentally and theoretically.
- The redox chemistry of thorium and uranium within this macrocyclic framework.

1.7 References for Chapter One

1. *Thorium*, Radiological and Chemical Fact Sheets to Support Health Risk Analyses for Contaminated Areas, Argonne National Laboratory, EVS, 2007.
2. *Uranium*, Radiological and Chemical Fact Sheets to Support Health Risk Analyses for Contaminated Areas, Argonne National Laboratory, EVS, 2007.
3. *Depleted Uranium*, Radiological and Chemical Fact Sheets to Support Health Risk Analyses for Contaminated Areas, Argonne National Laboratory, EVS, 2007.
4. P. L. Arnold, D. Patel, C. Wilson and J. B. Love, *Nature*, 2008, **451**, 315-317.
5. R. R. Langeslay, M. E. Fieser, J. W. Ziller, F. Furche and W. J. Evans, *Chem. Sci.*, 2015, **6**, 517-521.
6. M. R. MacDonald, M. E. Fieser, J. E. Bates, J. W. Ziller, F. Furche and W. J. Evans, *J. Am. Chem. Soc.*, 2013, **135**, 13310-13313.
7. H. S. La Pierre, A. Scheurer, F. W. Heinemann, W. Hieringer and K. Meyer, *Angew. Chem.*, 2014, **126**, 7286-7290.
8. D. H. Woen and W. J. Evans, in *Handbook on the Physics and Chemistry of Rare Earths*, eds. J.-C. G. Bünzli and V. K. Pecharsky, Elsevier, 2016, vol. 50, pp. 337-394.
9. R. Shannon, *Acta Crystallogr., Sect. A:*, 1976, **32**, 751-767.
10. N. Kaltsoyannis and P. Scott, *The f elements*, Oxford University Press, Oxford, 1999.
11. T. J. Marks, *Science*, 1982, **217**, 989-997.
12. J. G. Brennan, J. C. Green and C. M. Redfern, *J. Am. Chem. Soc.*, 1989, **111**, 2373-2377.
13. S. Cotton, in *Lanthanide and Actinide Chemistry*, John Wiley & Sons, Ltd, 2006, ch. 9, pp. 145-153.
14. N. Kaltsoyannis, *Inorg. Chem.*, 2013, **52**, 3407-3413.
15. E. R. Sigurdson and G. Wilkinson, *J. Chem. Soc., Dalton Trans.*, 1977, **0**, 812-818.
16. L. T. Reynolds and G. Wilkinson, *J. Inorg. Nucl. Chem.*, 1956, **2**, 246-253.
17. E. O. Fischer and Y. Hristidu, *Z. Naturforsch.*, 1962, **173**, 275-276.
18. E. O. Fischer and A. Treiber, *Z. Naturforsch.*, 1962, **173**, 276-277.

19. J. M. Birmingham and G. Wilkinson, *J. Am. Chem. Soc.*, 1956, **78**, 42-44.
20. A. Streitwieser, Jr. and U. Mueller-Westerhoff, *J. Amer. Chem. Soc.*, 1968, **90**, 7364.
21. Peter W. Roesky, *Eur. J. Inorg. Chem.*, 2001, **2001**, 1653-1660.
22. D. Seyferth, *Organometallics*, 2004, **23**, 3562-3583.
23. A. Streitwieser, Jr. and N. Yoshida, *J. Amer. Chem. Soc.*, 1969, **91**, 7528.
24. P. L. Arnold, *Chem. Commun.*, 2011, **47**, 9005-9010.
25. M. B. Jones and A. J. Gaunt, *Chem. Rev.*, 2012, **113**, 1137-1198.
26. P. L. Arnold and Z. R. Turner, *Nat. Rev. Chem.*, 2017, **1**, 0002.
27. J. M. O'Connor and C. P. Casey, *Chem. Rev.*, 1987, **87**, 307-318.
28. P. Jutzi and N. Burford, *Chem. Rev.*, 1999, **99**, 969-990.
29. R. D. Fischer, *Theor. Chim. Acta*, 1963, **1**, 418-431.
30. R. D. Ernst, W. J. Kennelly, C. S. Day, V. W. Day and T. J. Marks, *J. Am. Chem. Soc.*, 1979, **101**, 2656-2664.
31. T. J. Marks, A. M. Seyam and J. R. Kolb, *J. Am. Chem. Soc.*, 1973, **95**, 5529-5539.
32. T. J. Marks and W. A. Wachter, *J. Am. Chem. Soc.*, 1976, **98**, 703-710.
33. T. J. Marks and A. M. Seyam, *J. Am. Chem. Soc.*, 1972, **94**, 6545-6546.
34. A. E. Gebala and M. Tsutsui, *J. Am. Chem. Soc.*, 1973, **95**, 91-93.
35. G. Brandi, M. Brunelli, G. Lugli and A. Mazzel, *Inorg. Chim. Acta*, 1973, **7**, 319-322.
36. J. M. Manriquez, P. J. Fagan and T. J. Marks, *J. Am. Chem. Soc.*, 1978, **100**, 3939-3941.
37. J. M. Manriquez, P. J. Fagan, T. J. Marks, C. S. Day and V. W. Day, *J. Am. Chem. Soc.*, 1978, **100**, 7112-7114.
38. W. J. Evans, K. J. Forrestal and J. W. Ziller, *Angew. Chem., Int. Ed. Engl.*, 1997, **36**, 774-776.
39. W. J. Evans, G. W. Nyce and J. W. Ziller, *Organometallics*, 2001, **20**, 5489-5491.
40. D. G. Kalina, T. J. Marks and W. A. Wachter, *J. Am. Chem. Soc.*, 1977, **99**, 3877-3879.
41. T. Andrea and M. S. Eisen, *Chem. Soc. Rev.*, 2008, **37**, 550-567.
42. J. A. Pool, B. L. Scott and J. L. Kiplinger, *J. Am. Chem. Soc.*, 2005, **127**, 1338-1339.
43. J. L. Kiplinger, B. L. Scott, E. J. Schelter and J. A. Pool Davis Tournear, *J. Alloys Compd.*, 2007, **444–445**, 477-482.
44. W. J. Evans, N. A. Siladke and J. W. Ziller, *Chem. Eur. J.*, 2010, **16**, 796-800.
45. N. A. Siladke, J. W. Ziller and W. J. Evans, *J. Am. Chem. Soc.*, 2011, **133**, 3507-3516.
46. T. M. Gilbert, R. R. Ryan and A. P. Sattelberger, *Organometallics*, 1989, **8**, 857-859.
47. J.-C. Berthet, J.-F. Le Maréchal and M. Ephritikhine, *J. Organomet. Chem.*, 1994, **480**, 155-161.
48. O. T. Summerscales, F. G. N. Cloke, P. B. Hitchcock, J. C. Green and N. Hazari, *Science*, 2006, **311**, 829-831.
49. O. T. Summerscales, F. G. N. Cloke, P. B. Hitchcock, J. C. Green and N. Hazari, *J. Am. Chem. Soc.*, 2006, **128**, 9602-9603.
50. P. Roussel, P. B. Hitchcock, N. Tinker and P. Scott, *Chem. Commun.*, 1996, **0**, 2053-2054.
51. D. M. King, F. Tuna, E. J. L. McInnes, J. McMaster, W. Lewis, A. J. Blake and S. T. Liddle, *Science*, 2012, **337**, 717-720.
52. R. G. Ball, F. Edelmann, J. G. Matisons, J. Takats, N. Marques, J. Marcalo, A. Pires De Matos and K. W. Bagnall, *Inorg. Chim. Acta*, 1987, **132**, 137-143.
53. E. M. Matson, J. J. Kiernicki, P. E. Fanwick and S. C. Bart, *Eur. J. Inorg. Chem.*, 2016, **2016**, 2527-2533.
54. P. L. Arnold, N. A. Potter, N. Magnani, C. Apostolidis, J.-C. Griveau, E. Colineau, A. Morgenstern, R. Caciuffo and J. B. Love, *Inorg. Chem.*, 2010, **49**, 5341-5343.
55. P. L. Arnold, A. J. Blake, C. Wilson and J. B. Love, *Inorg. Chem.*, 2004, **43**, 8206-8208.

56. A. M. J. Devoille and J. B. Love, *Dalton Trans.*, 2012, **41**, 65-72.
57. P. L. Arnold, G. M. Jones, S. O. Odoh, G. Schreckenbach, N. Magnani and J. B. Love, *Nat. Chem.*, 2012, **4**, 221-227.
58. R. C. White, PhD Thesis, The University of Edinburgh, 2014.
59. P. L. Arnold, N. A. Potter, C. D. Carmichael, A. M. Z. Slawin, P. Roussel and J. B. Love, *Chem. Commun.*, 2010, **46**, 1833-1835.
60. D. L. Swartz II, L. P. Spencer, B. L. Scott, A. L. Odom and J. M. Boncella, *Dalton Trans.*, 2010, **39**, 6841-6846.
61. J. B. Love, A. J. Blake, C. Wilson, S. D. Reid, A. Novak and P. B. Hitchcock, *Chem. Commun.*, 2003, **0**, 1682-1683.
62. E. Campazzi, E. Solari, R. Scopelliti and C. Floriani, *Inorg. Chem.*, 1999, **38**, 6240-6245.
63. M. Ganesan, C. D. Bérubé, S. Gambarotta and G. P. Yap, *Organometallics*, 2002, **21**, 1707-1713.
64. I. Korobkov, S. Gambarotta and G. P. A. Yap, *Angew. Chem., Int. Ed. Engl.*, 2002, **41**, 3433-3436.
65. T. Dubé, J. Guan, S. Gambarotta and G. Yap, *Chem. Eur. J.*, 2001, **7**, 374-381.
66. C. Liu, S. Zhou, S. Wang, L. Zhang and G. Yang, *Dalton Trans.*, 2010, **39**, 8994-8999.
67. M. Nishiura, T. Mashiko and Z. Hou, *Chem. Commun.*, 2008, 2019-2021.
68. J. M. Tanski and G. Parkin, *Organometallics*, 2002, **21**, 587-589.
69. D. E. Morris, R. E. Da Re, K. C. Jantunen, I. Castro-Rodriguez and J. L. Kiplinger, *Organometallics*, 2004, **23**, 5142-5153.
70. G. Ionova, C. Madic and R. Guillaumont, *Polyhedron*, 1998, **17**, 1991-1995.
71. S. G. Bratsch and J. J. Lagowski, *J. Phys. Chem.*, 1986, **90**, 307-312.
72. L. J. Nugent, R. D. Baybarz, J. L. Burnett and J. L. Ryan, *J. Phys. Chem.*, 1973, **77**, 1528-1539.
73. B. Kanellakopulos, E. Dornberger and F. Baumgaertner, *Inorg. Nucl. Chem. Lett.*, 1974, **10**, 155-160.
74. P. C. Blake, N. M. Edelstein, P. B. Hitchcock, W. K. Kot, M. F. Lappert, G. V. Shalimoff and S. Tian, *J. Organomet. Chem.*, 2001, **636**, 124-129.
75. N. Kaltsoyannis and B. E. Bursten, *J. Organomet. Chem.*, 1997, **528**, 19-33.
76. J. W. Bruno, D. G. Kalina, E. A. Mintz and T. J. Marks, *J. Am. Chem. Soc.*, 1982, **104**, 1860-1869.
77. J. S. Parry, F. G. N. Cloke, S. J. Coles and M. B. Hursthouse, *J. Am. Chem. Soc.*, 1999, **121**, 6867-6871.
78. P. C. Blake, M. F. Lappert, J. L. Atwood and H. Zhang, *J. Chem. Soc., Chem. Commun.*, 1986, **0**, 1148-1149.
79. W. K. Kot, G. V. Shalimoff, N. M. Edelstein, M. A. Edelman and M. F. Lappert, *J. Am. Chem. Soc.*, 1988, **110**, 986-987.
80. F. Ortu, A. Formanuik, J. R. Innes and D. P. Mills, *Dalton Trans.*, 2016, **45**, 7537-7549.
81. A. Arunachalampillai, P. Crewdson, I. Korobkov and S. Gambarotta, *Organometallics*, 2006, **25**, 3856-3866.
82. I. Korobkov, B. Vidjayacoumar, S. I. Gorelsky, P. Billone and S. Gambarotta, *Organometallics*, 2010, **29**, 692-702.
83. M. Amme, T. Wiss, H. Thiele, P. Boulet and H. Lang, *J. Nucl. Mater.*, 2005, **341**, 209-223.
84. F. A. Cotton and G. Wilkinson, *Advanced Inorganic Chemistry, 5th ed.*, Wiley-Interscience, New York, 1988.
85. J.-C. Berthet, M. Nierlich and M. Ephritikhine, *Angew. Chem., Int. Ed. Engl.*, 2003, **42**, 1952-1954.

86. L. Natrajan, F. Burdet, J. Pécaut and M. Mazzanti, *J. Am. Chem. Soc.*, 2006, **128**, 7152-7153.
87. J.-C. Berthet, G. Siffredi, P. Thuéry and M. Ephritikhine, *Eur. J. Inorg. Chem.*, 2007, **2007**, 4017-4020.
88. G. M. Jones, P. L. Arnold and J. B. Love, *Angew. Chem., Int. Ed.*, 2012, **51**, 12584-12587.
89. J. L. Brown, G. Wu and T. W. Hayton, *J. Am. Chem. Soc.*, 2010, **132**, 7248-7249.
90. D. D. Schnaars, G. Wu and T. W. Hayton, *Inorg. Chem.*, 2011, **50**, 4695-4697.
91. E. A. Pedrick, G. Wu and T. W. Hayton, *Inorg. Chem.*, 2014, **53**, 12237-12239.
92. E. A. Pedrick, G. Wu and T. W. Hayton, *Inorg. Chem.*, 2015, **54**, 7038-7044.
93. J. J. Kiernicki, D. P. Cladis, P. E. Fanwick, M. Zeller and S. C. Bart, *J. Am. Chem. Soc.*, 2015, **137**, 11115-11125.
94. P. L. Arnold, A.-F. Pecharman, E. Hollis, A. Yahia, L. Maron, S. Parsons and J. B. Love, *Nat. Chem.*, 2010, **2**, 1056-1061.
95. G. M. Jones, P. L. Arnold and J. B. Love, *Chem. Eur. J.*, 2013, **19**, 10287-10293.
96. P. L. Arnold, A.-F. Pécharman, R. M. Lord, G. M. Jones, E. Hollis, G. S. Nichol, L. Maron, J. Fang, T. Davin and J. B. Love, *Inorg. Chem.*, 2015, **54**, 3702-3710.
97. N. L. Bell, P. L. Arnold and J. B. Love, *Dalton Trans.*, 2016, **45**, 15902-15909.
98. M. Zegke, G. S. Nichol, P. L. Arnold and J. B. Love, *Chem. Commun.*, 2015, **51**, 5876-5879.
99. L. Chatelain, F. Tuna, J. Pecaut and M. Mazzanti, *Dalton Trans.*, 2017, **46**, 5498-5502.
100. P. L. Arnold, E. Hollis, F. J. White, N. Magnani, R. Caciuffo and J. B. Love, *Angew. Chem., Int. Ed. Engl.*, 2011, **50**, 887-890.
101. J. R. Pankhurst, N. L. Bell, M. Zegke, L. N. Platts, C. A. Lamfsus, L. Maron, L. S. Natrajan, S. Sproules, P. L. Arnold and J. B. Love, *Chem. Sci.*, 2017, **8**, 108-116.
102. P. L. Arnold, A. F. Pecharman and J. B. Love, *Angew. Chem., Int. Ed.*, 2011, **50**, 9456-9458.
103. P. L. Arnold, E. Hollis, G. S. Nichol, J. B. Love, J.-C. Griveau, R. Caciuffo, N. Magnani, L. Maron, L. Castro, A. Yahia, S. O. Odoh and G. Schreckenbach, *J. Am. Chem. Soc.*, 2013, **135**, 3841-3854.
104. P. L. Arnold, B. Cowie, M. Suvova, M. Zegke, N. Magnani, E. Colineau, J.-C. Griveau, R. Caciuffo and J. Love, *Angew. Chem., Int. Ed. Engl.*, 2017, **56**, 10775-10779.
105. P. L. Arnold, M. S. Dutkiewicz, M. Zegke, O. Walter, C. Apostolidis, E. Hollis, A.-F. Pécharman, N. Magnani, J.-C. Griveau, E. Colineau, R. Caciuffo, X. Zhang, G. Schreckenbach and J. B. Love, *Angew. Chem., Int. Ed. Engl.*, 2016, **55**, 12797-12801.
106. T. J. Marks and A. M. Seyam, *J. Organomet. Chem.*, 1974, **67**, 61-66.
107. A. M Seyam, *Inorg. Chim. Acta*, 1983, **77**, L123-L125.
108. S. J. Kraft, P. E. Fanwick and S. C. Bart, *J. Am. Chem. Soc.*, 2012, **134**, 6160-6168.
109. G. Yagupsky, W. Mowat, A. Shortland and G. Wilkinson, *J. Chem. Soc. D*, 1970, **0**, 1369-1370.
110. L. A. Seaman, J. R. Walensky, G. Wu and T. W. Hayton, *Inorg. Chem.*, 2013, **52**, 3556-3564.
111. J. W. Bruno, T. J. Marks and L. R. Morss, *J. Am. Chem. Soc.*, 1983, **105**, 6824-6832.
112. T. M. Gilbert, R. R. Ryan and A. P. Sattelberger, *Organometallics*, 1988, **7**, 2514-2518.
113. O. P. Lam and K. Meyer, *Polyhedron*, 2012, **32**, 1-9.
114. P. J. Fagan, J. M. Manriquez, S. H. Vollmer, C. S. Day, V. W. Day and T. J. Marks, *J. Am. Chem. Soc.*, 1981, **103**, 2206-2220.
115. E. M. Matson, P. E. Fanwick and S. C. Bart, *Organometallics*, 2011, **30**, 5753-5762.

116. R. J. Batrice, C. E. Kefalidis, L. Maron and M. S. Eisen, *J. Am. Chem. Soc.*, 2016, **138**, 2114-2117.
117. H. Liu, M. Khononov, N. Fridman, M. Tamm and M. S. Eisen, *Inorg. Chem.*, 2017, **56**, 3153-3157.
118. C. A. P. Goodwin and D. P. Mills, *Organomet. Chem.*, 2017, **41**, 123-156.
119. K. G. Moloy and T. J. Marks, *Inorg. Chim. Acta*, 1985, **110**, 127-131.
120. A. Herve, N. Garin, P. Thuery, M. Ephritikhine and J.-C. Berthet, *Chem. Commun.*, 2013, **49**, 6304-6306.
121. P. J. Fagan, J. M. Manriquez, E. A. Maatta, A. M. Seyam and T. J. Marks, *J. Am. Chem. Soc.*, 1981, **103**, 6650-6667.
122. C. M. Fendrick, L. D. Schertz, V. W. Day and T. J. Marks, *Organometallics*, 1988, **7**, 1828-1838.
123. W. Ren, N. Zhao, L. Chen, H. Song and G. Zi, *Inorg. Chem. Commun.*, 2011, **14**, 1838-1841.
124. R. W. Broach, A. J. Schultz, J. M. Williams, G. M. Brown, J. M. Manriquez, P. J. Fagan and T. J. Marks, *Science*, 1979, **203**, 172-174.
125. A. K. Dash, J. Q. Wang and M. S. Eisen, *Organometallics*, 1999, **18**, 4724-4741.
126. E. Barnea, T. Andrea, M. Kapon, J.-C. Berthet, M. Ephritikhine and M. S. Eisen, *J. Am. Chem. Soc.*, 2004, **126**, 10860-10861.
127. E. Barnea, T. Andrea, J.-C. Berthet, M. Ephritikhine and M. S. Eisen, *Organometallics*, 2008, **27**, 3103-3112.
128. W. J. Evans, K. A. Miller, S. A. Kozimor, J. W. Ziller, A. G. DiPasquale and A. L. Rheingold, *Organometallics*, 2007, **26**, 3568-3576.
129. J. A. Higgins, F. G. N. Cloke and S. M. Roe, *Organometallics*, 2013, **32**, 5244-5252.
130. Z. E. Button, J. A. Higgins, M. Suvova, F. G. N. Cloke and M. Roe, *Dalton Trans.*, 2015, **44**, 2588-2596.
131. K. C. Jantunen, F. Haftbaradaran, M. J. Katz, R. J. Batchelor, G. Schatte and D. B. Leznoff, *Dalton Trans.*, 2005, **0**, 3083-3091.
132. M. R. Duttera, P. J. Fagan, T. J. Marks and V. W. Day, *J. Am. Chem. Soc.*, 1982, **104**, 865-867.
133. M. J. Monreal and P. L. Diaconescu, *Organometallics*, 2008, **27**, 1702-1706.
134. E. Mora, L. Maria, B. Biswas, C. Camp, I. C. Santos, J. Pécaut, A. Cruz, J. M. Carretas, J. Marçalo and M. Mazzanti, *Organometallics*, 2012, **32**, 1409-1422.
135. C. A. Cruz, D. J. H. Emslie, C. M. Robertson, L. E. Harrington, H. A. Jenkins and J. F. Britten, *Organometallics*, 2009, **28**, 1891-1899.
136. N. R. Andreychuk, S. Ilango, B. Vidjayacoumar, D. J. H. Emslie and H. A. Jenkins, *Organometallics*, 2013, **32**, 1466-1474.
137. C. E. Hayes and D. B. Leznoff, *Organometallics*, 2010, **29**, 767-774.
138. B. M. Gardner, P. A. Cleaves, C. E. Kefalidis, J. Fang, L. Maron, W. Lewis, A. J. Blake and S. T. Liddle, *Chem. Sci.*, 2014, **5**, 2489-2497.
139. T. Straub, A. Haskel, T. G. Neyroud, M. Kapon, M. Botoshansky and M. S. Eisen, *Organometallics*, 2001, **20**, 5017-5035.
140. A. Haskel, T. Straub and M. S. Eisen, *Organometallics*, 1996, **15**, 3773-3775.
141. A. Haskel, T. Straub, A. K. Dash and M. S. Eisen, *J. Am. Chem. Soc.*, 1999, **121**, 3014-3024.
142. R. J. Batrice, J. McKinven, P. L. Arnold and M. S. Eisen, *Organometallics*, 2015, **34**, 4039-4050.
143. P. L. Arnold, J. H. Farnaby, R. C. White, N. Kaltsoyannis, M. G. Gardiner and J. B. Love, *Chem. Sci.*, 2014, **5**, 756-765.
144. P. L. Arnold, M. W. McMullon, J. Rieb and F. E. Kühn, *Angew. Chem., Int. Ed. Engl.*, 2015, **54**, 82-100.

145. W. J. Evans, T. M. Champagne and J. W. Ziller, *J. Am. Chem. Soc.*, 2006, **128**, 14270-14271.
146. W. J. Evans, K. A. Miller, A. G. DiPasquale, A. L. Rheingold, T. J. Stewart and R. Bau, *Angew. Chem., Int. Ed. Engl.*, 2008, **47**, 5075-5078.
147. W. J. Evans, B. L. Davis, T. M. Champagne and J. W. Ziller, *Proc. Natl. Acad. Sci.*, 2006, **103**, 12678-12683.
148. J. Scott, F. Basuli, A. R. Fout, J. C. Huffman and D. J. Mindiola, *Angew. Chem., Int. Ed. Engl.*, 2008, **47**, 8502-8505.
149. Z. Jian, W. Rong, Z. Mou, Y. Pan, H. Xie and D. Cui, *Chem. Commun.*, 2012, **48**, 7516-7518.
150. D. M. King, F. Tuna, E. J. L. McInnes, J. McMaster, W. Lewis, A. J. Blake and S. T. Liddle, *Nat. Chem.*, 2013, **5**, 482-488.
151. A. S. Goldman and K. I. Goldberg, in *Activation and Functionalization of C-H Bonds*, American Chemical Society, 2004, vol. 885.
152. P. B. Arockiam, C. Bruneau and P. H. Dixneuf, *Chem. Rev.*, 2012, **112**, 5879-5918.
153. R. K. Thomson, T. Cantat, B. L. Scott, D. E. Morris, E. R. Batista and J. L. Kiplinger, *Nat. Chem.*, 2010, **2**, 723-729.
154. W. J. Evans, N. A. Siladke and J. W. Ziller, *C. R. Chim.*, 2010, **13**, 775-780.
155. L. E. Schock, A. M. Seyam, M. Sabat and T. J. Marks, *Polyhedron*, 1988, **7**, 1517-1529.
156. M. Aresta and A. Dibenedetto, *Dalton Trans.*, 2007, **0**, 2975-2992.
157. D. R. Lide, *Handbook of Chemistry and Physics*, CRC Press, 89th edn., 2008.
158. P. J. Fagan, K. G. Moloy and T. J. Marks, *J. Am. Chem. Soc.*, 1981, **103**, 6959-6962.
159. C. Elschenbroich, *Organometallics*, WILEY-VCH Verlag GmbH & Co. KGaA, Weinheim, 3rd edn., 2006.
160. C. Finn, S. Schnittger, L. J. Yellowlees and J. B. Love, *Chem. Commun.*, 2012, **48**, 1392-1399.
161. W. J. Evans, J. R. Walensky and J. W. Ziller, *Organometallics*, 2010, **29**, 945-950.
162. D. K. Cabbiness and D. W. Margerum, *J. Am. Chem. Soc.*, 1969, **91**, 6540-6541.
163. E. Campazzi, E. Solari, C. Floriani and R. Scopelliti, *Chem. Commun.*, 1998, 2603-2604.
164. M. G. Gardiner and D. N. Stringer, *Materials*, 2010, **3**, 841-862.
165. J. Wang, M. G. Gardiner, B. W. Skelton and A. H. White, *Organometallics*, 2005, **24**, 815-818.
166. N. W. Davies, A. S. Frey, M. G. Gardiner and J. Wang, *Chem. Commun.*, 2006, 4853-4855.
167. J. Jubb and S. Gambarotta, *J. Am. Chem. Soc.*, 1994, **116**, 4477-4478.
168. T. Dubé, S. Gambarotta and G. P. A. Yap, *Angew. Chem., Int. Ed. Engl.*, 1999, **38**, 1432-1435.
169. B. M. Rambo and J. L. Sessler, *Chem. Eur. J.*, 2011, **17**, 4946-4959.
170. I. Korobkov, S. Gambarotta and G. P. A. Yap, *Angew. Chem., Int. Ed. Engl.*, 2003, **42**, 814-818.
171. J. L. Sessler, W.-S. Cho, V. Lynch and V. Kral, *Chem. - Eur. J.*, 2002, **8**, 1134-1143.
172. A. S. P. Frey, PhD Thesis, University of Tasmania, 2009.
173. S. Ilango, B. Vidjayacoumar and S. Gambarotta, *Dalton Trans.*, 2010, **39**, 6853-6857.
174. P. L. Arnold, C. J. Stevens, J. H. Farnaby, M. G. Gardiner, G. S. Nichol and J. B. Love, *J. Am. Chem. Soc.*, 2014, **136**, 10218-10221.
175. M. S. Dutkiewicz, J. H. Farnaby, C. Apostolidis, E. Colineau, O. Walter, N. Magnani, M. G. Gardiner, J. B. Love, N. Kaltsoyannis, R. Caciuffo and P. L. Arnold, *Nat. Chem.*, 2016, **8**, 797-802.

Chapter Two: Actinide Alkyl and Amide Complexes: Synthesis, Characterisation and Reactivity

2.1 Introduction

As discussed in Chapter One, the vast majority of studies of actinide alkyl reactivity have been carried out on complexes supported by the *bis*-Cp* ligand system, with the general formula $[(Cp^*)_2AnR_2]$ (R = hydrocarbyl).[1-13] Our group has recently reported the synthesis of new *trans*-calix[2]benzene[2]pyrrolide, $(L)^{2-}$, complexes of thorium(IV) (**A** in Scheme 2.1), uranium(III) and uranium(IV) (**B** in Scheme 2.1).[14] The bis(pyrrolide)-containing macrocycle, $(L)^{2-}$, binds readily to the An^{IV} (An = actinide) cations through η^5-pyridyl coordination, affording complexes reminiscent of the metallocene dialkyls $[(Cp^*)_2An(R)_2]$. However, as discussed in part in Chapter One, Section 1.6, $(L)^{2-}$ has a greater flexibility and range of binding modes than that available to the $[(Cp^*)_2AnR_2]$ complexes.[15]

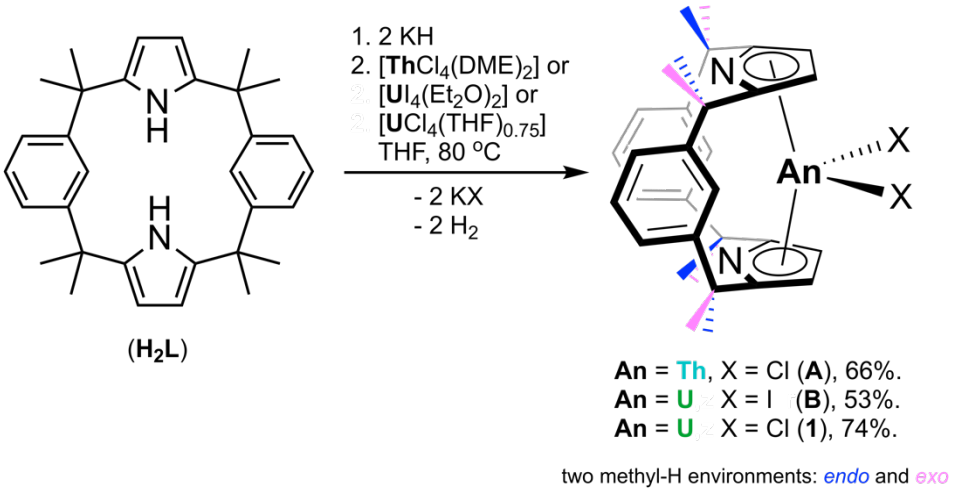

Scheme 2.1 Synthesis of $[(L)ThCl_2]$ (**A**), $[(L)UI_2]$ (**B**) and $[(L)UCl_2]$ (**1**). Symmetrically inequivalent methyl groups are shown in blue and pink.

2.2 Synthesis of Actinide(IV) Halide Complexes

As described in Scheme 2.1, after pro-ligand (H_2L) deprotonation with two equivalents of potassium hydride (KH) to afford K_2L, the actinide(IV) tetrahalides

$[ThCl_4(DME)_2]$ (DME = 1,2-dimethoxyethane), $[UI_4(Et_2O)]$ or $[UCl_4(THF)_{0.75}]$ were added and the reaction mixture was stirred for 18 hours at 80 °C. Following work-up to remove the volatiles and the insoluble KCl or KI by-products, $[(L)ThCl_2]$ (**A**),[14] $[(L)UI_2]$ (**B**)[14] and $[(L)UCl_2]$ (**1**) were obtained in 66, 53 and 74 % yield, respectively. Complexes **A** and **B** were synthesised by past group members.[14] Complex **1** was synthesised as a part of this work, in collaboration with a group member, Dr Joy H. Farnaby. Orange X-ray quality single crystals of **1** were grown by hexane diffusion into a saturated THF solution of **1**; the molecular structure of **1** displays C_{2v} symmetry and is isomorphous with **A** and **B** (Figure 2.1). The ^1H NMR spectroscopic resonances of **1** are paramagnetically shifted and broadened due the U^{IV} f^2 ion, however two resonances for the methyl groups of the macrocycle (*endo* and *exo*: shown in blue and pink in Scheme 2.1), integrating to 12H each, indicate that C_{2v} symmetry is retained in solution.

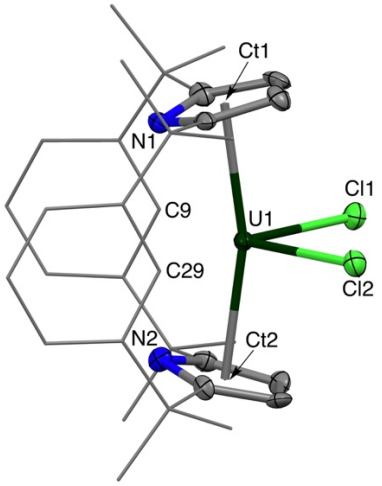

Figure 2.1 Solid-state structure of **1** (thermal ellipsoids set at 50 % probability level). Hydrogen atoms are omitted, with the phenyl rings and alkyl linkers depicted as wire-frame for clarity. Selected bond lengths (Å) and angles (°) for **1**: $[U1–Ct]_{avg}$ 2.498(3), U1–Cl1 2.620(2), U1–Cl2 2.633(2), Ct1–U1–Ct2 164.78, C9–U1–C29 120.88.

2.3 Synthesis of Actinide(IV) Borohydride Complexes

2.3.1 Introduction

Uranium(IV) borohydride complexes were targeted during the Manhattan project alongside their alkyl counterparts,[16] and some An^{IV} borohydride complexes with varying ligand systems have been reported since.[17-22] Examples include Marks' *tris*-Cp complexes $[(Cp)_3An(BH_4)]$ (An = Th (**2.1**), U (**2.2**), Figure 2.2),[17] Parkin's *bis*-permethylindenyl complex $[(Ind^*)_2Th(BH_4)_2]$ (**2.3** in Figure 2.2),[19] and Andersen's silylamide-supported complexes $[(BH_4)An(N(SiMe_3)_2)_3]$ (An = Th (**2.4**), U (**2.5**), Figure 2.2).[18] In some cases, the uranium(IV) borohydride complexes are thermally unstable and therefore only their

thorium(IV) borohydride counterparts are fully characterised. Actinide borohydride complexes can be used in salt metathesis reactions, similarly to halide complexes,[23] as well as potential sources of hydrides.[24]

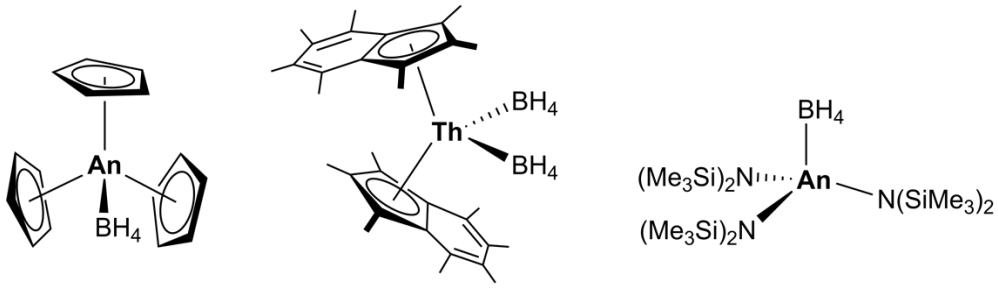

An = Th (**2.1**), U (**2.2**) (**2.3**) An = Th (**2.4**), U (**2.5**)

Figure 2.2 An^{IV} borohydride complexes.[17-19]

The borohydride group can coordinate to a transition metal, lanthanide or actinide centre by two main binding modes: κ^2-coordination through two hydrogen atoms or κ^3-coordination through three hydrogen atoms.[24] In solution at room temperature, these coordination modes tend to be fluxional and therefore NMR spectroscopy will not give a clear indication of the bonding. However, the two different coordination modes display a different range of stretching frequencies in the IR spectrum and the precise bonding can be determined.

2.3.2 Synthesis

Two equivalents of sodium borohydride, $NaBH_4$, were added to either **A** or **1** in THF and heated at 80 °C for 18 hours. Following work-up to remove the volatiles and the insoluble NaCl by-product, $[(L)Th(BH_4)_2]$ (**2**) and $[(L)U(BH_4)_2]$ (**3**) were isolated as yellow and orange solids in 63 and 57 % yield, respectively (Scheme 2.2).

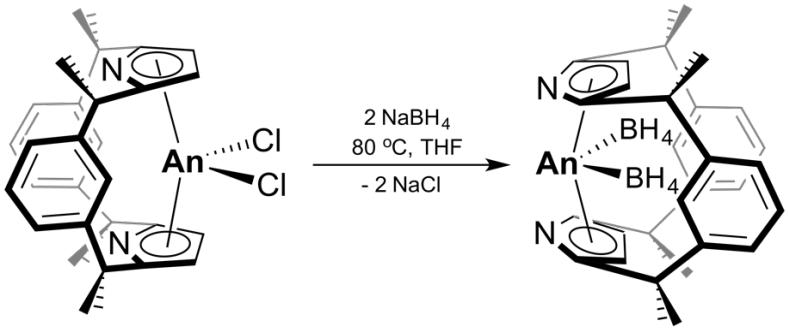

An = Th (**A**), U (**1**) **An** = Th (**2**), 63%, U (**3**), 57%.

Scheme 2.2 Synthesis of $[(L)Th(BH_4)_2]$ (**2**) and $[(L)U(BH_4)_2]$ (**3**). Here, the schematic representation of **2** and **3** is intended to highlight a notable change in ligand arrangement, however the reader is referred to the molecular structure of **2** in Figure 2.3 for an accurate depiction.

A resonance at −11 ppm in the $^{11}B\{^1H\}$ NMR spectrum of **2** is observed, which is within the region reported for thorium(IV) borohydride complexes.[25] The borohydride

resonance in the $^{11}B\{^1H\}$ NMR spectrum of **3** is found out 85.79 ppm, and in the ^1H NMR spectrum of **3** it is represented by two signals at -36.7 ppm (6H) and -57.9 ppm (2H), suggesting a tridentate coordination of the borohydride group. Borohydride ^1H NMR spectroscopic resonances for U^{IV} complexes have been reported at widely ranging chemical shifts due to the paramagnetism of U^{IV}: a direct comparison with chemical shifts for **3** is therefore not informative.[26] A very broad, partially obscured quintet resonance for the borohydride group in **2** is identifiable in the ^1H NMR spectrum, and a singlet at 2.10 ppm is observed in the $^1H\{^{11}B\}$ NMR spectrum, which is comparable to the ^1H chemical shift reported for the borohydride ligands in $[(Ind^*)_2Th(\kappa^3\text{-}H_3BH)_2]$ by Parkin and co-workers (2.84 ppm).[19]

The solid-state FTIR spectrum of complex **2** displays a terminal B−H stretch at 2478 cm^{-1}, bridging B−H stretches at 2230 cm^{-1} and 2145 cm^{-1} and a strong bridge deformation at 1083 cm^{-1}. The FTIR spectrum of complex **3** is comparable to that of **2** and displays a terminal B−H stretch at 2471 cm^{-1}, bridging B−H stretches at 2210 cm^{-1} and 2147 cm^{-1} and a strong bridge deformation at 1077 cm^{-1}. These absorption bands are characteristic of tridentate coordination of the borohydride group and therefore **2** and **3** can be more precisely described as $[(L)An(\kappa^3\text{-}H_3BH)_2]$.[19, 24]

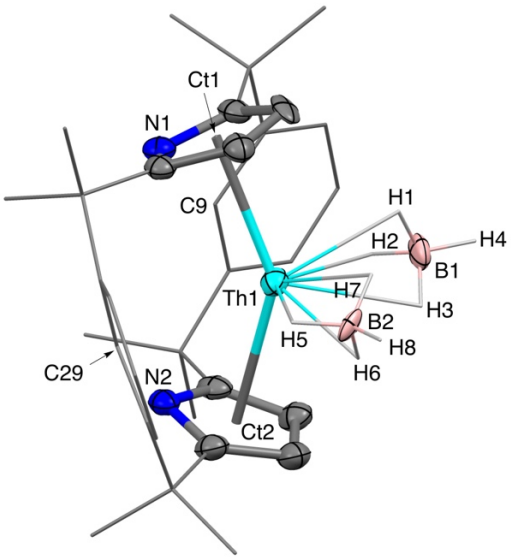

Figure 2.3 Solid state structure of **2** (thermal ellipsoids set at 50 % probability level). Hydrogen atoms are omitted except for BH_4, phenyl rings and alkyl linkers depicted as wire-frame for clarity. Selected bond lengths (Å) and angles (°) for **2** (Ct = centroid, avg = average): $[Th1–Ct]_{avg}$ 2.594(2), $[Th1–B]_{avg}$ 2.612(5), Ct1–Th1–Ct2 143.58, C9–Th1–C29 111.36.

X-ray quality single crystals of **2** were grown by hexane diffusion into a saturated solution of **2** in THF (Figure 2.3); attempts at recrystallizing **3** have not been successful. The solid-state structure of **2** displays the same bis(pyrrolic) η^5:η^5 binding

mode of $(L)^{2-}$ as complexes **A**, **B** and **1**, however the ligand rearranges itself so that the faces of the arene rings of the macrocycle are pointed towards the thorium centre (Figure 2.4). Although the arene planes are facing the borohydride groups, the average B–[aryl]$_{Ct(avg)}$ (Ct = centroid, avg = average) distance is 3.62 Å, indicating that a boron-arene bonding interaction is unlikely.[27] A comparison of **A** and **2** shows that the average Th−Cl distance in **A** is 2.6655(7) Å is longer than the average Th−B distance in **2** (2.612(5) Å). Although the ionic radius of tridentate BH_4^- is smaller than that of Cl^-,[28, 29] the three coordinating hydrides of each $(BH_4)^-$ are likely to occupy a relatively large volume close to the metal centre.[30] This increased steric repulsion close to the metal centre is likely to push the pyrrolic rings from the 163.60° Ct1–Th–Ct2 (Ct = centroid) angle in **A** to the 143.58° Ct1–Th1–Ct2 angle in **2**. The decrease in Ct1–Th–Ct2 angle is the probable cause of the distortion in and twisting of the macrocycle, forcing the arene rings to change conformation. This rearrangement demonstrates the adaptability of the ligand, indicating greater flexibility towards the accommodation of various potential substituents on the metal centre.

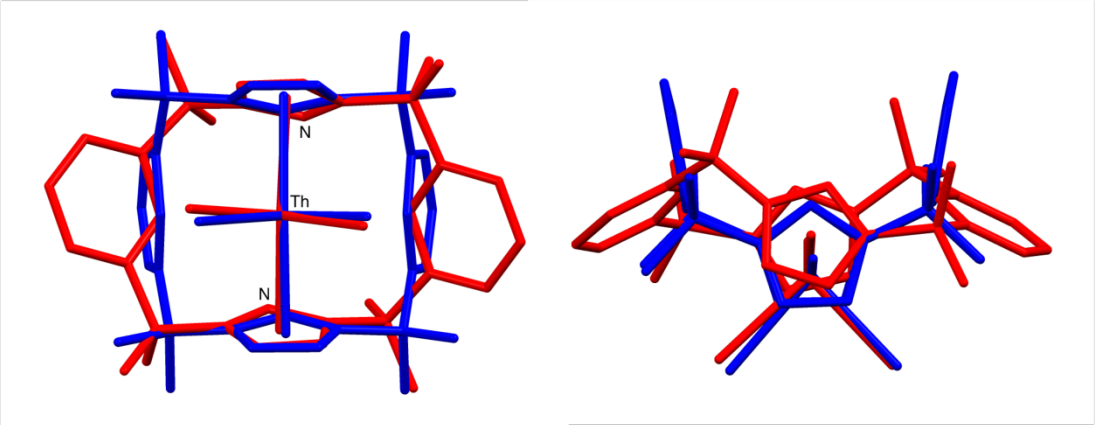

Figure 2.4 Overlaid solid state structures of **2** (red) and **A** (blue), demonstrating the flexibility of the $(L)^{2-}$ ligand.

2.3.3 Reactivity

With the aim of synthesising actinide hydride complexes of the form $[(L)AnH_2]$, BH_3 abstraction was attempted. Abstraction of BH_3 from borohydride ligands using either Lewis bases or thermal abstraction has been successful with a range of transition metal complexes, but it becomes more challenging with lanthanides and actinides. It has been suggested that the bulky ligands that stabilise larger metal centres can impede the process of BH_3 abstraction.[24]

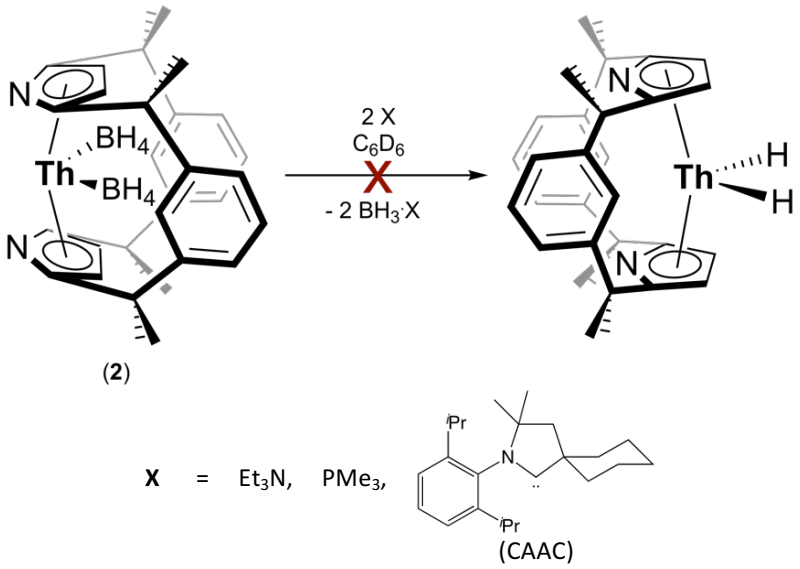

Scheme 2.3 Attempted synthesis of "[(L)AnH$_2$]" by abstraction of BH$_3$ from **2** using a Lewis base (X).

In this work, the Lewis bases Et_3N, PMe_3 or a cyclic alkyl amino carbene (CAAC) (Scheme 2.3) were added to **2** in C_6D_6 in attempts to abstract BH_3. In all cases an indistinguishable mixture of products was obtained. Thermal BH_3 abstraction was also attempted by heating **2** at 200 °C under a dynamic vacuum of 10^{-7} bar for 8 hours. On this occasion, starting material **2** was obtained together with some decomposition to hydrocarbon-insoluble yellow solids. Due to the flexibility of the ligand system, it is unlikely that the ligand environment would be too bulky to enable Lewis base coordination prior to BH_3 abstraction. Therefore, it is possible that although intractable mixtures of products were obtained, BH_3 abstraction did occur, however a lack of steric protection provided by $(L)^{2-}$ to stabilise "[(L)AnH$_2$]" may have resulted in subsequent reactivity (either intra- or inter-molecularly), such as oligomerisation, to achieve steric saturation of the metal centre.

Although the isolation of "[(L)AnH$_2$]" was not successful, it was found that **2** and **3** can be used as precursors for the synthesis of actinide alkyls in an analogous procedure to that described in Section 2.5 with **A** and **1**.

2.4 Synthesis of Actinide(IV) Amide Complexes

2.4.1 Introduction

Actinide amide complexes and their reactivity towards small molecules was discussed in Chapter One, Section 1.5. The main difference in reactivity of actinide alkyl and actinide amide complexes is the increased ionic-character and therefore strength of the An−N bond, resulting in greater stability of actinide amide complexes compared to their alkyl

counterparts.[31] The synthesis of complex C (Scheme 2.4) in poor yield, was previously reported by our group.[14] This reaction features a double deprotonation of the macrocyclic arenes, affording the tetradentate $(L^{-2H})^{4-}$ ligand, as a single $N(SiMe_3)_2$ is added onto the metal centre; potassium incorporation into the bis(arene) back pocket occurs simultaneously.

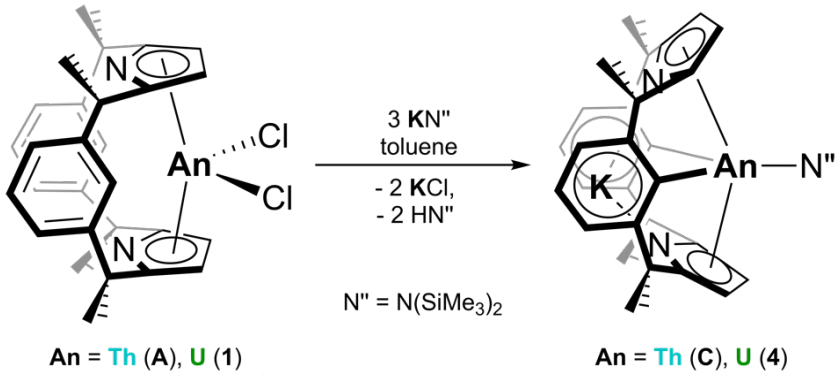

An = Th (**A**), U (**1**) **An** = Th (**C**), U (**4**)

Scheme 2.4 Synthesis of $[K(L^{-2H})Th(N")]$ (**C**) and $[K(L^{-2H})U(N")]$ (**4**) (where N" = $N(SiMe_3)_2$).

Complex **C** was synthesised using a published procedure previously reported by our group,[14] In this work, the reaction was repeated at 80 °C and at room temperature to afford **C** in a 74 % yield in both cases; a 2.5 fold increase on the published procedure.

2.4.2 Synthesis of a Uranium(IV) Amide Complex

With the aim of synthesising a U^{IV} amide analogue of **C**, **1** was treated with three equivalents of $KN(SiMe_3)_2$ in toluene at ambient temperature and stirred for 18 hours (Scheme 2.4). Following work-up to remove KCl and the volatiles, single crystals suitable for X-ray diffraction studies were grown by vapour diffusion of hexane into a saturated THF solution of $[K(L^{-2H})U(N(SiMe_3)_2)]$ (**4**) at ambient temperature; the solid-state structure of **4** is shown in Figure 2.5. The orange product, **4**, was isolated in a 50 % crystalline yield. Possibly due to the notable redox chemistry available to uranium(IV), the reaction did not proceed as cleanly as for the thorium(IV) analogue, resulting in multiple unidentifiable side-products and a comparatively lower yield of **4**.

Once again, this product displays double aryl metallation forming the $(L^{-2H})^{4-}$ ligand with an $\eta^5:\eta^1:\eta^5:\eta^1$ coordination mode. A single amide ligand is bound to the metal centre and a potassium counter-cation is incorporated into the bis(arene) pocket. A comparison of the solid-state structures **C** and **4** indicates that due to the smaller size of the uranium(IV) ion, the metal–ligand bond lengths are shorter in **4** than they are in **C**. In **4**, the C9–U–C29 (120.5(3)°) and Ct1–U–Ct2 (166.24°) angles are similar to **C** (119.58(4)° and 164.39°, respectively).

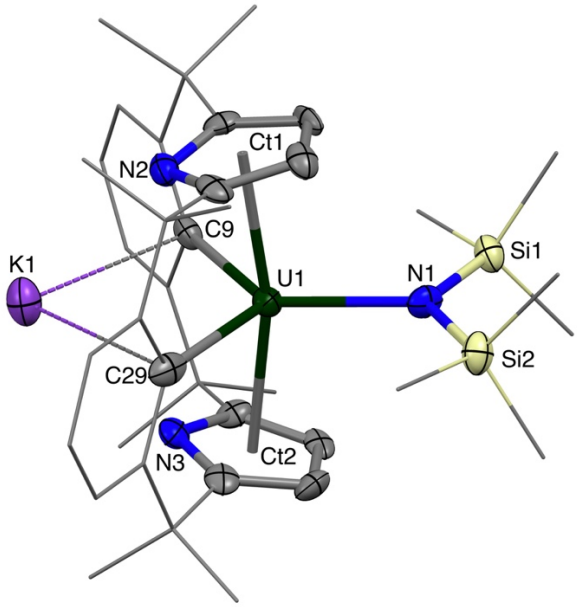

Figure 2.5 Solid-state structure of **4** (thermal ellipsoids set at 50 % probability level). Hydrogen atoms are omitted, with the phenyl rings and alkyl linkers depicted as wire-frame for clarity. Selected bond lengths (Å) and angles (°) for **11**: $[U1–Ct]_{avg}$ 2.484(5), U1–N1 2.336(10), U1–C9 2.679(12), U1–C29 2.680(15), $[Ct1–U1–Ct2]_{avg}$ 166.24, C9–U1–C29 120.5(3).

A survey of structurally comparable complexes of the general form $[(Cp^*)_2U(N\{SiMe_3\}_2)(X)]$ (X = heteroatom) indicates an average U–N bond length of 2.259 Å, which is slightly shorter than the U1–N1 bond length in **4** (2.336(10) Å).[32-34] In complex **4** the tetradentate binding of the macrocycle, with the potassium cation to balance the charge, could result in an increased negative charge on the uranium metal centre, resulting in a larger covalent radius of the uranium, which in turn could result in the slightly longer U1–N1 bond. The U–N average bond distance in complex $[U\{N(SiMe_3)_2\}_4]$ is reported as 2.2972(17) Å,[35] which is similar to the analogous bond distance in **4**; however $[U\{N(SiMe_3)_2\}_4]$ is a sterically strained structure, which is likely to result in elongated bonds in this complex.

In complex **4**, the ^{1}H NMR spectroscopic resonances are affected by the paramagnetism of the U^{IV} f^2 ion with the new resonances for the U–N(Si(C$\underline{H}_3$)$_3$)$_2$ methyl hydrogens represented by a broad singlet at −41.8 ppm in C_6D_6. The $^{29}Si\{^1H\}$ NMR spectrum in C_6D_6 shows a significantly shifted singlet resonance at -131.13 ppm compared to **C** (-10.51 ppm). The $^{29}Si\{^1H\}$ NMR spectroscopic resonances of two U^{IV}–$N(SiMe_3)_2$ containing complexes $[U\{N(SiMe_3)_2\}_4]$ and $[U\{N(SiMe_3)_2\}_2\{\eta^2$-$CH_2SiMe_2NSiMe_3\}]$ show values of -127 and -83 ppm, respectively, indicating **4** is in a similar range albeit not conclusively comparable due to the paramagnetism of the U^{IV} f^2 ion. Further literature analysis indicated that although complexes of the general form

$[(Cp^*)_2U(N\{SiMe_3\}_2)(X)]$ (X = heteroatom) have been isolated, the ^{29}Si NMR spectra of these complexes have not been recorded.[32-34] Complex **4** slowly decomposes in solution over approximately four weeks, therefore $HN(SiMe_3)_2$ ($^{29}Si\{^1H\}$ NMR spectrum: 2.01 ppm) and $KN(SiMe_3)_2$ ($^{29}Si\{^1H\}$ NMR spectrum: -21.78 ppm) are also often observed in the NMR spectra of **4**.

2.5 Synthesis of Actinide(IV) Alkyl Complexes

2.5.1 Introduction

As discussed in Chapter One, actinide alkyl complexes supported by non-carbocyclic[36-41] as well as metallocene-like ligand systems have been reported.[42-45] Particularly, actinide alkyl complexes supported by the *bis*-Cp* ligand system, with the general formula $[(Cp^*)_2AnR_2]$ (R = hydrocarbyl), have been studied in great detail.[1-13] Many of these complexes have shown interesting reactivity with small molecules, such as alkenes, CO, CO_2 or H_2.[46-49]

2.5.2 Synthesis

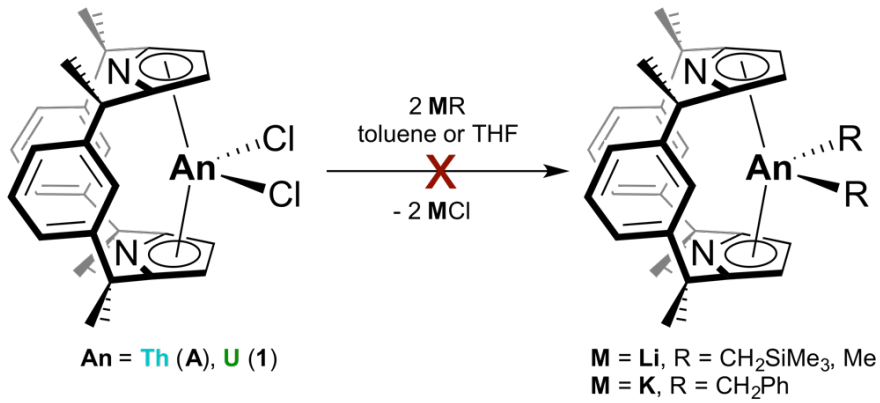

Scheme 2.5 Unsuccessful synthesis of $[(L)An(R)_2]$ (An = U, Th; M = Li, K; R = Me, CH_2SiMe_3, CH_2Ph).

Salt metathesis reactions, similar to those described for the synthesis of **2** and **3** in Section 2.3, were attempted with alkali metal alkyl reagents MR (M = K for R = CH_2Ph; M = Li for R = Me, CH_2SiMe_3) and **A** or **1** to target actinide(IV) dialkyl complexes of the form $[(L)An(R)_2]$ (An = U, Th; R = alkyl) (Scheme 2.5). However, these reactions did not undergo double salt metathesis to yield $[(L)An(R)_2]$. Similarly to the synthesis of **4** and **C**, the addition of two equivalents of MR to either **A** or **1** resulted in double aryl metallation, affording the tetradentate $(L^{-2H})^{4-}$ ligand and the addition of a single R group onto the metal centre; alkali-metal counter-cation incorporation into the bis(arene) back pocket occurred simultaneously. Unreacted

starting material **A** or **1** was also present in the reaction mixture. The yields of **5-10** were improved by treating **A** and **1** with three equivalents of MR (M = K for R = CH_2Ph; M = Li for R = Me, CH_2SiMe_3) in THF or toluene at ambient temperature over 18 hours (Scheme 2.6). The reactions proceeded cleanly and following work-up to remove the MX and HR by-products, the products [M(L^{-2H})An(R)] were isolated.

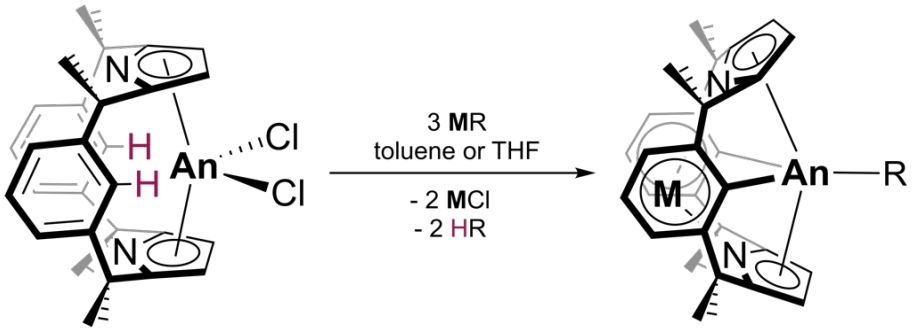

An = **Th** (**A**), **U** (**1**)

An = **Th**, **M** = Li, R = Me (**5**), 93%, CH_2SiMe_3 (**6**), 73%,
M = K, R = CH_2Ph (**7**), 71%.
An = **U**, **M** = Li, R = Me (**8**), 97%, CH_2SiMe_3 (**9**), 65%,
M = K, R = CH_2Ph (**10**), 46%.

Scheme 2.6 Synthesis of [M(L^{-2H})Th(R)] (R = Me (**5**), CH_2SiMe_3 (**6**), CH_2Ph (**7**) and [M(L^{-2H})U(R)] (R = Me (**8**), CH_2SiMe_3 (**9**), CH_2Ph (**10**)).

The new thorium(IV) alkyl complexes, [M(L^{-2H})Th(R)], were isolated as yellow solids in 93 % (R = Me (**5**)), 73 % (R = CH_2SiMe_3 (**6**)) and 71 % (R = CH_2Ph (**7**)) yield, respectively, and the new uranium(IV) complexes, [M(L^{-2H})U(R)], were isolated as dark orange solids in 97 % (R = Me (**8**)), 65 % (R = CH_2SiMe_3 (**9**)) and 46 % (R = Ch_2Ph (**10**)) yield, respectively.

A survey of the available literature indicates that complexes **5-7** are the first examples of mixed aryl/alkyl thorium complexes. Gambarotta reported the first example of a mixed aryl/alkyl complex of uranium(IV), supported by a 1,3-bis(methylaryliminatobenzene) ligand.[50] Gambarotta also reported the synthesis of a calix-pyrrolide-supported thorium butadienyl complex, [{(Et_8-calix-[4]tetrapyrrole)Th}{K(DME)}(η^4-$C_{10}H_8$)][Li(DME)$_3$]:[51] complexes **5-10** are therefore the second examples of pyrrolide-supported actinide alkyl complexes.

2.5.3 Characterisation of Actinide(IV) Methyl Complexes 5 and 8

The ^{1}H NMR spectra of **5** in THF-d_8 (Figure 2.6) and **8** in benzene-d_6 show that the macrocyclic ligand in the new complexes retains the C_{2v} symmetry observed for **A**, **B** and **1**, in which the methyl groups on the *endo* and *exo* faces of the macrocycle are represented by two singlets of equal intensity; the *exo* methyl groups in the thorium

complex are observed at 1.58 ppm and the *endo* methyl groups at 1.41 ppm. Aryl metalation in **5** is characterised by the disappearance of the *ipso*-hydrogen resonance in the ^{1}H NMR spectrum (formerly located at 7.71 ppm in **A**), and a shift in the *ipso*-carbon resonance in the $^{13}C\{^{1}H\}$ NMR spectrum (Figure 2.7) from 121.6 ppm for **A** to 217.6 ppm for **5**.

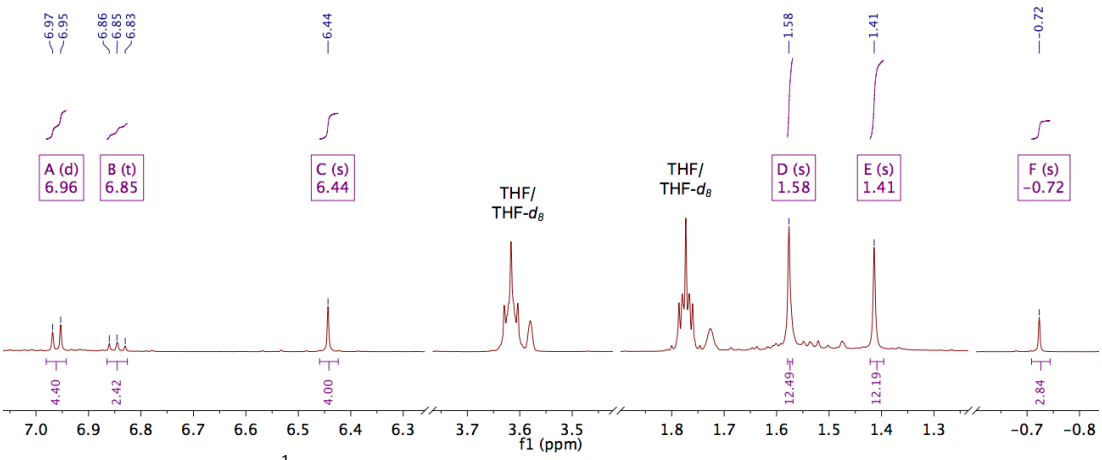

Figure 2.6 ^{1}H NMR spectrum of **5** in THF-d_8 containing trace *protio*-THF.

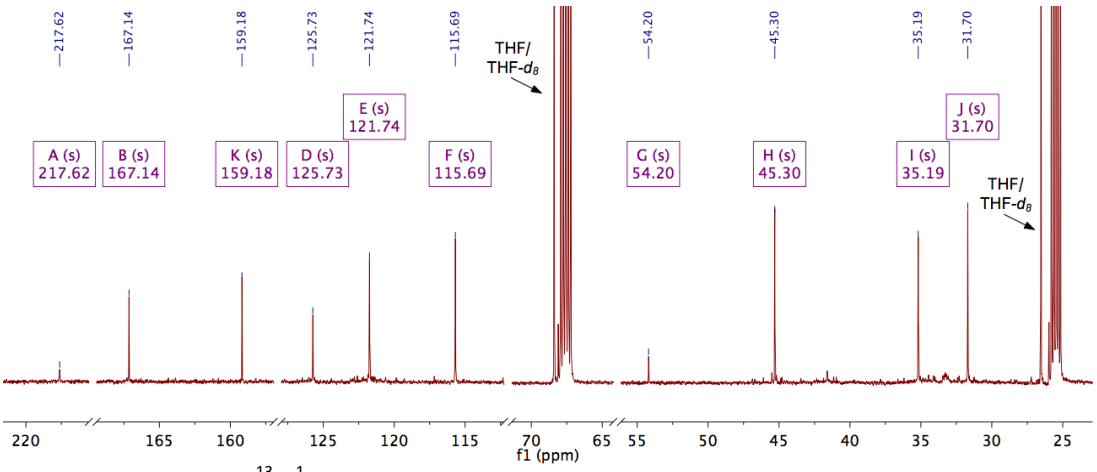

Figure 2.7 $^{13}C\{^{1}H\}$ NMR spectrum of **5** in THF-d_8 containing trace *protio*-THF.

In complex **8**, the ^{1}H NMR spectroscopic resonances are shifted and broadened due to the paramagnetism of the U^{IV} f^2 ion. The resonance for the U–CH_3 group in **8** overlaps with the resonances of the aryl-hydrogens. Unfortunately, the resonance for the *ipso*-carbon of the arene ring in the $^{13}C\{^{1}H\}$ NMR spectrum of **8** could not be definitively assigned due to broadening caused by the paramagnetism of the U^{IV} f^2 ion. The NMR spectra for **8** are therefore less diagnostic than those for **5**. Complex **8** slowly decomposes in solution over three weeks to products such as Li_2L and H_2L, a by-product easily identified by the characteristic ^{1}H NMR spectroscopic resonance of its

symmetrically equivalent methyl groups at 1.42 ppm in THF-d_8. Repeated attempts to crystallise **8** were therefore unsuccessful.

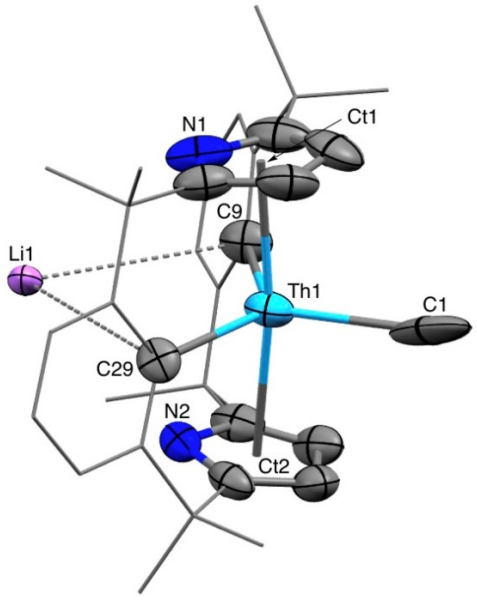

Figure 2.8 Solid state structure of **5** (thermal ellipsoids set at 50% probability level). Hydrogen atoms are omitted, with the phenyl rings and alkyl linkers depicted as wire-frame for clarity. Selected bond lengths (Å) and angles (°) for **5**: $[Th1–Ct]_{avg}$ 2.548(6), Th1–C1 2.65(2), Th1–C9 2.603(13), Th1–C29 2.603(11), Ct1–Th1–Ct2 172.26, C9–Th1–C29 129.9(4).

Single crystals suitable for X-ray diffraction were grown by vapour diffusion of hexane into a saturated THF solution of **5** at ambient temperature. The molecular structure of **5** (Figure 2.8) displays the η^5:η^1:η^5:η^1 $(L^{-2H})^{4-}$ binding mode, in which the pyrrolides are η^5-coordinated and aryls are η^1-coordinated. In **5**, the lithium counter-cation occupies the cavity between the arene rings of the macrocycle. The Ct1–Th–Ct2 angle in the molecular structure of **5** (172.26°) is, larger than that in **A** (163.60°). This increase in Ct1–Th–Ct2 angle is the likely result of aryl metallation as well as the exchange of two large chloride ligands for a small methyl substituent at thorium, prompting a more linear Ct1–Th–Ct2 angle to stabilise the metal centre. The C9–Th–C29 angle is altered from 120.50° in **A** to 129.9(4)° in **5**. Comparison of the C9–Th–C29 angle in **5** (129.9(4)°) with **C** (119.58(4)°) shows a ~10° increase for **5**: the wider angle in **C** can be attributed to the large $N(SiMe_3)_2$ substituent providing steric saturation to the metal centre, unlike the methyl group in **5**. The K–$[aryl]_{Ct(avg)}$ distance in **C** is 3.957 Å, with the orientation of the aryls towards K^+ indicating a notable π-interaction. The Li–$[aryl]_{Ct(avg)}$ distance of 4.292 Å and the orientation of the aryls in **5** indicates a weaker interaction between Li^+ and the aryl π-system than K^+ in **C**. A

Cambridge Structural Database (CSD) survey indicates that the literature average Li–[aryl]$_{Ct(avg)}$ distance is 2.512 Å, approximately 60 % of the distance in **5**.

These metrics demonstrate the ability of the macrocyclic ligand framework to stabilise the complex through subtle geometric adjustments adapting to the substituents on the thorium metal centre. A CSD survey indicates the Th1–C1 bond length in **5** (2.65(2) Å), is longer than the average reported Th^{IV}–Me bond lengths in metallocene-like complexes (2.53 Å).[2, 5, 12, 19, 52-57] Similarly to complex **4**, it could be suggested that due to the tetradentate binding of the macrocycle and presence of the lithium cation to balance the overall charge, the thorium metal centre could have an increased negative charge resulting in a slightly larger covalent radius and therefore longer Th1–C1 bond in **5**. It is also important to note, that the crystal diffraction data obtained for **5** were twinned. Despite twin separation and disorder-modelling (R_1 = 6.14 %, R_{int} = 8.66 %), the thermal ellipsoid of the alkyl ligand is prolate-like and pointed in the direction of the metal centre, which could indicate un-addressed residual electron density affecting the metrics for **5**.

It is interesting to note that **5** is only sparingly soluble in arene solutions, unlike **6**-**10**, which are soluble in arenes, and even sparingly soluble in hexanes. This difference is particularly remarkable when comparing **5** with **8**, where the smaller ionic radius of U^{IV} allows the ligand to encapsulate the metal centre more effectively by adopting a more linear Ct1−An−Ct2 geometry (observed also for **A** *vs* **1** and **6** *vs* **9**) resulting in greater solubility in non-polar solvents. This property of **5** allows for its more effective purification.

2.5.4 Characterisation of Actinide(IV) Neosilyl Complexes 6 and 9

The ^{1}H NMR spectra of **6** and **9** indicate that similarly to **5** and **8**, the macrocyclic ligand retains the C_{2v} symmetry observed for **A** and **B**. The *exo* methyl groups in the thorium complex are observed at 1.61 ppm and the *endo* methyl groups at 1.57 ppm. The aryl metalation in **6** is once again characterised by the disappearance of the *ipso*-hydrogen resonance in the ^{1}H NMR spectrum, and the shift in the *ipso*-carbon resonance in the ^{13}C{^{1}H} NMR spectra from 121.6 for **A** to 213.6 ppm for **6**. As in complex **8**, in complex **9**, the ^{1}H NMR spectroscopic resonances are affected by the paramagnetism of the U^{IV} f^2 ion; however, in this case, the new U–$C\underline{H_2}SiMe_3$ alkyl hydrogens resonate at −12.9 ppm. The ^{13}C{^{1}H} NMR spectroscopic resonance for the *ipso*-carbon of the arene ring in **9** cannot be accurately assigned.

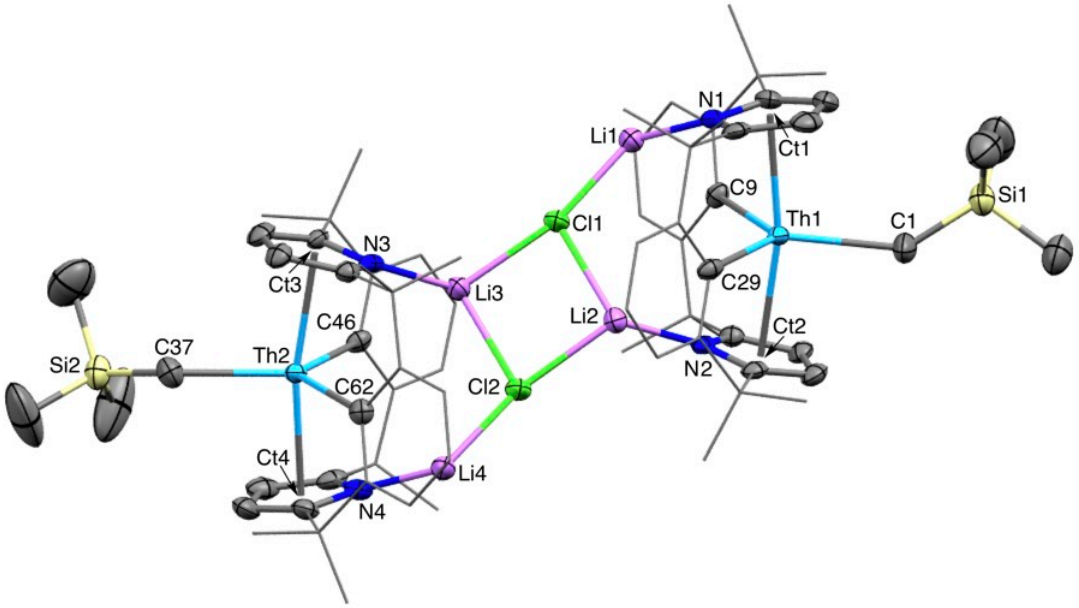

Figure 2.9 Solid-state structure of **6**·LiCl (thermal ellipsoids set at 50 % probability level). Hydrogen atoms are omitted, with the phenyl rings and alkyl linkers depicted as wire-frame for clarity. Selected bond lengths (Å) and angles (°) for **6**·LiCl: $[Th–Ct]_{avg}$ 2.54(2), Th1–C1 2.533(5), Th2–C37 2.530(5), Th1–C9 2.608(4), Th1–C29 2.598(4), Th2–C46 2.614(4), Th2–C62 2.627(4), $[Ct1–Th–Ct2]_{avg}$ 168.48, C9–Th1–C29 120.73(13), C46–Th2–C62 121.17(14).

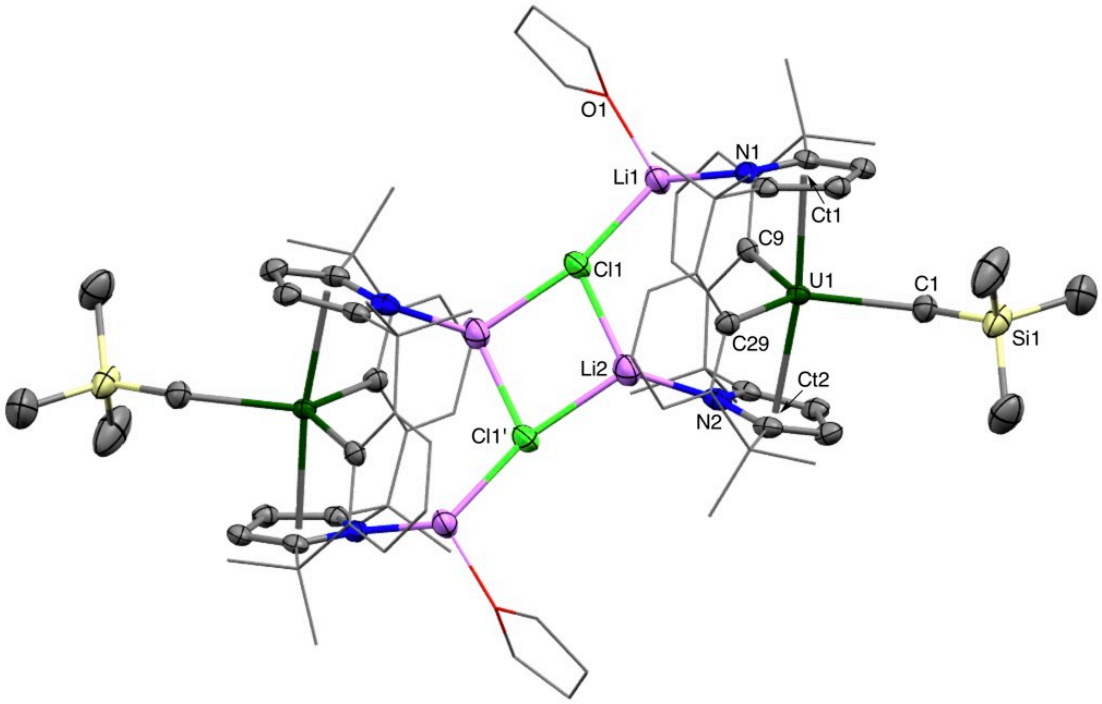

Figure 2.10 Solid-state structure of **9**·LiCl·THF (thermal ellipsoids set at 50 % probability level). Hydrogen atoms are omitted, with the phenyl rings and alkyl linkers depicted as wire-frame for clarity. Selected bond lengths (Å) and angles (°) for **9**·LiCl·THF: $[U1–Ct]_{avg}$ 2.47(2), U1–C1 2.489(4), U1–C9 2.564(4), U1–C29 2.572(4), Ct1–U1–Ct2 172.03, C9–U1–C29 124.33(12).

The crystallisation of **6** and **9** was initially attempted in the absence of LiCl, however it was found that the presence of LiCl facilitated salt-bridged dimerization and

the growth of X-ray quality crystals. Single crystals suitable for X-ray diffraction studies were grown by vapour diffusion of hexanes into saturated THF solutions of **6** and **9** at ambient temperature in the presence of LiCl by-product; the solid-state structures of **6**·LiCl and **9**·LiCl·THF are shown in Figure 2.9 and Figure 2.10, respectively.

The molecular structures of **6**·LiCl and **9**·LiCl·THF also display the η^5:η^1:η^5:η^1 $(L^{-2H})^{4-}$ binding mode seen in **5**. The Ct1−An−Ct2 angles in the molecular structures of **6**·LiCl and **9**·LiCl·THF are 168.48° and 172.03°, respectively, whereas in **A** and **1** this angle is smaller at 163.60° and 164.97°, respectively. The C9−An−C29 angles are altered from 120.50° and 120.88° in **A** and **1** to 120.95(14)° and 124.33(12)° in **6**·LiCl and **9**·LiCl·THF, respectively. Similarly to **4** and **5**, these trends demonstrate the flexibility of the macrocyclic ligand framework. In **6**·LiCl and **9**·LiCl·THF, this flexibility allows for lithium coordination to each of the pyrrolic nitrogen atoms, forming a LiCl bridge between two [Li(L^{-2H})An(CH_2SiMe_3)] units. The average Th1−C1/C37 bond lengths in **6**·LiCl (2.532(5) Å) and the U1–C1 bond length in **9**·LiCl·THF **(**2.489(4) Å), are similar to literature values.[38, 39, 41-43, 58-64] Literature examples include the Th–C average bond length in *ansa*-bridged metallocene complex [(Me_2Si-{Me_4C_5}$_2$)Th(CH_2SiMe_3)$_2$] (2.51(2) Å),[61] and the U–C bond length in the "mixed-sandwich" complex [(Cp*)(COT^{TIPS2})U(CH_2SiMe_3)] (2.464(4) Å).[43]

2.5.5 Characterisation of Actinide(IV) Benzyl Complexes 7 and 10

The ^{1}H NMR spectra of **7** and **10** indicate that similarly to **5**, **6**, **8** and **9**, the macrocyclic ligand retains C_{2v} symmetry. The *exo* methyl groups in the thorium complex are observed at 1.63 ppm and the *endo* methyl groups at 1.49 ppm. The aryl metalation in **7** is also characterised by the disappearance of the *ipso*-hydrogen resonance in the ^{1}H NMR spectrum, and the shift in the *ipso*-carbon resonance in the ^{13}C{^{1}H} NMR spectra from 121.6 for **A** to 215.8 ppm for **7** and 225.8 ppm in **10**. As in complex **8** and **9**, in complex **10**, the ^{1}H NMR spectroscopic resonances are shifted and broadened by the paramagnetism of the U^{IV} f^2 ion with the new resonances for the U–$C\underline{H}_2$Ph alkyl hydrogens represented by a very broad singlet at −57.8 ppm. Complex **10** decomposes slowly in solution over three weeks to products such as K_2L and H_2L, a by-product easily identified by the characteristic ^{1}H NMR spectroscopic resonance of its symmetrically equivalent methyl groups at 1.47 ppm in benzene-d_6. Repeated attempts to crystallise **10** were therefore unsuccessful.

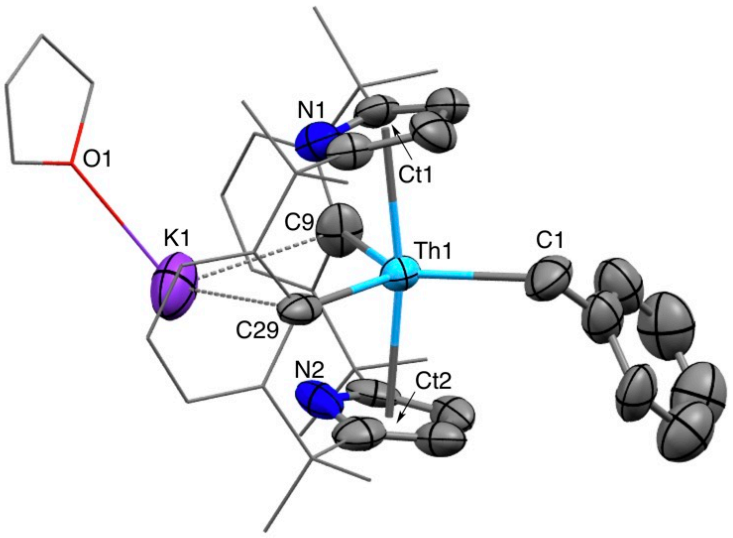

Figure 2.11 Solid-state structure of **7**·THF (thermal ellipsoids set at 50 % probability level). Hydrogen atoms are omitted, with the phenyl rings and alkyl linkers depicted as wire-frame for clarity. Selected bond lengths (Å) and angles (°) for **7**·THF: $[Th1–Ct]_{avg}$ 2.53(1), Th1–C1 2.58(2), Th1–C9 2.55(3), Th1–C29 2.59(2), $[Ct1–Th1–Ct2]_{avg}$ 170.16, C9–Th1–C29 115.4(6).

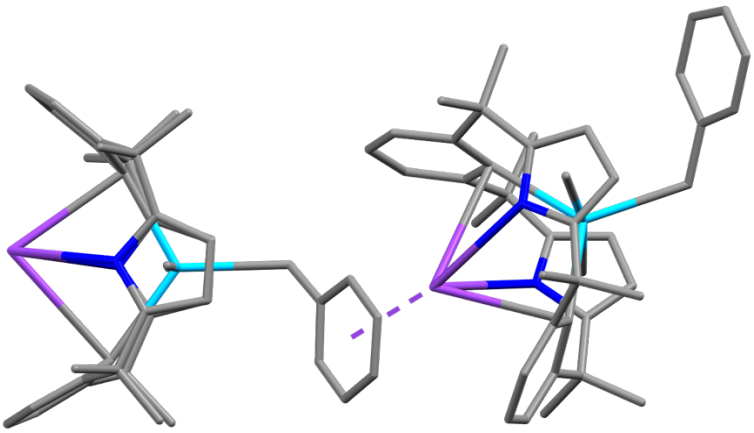

Figure 2.12 Capped-stick representation of the coordination of the potassium counter-ion in **7**·THF to the benzyl group of the adjacent complex resulting in the one-dimensional polymer $[K(L^{-2H})Th(CH_2Ph)]_\infty$. Hydrogen atoms and THF molecules omitted for clarity.

Single crystals suitable for X-ray diffraction studies were grown by vapour diffusion of hexane into a saturated THF solution of **7** at ambient temperature; the solid-state structure of **7**·THF is shown below in Figure 2.11. The molecular structure of **7**·THF once again displays the $\eta^5{:}\eta^1{:}\eta^5{:}\eta^1$ $(L^{-2H})^{4-}$ binding mode seen in **5**, **6**·LiCl and **9**·LiCl·THF. Similarly to the molecular structures of **5** and **C**, the potassium counter-cation in **7**·THF occupies the cavity between the arene rings of the macrocycle. In **7**·THF, the potassium counter-ion is coordinated to a THF molecule in addition to the benzyl group of the adjacent complex (Figure 2.12). Complex **7**·THF is therefore a one-dimensional coordination polymer in the solid state and is best described as $[K(L^{-2H})Th(CH_2Ph)]_\infty$.

The Ct1−An−Ct2 angle in the molecular structure of **7**·THF is 170.16°; larger than in **A** (163.60°). The trend observed for complexes **5**, **6**·LiCl, **7**·THF and **9**·LiCl·THF indicates that the Ct1−An−Ct2 angle becomes larger upon the synthesis of complexes [M(L^{-2H})An(R)] (M = Li for R = Me (**5**, **8**), CH_2SiMe_3 (**6**, **9**); M = K for R = CH_2Ph (**7**, **10**)). The C9−An−C29 angle decreases from 120.50° in **A** to 115.4(6)° in **7**·THF, which is a contrast to the increases in this angle for complexes **5**, **6**·LiCl and **9**·LiCl·THF. This is likely to be the result of a stronger π-interaction between potassium and arene rings in **7**·THF compared to the lithium counter ions in **5**, **6**·LiCl and **9**·LiCl·THF, and is comparable to the angles in **C** (119.59(4)°) and complex [$K(THF)_2$(L^{-2H})Th(μ-Cl)]$_2$ (112.21(3)°; **1DG** in Chapter One), synthesised previously in our group.[14] The crystallographically characterised complexes **5**, **6**·LiCl, **7**·THF and **9**·LiCl·THF demonstrate the ability of the macrocyclic ligand framework to stabilise the complex through subtle geometric adjustments depending on the nature and size of both the counter ion in the cavity between the arene rings and the alkyl co-ligand.

The Th1−C1 average bond length of 2.58(2) Å in **7**·THF is similar to literature values,[38, 39, 41-43, 58-64] such as the Th–C average bond length in the metallocene complex [(η^5-1,2,4-{Me_3C}$_3C_5H_2$)$_2$Th(CH_2Ph)$_2$] (2.524(3) Å) reported by Zi and co-workers.[63]

2.5.6 Grignard Reagents

An alternative synthetic route to actinide dialkyl complexes of the form [(L)]An($R)_2$] (R = alkyl) was explored by using slightly less basic Grignard reagents. Two equivalents of $PhCH_2MgCl$ were added to a solution of **A** in toluene and stirred for 18 hours. Following work-up to remove the volatiles and $MgCl_2$ by-products, ^{1}H and $^{13}C\{^1H\}$ NMR spectroscopy indicated that an analogous reaction to that which makes **7** occurred to yield [MgCl(L^{-2H})Th(CH_2Ph)] (**11**), an analogue of **7**; approximately 30 % of starting material **A** remained unreacted. The procedure was then repeated using three equivalents of $PhCH_2MgCl$ (Scheme 2.7). The reaction of $PhCH_2MgCl$ with **A** is slower than that of KCH_2Ph with **A** and it was found that adding an excess of $PhCH_2MgCl$ promoted the reaction. After work-up to remove the insoluble salts and volatiles, **11** was obtained as an off-white solid in 43 % yield. Although the reactivity of **11** is similar to that of **7**, single crystals suitable for X-ray diffraction studies could not be obtained. As a result, the exact coordination of $[MgCl]^+$ could not be ascertained and **11** in Scheme 2.7 is therefore depicted as a separated ion pair for simplicity.

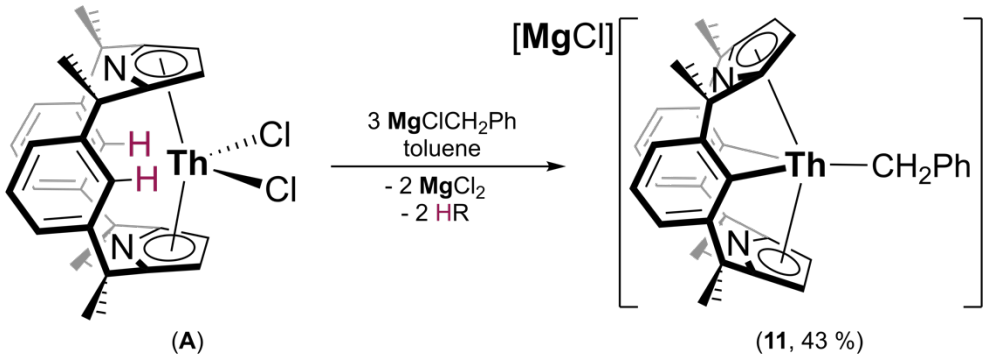

(**A**) (**11**, 43 %)

Scheme 2.7 Synthesis of [MgCl(L^{-2H})Th(CH_2Ph)] (**11**).

With the aim of investigating whether Th^{IV}-allyl complexes could be synthesised using this method, the analogous procedure to the synthesis of **11** was repeated using two, and subsequently three equivalents of 2-methylallylmagnesium chloride, however these reactions afforded inseparable mixtures of products that could not be identified.

2.5.7 Discussion of Ligand Non-Innocence

The deprotonation of the $(L)^{2-}$ ligand to yield $(L^{-2H})^{4-}$ is a process mediated by the actinide metal centre, because the addition of four equivalents of $KN(SiMe_3)_2$ or KH to H_2L yields K_2L but not $K_4(L^{-2H})$. It is likely that the synthesis of tetradentate $(L^{-2H})^{4-}$ is in-part promoted by the stability gained from the macrocyclic effect.[65] Previous work by our group found that addition of DHA (DHA = dihydroanthracene) to the reaction mixture, which affords **C**, also yields anthracene.[66] It was subsequently concluded that the synthesis of **C** proceeds *via* a radical mechanism. Although no intermediates have been isolated to date, two mechanisms for the formation of **C** were proposed by White.[66] One pathway assumed that two $N(SiMe_3)_2$ ligands would initially coordinate to the metal centre to form a "$[(L)Th(N(SiMe_3)_2)_2]$" intermediate and the bulkiness of the silyl groups would cause sterically-induced reduction (SIR), ultimately forming **C**.[66] Although a plausible pathway for large substituents, the SIR route is unlikely for $[M(L^{-2H})Th(R)]$ because when R = Me, the methyl groups are too small to cause SIR. The second suggested pathway proposed a coordinatively unsaturated "$[(L^{-2H})Th]$" intermediate. A number of experiments performed in this work suggest that such an intermediate would be too unstable to drive the reaction forward. As a result, an alternative mechanism is proposed, ensuring the coordinative saturation of the complex at each stage during the formation of **C** and **4**-**11** (Figure 2.13).

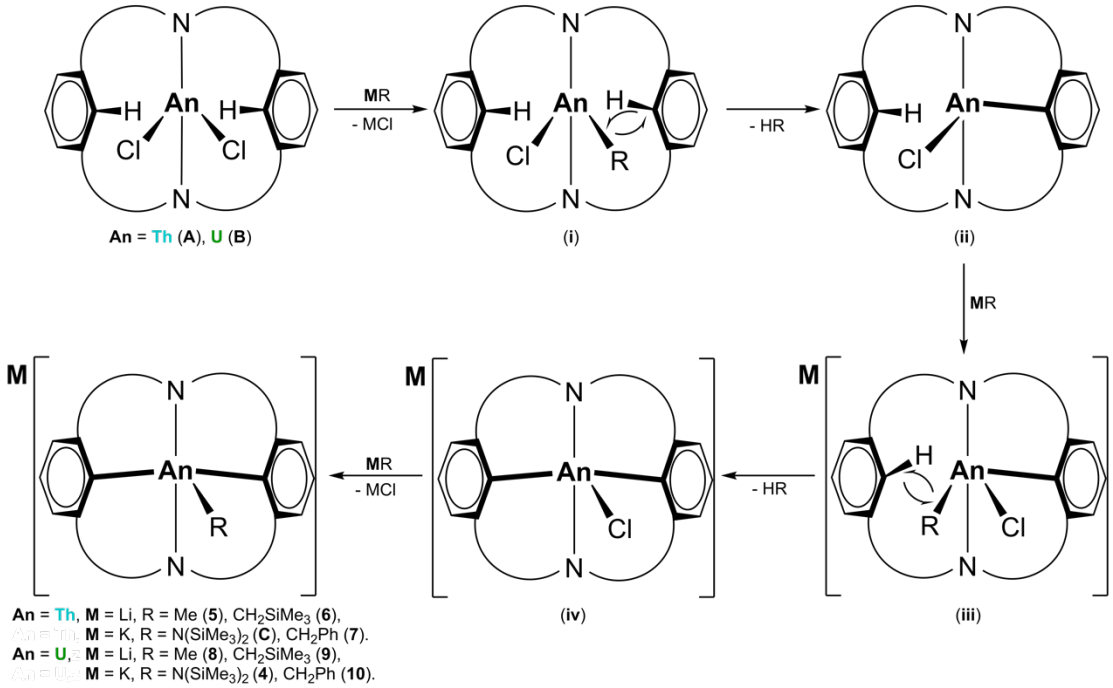

Figure 2.13 Proposed mechanism of formation of **C** and **4**-**11**.

The proposed mechanism in Figure 2.13 begins with a salt metathesis reaction of one equivalent of MR (M = Li, K; R = CH_3, CH_2SiMe_3, CH_2Ph, $N(SiMe_3)_2$) with **A** or **B** to give intermediate **i**, followed by HR elimination to yield a singly-deprotonated intermediate **ii**. A second equivalent of MR then coordinates to the complex to give "ate"-intermediate **iii** followed by the elimination of a second equivalent of HR to give **iv**. White isolated a dimer of intermediate **iv**, $[K(THF)_2(L^{-2H})Th(\mu\text{-}Cl)]_2$, accessed in low yields *via* the addition of two equivalents of potassium naphthalenide in THF to **A**, and subsequently added $KN(SiMe_3)_2$ to ascertain whether **C** could be formed; however, no reaction occurred.[66] White therefore suggested that the last step in the mechanism proposed in Figure 2.13 could not occur. The synthesis of $[K(THF)_2(L^{-2H})Th(\mu\text{-}Cl)]_2$ was repeated in this work according to the reported procedure.[14] It was found that upon isolation, complex of $[K(THF)_2(L^{-2H})Th(\mu\text{-}Cl)]_2$ became entirely insoluble in THF. It is therefore suggested that although the addition of $KN(SiMe_3)_2$ to $[K(THF)_2(L^{-2H})Th(\mu\text{-}Cl)]_2$ did not form **C**, this could be the result of the insolubility of the dimer of **iv**. It is proposed that if **iv** is formed as a transient intermediate *in situ*, the elimination of MCl will drive the synthesis of **C** and **4**-**11**.

2.6 Synthesis of Actinide(IV) Alkynyl Complexes

The advances in C–H bond activation by organometallic *f*-block complexes are discussed in Chapter One, Section 1.5.3. The actinide-aryl bonds to the macrocyclic ligand in the metallated $[M(L^{-2H})An(R)]$ complexes **5**-**10** have been found to provide a

useful route to new hydrocarbon C−H bond reactivity pathways, exemplified by the reaction with terminal alkynes described in Scheme 2.8. An excess of HC≡CR' (R' = $SiMe_3$, Si^iPr_3) was added to a suspension of **5** or **8** in hexanes at room temperature and stirred for 16 hours. Following work-up to remove the volatiles and unusual by-product LiMe, [(L)Th(C≡C$SiMe_3$)$_2$] (**12**) and [(L)Th(C≡CSi^iPr_3)$_2$] (**13**) were isolated as pale yellow solids in 44 and 54 % yield, respectively, and [(L)U(C≡C$SiMe_3$)$_2$] (**14**) and [(L)U(C≡CSi^iPr_3)$_2$] (**15**) were isolated as red solids, each in 50 % yield. The macrocyclic ligand in complexes **12-15** was selectively reprotonated to form bidentate $(L)^{2-}$ from tetradentate $(L^{-2H})^{4-}$ in **5** or **8**. The synthesis of **12** and **13** was also attempted from **6**, however the alkyl lithium by-product, $LiCH_2SiMe_3$, has a similar solubility to the products and subsequently reacts with them in solution, preventing the isolation of pure material.

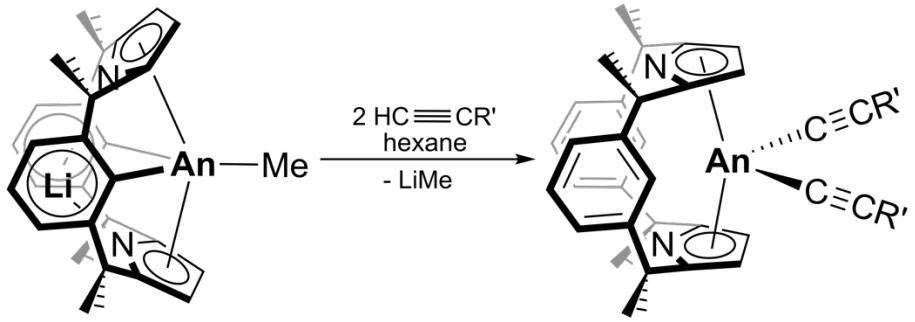

An = **Th** (**5**), **U** (**8**)

An = **Th**, R' = $SiMe_3$ (**12**), 44%, Si^iPr_3 (**13**), 54%.
An = **U**, R' = $SiMe_3$ (**14**), 50%, Si^iPr_3 (**15**), 50%.

Scheme 2.8 Synthesis of [(L)Th(C≡C$SiMe_3$)$_2$] (**12**), [(L)Th(C≡CSi^iPr_3)$_2$] (**13**), [(L)U(C≡C$SiMe_3$)$_2$] (**14**) and [(L)U(C≡CSi^iPr_3)$_2$] (**15**).

2.6.1 Characterisation

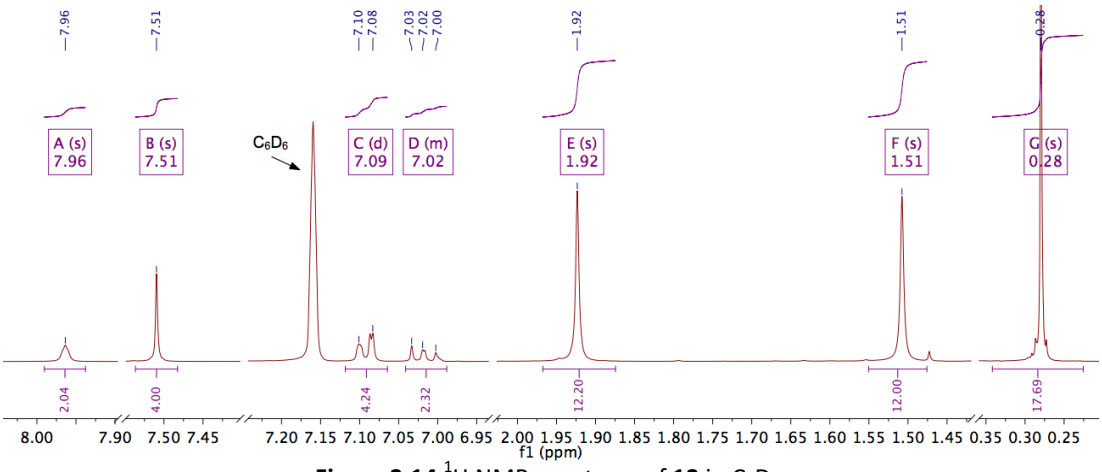

Figure 2.14 ^{1}H NMR spectrum of **12** in C_6D_6.

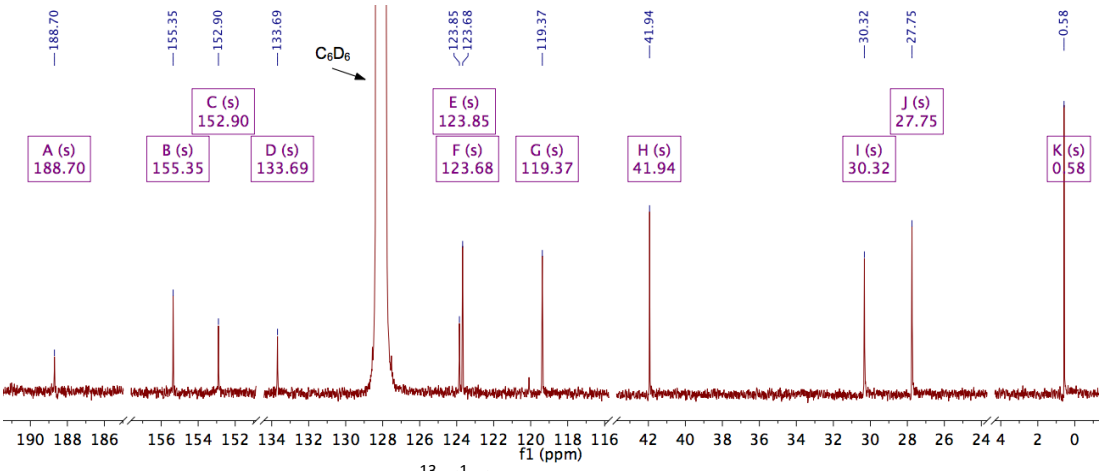

Figure 2.15 $^{13}C\{^{1}H\}$ NMR spectrum of **12** in C_6D_6.

^{1}H and $^{13}C\{^{1}H\}$ NMR spectra in C_6D_6 (Figure 2.14 and Figure 2.15, respectively for **12**) were used to determine that complexes **12** and **13** had retained C_{2v} symmetry in solution. The *ipso*-hydrogen resonances in the ^{1}H NMR spectra were once again assigned at 7.96 and 7.90 ppm in **12** and **13**. In the $^{13}C\{^{1}H\}$ NMR spectra the *ipso*-carbon resonances shifted from 217.6 ppm in **5** to 123.9 and 123.7 ppm in **12** and **13**, respectively. Once again, the ^{1}H NMR spectroscopic resonances of **14** and **15** were shifted and broadened and many of the $^{13}C\{^{1}H\}$ NMR spectroscopic resonances could not be definitively assigned due to the paramagnetism of the U^{IV} f^2 ion.

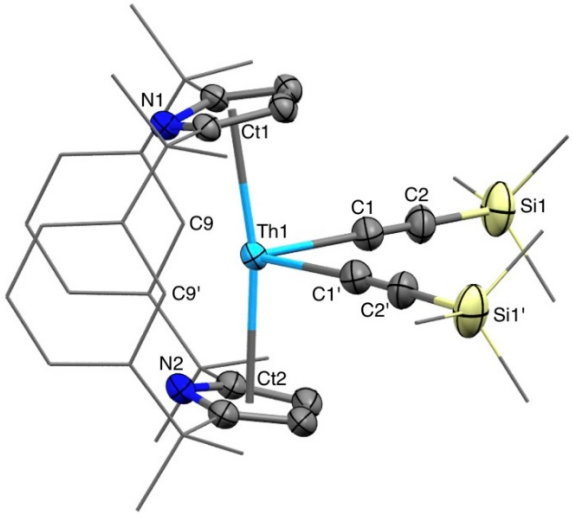

Figure 2.16 Solid state structure of **12** (thermal ellipsoids set at 50 % probability level). Hydrogen atoms are omitted, with the phenyl rings and alkyl linkers depicted as wire-frame for clarity. Selected bond lengths (Å) and angles (°) for **12**: $[Th1–Ct]_{avg}$ 2.525(2), Th1–C1 2.479(4), C1–C2 1.220(5), Ct1–Th1–Ct2 169.49, C9–Th1–C9' 128. 10.

Pale yellow single X-ray quality crystals of **12** and **13** and dark orange X-ray quality crystals of **15** were isolated from the slow evaporation of benzene from saturated solutions of **12**, **13** and **15** at room temperature. Similarly to complexes **4-10**, it was observed that uranium

analogues displayed a darker colour to their nearly-colourless thorium counterparts. This darker colour can be attributed to $f \rightarrow f$ electron transitions in U^{IV} complexes (Th^{IV} has no valence *f*-electrons).[67] The molecular structures of **12**, **13** and **15** (Figure 2.16 - Figure 2.18) exhibit bidentate η^5:η^5 binding, analogous to that of **A**. The Ct1–An–Ct2 angles in **12**, **13** and **15** are 169.49, 169.43 and 170.44°, respectively, and are larger than in **A** (163.60°), **B** (163.26°) and **1** (164.78°). This subtle increase in Ct1–An–Ct2 angle is likely the result of the smaller covalent radius of carbon compared to that of chlorine,[68] sterically allowing the macrocyclic ligand to adopt a more linear Ct1–An–Ct2 in **12**, **13** and **15**.

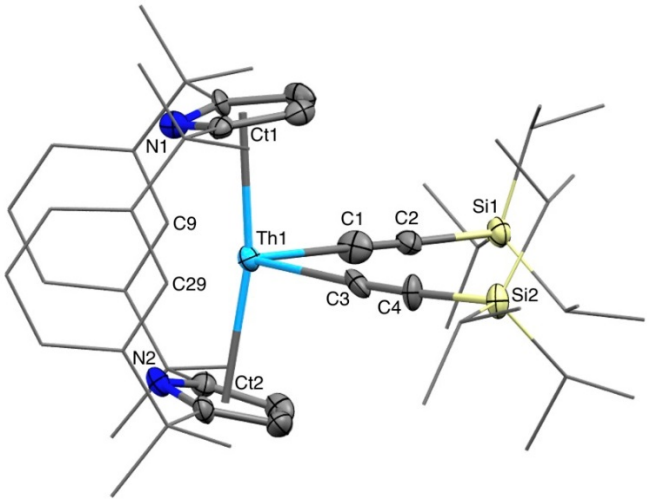

Figure 2.17 Solid state structure of **13** (thermal ellipsoids set at 50 % probability level). Hydrogen atoms are omitted, with the phenyl rings and alkyl linkers depicted as wire-frame for clarity. Selected bond lengths (Å) and angles (°) for **13**: $[Th1–Ct]_{avg}$ 2.54(1), Th1–C1 2.482(3), Th1–C3 2.471(3), C1–C2 1.219(4), C3–C4 1.207(4), Ct1–Th1–Ct2 168.36, C9–Th1–C29 124.15.

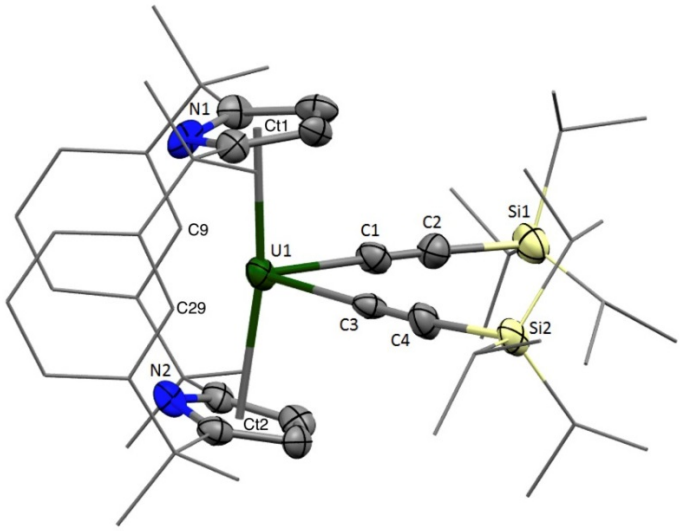

Figure 2.18 Solid state structure of **15** (thermal ellipsoids set at 50 % probability level). Hydrogen atoms are omitted, with the phenyl rings and alkyl linkers depicted as wire-frame for clarity. Selected bond lengths (Å) and angles (°) for **15**: $[U1–Ct]_{avg}$ 2.479(4), U1–C1 2.378(9), U1–C3 2.437(8), C1–C2 1.236(11), C3–C4 1.205(11), Ct1–U1–Ct2 170.44, C9–U1–C29 124.91.

Although reactivity involving Th^{IV} alkynyl complexes has been invoked,[46, 69, 70] **12** and **13** are the first crystallographically characterised thorium alkynyl complexes. A small number of fully characterised U^{IV} alkynyl complexes have been reported to date,[2, 71-76] such as the $[(Cp^*)_2U(NPh_2)(C{\equiv}C\text{-}p\text{Tol})]$ (*p*Tol = *para*-tolyl) complex (U–C bond length: 2.418(5) Å).[71] A CSD survey indicates that the average U–C bond length in U^{IV} alkynyl complexes is 2.423 Å: similar to the $[U1{-}C1/C3]_{avg}$ bond distance in **15** (2.408(9) Å). The $[Th1{-}C1/C3]_{avg}$ distances in **12** (2.479(4) Å) and **13** (2.477(9) Å) are equivalent, and longer than the $[U1{-}C1/C3]_{avg}$ bond length in **15** (2.408(9) Å), which is likely the result of the larger covalent radius of Th^{IV} when compared to U^{IV}.[68]

A comparison with the C≡C bond length of free $HC{\equiv}CSiMe_3$ (1.194(8) Å)[77] shows that the C1≡C2 bond lengths in complexes **12** (1.220(5) Å), **13** ($[C1/C3{\equiv}C2/C4]_{avg}$: 1.213(4) Å) and **15** ($[C1/C3{\equiv}C2/C4]_{avg}$: 1.221(11) Å) are unaffected by complexation, within ESD. This is further supported by solid-state FTIR spectroscopy where C≡C stretching frequencies were recorded at 2140 cm^{-1}, 2032 cm^{-1} and 2032 cm^{-1} for **12**, **13** and **15**, respectively, all of which are in the region of C≡C triple bond stretching frequencies and are comparable to the stretching frequency of free $HC{\equiv}CSiMe_3$ (2037 cm^{-1}).[78]

2.6.2 Discussion of Reversible Aryl Deprotonation

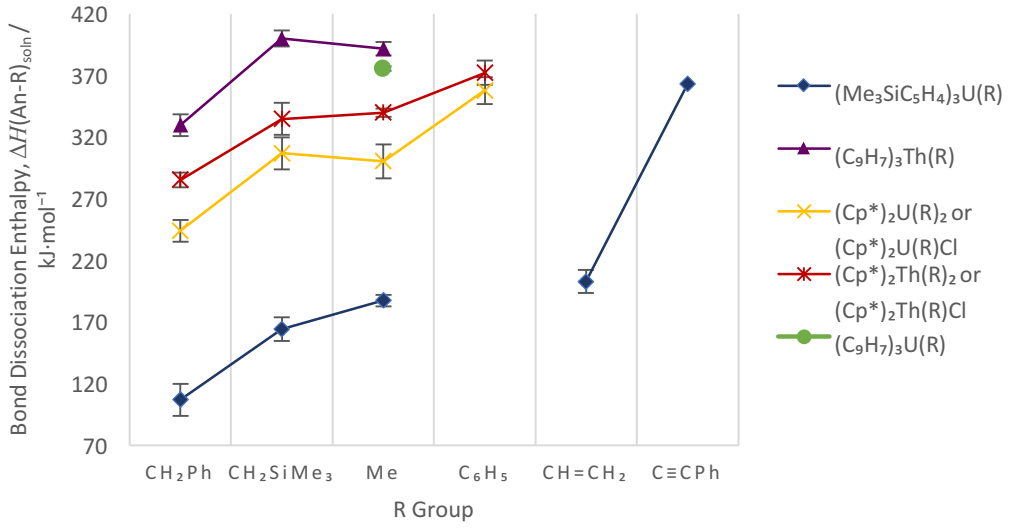

Figure 2.19 Summary of the bond dissociation enthalpies of $(C_9H_7)_3Th(R)$ (purple), $(C_9H_7)_3U(R)$ (green), $(Cp^*)_2Th(R)_2$ or $(Cp^*)_2Th(R)Cl$ (red), $(Cp^*)_2U(R)_2$ or $(Cp^*)_2U(R)Cl$ (yellow) and $(Me_3SiC_5H_4)_3U(R)$ (dark blue), where R = CH_2Ph, CH_2SiMe_3, Me, $CH{=}CH_2$ or C≡CPh.[10, 79-81]

A literature survey of bond dissociation energies of An–alkyl bonds in metallocene-like Th^{IV} and U^{IV} complexes is summarised in Figure 2.19.[10, 79-81] It is important to note that

although all bond dissociation enthalpies shown in Figure 2.19 were obtained via oxygen-free titration calorimetry, the bond dissociation enthalpies of the [$(Me_3SiC_5H_4)_3U(R)$] series (dark blue) were recorded using an improved method, which resulted in large energy differences when compared with the other data sets. As such, Figure 2.19 is presented herein to demonstrate trends, rather than for the comparison of exact numerical values.

Figure 2.19 shows that the bond dissociation energies of An–alkyl bonds are generally lower than those of An–aryl bonds.[10, 79-81] Interestingly, Marks showed that the U–alkynyl bond dissociation enthalpy in complex [$Cp''_3U(C{\equiv}CPh)$] ($Cp'' = \eta^5$-$C_5H_4SiMe_3$) is nearly twice that of U–Me in the analogous methyl complex [$Cp''_3U(Me)$], however Marks did not make a direct comparison with U–aryl bond enthalpies.[81] Evans showed that the addition of two equivalents of HC≡CPh to the complex [$(Cp^*)_2U(Me)_2$] resulted in the synthesis of [$(Cp^*)_2U(C{\equiv}CPh)_2$] and methane elimination.[72] In this work, An–arene bonds in complexes **5** or **8** have been reprotonated to give $(L)^{2-}$ by the alkynes HC≡CR′ (R′ = $SiMe_3$, Si^iPr_3) (pKa of acetylenes in DMSO: ~28)[82]. These findings, together with the elimination of the unusual by-product LiMe, suggest that the synthesis of **12-15** is not only driven by the acidity of the acetylenes, but also by the strength of the An–alkynyl bond.

2.7 Attempted Syntheses of Thorium(IV) Imido Complexes

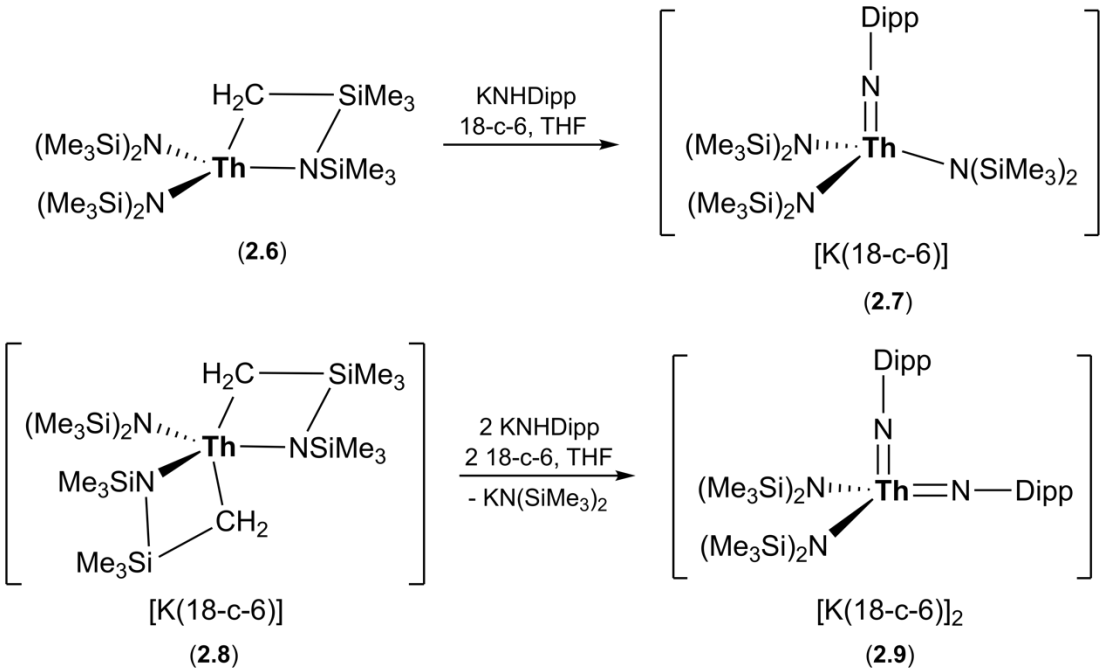

(**2.6**) (**2.7**) (**2.8**) (**2.9**)

Scheme 2.9 Synthesis of Th^{IV} mono(imido) (**2.7**) and bis(imido) (**2.9**) complexes from thorium metallacycles **2.6** and **2.8** (Dipp = 2,6-$^iPr_2C_6H_3$).[83]

Recent work in our group has shown that Th^{IV} mono(imido) (**2.7** in Scheme 2.9) and bis(imido) (**2.9** in Scheme 2.9) complexes can be accessed by the addition of KNHDipp (Dipp = 2,6-$^{i}Pr_2C_6H_3$) to Th^{IV} metallacycle [(N{$SiMe_3$}$_2$)$_2$Th(N{$SiMe_3$}{$SiMe_2$}CH_2)] (**2.6** in Scheme 2.9) or bis(metallacycle) [(N{$SiMe_3$}$_2$)Th(N{$SiMe_3$}{$SiMe_2$}CH_2)$_2$] (**2.8** in Scheme 2.9).[83] During these reactions, the reprotonation of the cyclometallated carbon occurs as the KNHDipp N–H bond undergoes σ-bond metathesis with the Th–CH_2 bond.

Following the successful syntheses of complexes **12-15** *via* the reprotonation of $(L^{-2H})^{4-}$ to $(L)^{2-}$ and elimination of LiMe, it was postulated that the addition of one equivalent of secondary amine NH_2Ph or NH_2Dipp to [Li(L^{-2H})Th(Me)] (**5**) may reprotonate the macrocycle and eliminate LiMe to yield a Th^{IV} mono(imido) complex "[(L)Th=NR]" (R = Ph, Dipp) (Scheme 2.10). In both cases mixtures of products were immediately obtained, however ^{1}H and $^{13}C\{^{1}H\}$ NMR spectroscopy indicated that the *ipso*-carbons of the macrocycle had been reprotonated. The reaction mixtures were allowed to stand at room temperature for 24 hours after which time the products had decomposed to H_2L. Addition of an excess of NH_2Ph or NH_2Dipp to **5** resulted in the complete protonation of the ancillary ligand to yield H_2L. Na_2L was isolated from the addition of $NaNH_2$ to **5**. It has been established that electrophilic nitrogen donor atoms readily form bonds with actinides,[84] it is therefore likely that the decomplexation occurring in reactions described herein was driven by the formation of multiple Th–N bonds. These reactions were attempted in a THF, toluene and hexane, however changing the solvent did not have an impact on reaction outcomes. No immediate reaction occurred upon the addition of NH_2Dipp, KNHDipp or KNHPh to the Th^{IV} amide [K(L^{-2H})Th(N($SiMe_3$)$_2$)] (**C**), however over two weeks, in C_6D_6 solutions, **C** slowly decomposed to H_2L and other decomposition products.

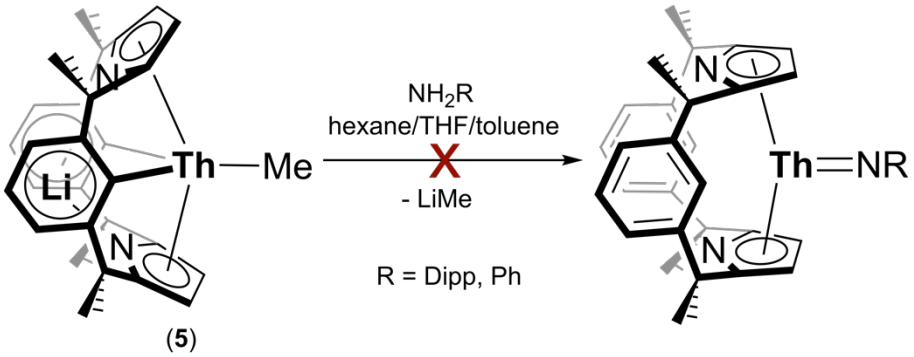

(**5**)

Scheme 2.10 Attempted synthesis of a Th^{IV} mono(imido) complex "[(L)Th=NR]" (R = Dipp, Ph).

2.8 Reactivity of Actinide(IV) Alkyl and Alkynyl Complexes

The reactivity of complexes **5-10** was explored, using **5** as a representative example for the series, due to its ease of purification (see above), which resulted in increased control over reaction progress and increased ease of reaction mixture separation. The reactivity of complexes **12-15** was also explored, using **12** as a representative example.

2.8.1 Reactivity with Alkenes

2.8.1.1 Attempted 1,2-insertion into An–C Bonds of Complexes 5-10

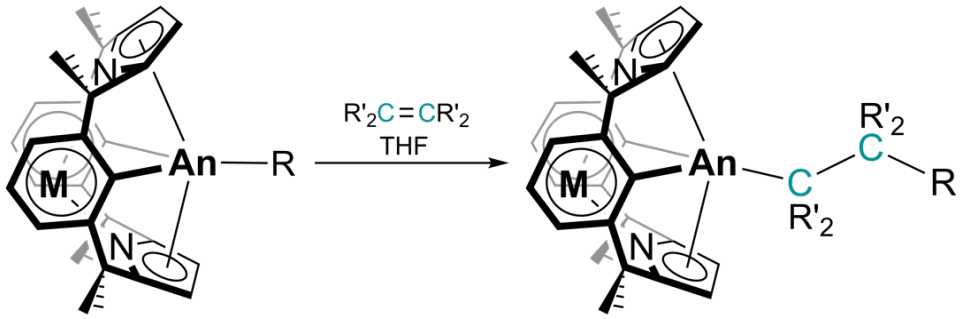

(**5** - **10**) R' = hydrocarbyl

Scheme 2.11 Proposed 1,2-insertion of alkenes into An–C bonds of complexes **5-10** (R' = hydrocarbyl).

Complexes **5-10** contain three An−C σ-bonds, two of which are to the arene rings of the macrocyclic ligand. It was postulated that alkenes may undergo 1,2-insertion into all three bonds, although it was anticipated that the macrocyclic effect and the accessibility of the alkyl ligand may promote 1,2-insertion into the An−R bond (Scheme 2.11). Initial attempts were made by adding an excess of 1,1-diphenyl ethylene to **5** in THF whilst heating at 80 °C. After 48 hours, no reaction had occurred. The reactivity of less bulky alkenes (styrene, 1-hexene, cyclohexene and 1-methyl-1-cyclohexene) with **5** was tested in an analogous procedure. No reactivity with styrene and 1-hexene was observed. It was found that cyclohexene and 1-methyl-1-cyclohexene displayed some reactivity after 48 hours at 80 °C. The products formed from these reactions could not be conclusively assigned as single insertion products into the Th−Me bond of **5**, multiple insertion products into all three Th−C bonds of **5** or a mixture thereof. This difficulty was also caused by the partial decomposition of **5** to Li_2L, H_2L and other decomposition products, which had occurred upon prolonged heating. These decomposition products could have also potentially reacted with cyclohexene or 1-methyl-1-cyclohexene. Thus, the isolation and characterisation of clean material from a mixture containing starting material and a range of decomposition products was not possible.

2.8.1.2 Attempted [2+2+2] Cycloaddition Reactions with Complex 12

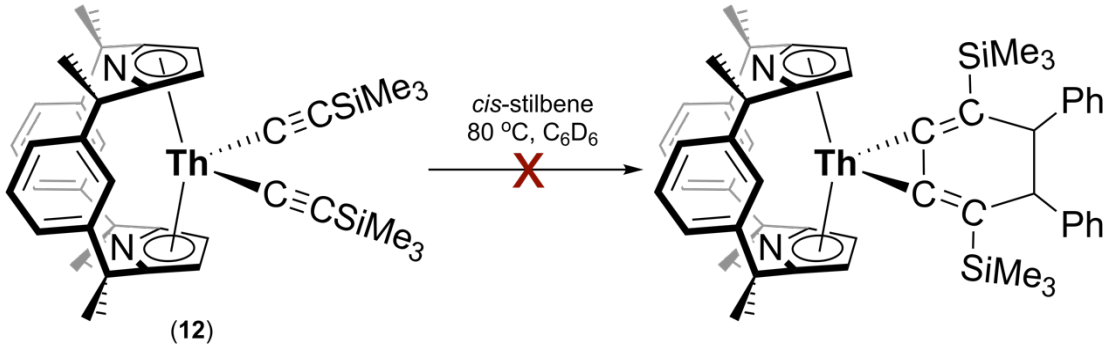

Scheme 2.12 Attempted [2+2+2] cycloaddition of **12** and *cis*-stilbene.

[2+2+2] cycloaddition reactions are well established and can be catalysed by a range of transition metals, including Ni, Pd, Rh, Ru, Ir, Fe, Co and Zr.[85] In an attempt to induce a [2+2+2] cycloaddition, *cis*-stilbene was added to **12** in benzene-d_6 and the reaction heated to 80 °C for 16 hours (Scheme 2.12); no reaction occurred during this time. The [2+2+2] cycloaddition reaction could potentially result in the formation of a thorium metallocyclopropane, which could be too strained. However, Zi and co-workers recently reported syntheses of a stable Th^{IV} and U^{IV} metallocyclopropene complexes [(η^5-1,2,4-{Me_3C}$_3C_5H_2$)$_2$Th(η^2-C_2Ph_2)] and [$Cp^*_2U(\eta^2$-$C_2(SiMe_3)_2)$].[86, 87] It is possible that the phenyl groups on the *cis*-stilbene may have been too bulky, preventing reactivity. Future investigations using ethene may be of interest.

2.8.2 Reactivity with Silanes

It has been established that silanes can act as sources of hydrides and have been used for this purpose in actinide hydride-mediated hydrosilylation catalysis, where actinide hydrides were synthesised from both actinide methyl complexes [$(Cp^*)_2An(Me)_2$] and alkynyl complexes [$(Cp^*)_2An(C{\equiv}C^iPr)_2$] (An = Th, U).[88] Attempts to synthesise actinide hydride analogues of complexes **5**-**7** *via* σ-bond metathesis were made using $PhSiH_3$ and Et_3SiH (Scheme 2.13). These silanes were chosen based on their hydride-donor abilities: both silanes are less reducing than H_2, with $PhSiH_3$ more reducing than Et_3SiH.[89] One equivalent of Et_3SiH or $PhSiH_3$ was added to a solution of **5** in THF, however mixtures of products were obtained, with H_2L also observed in the ^{1}H NMR spectra. Th^{IV} hydride ^{1}H NMR spectral resonances have most commonly been reported at chemical shifts above 9 ppm,[42] however no resonances were observed in this region, suggesting that none of the many products formed were Th^{IV} hydrides. ^{29}Si{^{1}H} NMR spectroscopic resonances also suggested a mixture of several products.

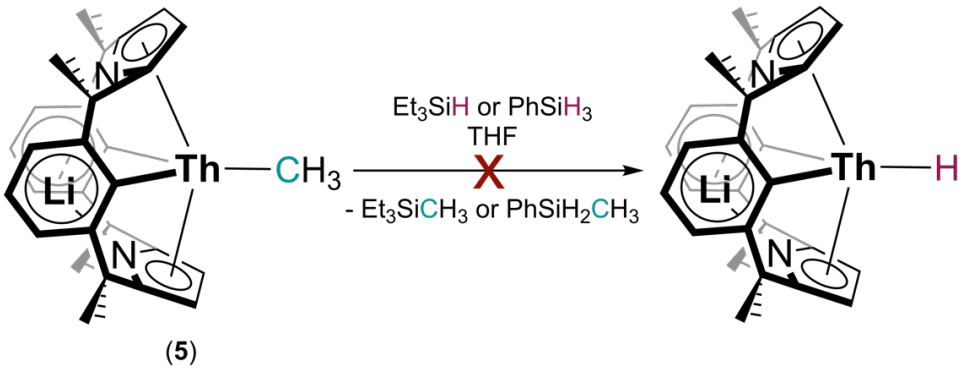

Scheme 2.13 Attempted σ-bond metathesis of Th–CH_3 bond in complex **5** with silanes.

This procedure was repeated with complex **12** in attempts to synthesise actinide dihydride analogues of **12**-**15**. One equivalent of Et_3SiH or $PhSiH_3$ was added to **12** in C_6D_6. After stirring at ambient conditions for 16 hours, it was found that no reaction had occurred. The solutions were subsequently heated at 80 °C for two hours, after which ^{1}H NMR spectroscopic analysis showed that mixtures of products had formed. Some ancillary ligand reprotonation to H_2L was also observed in the ^{1}H NMR spectra of the products. No resonances were observed above a chemical shift of 9 ppm in the ^{1}H NMR spectra of the mixtures of products suggesting that Th^{IV} hydrides had not been synthesised. ^{29}Si{^{1}H} NMR spectroscopic analysis suggested mixtures of at least five products.

2.8.3 Reactivity with a Tin Hydride

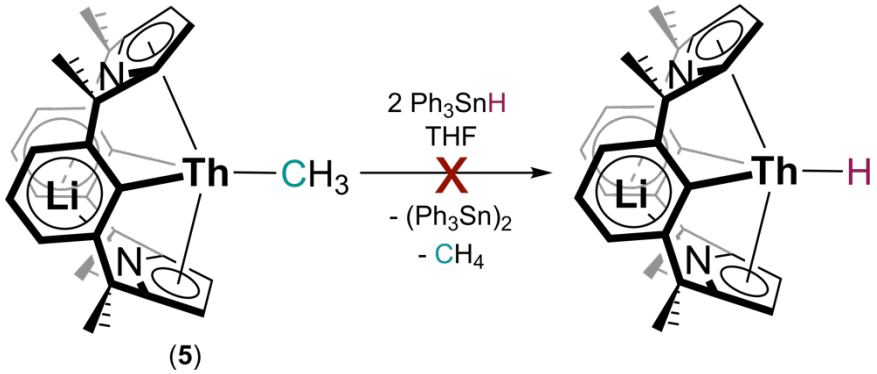

Scheme 2.14 Attempted reaction of Th–CH_3 bond in complex **5** with Ph_3SnH *via* a radical mechanism.

Tin hydrides are commonly used as mild hydride sources in catalytic organic transformations, such as the reduction of ketones to alcohols.[90] Tin hydrides undergo radical reactions and are better described as sources of H• rather than H^-, and were examined as alternatives to silanes in attempts to synthesise actinide hydride analogues of complexes **5**-**7** (Scheme 2.14). Two equivalents of Ph_3SnH were added to **5** at −20 °C and the reaction stirred for 20 minutes while gas, found to be methane, evolved. ^{1}H, ^{7}Li and ^{119}Sn{^{1}H} NMR spectroscopy indicated that a mixture of at least three products was obtained. No resonance

was observed above 9 ppm in the ^{1}H NMR spectrum, where Th^{IV} hydride signals are commonly reported, suggesting that none of the products contained a Th^{IV} hydride.[42] No ^{119}Sn satellites could be discerned in the regions attributed to ancillary ligand resonances in the ^{1}H NMR spectrum of the products: this suggested that no new Sn–ancillary ligand bonds had formed. To determine the identity of the obtained products, fractional crystallisation was attempted, however crystals of $(Ph_3Sn)_2$ were instead repeatedly isolated from the reaction mixture. The formation of $(Ph_3Sn)_2$ and methane suggests that here, as well as in Section 2.8.2, a transient Th^{IV} hydride may have formed but was unstable and decomposed prior to detection. Mixtures of products may have been obtained due to the presence of three An−C bonds, two of which are bonds to the arene rings of the macrocyclic ligand, which are also susceptible to nucleophilic attack and may have reacted with Ph_3SnH.

2.8.4 Reactivity of 8 with Silicone Grease

As mentioned in Section 2.5.3, complex **8** decomposes slowly in solution over three weeks. It was found however that in the presence of an excess of silicone grease in THF, activation of silicone grease by **8** occurred over a period of two weeks to afford $[(L^{-2H})U(\eta^2\text{-}O_2SiMe_2)(Li\{THF\})_2]$ (**16**) (Scheme 2.15). Orange single crystals suitable for X-ray diffraction studies were obtained in 13 % yield from a saturated solution of **16** in THF (Figure 2.20). Decomposition products such as H_2L, Li_2L and Li_4L were also present in the mother-liquor.

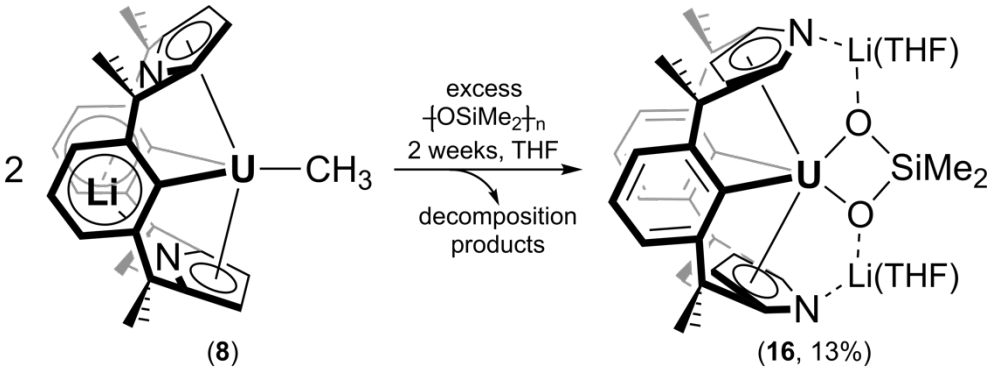

Scheme 2.15 Silicone grease activation by **8** to afford $[(L^{-2H})U(\eta^2\text{-}O_2SiMe_2)(Li\{THF\})_2]$ (**16**).

Complex **16** is overall charge-neutral with two lithium counterions rendering the uranium centre in a formally +4 oxidation state. It is postulated that the second equivalent of Li^+ is obtained from a second molecule of **8**, which then either triggers its decomposition, or is obtained from a molecule of **8** that may already be in the process of decomposing. Silicone grease activation by inorganic substrates and organometallic complexes has been previously reported.[91] An example of silicone grease activation by an actinide complex was reported by

Gambarotta and showed that the addition of potassium naphthalenide in DME to a U^{III} calix-pyrrole-supported "ate"-complex [K(DME)(Et_8-calix-[4]tetrapyrrole)U(DME)], in the presence of silicone grease, resulted in a μ-O_2SiMe_2 bridged U^{III} complex [K(DME)(Et_8-calix-[4]tetrapyrrole)U(μ-O_2SiMe_2)(μ-K)(DME)][K(DME)$_4$].[92] In the synthesis of **16**, a reducing agent was not added, which suggests that complex **8** is highly reactive.

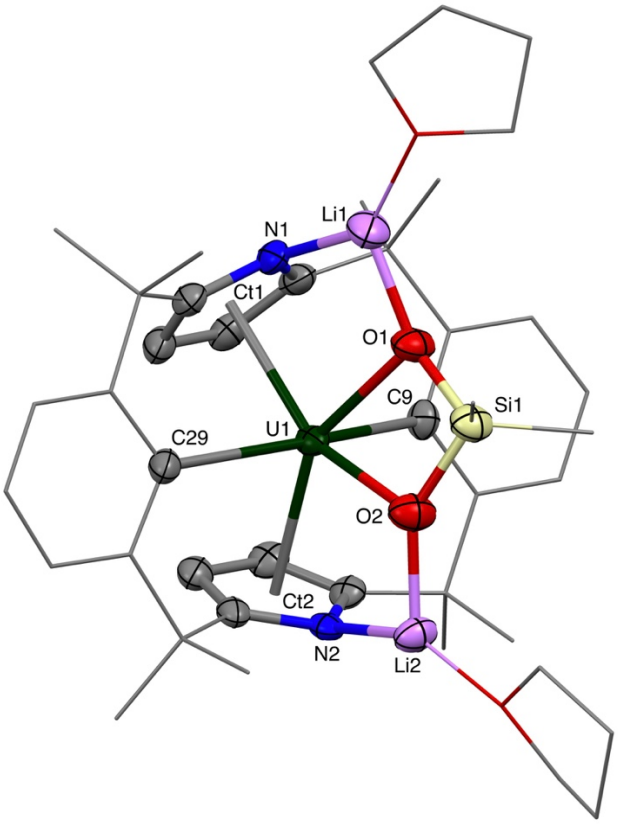

Figure 2.20 Solid-state structure of **16** (thermal ellipsoids set at 50 % probability level). Hydrogen atoms are omitted, with the phenyl rings and alkyl linkers depicted as wire-frame for clarity. Selected bond lengths (Å) and angles (°) for **16**: $[U1–Ct]_{avg}$ 2.509(2), U1–O1 2.364(3), U1–O2 2.362(3), U1–C9 2.505(4), U1–C29 2.607(4), Ct1–U1–Ct2 117.60, C9–U1–C29 164.22(13).

The solid-state structure of **16** is interesting because similarly to **2**, the pyrrolic-nitrogens are facing the η^2-O_2SiMe_2 substituent, rather than pointing away, as seen in complexes **5-7**, **9**, **12**, **13** and **15**. In structure **16**, this is likely the consequence of the lithium bridges between the oxygens and pyrrolic-nitrogens. The Ct1–U1–Ct2 angle in **16** (117.60°) is the smallest seen in complexes of this macrocycle, smaller than the Ct1–Th1–Ct2 angle in **2** (143.58°). The C9–U1–C29 angle in **16** is 164.22(13)° and is the most linear C9–An–C29 angle seen in complexes of this macrocycle.[14, 93] The need to accommodate η^2-O_2SiMe_2 and two bridging lithium counterions is likely to cause a decrease in Ct1–U1–Ct2 angle, which in turn is likely to push the arene rings into nearly one plane causing the large C9–U1–C29 angle. Unlike **2**, where the arene rings arrange to envelope the borohydride ligands, the actinide metal

centre in **16** is bound to C9 and C29, which significantly restricts the movement of the arene rings.

In complex **16**, the ^{1}H NMR spectroscopic resonances are broadened by the paramagnetism of the U^{IV} f^2 ion. The new resonances for the U–O_2SiMe_2 methyl hydrogens are assigned at 30.3 ppm in THF-d_8. A $^{13}C\{^{1}H\}$ NMR spectrum obtained from a four hour-long measurement cannot be definitely assigned, with the four quaternary carbon resonance signals of the macrocycle too weak to observe. No signals were observed in the $^{29}Si\{^{1}H\}$ and $^{7}Li\{^{1}H\}$ NMR spectra of **16** in THF-d_8, which is also likely to be a consequence of broadening caused by the paramagnetism of U^{IV}.

2.8.5 Reactivity of Alkyl Complexes with Small Molecules

2.8.5.1 Attempted Small Molecule Activation by Complexes 5-10

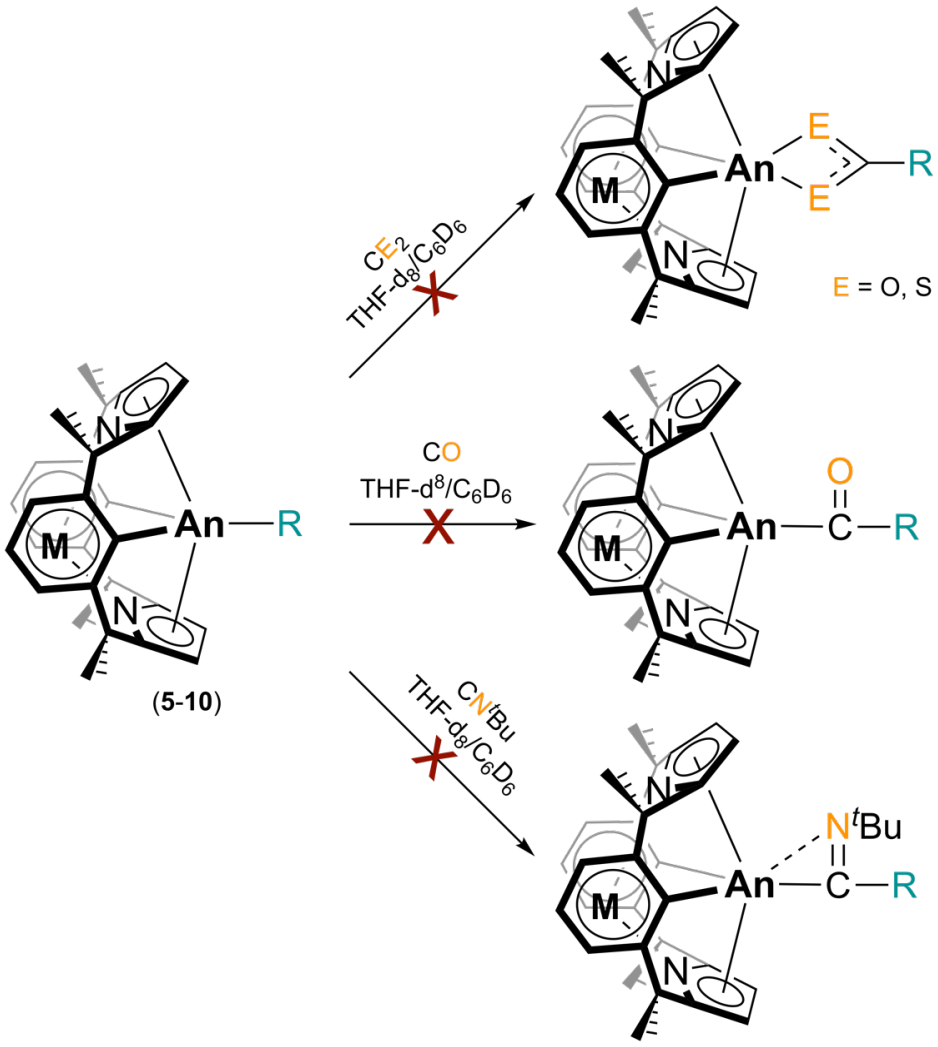

Scheme 2.16 Attempted CO, CO_2, CS_2 and CN^tBu insertion reactions into An–R bonds of complexes **5-10**.

The importance of and recent advances in the activation of small molecules such as CO, CO_2, CS_2, isonitriles or H_2 was discussed in detail in Chapter One. Complexes **5-10**, present three reactions to target as they contain three An−C bonds, two of which are bonds to the arene rings of the macrocyclic ligand. Small molecule insertion reactions into the An−C bonds of complexes **5-10** were attempted to determine whether the alkyl substituents would influence the reactivity of the complexes. Complexes **5-10** in benzene-d_6 or THF-d_8 were reacted with an excess or 1, 2 or 3 equivalents of CO, CO_2, CS_2 or ^{t}BuNC (Scheme 2.16). In all cases, inseparable mixtures of products were obtained immediately.

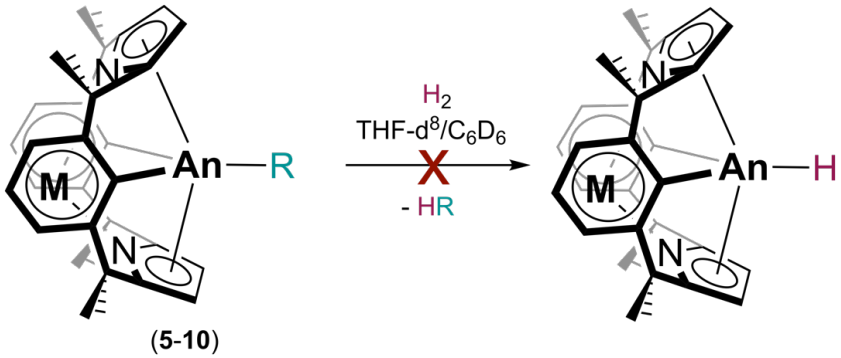

Scheme 2.17 Attempted σ-bond metathesis of An–R bonds in complexes **5-10** and H_2.

The potential for the An−C bonds of complexes **5-10** to undergo σ-bond metathesis with H_2 was also investigated (Scheme 2.17). Once again, an excess or 1, 2 or 3 equivalents of H_2 were added to **5-10**. All of the reactions occurred instantly and resulted in inseparable mixtures of products. These results are likely to stem from a lack of small molecule selectivity for reaction with any of the An−C bonds and/or a lack of stability of the resulting products. This observation is further supported by the presence of large amounts of H_2L, Li_2L or K_2L in all product mixtures; these reaction by-products were identified by their characteristic methyl ^{1}H NMR spectroscopic resonances at 1.47, 1.73 and 1.65 ppm in C_6D_6, respectively.

2.8.5.2 Reactivity of Complexes 12-15 with CO, CO_2 and H_2

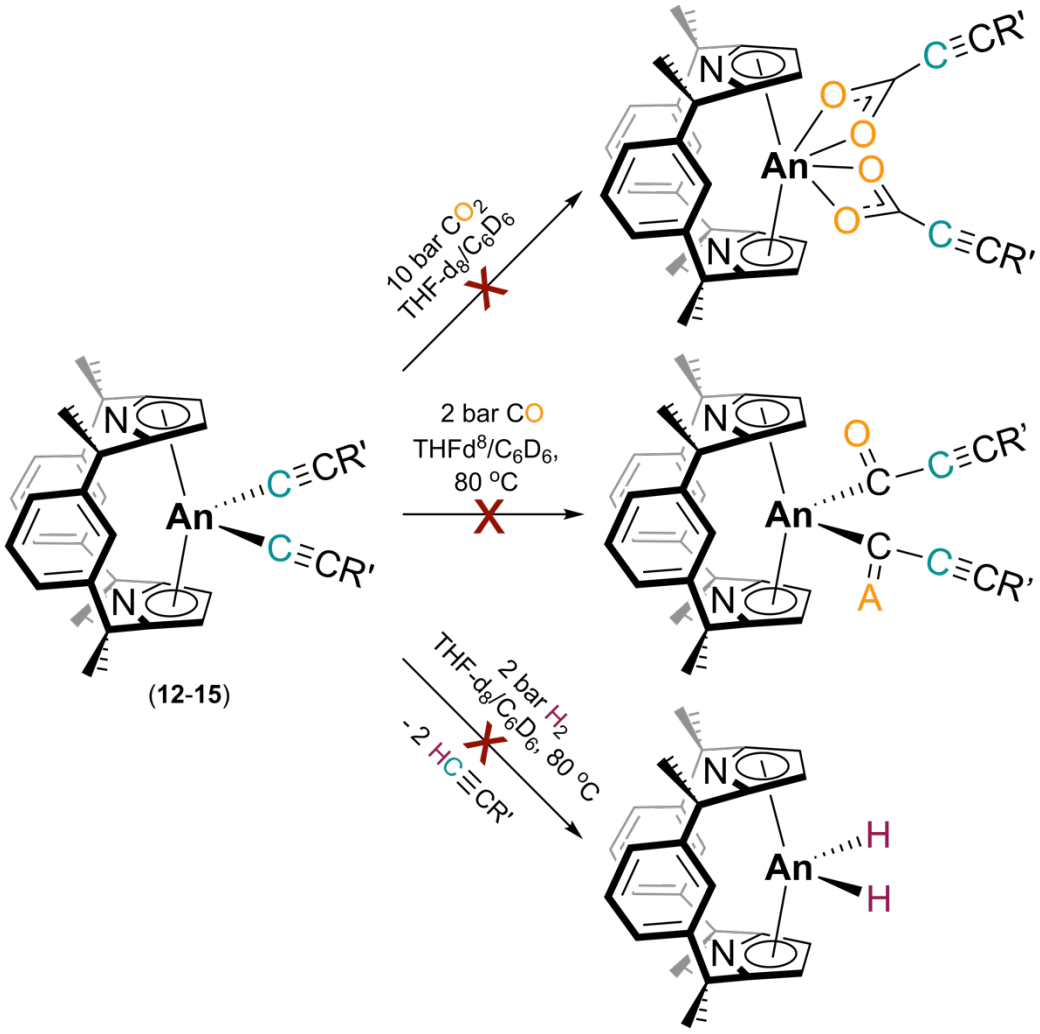

Scheme 2.18 Attempted CO and CO_2 insertion reactions into An–C bonds of complexes **12-15** and attempted σ-bond metathesis of An–C bonds in complexes **12-15** and H_2.

The reactivity of the An−C alkynyl bonds in complexes **12-15** with CO, CO_2 or H_2 was investigated. It was found that these bonds are stable towards insertion of CO into the An−C bond, as well as σ-bond metathesis with H_2 up to a pressure of 2 bar, even upon heating to 80 °C (Scheme 2.18). Due to the combustibility of H_2 and toxicity of CO, reactivities of **12-15** at higher pressures of H_2 and CO were not investigated. Insertion of CO_2 into the An−C bonds of **12-15** was attempted at a pressure of 10 bar and ambient temperature, however no reaction occurred. The stability of uranium(IV)-alkynyl bonds towards CO_2 insertion in metallocene-like complexes has previously been reported to require pressures of up to 5.51 bar.[74]

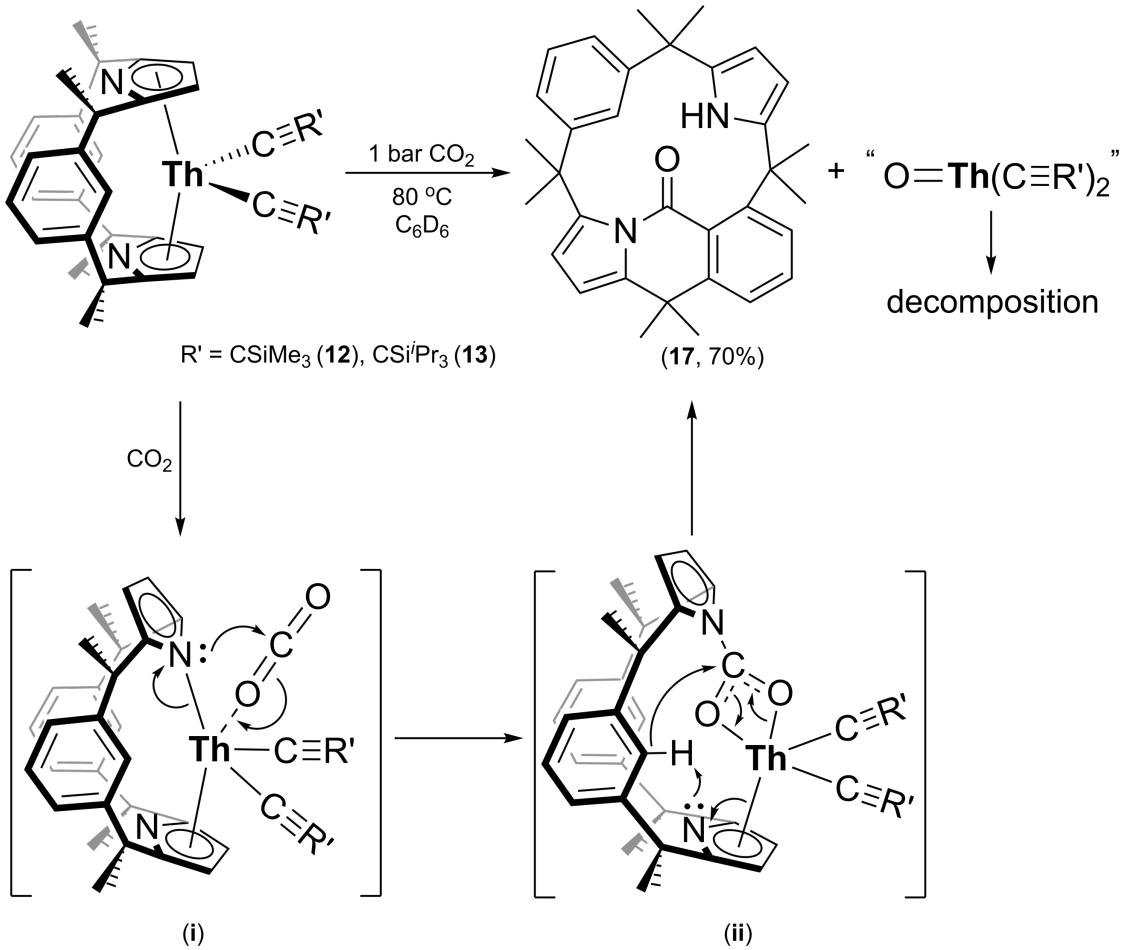

Scheme 2.19 Proposed reaction mechanism of ancillary ligand functionalisation and abstraction from the thorium-metal centres of complexes **12** or **13** to form **17**.

It was found however, that heating complexes **12** or **13** at 80 °C in C_6D_6 under 1 bar of CO_2 for 16 hours resulted in *trans*-calix[2]benzene[2]pyrrolide ligand functionalisation and abstraction from the metal centre (Scheme 2.19), resulting in the formation of a new organic macrocycle, 1^{10},1^{10},2,2,4,4,6,6-octamethyl-1^{5},1^{10}-dihydro-$3^{1}H$-1(6,3)-pyrrolo[1,2-*b*]isoquino-lina-3(2,5)-pyrrola-5(1,3)-benzenacyclohexaphan-1^{5}-one, referred to for simplicity as LCO (**17**) (Figure 2.21; yield = 70 %). Colourless X-ray quality single crystals of **17** were grown from saturated hexane solutions at -20 °C. It was postulated that transient Th^{IV}-oxo complexes form as by-products and rapidly decompose, yielding white insoluble solids. These thorium(IV) by-products could not be conclusively characterised; they have been drawn as Th^{IV}-monooxo for simplicity, however it is likely that oxo-bridged dimers or clusters form instead.

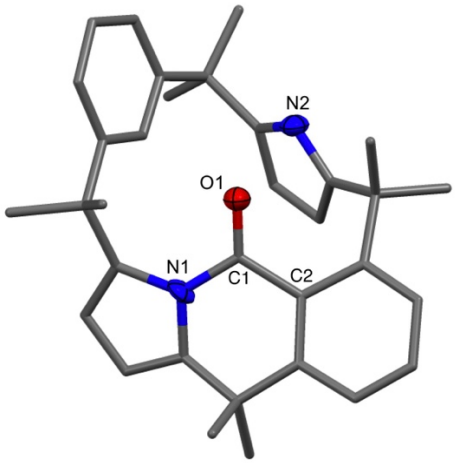

Figure 2.21 Solid-state structure of **17** (thermal ellipsoids set at 50 % probability level). Hydrogen atoms are omitted, with only heteroatoms depicted as thermal ellipsoids for clarity. Selected bond lengths (Å) and angles (°) for **17**: O1-C1 1.205(9), C1-N1 1.407(9), C1-C2 1.512(10).

Although, the detailed mechanism of the formation of **17** was not investigated, a route to its formation can be proposed (Scheme 2.19) based on actinide reactivity reported in the literature.[94, 95] In the first step of the mechanism shown in Scheme 2.19, it is proposed that CO_2 coordinates to the metal centre, creating steric crowding, in part due to the rigidity of the Th^{IV}–alkynyl bonds, which causes a pyrrolide to adopt κ^1-N coordination to the metal centre. NMR spectroscopic analysis does not provide any evidence to suggest CO_2 insertion into Th–C bonds of **12**-**13**. It has been established that CO_2 can insert into actinide-nitrogen bonds to form carbamate,[95, 96] which is suggested to be intermediate **ii** in the mechanism in Scheme 2.19. Our group previously reported the activation and reductive disproportionation of CO_2 by the uranium(III) complex $[U(N'')_3]$ (N'' = $N(SiMe_3)_2$), yielding the U^{IV} complex $[U(OSiMe_3)_4]$ and $O{=}C{=}NSiMe_3$.[97] The Th^{IV} metal centre in complexes **12** and **13** does not undergo oxidation state change, however the participation of the ancillary ligand in CO_2 disproportionation may allow the reaction to follow a similar reaction pathway to that previously reported by our group. Specifically, the *ipso*-hydrogen migration to the pyrrolide facilitates the formation of a demetallated piperidinone derivative and a transient Th^{IV}-oxo complex.

To further show that the synthesis of **17** is mediated by the Th^{IV} metal centre and is aided by the presence of the alkynyl substituents, 1 bar of CO_2 was added to solutions of **A**, H_2L or K_2L in C_6D_6 and the solutions heated at 80 °C for 16 hours. No reactions occurred with **A** or K_2L. With H_2L, approximately 25 % of the starting material was converted to a mixture of products, none of which had NMR spectroscopic resonances comparable to **17**; these products were likely the mono- and di-carbamates, formed by CO_2 insertion into one or both N−H bonds of the starting material. Isolation of these organic insertion products was not

attempted. The observation that the reaction of CO_2 and **A** does not give **17** led to the suggestion that the alkynyl substituents help stabilise the metal centre in **12**-**13** during the synthesis of **17**.

2.8.6 Reactivity of Complex 12 with $[Co_2(CO)_8]$ and $[Re_2(CO)_{10}]$

The coordination and subsequent activation of acetylenes by $[Co_2(CO)_8]$ has been investigated in great depth due to its application in the Pauson-Khand reaction, where reactivity between an alkyne, alkene and CO is initiated photochemically to form α,β-cyclopentenone.[98-102] $[Re_2(CO)_{10}]$ also coordinates to acetylenes and can subsequently be used as a radical polymerisation initiator after exposure to UV light.[103] Additions of $[Co_2(CO)_8]$ and $[Re_2(CO)_{10}]$ to **12** in THF were attempted, however no evidence of coordination was observed. Exposure of the reaction mixtures to UV radiation (λ = 351 nm) over 10 hours in a Quartz tube did not promote coordination or activation of the alkynyl groups of **12**.

2.8.7 Reactivity of Complex 12 with P_4

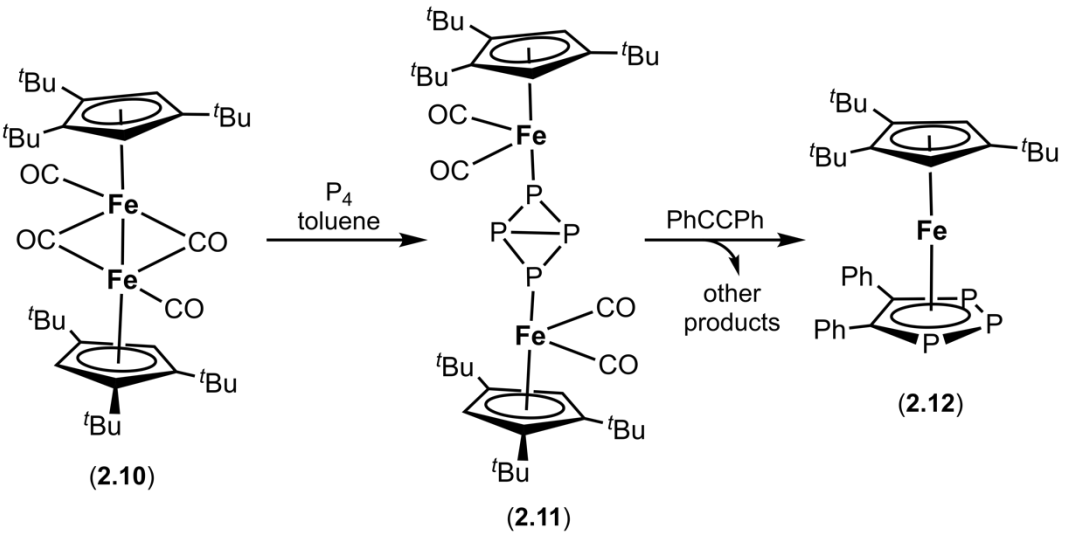

Scheme 2.20 Synthesis of a 1,2,3-triphospholyl aromatic Cp analogue (coordinated to iron in complex **2.12**) from the reaction of diphenyl acetylene with P_4, mediated by $[\{(C_5H_2{}^tBu_3\text{-}1,2,4)(CO)_2Fe\}_2]$ (**2.10**).[104]

An interesting range of reactivity has been reported in the literature involving P_4 and alkynes, commonly mediated by transition metal complexes.[104, 105] One such example reports the synthesis of a 1,2,3-triphospholyl aromatic Cp analogue (shown coordinated to iron in complex **2.12**, Scheme 2.20) from the reaction of diphenyl acetylene with a bimetallic P_4-bridged iron complex **2.11** (Scheme 2.20), formed from the activation of P_4 by a dinuclear iron complex, $[\{(C_5H_2{}^tBu_3\text{-}1,2,4)(CO)_2Fe\}_2]$ (**2.10** in Scheme 2.20).[104] In order to explore the

reactivity of the alkynyl groups of **12**, P_4 was added to a solution of **12** in THF. Exposure of the reaction mixture to UV radiation (λ = 351 nm) did not trigger a reaction. The reaction mixture was then heated at 80 °C for 20 minutes, resulting in partial decomposition of the starting material to H_2L and an unidentifiable mixture of products. Further heating resulted in full decomposition of the starting material.

2.9 Cation Exchange Reactions

Complexes **5**-**11** show that $(L^{-2H})^{4-}$ can incorporate several different counterions. Our group also previously reported the synthesis of a U^{III} bimetallic complex supported by $(L)^{2-}$, $[(L)U_2I_4]$ (**2.13** in Scheme 2.21),[66] synthesised from the reaction of Li_2L with two equivalents of UI_3 in toluene.[66] The coordination of two large U^{III} centres to $(L)^{2-}$ (one η^5-coordinated to the pyrrolides and the other κ^1-N bound to the pyrrolic nitrogens and η^6-coordinated to the arenes) suggests that other bimetallic complexes of this ligand system could form. Cation, such as caesium, capture has applications in the separation of nuclear waste.[106, 107] The aim of this Section is therefore to ascertain whether $(L^{-2H})^{4-}$ can support bimetallic systems accessed *via* cation exchange.

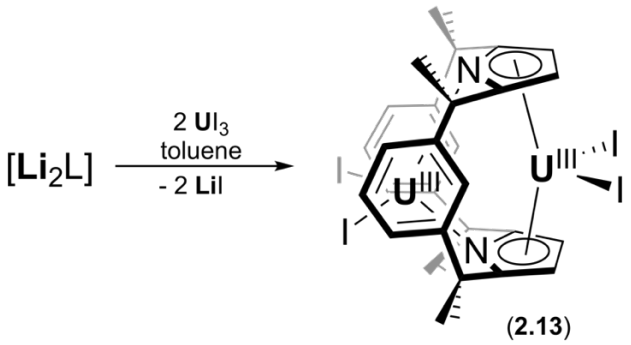

Scheme 2.21 Synthesis of $[(L)U_2I_4]$ (**2.13**).[14]

2.9.1 Group 1 Metal Exchange

Two analogues of complex **C** were synthesised by the reaction of **A** with three equivalents of $LiN(SiMe_3)_2$ or $NaN(SiMe_3)_2$ in toluene to yield $[Li(L^{-2H})Th(N(SiMe_3)_2)]$ (**18**) after 48 hours and $[Na(L^{-2H})Th(N(SiMe_3)_2)]$ (**19**) after 18 hours in 45 and 56 % yield, respectively (Scheme 2.22). ^{1}H NMR spectra of **18** and **19** displayed resonances that were subtly shifted from those of **A**. Elemental analysis agreed with the composition of **18** and **19**. X-ray quality crystals of **18** or **19** could not be obtained. It is interesting to note that the synthesis of **C** in this work proceeded most cleanly with highest overall yield (74 %). It is possible that the potassium-arene π-interaction acts as a driving force.

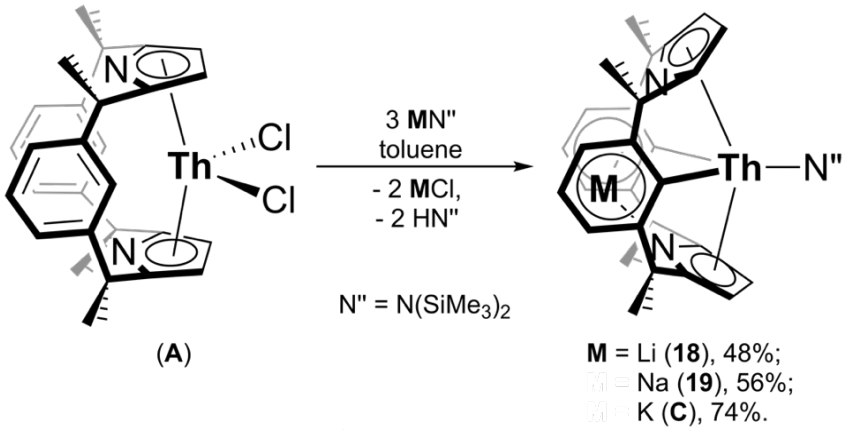

Scheme 2.22 Synthesis of $[M(L^{-2H})Th(N(SiMe_3)_2)]$ (M = Li (**18**), Na (**19**) or K (**C**)).

It was found that if an excess of a salt, such as LiCl or NaCl was added to a solution of **19** or **18**, respectively, the cations in the cavity between the arenes of the macrocycle would exchange. This lead to the investigation of the exchange of M^+ (M = Li, Na, K) for other alkali metal cations such as caesium.

An ion exchange reaction of potassium for caesium was attempted by heating **C** and excess Cs_2CO_3 in THF at 80 °C for 16 hours to yield $[Cs(L^{-2H})Th(N'')]$ (**20**) in 68 % yield (Scheme 2.23). The low yield is attributed to heating at 80 °C resulting in some decomposition. After work-up ^{1}H NMR spectroscopy indicated resonances that were shifted from those of **A**. X-ray quality crystals of **20** could not be obtained, however elemental analysis agreed with the composition of **20**. Complex **20** can be converted back to **C** in the presence of an excess of a potassium salt, such as KCl using the same procedure as for the synthesis of **20**; this process takes approximately 48 hours.

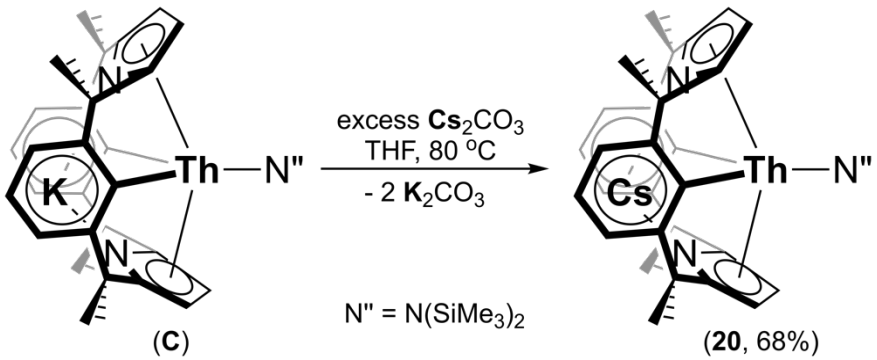

Scheme 2.23 Synthesis of $[Cs(L^{-2H})Th(N'')]$ (**20**).

2.9.2 Attempted Exchange of Group 1 Cations for *f*-Elements

In order to ascertain whether *f*-elements could be exchanged for potassium in **C**, an excess of SmI_3, $EuI_2(THF)_2$, $UI_3(dioxane)_{1.5}$, $UCl_4(THF)_{0.75}$ or $ThCl_4(DME)_2$ was added to a solution of **C** in THF. The reaction mixtures were sonicated for 15 minutes and then stirred

for 18 hours at 80 °C. Following work-up, it was found that no ion exchange reactions had taken place, with starting material and some decomposition visible in the NMR spectra.

2.10 Cationic Complexes

2.10.1 Synthesis

The C−H addition route described in Section 2.6, reprotonates the ligand aryl rings from $(L^{-2H})^{4-}$ to $(L)^{2-}$ and replaces the Th−R alkyl groups in **5**-**7** with two new Th–R' alkynyl groups to yield **12** and **13**. It was found that the R group can be retained, and a cationic alkyl complex formed, if two equivalents of the weak acid $[Et_3NH][BPh_4]$ (pKa of 9 in DMSO)[108] are used to reprotonate the ligand aryl rings. An excess of $[Et_3NH][BPh_4]$ was added to a solution of $[K(L^{-2H})Th(CH_2Ph)]$ (**7**) or $[MgCl(L^{-2H})Th(CH_2Ph)]$ (**11**) in THF and the suspension stirred at ambient temperature for two hours (Scheme 2.24). After work-up to remove Et_3N and the $K[BPh_4]$ or $MgCl[BPh_4]$ by-products, $[(L)Th(CH_2Ph)][BPh_4]$ (**21**) was isolated as an off-white solid in 31 % yield. The analogous amido complex, $[(L)Th(N(SiMe_3)_2)][BPh_4]$ (**22**), was accessed from $[K(L^{-2H})Th(N(SiMe_3)_2)]$ (**C**) and $[Et_3NH][BPh_4]$ and obtained in 68 % yield. The driving forces for these reactions are likely to be both the formation of the conjugate-base Et_3N and precipitation of the salt $K[BPh_4]$.

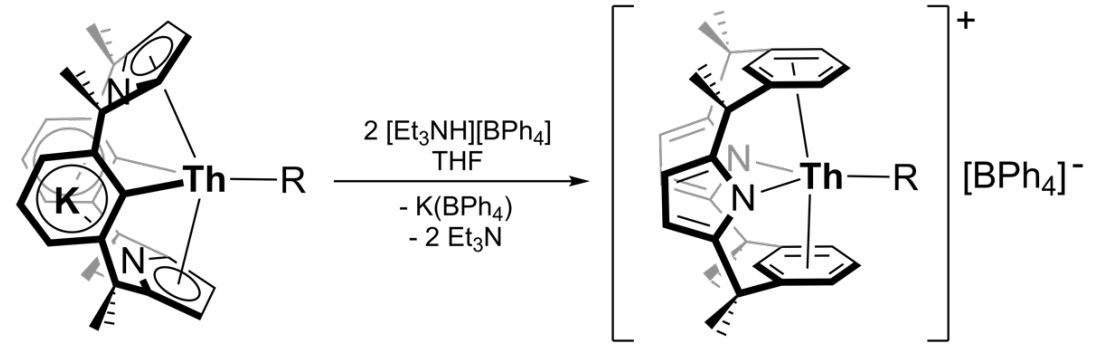

R = CH_2Ph (**7**), $N(SiMe_3)_2$ (**C**) R = CH_2Ph (**21**), 31%, $N(SiMe_3)_2$ (**22**), 68%.

Scheme 2.24 Synthesis of $[(L)Th(CH_2Ph)][BPh_4]$ (**21**) and $[(L)Th(N(SiMe_3)_2)][BPh_4]$ (**22**).

Although an X-ray structural determination for the alkyl cation **21** could not be obtained, multinuclear NMR spectroscopy confirmed its similarity to the amido complex **22**, for which single crystals were obtained. The *ipso*-proton resonances are assigned at 7.72 and 8.23 ppm in the ^1H NMR spectra of **21** and **22**, respectively. The $^{13}C\{^1H\}$ NMR spectra recorded in THF-d_8 no longer show quaternary *ipso*-carbon resonances above 158.3 ppm found at 215.8 ppm in **7** and at 211.7 ppm in **C**.

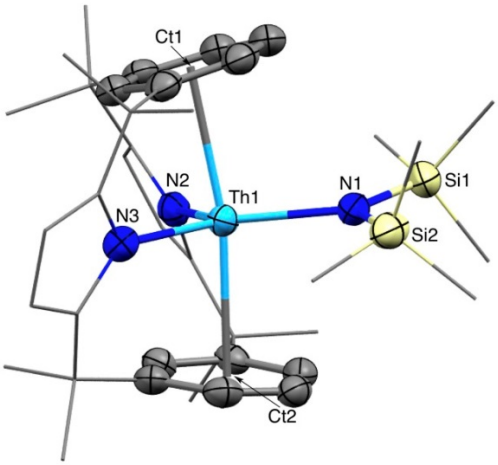

Figure 2.22 Solid-state structure of **22** (thermal ellipsoids set at 50 % probability level). The $[BPh_4]^-$ counterion and hydrogen atoms are omitted, and the pyrrolic rings and alkyl linkers depicted as wire-frame for clarity. Selected bond lengths (Å) and angles (°) for **22**: Th1–$Ct_{(avg)}$ 2.690(2), Th1–N1 2.276(5), Th1–N2 2.469(5), Th1–N3 2.483(5), Ct1–Th1–Ct2 169.41, N2–Th1–N3 115.47(16).

In **22**, the macrocyclic ligand $(L)^{2-}$ was found to coordinate $\eta^6{:}\kappa^1{:}\eta^6{:}\kappa^1$ to the Th^{IV} cation. **22** is shown in Figure 2.22 and is a rare example of a bis(arene) 'sandwich' complex of a thorium ion. A small number of Th^{IV}-η^6-arene complexes have been reported to date, including other cationic Th^{IV} complexes.[22, 39, 51, 59, 109] Only two of these examples display thorium coordination to two arenes.[22, 39] This binding mode has not been previously observed for this macrocyclic ligand with An^{IV}, but has been dominant in the more electron-rich U^{III} and Np^{III} complexes of the form [(L)AnX] (X = I, BH_4, $N(SiMe_3)_2$, O-2,6-$^tBu_2$-C_6H_3 for U^{III} and X = Cl for Np^{III}) and $[(L)Np_2Cl_4(THF)_3]$.[14, 23, 93, 110] A survey of the available ^1H NMR data for Th^{IV} $(L)^{2-}$-supported complexes does not display any characteristics that could be used to distinguish between coordination modes $\eta^6{:}\kappa^1{:}\eta^6{:}\kappa^1$ and $\eta^5{:}\eta^5$ of the macrocycle.

The Th1−$Ct_{(avg)}$ distance in **22** is comparable to that in a similar polydentate pyrrolide-containing thorium(IV) arene complex reported by Gambarotta, $[Li(DME)_3][\eta^6$-{1,3-[(2-$C_4H_3N)(CH_3)_2C]_2C_6H_4$}$ThCl_3]$ (2.701(8) Å).[109] Examples of interactions between Th^{IV} and η^6-coordinated arenes in the literature exhibit bond lengths between 2.815(3) Å and 4.05(1) Å, which are longer than the Th1−$Ct_{(avg)}$ bond distance in **22**, suggesting a weaker Th^{IV}-arene interaction in the literature examples.[22, 39, 59] Due to the cationic nature of **22**, an expected decrease of the Th1–N3 bond from 2.375(12) Å in **C** to 2.276(5) Å in **22** was observed.[14] The Th–N distance in **22** is therefore also shorter than other Th^{IV}–$N(SiMe_3)_2$ literature bonds.[18, 31, 51, 111, 112]

The unsolvated η^6-arene-bound U^{III} [(L)UI] and [(L)UI(THF)] complexes have $[aryl]_{Ct1}$–U–$[aryl]_{Ct2}$ angles of 173.55° and 171.61°, respectively,[14] and the samarium(III)

[(L)SmCl] complex has a $[aryl]_{Ct1}$–Sm–$[aryl]_{Ct2}$ angle of 179°.[15] The base-free U^{III} and Sm^{III} complexes display larger angles, whilst the angle in [(L)UI(THF)] is decreased, most likely as a result of steric repulsion caused by the THF molecule. This can be used to explain the notably smaller $[aryl]_{Ct1}$–Th1–$[aryl]_{Ct2}$ angle in **22** (169.41°) that is likely to be the result of steric repulsion caused by the bulky $N(SiMe_3)_2$ ligand. Although the U^{III} analogue of **22**, $[(L)U(N(SiMe_3)_2)]$,[110] displays a larger $[aryl]_{Ct1}$–U–$[aryl]_{Ct2}$ angle (176.05°) than that in **22**, the bulky $N(SiMe_3)_2$ ligand is further away from the metal centre in the U^{III} complex: the U1–N3 bond (2.364(3) Å) is longer than the Th1–N3 bond in **22** (2.276(5) Å).

Attempts at $(L^{-2H})^{4-}$ arene reprotonation were also made using $[Et_3NH]Cl$ instead of $[Et_3NH][BPh_4]$ in an analogous procedure to that in Scheme 2.24, to establish whether an analogous reaction to that of **22** can occur whilst introducing an inner-sphere anion. Although NMR spectroscopy provided evidence of the formation of an analogue of **22**, this reaction did not proceed cleanly, perhaps due to increased steric crowding, and the product could not be isolated and characterised. Finally, no reaction occurred upon the addition of $[NH_4][BPh_4]$ (pKa of 10.5 in DMSO)[82] to **C**.

2.10.2 Reactivity with Small Molecules

The addition of small molecules such as CO or CO_2 to **22** was attempted in THF-d_8 at a pressure of 1 bar. An unidentifiable mixture of products and H_2L was obtained immediately, similarly to attempts described in Section 2.8.2. It is therefore likely that the products of the reactions of **22** with small molecules are unstable and prone to decomposition. This theory may be further supported by the reactivity observed for **12** and **13** with CO_2 (Section 2.8.5.2), which resulted in the functionalisation of the ancillary ligand. Consequently, it was proposed that in the case of **22**, and perhaps in analogous reactions with **5**-**10**, the An−N bonds of the ancillary ligand undergo insertion, resulting in the formation of a range of complexes, some of which are unstable and undergo decomposition to H_2L.

2.10.3 Reactivity with Reducing Agents and Bases

Gambarotta reported the reduction of a thorium(IV) complex of a similar dipyrrolic ligand containing a single arene group, $[Li(DME)_3][\eta^6\text{-}\{1,3\text{-}[(2\text{-}C_4H_3N)(CH_3)_2C]_2C_6H_4\}ThCl_3]$, with potassium metal to yield a paramagnetic complex, $[Li(DME)_3][\{\eta^5\text{-}1,3\text{-}[(\eta^5\text{-}2\text{-}C_4H_3N)(CH_3)_2C]_2C_6H_4\}ThK\text{-}(\mu\text{-}Cl)_3]$, which could be regarded as containing thorium(III).[109] The bond distance between thorium and the cyclohexadienide

centroid in the reduced complex is 2.463(7) Å,[109] and is significantly shorter than that in the unreduced complex. The Th−arene interaction is therefore likely to play a key role in this chemistry. Consequently, the Th^{IV}/Th^{III} reduction chemistry of **22** was investigated. Addition of one equivalent of KC_8 to **22** at -20 °C resulted in a mixture of products, none of which were paramagnetic, as would be expected for Th^{III}; however $K(BPh_4)$ was identified as a reaction by-product. Most of the products could not be isolated and conclusively characterised, however some evidence suggests that one of the products formed was a metallacycle from the activation of a methyl group C–H bond of the bis(trimethylsilyl)amide substituent (Scheme 2.25). The 'tuck-in' complex was not isolated cleanly and therefore was not conclusively characterised; its identity was suggested based on further reactivity and methods of exclusion, namely: (1) the addition of $[Et_3NH][BPh_4]$ to the reaction mixture resulted in the reformation of **22**, indicating that the intermediate had been deprotonated in the attempted reduction, (2) the lack of a characteristic resonance at a high chemical shift in the $^{13}C\{^1H\}$ NMR spectrum suggested that the deprotonation had not occurred at the arene rings of the macrocycle, and (3) a de-symmetrisation of the ligand environment was observed in the ^1H NMR spectrum of the deprotonated product. It was concluded that **22**, as well as other complexes supported by this non-innocent macrocyclic ligand system, were not suitable candidates for Th^{IV}/Th^{III} reduction chemistry.

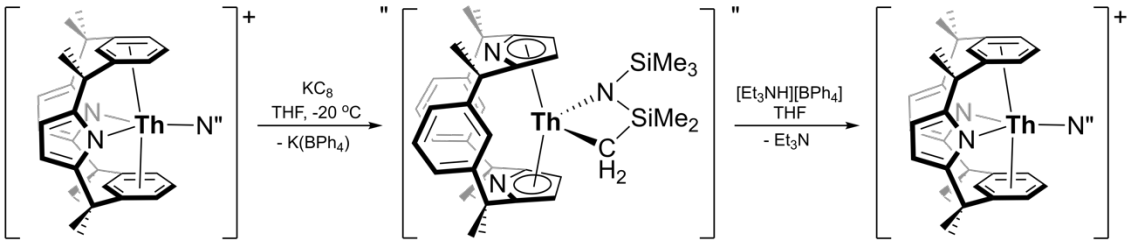

Scheme 2.25 Synthesis of a tuck-in complex of the bis(trimethylsilyl)amido ligand and subsequent reprotonation and reformation of **22** (N'' = $N(SiMe_3)_2$).

It is interesting to note that the addition of two equivalents of base such as $KN(SiMe_3)_2$ or KCH_2Ph to **22** resulted in the double deprotonation of the macrocyclic arene rings to afford **C**, however in these reactions ^1H NMR spectroscopy did not show any evidence of the tuck-in intermediate proposed in Scheme 2.25.

2.11 Heterobimetallic Complexes: 12 and 13 with Group 10

It has been established that group 10 metals readily coordinate to and activate multiple bonds.[113] In bis(cyclopentadienyl) group 4 transition metal bis-alkynyl complexes $[(Cp)_2TM(C{\equiv}CSiMe_3)_2{\cdot}NiPPh_3]$ (TM = Ti (**2.16**), Zr (**2.17**), Scheme 2.26), nickel

incorporation was found to be accompanied by the activation of a TM^{IV}–C bond in complexes $[(Cp)_2TM(\eta^2\text{-}C_2(SiMe_3)_2)]$ (TM = Ti (**2.14**), Zr (**2.15**), Scheme 2.26), and subsequent rearrangement of the alkynyl groups to coordinate η^1:η^2 to each metal.[114]

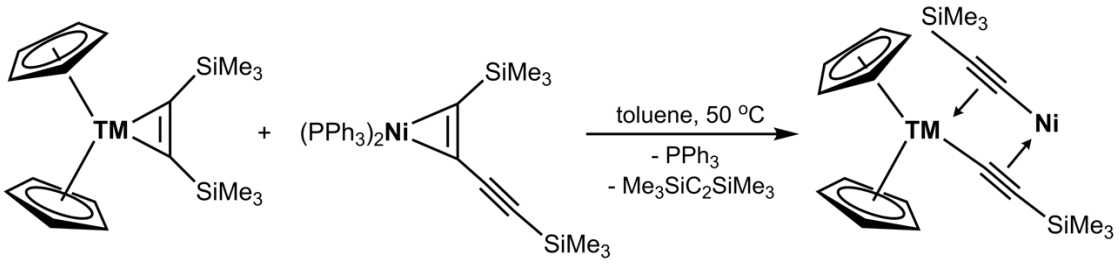

TM = Ti (**2.14**), Zr (**2.15**) **TM** = Ti (**2.16**), Zr (**2.17**)

Scheme 2.26 Synthesis of complexes $[(Cp)_2TM(C{\equiv}CSiMe_3)_2{\cdot}NiPPh_3]$ (TM = Ti (**2.16**), Zr (**2.17**)) from $[(Cp)_2TM(\eta^2\text{-}C_2(SiMe_3)_2)]$ (TM = Ti (**2.14**), Zr (**2.15**)).[114]

2.11.1 Nickel Coordination to 12

To establish whether Th^{IV} analogues of complexes $[(Cp)_2TM(C{\equiv}CSiMe_3)_2{\cdot}NiPPh_3]$ could be synthesised, $[(L)Th(C{\equiv}CSiMe_3)_2]$ (**12**) was initially reacted with one equivalent of $[Ni(COD)_2]$ (COD = cyclooctadiene) (Scheme 2.27). The reaction reached completion within several minutes, with the ^{1}H NMR spectrum indicating that only free COD was present. After work-up to remove the volatile COD, an orange solid was isolated in 21 % crude yield. A significant shift in ancillary ligand ^{1}H NMR spectroscopic resonances from those of **12** (Figure 2.23) was observed, most notably for the resonances of the *ipso*-hydrogens and pyrrolic-hydrogens of the macrocycle, which shifted from 7.96 and 7.50 ppm in **12** to 9.43 and 6.11 ppm in $[(L)Th(C{\equiv}CSiMe_3)_2{\cdot}Ni]$ (**23**), respectively (Figure 2.23). NMR spectroscopy and elemental analysis support the description of this orange product as $[(L)Th(C{\equiv}CSiMe_3)_2{\cdot}Ni]$ (**23**) (Scheme 2.27).

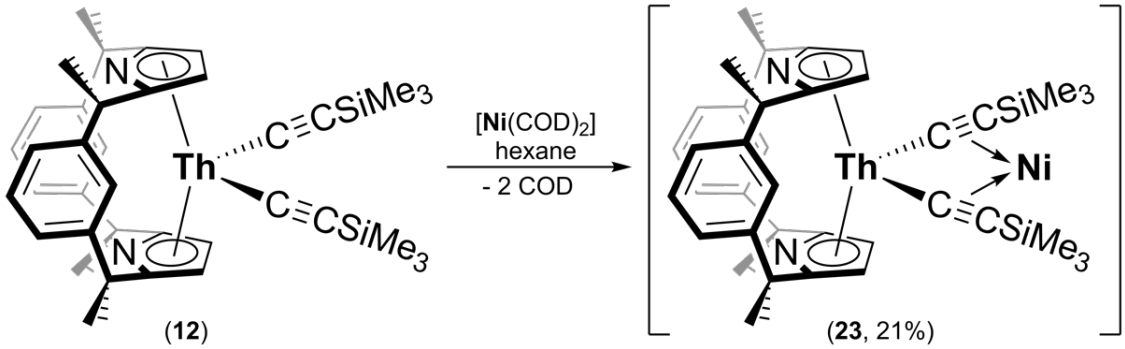

(**12**) (**23**, 21%)

Scheme 2.27 Synthesis of $[(L)Th(C{\equiv}CSiMe_3)_2{\cdot}Ni]$ (**23**).

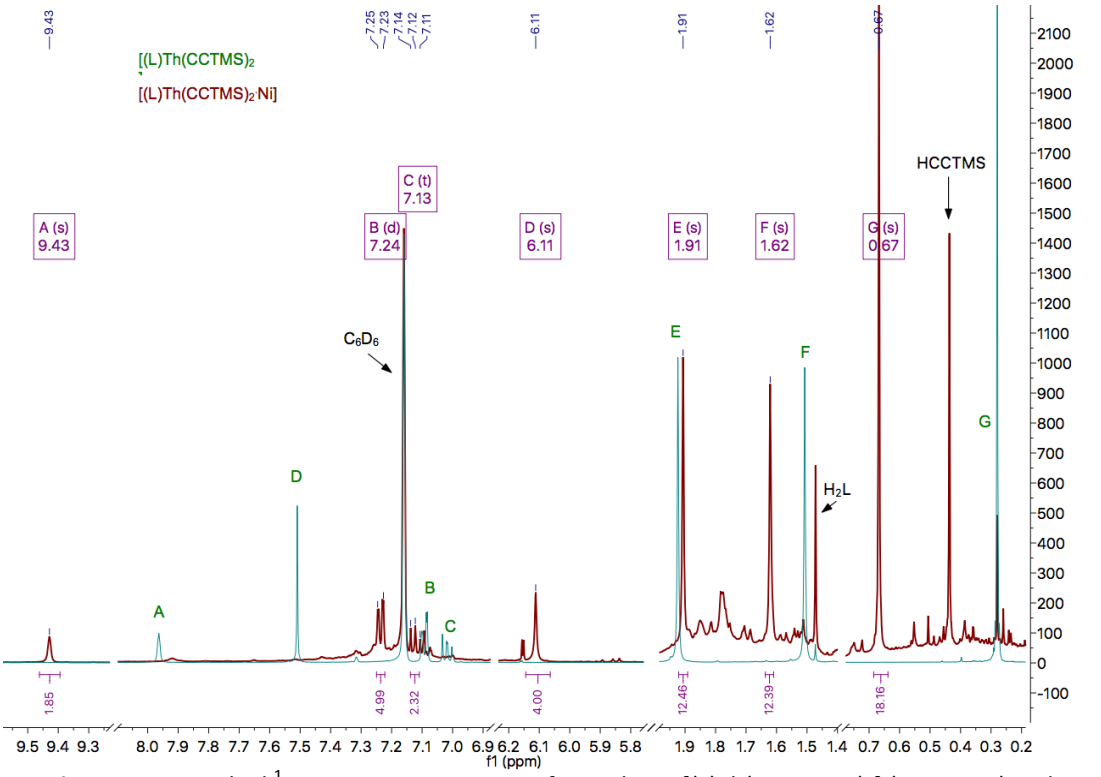

Figure 2.23 Overlaid ^{1}H NMR spectra in C_6D_6 of complexes [(L)Th(C≡CSiMe$_3$)$_2$] (**12**, green) and [(L)Th(C≡CSiMe$_3$)$_2$·Ni] (**23**, red). Resonances in green are labelled A-G, to correspond to resonances in red, and emphasise the differences in chemical shifts between **12** and **23**.

Solid-state FTIR of **23** shows a C≡C stretch at 2143 cm^{-1}, which is unchanged from that of **12**, indicating no significant C≡C bond activation. It is possible however that due to weak binding of Ni within the complex, upon drying, Ni is displaced from the complex entirely, resulting in no observable change in FTIR stretching frequency from that of the starting material.

Over the course of several hours in solution, **23** begins decomposing to complex **12** during which time metallic-grey solids are seen precipitating from solution. As a result, X-ray quality single crystals of **23** could not be grown. However, experiments to verify nickel coordination to the triple bonds of the alkynyl groups were performed. One equivalent of [Ni(COD)$_2$] was added to **A** and no reaction was observed. This result indicated that Ni^0 was not coordinated to the multiple bonds of the ancillary ligand, and was therefore likely to be coordinated to the triple bonds of the alkynyl groups. Furthermore, no reaction occurred upon the addition of one equivalent of [Ni(COD)$_2$] to **13**, indicating that the steric bulk of *iso*-propyl groups on the alkynyl ligands likely prevented the approach and subsequent coordination of Ni to these triple bonds. The possibility of Ni coordination to triple bonds of an adjacent complex and subsequent dimer formation cannot be excluded.

Assuming Ni^0 coordination to the triple bonds of the alkynyl groups in complex **23**, the nickel centre has a *d*-electron count of 14. Examples of 14-electron Ni^0 have been reported, such as the complex [Ni(dtbpm] (dtbpm = bis(di-*tert*-butylphosphanyl)methane),[115] but such examples are rare due to insufficient electronic stabilisation of the nickel centre.

2.11.2 Nickel Coordination to 12 Supported by Phosphine Donors

In order to offer the nickel centre sufficient electron density, several two electron donors were considered to increase the electronic count to 16. The two-electron donors that yielded the best results were PPh_3 and PCy_3 (Cy = cyclohexyl) (Scheme 2.28). One equivalent of PPh_3 or PCy_3, **12** and $[Ni(COD)_2]$ were combined in a reaction vessel in hexanes. The reaction reached completion within several minutes and after work-up, it was found that no bound COD remained. Dark orange-red X-ray quality single crystals of $[(L)Th(C{\equiv}CSiMe_3)_2{\cdot}NiPPh_3]$ (**24a**) (Figure 2.24) and of $[(L)Th(C{\equiv}CSiMe_3)_2{\cdot}NiPCy_3]$ (**25a**) (Figure 2.25) were isolated from saturated hexane solutions in 7 and 18 % crystalline yields, respectively.

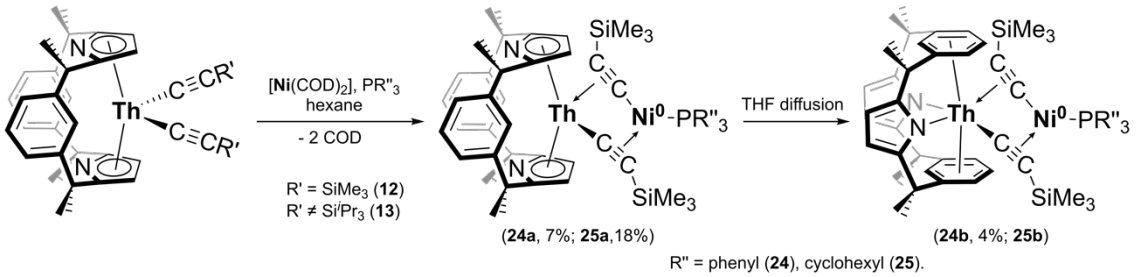

Scheme 2.28 Synthesis of $[(L)Th(C{\equiv}CSiMe_3)_2{\cdot}NiPR_3]$ (where R = phenyl (**24**) or cyclohexyl (**25**)).

As an alternative crystallisation method for **25**, hexane vapour was allowed to diffuse into a saturated THF solution of **25**, affording dark orange-red X-ray quality single crystals of $[(L)Th(C{\equiv}CSiMe_3)_2{\cdot}NiPCy_3]$ (**25b**) in 4 % yield (with respect to **12**), the molecular structure of which is shown in Figure 2.26. Surprisingly, the two methods of crystallisation of **25** yield two different structures. When crystallised from THF, ligand $(L)^{2-}$ coordination to the Th^{IV} cation is $\eta^6{:}\kappa^1{:}\eta^6{:}\kappa^1$ (**25b**), similarly to **22**, and when crystallised from hexanes $(L)^{2-}$ coordination is metallocene-like $\eta^5{:}\eta^5$ (**25a**).

A survey of the available literature indicates that only two heterobimetallic complexes featuring thorium and nickel adjacent to each other have been reported to date,[116, 117] one of which is a Th^{IV} *bis*-Cp* nickel phosphido complex $[(Cp^*)_2Th(\mu\text{-}PPh_2)_2Ni(CO)_2]$ (Th–Ni distance: 3.206(2) Å), where the authors suggest that an interaction between nickel and thorium exists.[117] It was found that the Th1–Ni1

distances in complexes **24a** (3.068 Å), **25a** (3.0559(7) Å) and **25b** (3.053 Å) are notably shorter than those reported in the literature, and on average approximately 0.25 Å shorter than the sum of the covalent radii of nickel and thorium.[68]

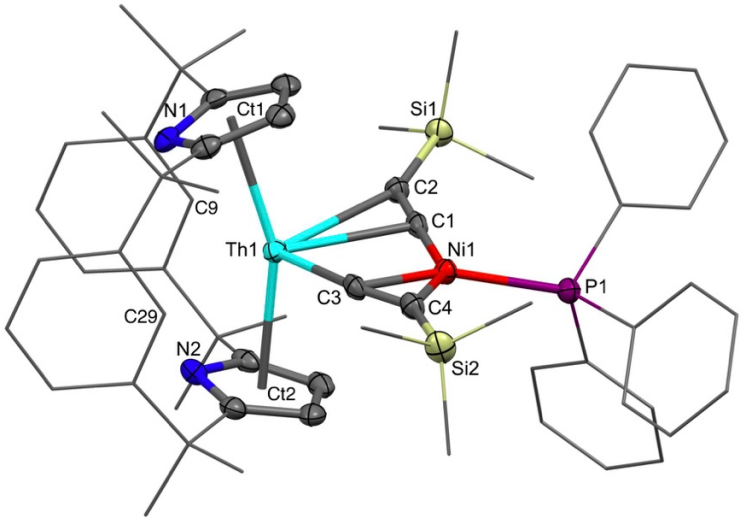

Figure 2.24 Solid-state structure of **24a** (thermal ellipsoids set at 50 % probability level). Hydrogen atoms are omitted, with the phenyl rings and alkyl linkers depicted as wire-frame for clarity. Selected bond lengths (Å) and angles (°) for **24a**: $[Th1–Ct]_{avg}$ 2.563(1), Th1–C1 2.614(3), Th1–C3 2.423(3), C1–C2 1.246(4), C3–C4 1.272(4), Ni1–C1 1.829(3), Ni1–C3 1.932(3), Ni1–C4 2.015(3), Ni1–P1 2.1806(9), Th1–Ni1 3.068, Ct1–Th1–Ct2 157.64, C9–Th1–C29 114.70.

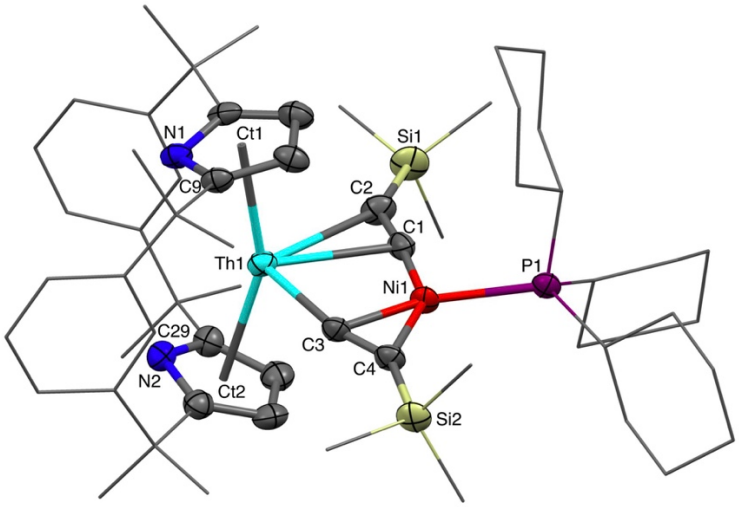

Figure 2.25 Solid-state structure of **25a**, where single crystals were grown from a saturated solution of **25a** in hexane (thermal ellipsoids set at 50 % probability level). Hydrogen atoms are omitted, with the phenyl rings and alkyl linkers depicted as wire-frame for clarity. Selected bond lengths (Å) and angles (°) for **25a**: $[Th1–Ct]_{avg}$ 2.557(3), Th1–C1 2.645(5), Th1–C2 2.937(6), Th1–C3 1.938(5), C1–C2 1.267(8), C3–C4 1.268(8), Ni1–C1 1.814(6), Ni1–C3 1.938(5), Ni1–C4 2.025(6), Ni1–P1 2.2053(16), Th1–Ni1 3.0559(7), Ct1–Th1–Ct2 155.61, C9–Th1–C29 113.86.

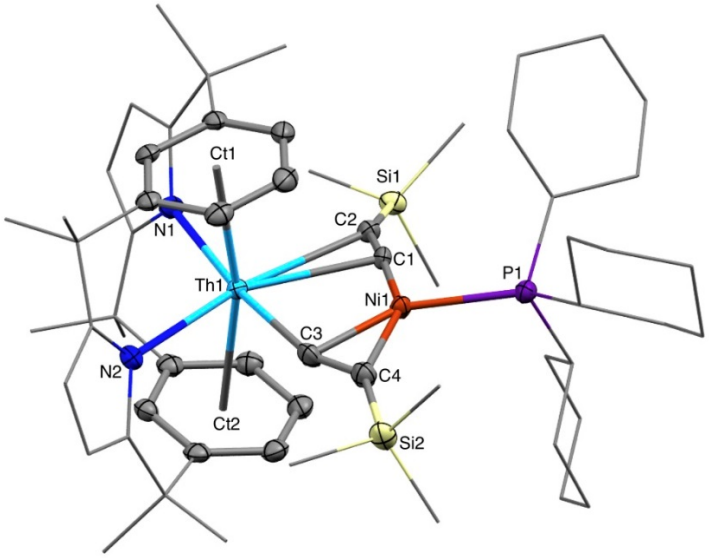

Figure 2.26 Solid-state structure of **25b**, where single crystals were grown from vapour diffusion of hexanes into a saturated solution of **25b** in THF (thermal ellipsoids set at 50 % probability level). Hydrogen atoms are omitted, with the pyrrolic rings and alkyl linkers depicted as wire-frame for clarity. Selected bond lengths (Å) and angles (°) for **25b**: $[Th1–Ct]_{avg}$ 2.665(1), Th1–C1 2.653(3), Th1–C3 2.436(3), C1–C2 1.250(4), C3–C4 1.272(4), Th1–N1 2.604(2), Th1–N2 2.587(2), Ni1–C1 1.830(3), Ni1–C3 1.933(3), Ni1–C4 2.005(3), Ni1–P1 2.1999(8) Th1–Ni1 3.053, Ct1–Th1–Ct2 166.55.

The solid-state structures of **24** and **25** show that the interaction with the Ni^0 centre is strong enough to reorganise the Th−C alkynyl groups from bis(η^1) to Th^{IV} to η^1 to one metal and η^2 to the other. As mentioned above, this asymmetry was previously noted by Rosenthal for the zirconium and titanium metallocene complexes, $[(Cp)_2TM(C{\equiv}CSiMe_3)_2{\cdot}NiPPh_3]$ (TM = Ti (**2.16**), Zr (**2.17**), Scheme 2.26).[114] Rosenthal reasoned that the $SiMe_3$ groups on the alkynyl substituents and the phenyl groups on $NiPPh_3$ are too bulky to allow the η^2-coordination of Ni^0 to both alkynyl triple bonds. This therefore results in the alkynyl rearrangement to bind η^1:η^2 to each metal.

Rosenthal and co-workers report a slight lengthening of the triple bonds of the alkynyl ligands upon nickel coordination, the FTIR stretching frequencies for which are reported as 1780 and 1911 cm^{-1} for the titanium complex and 1771 and 1876 cm^{-1} for the zirconium complex.[114] These data disagree with those for **24**, where the observed solid-state FTIR stretching frequencies are 2120 and 2071 cm^{-1}, which indicates a slight change from the stretching frequency of the staring material **12**, which was found to be 2140 cm^{-1} and comparable to the stretching frequency of free $HC{\equiv}CSiMe_3$ (2038 cm^{-1}).[78] The solid-state structures of **24** and **25** also display a very slight lengthening in C≡C bond lengths compared to that of free $HC{\equiv}CSiMe_3$ (1.194(8) Å) within ESD.[77]

A combination of variable temperature NMR spectroscopy and DFT computational studies (Section 2.11.4) were undertaken to interrogate the ligand flexibility and dynamic equilibria. Given the low isolated yields of **25**, the variable temperature NMR spectral study of just **24** was undertaken. Computational analysis (Section 2.11.4, Table 2.1) shows that the Gibbs free energy difference between complexes **24** and **25** is negligible (3.4 kJ·mol^{-1}).

The ^{1}H NMR spectroscopic resonances of **24** are better resolved in toluene-d_8 than in THF-d_8, therefore toluene-d_8 was initially used for variable temperature NMR experiments. At temperatures below 210 K however, toluene-d_8 became viscous and resonances became broad. Consequently, THF-d_8 was used for measurements at temperatures below 210 K. The ^{1}H NMR spectra of **24** and **25** at 298 K correspond to a molecule with overall C_{2v} symmetry, indicating a symmetrical bis(alkynide) coordination on the NMR timescale in solution, but this is lowered to C_s as solutions are cooled to 190 K. Figure 2.27 shows the two halves of **24** and **25** in the **a** (η^5:η^5) and **b** (η^6:κ^1:η^6:κ^1) binding modes, which become inequivalent from the asymmetric alkynyl coordination in the solid state structures and at low temperatures in solution NMR spectroscopy. The flexibility of $(L)^{2-}$ also offers other dynamic equilibria processes that decoalesce sequentially as the temperature of either THF-d^8 or toluene-d^8 solutions of **24** are warmed from 190 K.

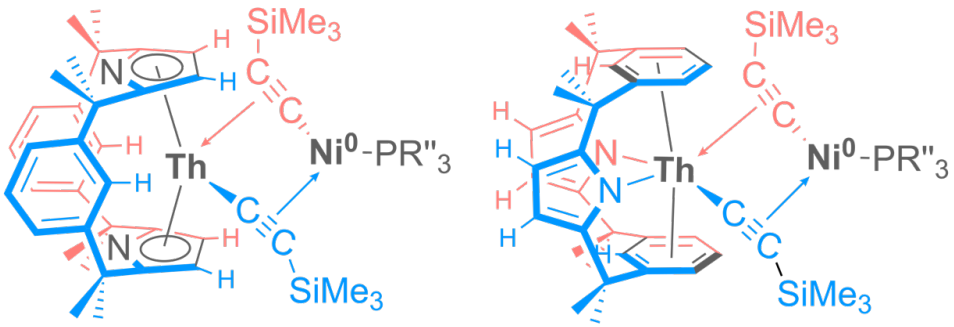

(**24a**, **25a**) (**24b**, **25b**)

Figure 2.27 Planes of asymmetry (blue and pink) introduced into **24** and **25** by alkynyl asymmetry in solid-state and low temperature solutions changes depending on coordination of $(L)^{2-}$.

Careful inspection of the spectra at 193 K in THF-d^8 shows the two pyrrolide-hydrogen resonances of the macrocycle are doublets. Given that the hydrogens of the same pyrrolide ring are not in the same plane of symmetry in conformation **a** (Figure 2.27, left) unlike in **b** (Figure 2.27, right), they will couple, resulting in signal splitting, which is therefore consistent with structure **24a**. There are multiple coalescence temperatures for the various dynamic processes in the molecule, with the *ipso*-protons

of the $(L)^{2-}$ ligand visible as two well-defined resonances up to 230 K, but above this, the resonances coalesce to a single, average chemical shift. This suggests there is sufficient flexibility in the ligand binding that even at lowered temperatures when the alkynyl ligands are bound asymmetrically (on the NMR timescale) the macrocycle can flex such that an average C_{2v} can be maintained. It is noted that $^{13}C\{^1H\}$ NMR spectra of **24** and **25** do not show coupling of ^{31}P to ^{13}C of the alkynyl substituents.

For comparison, the coalescence temperature for the process that renders the $SiMe_3$ groups equivalent in $[(Cp)_2Ti(C{\equiv}CSiMe_3)_2][NiPPh_3]$ (**2.16**) is just above 190 K.[114] The ^1H NMR spectra of the Th^{IV} dichloride **A** show no dynamic processes; spectra in THF-d^8 are the same at 193 K and 298 K.

Complexes **24** and **25** are stable in the solid-state for a number of weeks, however decompose readily when heated or in solution over several days. As a result, H_2L can be seen in NMR spectra of **24** and **25**. To further stabilise these coordination complexes, attempts were made to increase the electron count around the nickel centre by using the bidentate, four electron phosphine donor dppf (dppf = 1,1′-Ferrocenediyl-bis(diphenylphosphine)). [Ni(dppf)(COD)] was therefore prepared and subsequently added to **12**, however no reaction occurred. It is likely that the dppf ligand is too bulky, preventing the coordination of nickel to the alkynyl groups of **12**.

2.11.2.1 Reactivity with CO and CO_2

It was postulated that the alkynyl interaction with the Ni^0 centre resulting in alkynyl $\eta^1{:}\eta^2$ coordination in both **24** and **25** may have resulted in some degree of Th–C or Ni–C alkynyl bond activation and potentially increased reactivity of complexes **24** or **25** *vs* **12**. The reactivity of **24** towards CO (2 bar) and CO_2 (10 bar) was therefore examined. It was found that **24** is stable against CO or CO_2 insertion at room temperature.

2.11.3 Attempted Platinum Incorporation

Attempts were made to synthesise platinum analogues of complexes **23-25**, using $[Pt(nb)_3]$ (nb = norbornene) instead of $[Ni(COD)_2]$ (Scheme 2.29). Reaction of **12** with $[Pt(nb)_3]$ in donor solvent such as THF resulted in the formation of a mixture of products. Electronic stabilisation was attempted by using various phosphine donors such as PCy_3 or PPh_3, however a clean product could not be isolated. Multiple product formation precluded conclusive identification of ^{195}Pt satellites in the ^1H, $^{13}C\{^1H\}$ or ^{29}Si NMR spectra of these reactions. No reaction occurred upon the addition of [Pt(dppf)(nb)] to **12**. None of the above

reactions proceeded in non-donor solvents. It is possible that Pt^0 is too large to coordinate to both alkynes in an analogous manner to Ni^0 in **24** and **25**, resulting in insufficient electronic stabilisation of the metal centre. It is also possible that the use of different supporting ligands for the group 10 starting material ([Ni(COD)$_2$] *vs* [Pt(nb)$_3$]) may have caused differences in reactivity. Computational analysis compares hypothetical platinum analogues, **24′** and **25′**, to nickel-containing complexes, **24** and **25**, and is discussed in Section 2.11.4.

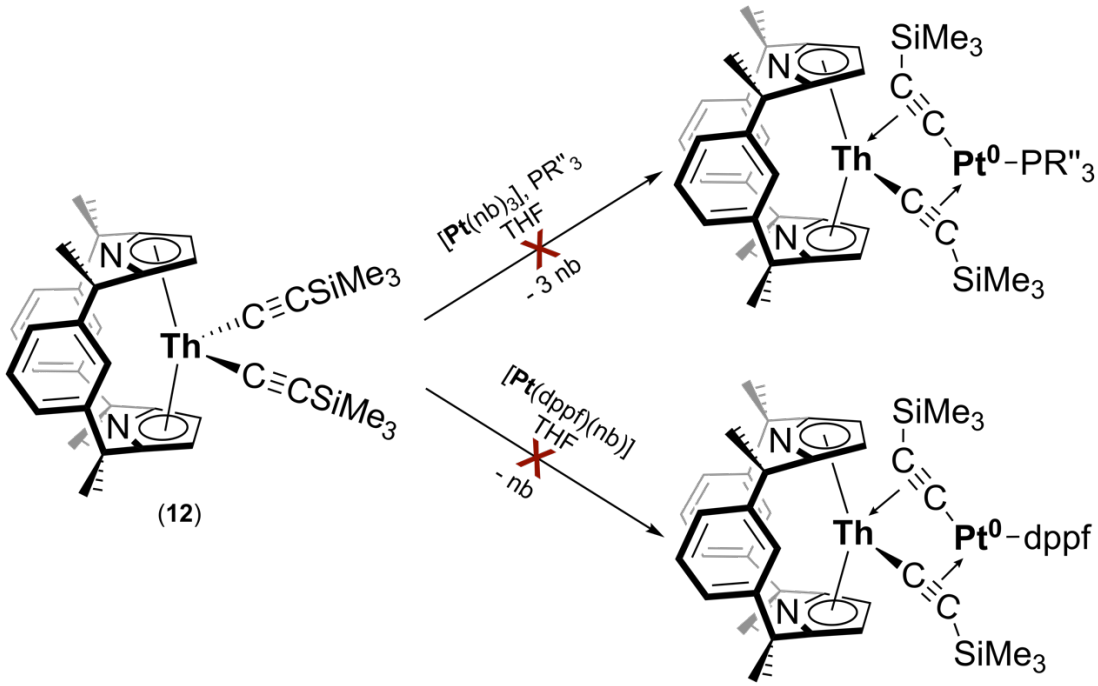

Scheme 2.29 Attempted reactions of **12** with [Pt(nb)$_3$] in the presence of PR′′$_3$ and with [Pt(dppf)(nb)] (dppf = 1,1′-Ferrocenediyl-bis(diphenylphosphine), nb = norbornene, R′′ = phenyl, cyclohexyl).

2.11.4 Computational Analysis and Discussion of Ancillary Ligand Rearrangement

The computational analyses described in this section were performed by collaborators Prof. Nikolas Kaltsoyannis and Kieran O'Brien at the University of Manchester, UK, in order to further probe the different coordination modes of the ancillary $(L)^{2-}$ ligand in complexes **24** and **25**. Scalar relativistic, hybrid density functional theory (DFT) was used to examine **24**, **25** as well as their hypothetical platinum analogues **24′** and **25′**, in order to ascertain whether the group 10 metal has an effect on ligand arrangement. The total self-consistent field (SCF) (*E*) and Gibbs (*G*) energy differences between the **a** (η^5:η^5) and **b** (η^6:κ^1:η^6:κ^1) forms of all four complexes are shown in Table 2.1, which shows that in all cases the **a** form is the more stable, with an increased preference for this conformation in the PPh_3 systems. There appears to be no significant difference between the energies of **24** or **25** *vs* **24′** or **25′**, indicating that exchanging Ni for Pt has little effect on $(L)^{2-}$ coordination. The energies summarised in

Table 2.1 were also recalculated in the presence of a continuum solvent of THF or hexane. It was found that the solvent had little effect, with Gibbs free energies differing from those in Table 2.1 by negligible amounts for **24** (1.6 kJ·mol^{-1}) and **25** (2.2 kJ·mol^{-1}).

Table 2.1 Δ*E* and Δ*G* values (kJ·mol^{-1}) for the ligand interconversion between the **a** (η^5:η^5) and **b** (η^6:κ^1:η^6:κ^1) forms of **24**, **25**, **24'** and **25'**.

Ligand Interconversion	Δ*E*	Δ*G*
24b to 24a	−33.7	−27.2
25b to 25a	−24.8	−23.8
24b′ to 24a′	−30.5	−27.3
25b′ to 25b′	−25.6	−24.1

Single-point SCF energy calculations on the $[(L)Th^{IV}]^{2+}$ fragment have shown that the bis(arene) **b** (η^6:κ^1:η^6:κ^1) coordination is 19.0 kJ·mol^{-1} more favourable. The $[(CCSiMe_3)_2NiPCy_3]^{2-}$ fragment single-point SCF energy remained nearly unchanged (1.0 kJ mol^{-1} difference) between **25a** and **25b**. It was therefore proposed that the energetic preference for conformation **a** in the full molecules must be caused by bonding differences between the $[(CCSiMe_3)_2NiPCy_3]^{2-}$ and $[(L)Th^{IV}]^{2+}$ fragments arising from different orientations of $(L)^{2-}$.

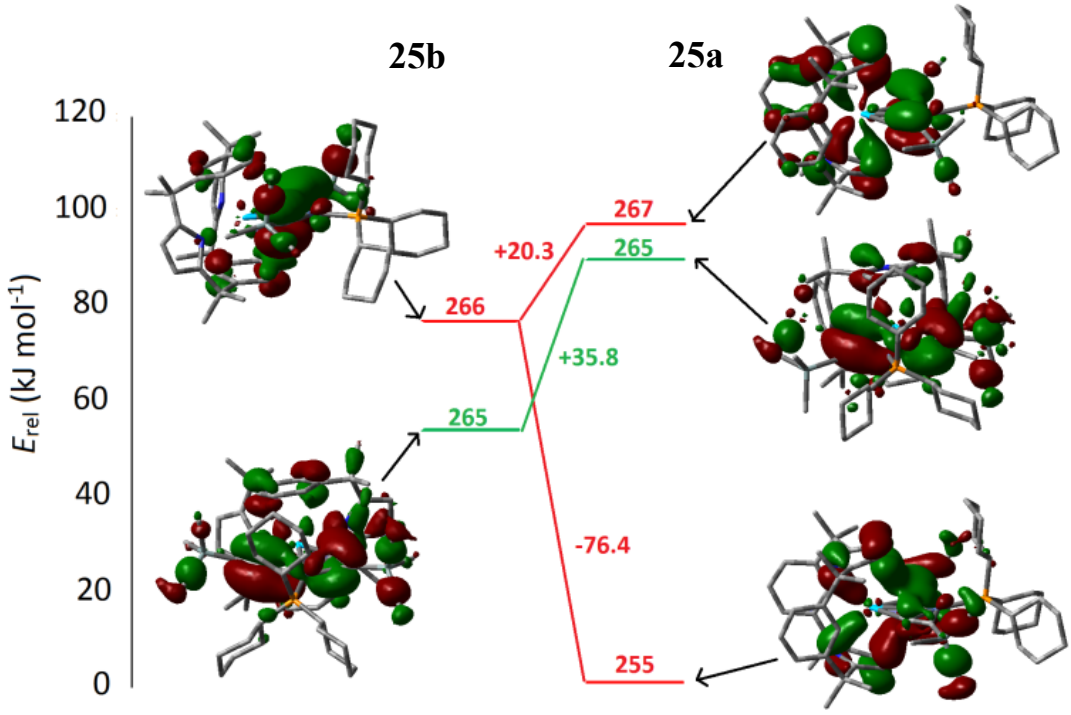

Figure 2.28 Selected MOs of complexes **25a** and **25b**. Energies are plotted relative to MO 255 in the η^5:η^5 conformation. Hydrogens omitted for clarity. Isovalue = 0.025.

To understand the origin of the energetic preference for the **a** (η^5:η^5) bonding mode, the valence Kohn-Sham molecular orbitals (MOs) of **24** and **25** were examined. The energies and isosurfaces for MOs of **25** are shown in Figure 2.28 with MOs 255 and 266 (**25a** and **25b**, respectively, labelled in red) containing Ni-alkynyl interactions with in-phase combinations of Ni *d*- and alkynyl π-orbitals. MO 267 (**25a**, labelled in red) is the out-of-phase counterpart to MO 255. This splitting and stabilisation of MO 255 arises from the energetic proximity of Ni-alkynyl and Th-pyrrolide bonding MOs in ligand conformation **a**. A detailed view of MO 255 is presented in Figure 2.29, where the source of the η^5:η^5-conformation stability is a result of a bonding interaction involving nickel, the alkynyl groups and the pyrrolide ring.

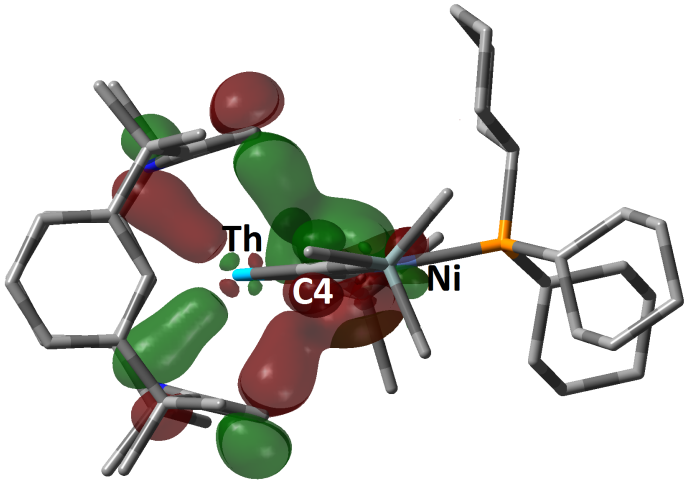

Figure 2.29 Detailed view of MO 255 and the stabilising bonding interaction involving nickel, the alkynyl groups and the pyrrolide ring.

MO 265 (labelled in green) in Figure 2.28 is more stable in **25b** than in **25a**, and its character doesn't split between conformation **a** and **b**. This 35.8 kJ·mol^{-1} destabilisation from **b** to **a** can be attributed to a small admixture of $(L)^{2-}$ arene ring π-character in **25b**, which in isolated $[(L)Th^{IV}]^{2+}$ fragments is stabilised by 223.1 kJ·mol^{-1}. The MOs shown in Figure 2.28 change most significantly between the **a** and **b** forms. MO 255 is therefore likely to be the source of stability for the **a** (η^5:η^5) coordination.

The MO diagram for **24** is shown in Figure 2.30 with MOs 250, 251 and 245 (labelled in green) displaying different behaviour from those in **25a** and **25b**. MOs 250 and 251 in **24b** represent two Ni–alkynyl bonding interactions in which the alkynyl ligands are out of phase with each other as a result of π-contributions from the PPh_3 aromatic rings, character which cannot be present in **25**. The character of MOs 250 and 251 (**25b**) is distributed amongst three MOs in **24a** (245, 249 and 254), with only MO 245 displaying Ni−alkynyl character. As π-

contributions from the PPh_3 aromatic rings move to MOs 249 and 254 in **25a**, MO 245 is stabilised *vs* MOs 250 and 251 of **24b**.

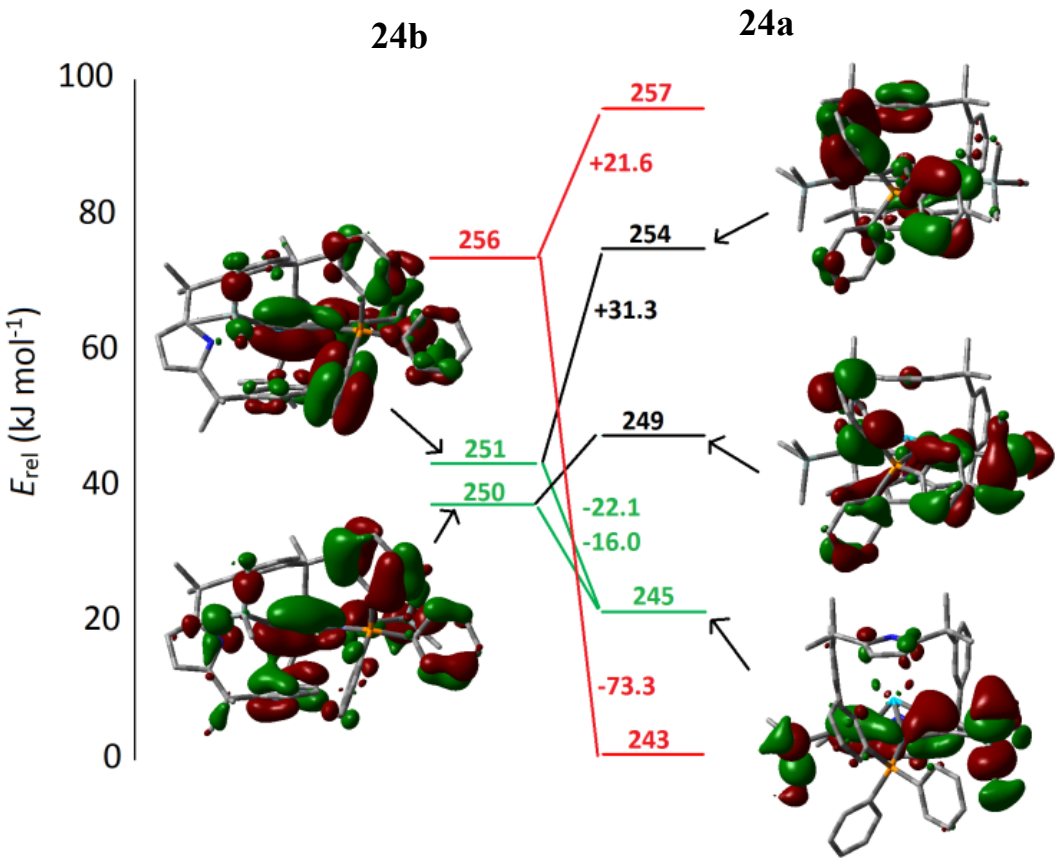

Figure 2.30 Selected MOs of complexes **24a** and **24b**. Energies are plotted relative to MO 243 in the η^5:η^5 conformation. Hydrogens omitted for clarity. Isovalue = 0.025.

The DFT calculations therefore conclude that the **a** (η^5:η^5) ligand conformation is the more stable coordination mode in both **24** and **25**. This agrees with low temperature NMR spectroscopic studies on complex **24**. Figure 2.30 suggests that similarly to MO 255 in complex **25a**, the increased stability of **24a** results from the formation of MO 243. It is also possible that the increased stability of **24a** *vs* **25a** is a direct result of the behavioural differences between the orbitals labelled in green in Figure 2.28 and Figure 2.30. It therefore remains unclear how structural isomer **b** forms. **25b** may be a minor product in the reaction mixture that is not resolved in the NMR spectrum. **25b** could also be the result of a packing effect imparted by lattice solvent and formed over several days in a slow rearrangement. Perhaps fluxionality would be promoted at higher temperatures, however complexes **24** and **25** readily decompose in solution when heated, precluding high temperature NMR studies.

2.12 General Trends

Table 2.2 summarises the Ct–An–Ct angles in An^{IV} η^5-pyrrolide complexes of $(L)^{2-}$ and $(L^{-2H})^{4-}$, listed in order of increasing angle. Generally, a larger Ct–An–Ct angle is observed in U^{IV} complexes when compared with their Th^{IV} analogues. In the macrocyclic framework, the distance between the pyrrolides is fixed and therefore the smaller size of uranium, allows for the ligand to adopt a more linear geometry when encapsulating the metal centre. Table 2.2 also suggests that the substituents on the metal centre and the sizes of and interactions with counterions have a greater effect on the Ct–An–Ct angle than the form of the ligand, $(L)^{2-}$ or $(L^{-2H})^{4-}$, itself. The smallest Ct–An–Ct angle is observed in **16** (supported by $(L^{-2H})^{4-}$), where the pyrrolic-nitrogens coordinate to lithium bridges whilst facing the η^2-O_2SiMe_2 substituent, and as a result, the arene planes become nearly perpendicular to the pyrrolide planes. The second smallest Ct–An–Ct angle is observed in **2** (supported by $(L)^{2-}$), where the pyrrolic-nitrogens face the two η^3-BH_4 substituents; the arenes are not bound to the metal centre in **2** and also face the η^3-BH_4 substituents.

Table 2.2 Comparison of Ct–An–Ct angles (°) in An^{IV} η^5-pyrrolide complexes of $(L)^{2-}$ and $(L^{-2H})^{4-}$.

Complex	Ct–An–Ct (°)
$[(L^{-2H})U(\eta^2\text{-}O_2SiMe_2)(Li\{THF\})_2]$ (**16**)	117.60
$[(L)Th(BH_4)_2]$ (**2**)	143.58
$[(L)Th(C{\equiv}CSiMe_3)_2{\cdot}NiPCy_3]$ (**25a**)	155.61
$[(L)Th(C{\equiv}CSiMe_3)_2{\cdot}NiPPh_3]$ (**24a**)	157.64
$[(L)UI_2]$ (**B**)[14]	163.26
$[(L)ThCl_2]$ (**A**)[14]	163.60
$[K(L^{-2H})Th(N(SiMe_3)_2)]$ (**C**)[14]	164.39
$[(L)UCl_2]$ (**1**)	164.78
$[K(L^{-2H})U(N(SiMe_3)_2)]$ (**4**)	166.24
$[(L)Th(C{\equiv}CSi^iPr_3)_2]$ (**13**)	168.38
$[Li(L^{-2H})Th(CH_2SiMe_3){\cdot}LiCl]$ (**6·LiCl**)	168.48
$[(L)Th(C{\equiv}CSiMe_3)_2]$ (**12**)	169.49
$[K(L^{-2H})Th(CH_2Ph){\cdot}THF]$ (**7·THF**)	170.16
$[(L)U(C{\equiv}CSi^iPr_3)_2]$ (**15**)	170.44
$[Li(L^{-2H})U(CH_2SiMe_3){\cdot}LiCl{\cdot}THF]$ (**9·LiCl·THF**)	172.03
$[Li(L^{-2H})Th(Me)]$ (**5**)	172.26

All remaining crystallographically characterised An^{IV} complexes feature pyrrolic-nitrogens facing away from the substituents on the metal centre, and where relevant,

interacting with alkali metal counterions. A comparison of analogues [K(L^{-2H})Th(CH_2Ph)·THF] (**7·THF**) and [K(L^{-2H})Th($N(SiMe_3)_2$)] (**C**) shows that the larger $N(SiMe_3)_2$ ligand causes the Ct–An–Ct angle to decrease. The largest Ct–An–Ct angle is observed for **5** (supported by $(L^{-2H})^{4-}$), which features the smallest substituent on the thorium centre, with a weakly coordinating lithium counterion. The An^{IV} alkynyl complexes **12**, **13** and **15** have comparatively large Ct–An–Ct angles, a likely result of the small volume occupied by the alkynyl quaternary carbons. This angle is significantly decreased upon the coordination of $NiPR''_3$ (R = Ph, Cy) in **24a** and **25a**, whereupon the coordination of the alkynyl groups changes to occupy a larger volume closer to the metal centre.

2.13 Summary and Conclusions for Chapter Two

A series of new Th^{IV} and U^{IV} complexes supported by a *trans*-calix[2]benzene[2]pyrrolide ligand have been synthesised. This macrocyclic ligand system has been shown to display remarkable flexibility and a range of binding modes. This ligand flexibility has allowed for the addition and stabilisation of a range of substituents and facile incorporation and abstraction of cations in the bis(arene) pocket. Complexes **2** and **3** are two examples of a small number of thermally stable actinide borohydride complexes reported to date.

Complexes **5-7** are the first mixed aryl/alkyl complexes of thorium. Complexes **5-10** are the second examples of pyrrolide-supported actinide alkyl complexes. Complexes **12**, **13**, **24** and **25** are the first crystallographically characterised thorium alkynyl complexes. The macrocyclic ligand non-innocence has demonstrated reversible C–H bond activation chemistry and formed a new route to alkynyl complexes **12-15**, and alkyl cations of Th^{IV}, **21** and **22**. Complex **22** is a rare example of a thorium bis(arene) 'sandwich' complex. Alkynyl complexes **12-15** were found to be remarkably stable, when compared to the reactive monoalkyl complexes **5-10**. In an unusual case of ligand non-innocence, a new organic ketone-functionalised macrocycle **17**, was synthesised from the cleavage of a C=O bond in CO_2, upon heating complexes **12** or **13** under 1 bar of CO_2.

New heterobimetallic complexes **24** and **25**, incorporating nickel, were synthesised, and display the shortest Th–Ni distances reported to date: on average 0.25 Å shorter than the sum of the covalent radii of nickel and thorium. Complex **25** was isolated as two conformers **a** (η^5:η^5) and **b** (η^6:κ^1:η^6:κ^1); the first instance of two structural isomers of $(L)^{2-}$ in the same complex. Complex **25b** is also an example of a thorium bis(arene) 'sandwich' complex. DFT calculations show that in complexes **24** and **25**, the **a** conformation of the ancillary $(L)^{2-}$ ligand

is favoured, independent of the transition metal (Ni or Pt). The source of the energetic preference for **a** may stem from the mixing of a Th-pyrrolide π-bonding orbital with a Ni–alkynyl interaction.

2.14 References for Chapter Two

1. J. M. Manriquez, P. J. Fagan and T. J. Marks, *J. Am. Chem. Soc.*, 1978, **100**, 3939-3941.
2. W. J. Evans, J. R. Walensky, J. W. Ziller and A. L. Rheingold, *Organometallics*, 2009, **28**, 3350-3357.
3. T. Andrea, E. Barnea and M. S. Eisen, *J. Am. Chem. Soc.*, 2008, **130**, 2454-2455.
4. K. C. Jantunen, C. J. Burns, I. Castro-Rodriguez, R. E. Da Re, J. T. Golden, D. E. Morris, B. L. Scott, F. L. Taw and J. L. Kiplinger, *Organometallics*, 2004, **23**, 4682-4692.
5. J. A. Pool, B. L. Scott and J. L. Kiplinger, *J. Am. Chem. Soc.*, 2005, **127**, 1338-1339.
6. P. J. Fagan, J. M. Manriquez, E. A. Maatta, A. M. Seyam and T. J. Marks, *J. Am. Chem. Soc.*, 1981, **103**, 6650-6667.
7. L. Jia, X. Yang, C. L. Stern and T. J. Marks, *Organometallics*, 1997, **16**, 842-857.
8. A. Haskel, T. Straub and M. S. Eisen, *Organometallics*, 1996, **15**, 3773-3775.
9. Y.-X. Chen, M. V. Metz, L. Li, C. L. Stern and T. J. Marks, *J. Am. Chem. Soc.*, 1998, **120**, 6287-6305.
10. J. W. Bruno, T. J. Marks and L. R. Morss, *J. Am. Chem. Soc.*, 1983, **105**, 6824-6832.
11. J. K. Pagano, J. M. Dorhout, K. R. Czerwinski, D. E. Morris, B. L. Scott, R. Waterman and J. L. Kiplinger, *Organometallics*, 2016, **35**, 617-620.
12. N. A. Siladke, C. L. Webster, J. R. Walensky, M. K. Takase, J. W. Ziller, D. J. Grant, L. Gagliardi and W. J. Evans, *Organometallics*, 2013, **32**, 6522-6531.
13. R. R. Langeslay, M. E. Fieser, J. W. Ziller, F. Furche and W. J. Evans, *J. Am. Chem. Soc.*, 2016, **138**, 4036-4045.
14. P. L. Arnold, J. H. Farnaby, R. C. White, N. Kaltsoyannis, M. G. Gardiner and J. B. Love, *Chem. Sci.*, 2014, **5**, 756-765.
15. S. Ilango, B. Vidjayacoumar and S. Gambarotta, *Dalton Trans.*, 2010, **39**, 6853-6857.
16. H. I. Schlesinger and H. C. Brown, *J. Am. Chem. Soc.*, 1953, **75**, 219-221.
17. T. J. Marks, W. J. Kennelly, J. R. Kolb and L. A. Shimp, *Inorg. Chem.*, 1972, **11**, 2540-2546.
18. H. W. Turner, R. A. Andersen, A. Zalkin and D. H. Templeton, *Inorg. Chem.*, 1979, **18**, 1221-1224.
19. T. M. Trnka, J. B. Bonanno, B. M. Bridgewater and G. Parkin, *Organometallics*, 2001, **20**, 3255-3264.
20. S. Bettonville and J. Goffart, *J. Organomet. Chem.*, 1988, **356**, 297-305.
21. P. Zanella, N. Brianese, U. Casellato, F. Ossola, M. Parchia, G. Rossetto and R. Graziani, *Inorg. Chim. Acta*, 1988, **144**, 129-134.
22. J. McKinven, G. S. Nichol and P. L. Arnold, *Dalton Trans.*, 2014, **43**, 17416-17421.
23. P. L. Arnold, C. J. Stevens, J. H. Farnaby, M. G. Gardiner, G. S. Nichol and J. B. Love, *J. Am. Chem. Soc.*, 2014, **136**, 10218-10221.
24. T. J. Marks and J. R. Kolb, *Chem. Rev.*, 1977, **77**, 263-293.
25. A. C. Dunbar, J. E. Gozum and G. S. Girolami, *J. Organomet. Chem.*, **695**, 2804-2808.
26. D. Baudry, E. Bulot, P. Charpin, M. Ephritikhine, M. Lance, M. Nierlich and J. Vigner, *J. Organomet. Chem.*, 1989, **371**, 163-174.
27. X. Zhang, H. Dai, H. Yan, W. Zou and D. Cremer, *J. Am. Chem. Soc.*, 2016, **138**, 4334-4337.

28. E. R. Bernstein, W. C. Hamilton, T. A. Keiderling, S. J. La Placa, S. J. Lippard and J. J. Mayerle, *Inorg. Chem.*, 1972, **11**, 3009-3016.
29. R. Shannon, *Acta Crystallogr., Sect. A:*, 1976, **32**, 751-767.
30. D. Hohl and N. Roesch, *Inorg. Chem.*, 1986, **25**, 2711-2718.
31. T. M. Gilbert, R. R. Ryan and A. P. Sattelberger, *Organometallics*, 1988, **7**, 2514-2518.
32. R. K. Thomson, B. L. Scott, D. E. Morris and J. L. Kiplinger, *C. R. Chim.*, 2010, **13**, 790-802.
33. R. K. Thomson, T. Cantat, B. L. Scott, D. E. Morris, E. R. Batista and J. L. Kiplinger, *Nat. Chem.*, 2010, **2**, 723-729.
34. C. R. Graves, E. J. Schelter, T. Cantat, B. L. Scott and J. L. Kiplinger, *Organometallics*, 2008, **27**, 5371-5378.
35. A. J. Lewis, U. J. Williams, P. J. Carroll and E. J. Schelter, *Inorg. Chem.*, 2013, **52**, 7326-7328.
36. S. J. Kraft, P. E. Fanwick and S. C. Bart, *J. Am. Chem. Soc.*, 2012, **134**, 6160-6168.
37. C. E. Hayes and D. B. Leznoff, *Organometallics*, 2010, **29**, 767-774.
38. K. C. Jantunen, F. Haftbaradaran, M. J. Katz, R. J. Batchelor, G. Schatte and D. B. Leznoff, *Dalton Trans.*, 2005, **0**, 3083-3091.
39. C. A. Cruz, D. J. H. Emslie, L. E. Harrington and J. F. Britten, *Organometallics*, 2008, **27**, 15-17.
40. E. Lu, O. J. Cooper, J. McMaster, F. Tuna, E. J. L. McInnes, W. Lewis, A. J. Blake and S. T. Liddle, *Angew. Chem., Int. Ed. Engl.*, 2014, **53**, 6696-6700.
41. E. Mora, L. Maria, B. Biswas, C. Camp, I. C. Santos, J. Pécaut, A. Cruz, J. M. Carretas, J. Marçalo and M. Mazzanti, *Organometallics*, 2012, **32**, 1409-1422.
42. Z. E. Button, J. A. Higgins, M. Suvova, F. G. N. Cloke and M. Roe, *Dalton Trans.*, 2015, **44**, 2588-2596.
43. J. A. Higgins, F. G. N. Cloke and S. M. Roe, *Organometallics*, 2013, **32**, 5244-5252.
44. G. Paolucci, G. Rossetto, P. Zanella, K. Yünlü and R. D. Fischer, *J. Organomet. Chem.*, 1984, **272**, 363-383.
45. J.-C. Berthet, J.-F. Le Maréchal and M. Ephritikhine, *J. Organomet. Chem.*, 1994, **480**, 155-161.
46. A. Haskel, T. Straub, A. K. Dash and M. S. Eisen, *J. Am. Chem. Soc.*, 1999, **121**, 3014-3024.
47. K. G. Moloy and T. J. Marks, *Inorg. Chim. Acta*, 1985, **110**, 127-131.
48. J. M. Manriquez, P. J. Fagan, T. J. Marks, C. S. Day and V. W. Day, *J. Am. Chem. Soc.*, 1978, **100**, 7112-7114.
49. P. J. Fagan, K. G. Moloy and T. J. Marks, *J. Am. Chem. Soc.*, 1981, **103**, 6959-6962.
50. I. Korobkov, S. Gorelsky and S. Gambarotta, *J. Am. Chem. Soc.*, 2009, **131**, 10406-10420.
51. I. Korobkov, S. Gambarotta and G. P. A. Yap, *Angew. Chem., Int. Ed. Engl.*, 2003, **42**, 814-818.
52. Z. Lin, J. F. Le Marechal, M. Sabat and T. J. Marks, *J. Am. Chem. Soc.*, 1987, **109**, 4127-4129.
53. X. Yang, W. A. King, M. Sabat and T. J. Marks, *Organometallics*, 1993, **12**, 4254-4258.
54. W. Ren, G. Zi, D.-C. Fang and M. D. Walter, *Chem. Eur. J.*, 2011, **17**, 12669-12682.
55. R. R. Langeslay, J. R. Walensky, J. W. Ziller and W. J. Evans, *Inorg. Chem.*, 2014, **53**, 8455-8463.
56. X. Yang, C. Stern and T. J. Marks, *Organometallics*, 1991, **10**, 840-842.
57. S. W. Hall, J. C. Huffman, M. M. Miller, L. R. Avens, C. J. Burns, A. P. Sattelberger, D. S. J. Arney and A. F. England, *Organometallics*, 1993, **12**, 752-758.
58. C. E. Hayes, R. H. Platel, L. L. Schafer and D. B. Leznoff, *Organometallics*, 2012, **31**, 6732-6740.

59. C. A. Cruz, D. J. H. Emslie, C. M. Robertson, L. E. Harrington, H. A. Jenkins and J. F. Britten, *Organometallics*, 2009, **28**, 1891-1899.
60. C. M. Fendrick, L. D. Schertz, V. W. Day and T. J. Marks, *Organometallics*, 1988, **7**, 1828-1838.
61. C. M. Fendrick, E. A. Mintz, L. D. Schertz and T. J. Marks, *Organometallics*, 1984, **3**, 819-821.
62. P. G. Edwards, R. A. Andersen and A. Zalkin, *Organometallics*, 1984, **3**, 293-298.
63. W. Ren, N. Zhao, L. Chen and G. Zi, *Inorg. Chem. Commun.*, 2013, **30**, 26-28.
64. S. Fortier, B. C. Melot, G. Wu and T. W. Hayton, *J. Am. Chem. Soc.*, 2009, **131**, 15512-15521.
65. D. K. Cabbiness and D. W. Margerum, *J. Am. Chem. Soc.*, 1969, **91**, 6540-6541.
66. R. C. White, PhD Thesis, The University of Edinburgh, 2014.
67. I. Grenthe, J. Drożdżyński, T. Fujino, E. C. Buck, T. E. Albrecht-Schmitt and S. F. Wolf, in *The Chemistry of the Actinide and Transactinide Elements*, eds. L. R. Morss, N. M. Edelstein and J. Fuger, Springer Netherlands, Dordrecht, 2006, DOI: 10.1007/1-4020-3598-5_5, pp. 253-698.
68. B. Cordero, V. Gomez, A. E. Platero-Prats, M. Reves, J. Echeverria, E. Cremades, F. Barragan and S. Alvarez, *Dalton Trans.*, 2008, DOI: 10.1039/B801115J, 2832-2838.
69. A. K. Dash, J. Q. Wang, J. Wang, I. Gourevich and M. S. Eisen, *J. Nucl. Sci. Technol.*, 2002, **39**, 386-392.
70. A. K. Dash, J. Q. Wang and M. S. Eisen, *Organometallics*, 1999, **18**, 4724-4741.
71. R. K. Thomson, C. R. Graves, B. L. Scott and J. L. Kiplinger, *Eur. J. Inorg. Chem.*, 2009, **2009**, 1451-1455.
72. W. J. Evans, N. A. Siladke and J. W. Ziller, *C. R. Chim.*, 2010, **13**, 775-780.
73. E. Montalvo, J. W. Ziller, A. G. DiPasquale, A. L. Rheingold and W. J. Evans, *Organometallics*, 2010, **29**, 2104-2110.
74. W. J. Evans, J. R. Walensky and J. W. Ziller, *Organometallics*, 2010, **29**, 945-950.
75. C. R. Graves, B. L. Scott, D. E. Morris and J. L. Kiplinger, *Organometallics*, 2008, **27**, 3335-3337.
76. B. S. Newell, A. K. Rappé and M. P. Shores, *Inorg. Chem.*, 2010, **49**, 1595-1606.
77. A. D. Bond and J. E. Davies, *Acta Crystallogr., Sect. E*, 2002, **58**, o777-o778.
78. H. Čičak, H. Vančik and Z. Mihalić, *J. Org. Chem.*, 2010, **75**, 6969-6972.
79. Bettonville, S., Goffart, J., Fuger and J., *Organo-f-element thermochemistry. Actinide-ligand bond disruption enthalpies in tris(indenyl)actinide hydrocarbyls*, Elsevier, Lausanne, SUISSE, 1989.
80. J. W. Bruno, H. A. Stecher, L. R. Morss, D. C. Sonnenberger and T. J. Marks, *J. Am. Chem. Soc.*, 1986, **108**, 7275-7280.
81. L. E. Schock, A. M. Seyam, M. Sabat and T. J. Marks, *Polyhedron*, 1988, **7**, 1517-1529.
82. F. G. Bordwell, *Acc. Chem. Res.*, 1988, **21**, 456-463.
83. N. L. Bell, L. Maron and P. L. Arnold, *J. Am. Chem. Soc.*, 2015, **137**, 10492-10495.
84. C. A. P. Goodwin and D. P. Mills, *Organomet. Chem.*, 2017, **41**, 123-156.
85. G. Dominguez and J. Perez-Castells, *Chem. Soc. Rev.*, 2011, **40**, 3430-3444.
86. L. Zhang, G. Hou, G. Zi, W. Ding and M. D. Walter, *J. Am. Chem. Soc.*, 2016, **138**, 5130-5142.
87. B. Fang, W. Ren, G. Hou, G. Zi, D.-C. Fang, L. Maron and M. D. Walter, *J. Am. Chem. Soc.*, 2014, **136**, 17249-17261.
88. T. Andrea and M. S. Eisen, *Chem. Soc. Rev.*, 2008, **37**, 550-567.
89. Z. M. Heiden and A. P. Lathem, *Organometallics*, 2015, **34**, 1818-1827.
90. E. Vedejs, S. M. Duncan and A. R. Haight, *J. Org. Chem.*, 1993, **58**, 3046-3050.
91. I. Haiduc, *Organometallics*, 2004, **23**, 3-8.
92. I. Korobkov, S. Gambarotta and G. P. A. Yap, *Angew. Chem., Int. Ed. Engl.*, 2002, **41**, 3433-3436.

93. M. S. Dutkiewicz, J. H. Farnaby, C. Apostolidis, E. Colineau, O. Walter, N. Magnani, M. G. Gardiner, J. B. Love, N. Kaltsoyannis, R. Caciuffo and P. L. Arnold, *Nat. Chem.*, 2016, **8**, 797-802.
94. O. P. Lam and K. Meyer, *Polyhedron*, 2012, **32**, 1-9.
95. P. L. Arnold and Z. R. Turner, *Nat. Rev. Chem.*, 2017, **1**, 0002.
96. E. M. Matson, P. E. Fanwick and S. C. Bart, *Organometallics*, 2011, **30**, 5753-5762.
97. S. M. Mansell, N. Kaltsoyannis and P. L. Arnold, *J. Am. Chem. Soc.*, 2011, **133**, 9036-9051.
98. W. G. Sly, *J. Am. Chem. Soc.*, 1959, **81**, 18-20.
99. F. A. Cotton, J. D. Jamerson and B. R. Stults, *J. Am. Chem. Soc.*, 1976, **98**, 1774-1779.
100. Y. Iwashita, F. Tamura and A. Nakamura, *Inorg. Chem.*, 1969, **8**, 1179-1183.
101. M. Zirngast, C. Marschner and J. Baumgartner, *Organometallics*, 2006, **25**, 4897-4908.
102. S. M. Draper, C. Long and B. M. Myers, *J. Organomet. Chem.*, 1999, **588**, 195-199.
103. C. H. Bamford and S. U. Mullik, *J. Chem. Soc., Faraday Trans.*, 1976, **72**, 368-375.
104. M. Peruzzini, R. R. Abdreimova, Y. Budnikova, A. Romerosa, O. J. Scherer and H. Sitzmann, *J. Organomet. Chem.*, 2004, **689**, 4319-4331.
105. M. Peruzzini, L. Gonsalvi and A. Romerosa, *Chem. Soc. Rev.*, 2005, **34**, 1038-1047.
106. D. Yang, S. Sarina, H. Zhu, H. Liu, Z. Zheng, M. Xie, S. V. Smith and S. Komarneni, *Angew. Chem., Int. Ed. Engl.*, 2011, **50**, 10594-10598.
107. T. Sangvanich, V. Sukwarotwat, R. J. Wiacek, R. M. Grudzien, G. E. Fryxell, R. S. Addleman, C. Timchalk and W. Yantasee, *J. Hazard. Mater.*, 2010, **182**, 225-231.
108. M. R. Crampton and I. A. Robotham, *J. Chem. Res., Synop.*, 1997, DOI: 10.1039/A606020J, 22-23.
109. I. Korobkov, B. Vidjayacoumar, S. I. Gorelsky, P. Billone and S. Gambarotta, *Organometallics*, 2010, **29**, 692-702.
110. P. L. Arnold, J. H. Farnaby, M. G. Gardiner and J. B. Love, *Organometallics*, 2015, **34**, 2114-2117.
111. B. D. Stubbert and T. J. Marks, *J. Am. Chem. Soc.*, 2007, **129**, 6149-6167.
112. R. J. Butcher, D. L. Clark, S. K. Grumbine and J. G. Watkin, *Organometallics*, 1995, **14**, 2799-2805.
113. B. L. Edelbach, R. J. Lachicotte and W. D. Jones, *Organometallics*, 1999, **18**, 4660-4668.
114. U. Rosenthal, S. Pulst, P. Arndt, A. Ohff, A. Tillack, W. Baumann, R. Kempe and V. V. Burlakov, *Organometallics*, 1995, **14**, 2961-2968.
115. P. Hofmann, A. Perez-Moya Luis, E. Krause Martin, O. Kumberger and G. Müller, *Journal*, 1990, **45**, 897.
116. D. Shang-Chao, T. Hua-Qiao, B. Yan-Feng, Y. Yang and L. Wu-Ping, *Chin. J. Inorg. Chem.*, 2014, **30**, 749-756.
117. J. M. Ritchey, A. J. Zozulin, D. A. Wrobleski, R. R. Ryan, H. J. Wasserman, D. C. Moody and R. T. Paine, *J. Am. Chem. Soc.*, 1985, **107**, 501-503.

Chapter Three: Oxidation of Uranium *Trans*-Calix[2]Benzene[2]Pyrrolide Complexes

3.1 Accessing Uranium-Oxo Complexes

A literature survey of U^{V}-dioxo complexes was presented in Chapter One, Section 1.4. This showed that the majority of U^{V}-dioxo complexes are accessed by the reduction of uranyl, with only one example of systematic and reproducible oxidation of U^{IV} to afford the U^{V}-dioxo coordination polymer $\{[UO_2(py)_5][KI_2(py)_2]\}_n$.[1] Additionally, Hayton reported the synthesis of a silylamide-supported U^{V}-monooxo complex, $[OU(N(SiMe_3)_2)_3]$ (**3.2** in Figure 3.1), *via* the oxidation of U^{III} complex $[U(N(SiMe_3)_2)_3]$ with pyridine-*N*-oxide.[2] An anionic U^{IV}-monooxo complex $[OU(N(SiMe_3)_2)_3{\cdot}K(18\text{-c-}6)]$ (**3.1** in Figure 3.1) was also synthesised by the removal of a trityl anion from U^{IV} complex $[(Ph_3CO)U(N(SiMe_3)_2)_3]$ using KC_8 in the presence of 18-crown-6.[3] Although U^{VI} uranyl is a thermodynamic sink, some examples of U^{VI}-monooxo complexes have been reported to date,[4-6] such as complexes $[OU(R)(N(SiMe_3)_2)_3]$ (R = Me (**3.3a**), C≡CPh (**3.3b**) in Figure 3.1) synthesised *via* the addition of *N*-methylmorpholine-*N*-oxide to U^{IV} alkyl complexes $[U(R)(N(SiMe_3)_2)_3]$.[5]

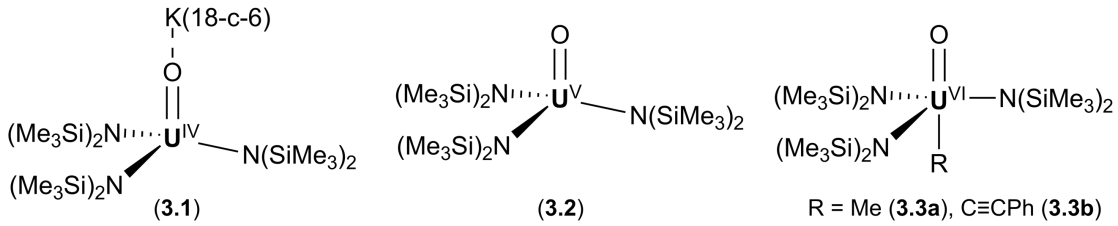

Figure 3.1 Uranium-monooxo complexes $[OU(N(SiMe_3)_2)_3{\cdot}K(18\text{-c-}6)]$ (**3.1**), $[OU(N(SiMe_3)_2)_3]$ (**3.2**) and $[OU(R)(N(SiMe_3)_2)_3]$ (R = Me (**3.3a**), C≡CPh (**3.3b**)).[2, 3, 5]

3.2 Uranium(V)-Dioxo Complex

It was mentioned in Chapter Two, Section 2.5.3 that complex $[Li(L^{-2H})U(Me)]$ (**8**) decomposes slowly in solution over three weeks. It was found that the crystallisation of An^{IV} alkyl complexes $[Li(L^{-2H})An(CH_2SiMe_3)]$ (An = Th (**6**), U (**9**)) was successful in the presence of LiCl. An attempt was therefore made to crystallise **8** in the presence of residual LiI from its synthesis using $[(L)UI_2]$ (**B**) rather than $[(L)UCl_2]$ (**1**). A saturated solution of **8** and trace LiI

in THF was stored at -20 °C, however it was found that the THF used contained trace amounts of H_2O. After two weeks red X-ray quality crystals of a U^V-dioxo complex $[(L)U(OLi\{THF\}_3)_2]I$ (**26**) were isolated in 20 % yield (Figure 3.2). NMR spectra of **26** could not be obtained because **26** did not dissolve in C_6D_6, THF-d_8 or pyridine-d_5 and decomposed in $CDCl_3$. Elemental analysis confirmed the composition of **26**. An insufficient amount of material remained for FTIR spectroscopic analysis.

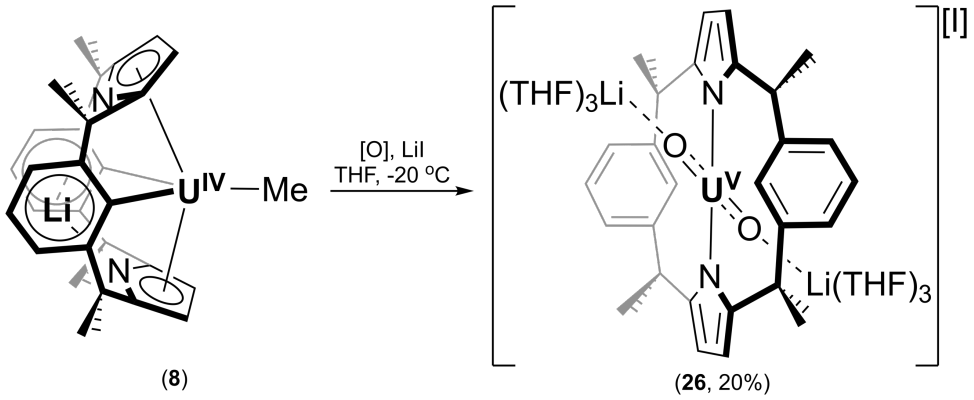

(**8**) (**26**, 20%)

Scheme 3.1 Synthesis of $[(L)U(OLi\{THF\}_3)_2]I$ (**26**) from **8** using an oxidant, [O].

The formation of **26** is described in Scheme 3.1 with a proposed mechanism given in Scheme 3.2. The synthesis of **26** could not be reproduced, the mechanism is therefore speculative. However, three key events must happen for **26** to form, namely: (1) protonation of the methyl group to give methane (Scheme 3.2, step 2), (2) reprotonation of the arene rings (Scheme 3.2, steps 3 and 4), (3) oxidation of U^{IV} to U^V. It is unclear how the oxidation step occurs in this reaction, however Meyer recently isolated intermediates in the oxidation reaction of a U^{III} to U^{IV} using H_2O (Scheme 3.3).[7] These intermediates suggest that during the oxidation of one equivalent of U^{III} with one equivalent of H_2O, a U^V-hydroxo-hydrido intermediate forms, which then eliminates H_2 and forms a U^V-monooxo. A comproportionation reaction between a U^{III}-hydrate and a U^V-monooxo then occurs to give two equivalents of a U^{IV}-hydroxide complex.[7]

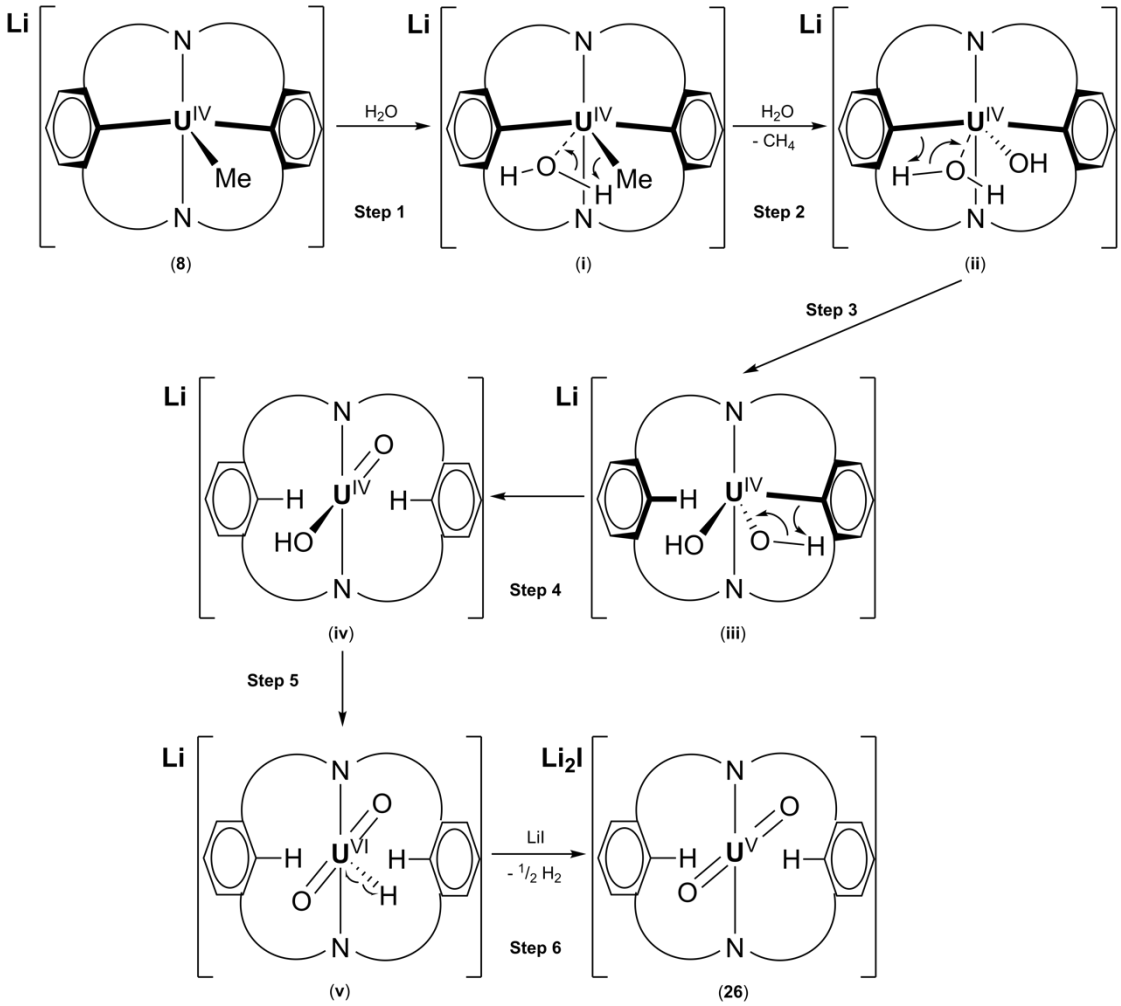

Scheme 3.2 Proposed mechanism of formation of **26** from **8**.

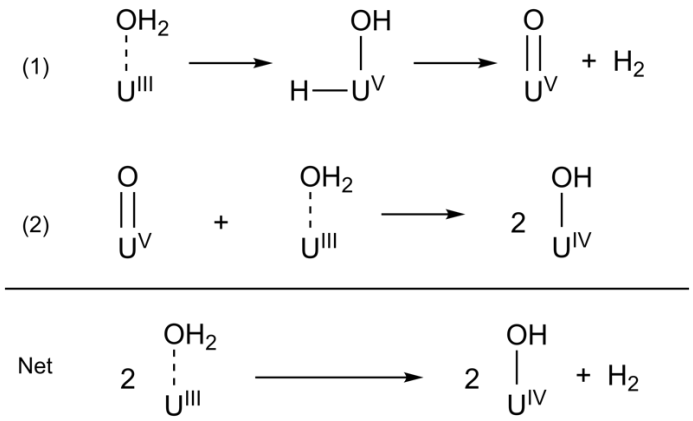

Scheme 3.3 Intermediates isolated in the oxidation reaction of a U^{III} to U^{IV} using H_2O.[7]

It is possible that a similar reaction mechanism is taking place during the formation of **26**, where intermediate **iv** (Scheme 3.2) is a U^{IV}-oxohydroxo complex in which the O–H bond metallates to give intermediate **v**, a U^{VI}-oxohydroxo-hydrido complex. The hydride is then lost

in step 6 as a radical H·, which combines with another equivalent of H· to give H_2 and **26**. Potentially, intermediates **iv** and **v** could be dimeric facilitating the formation of H_2.

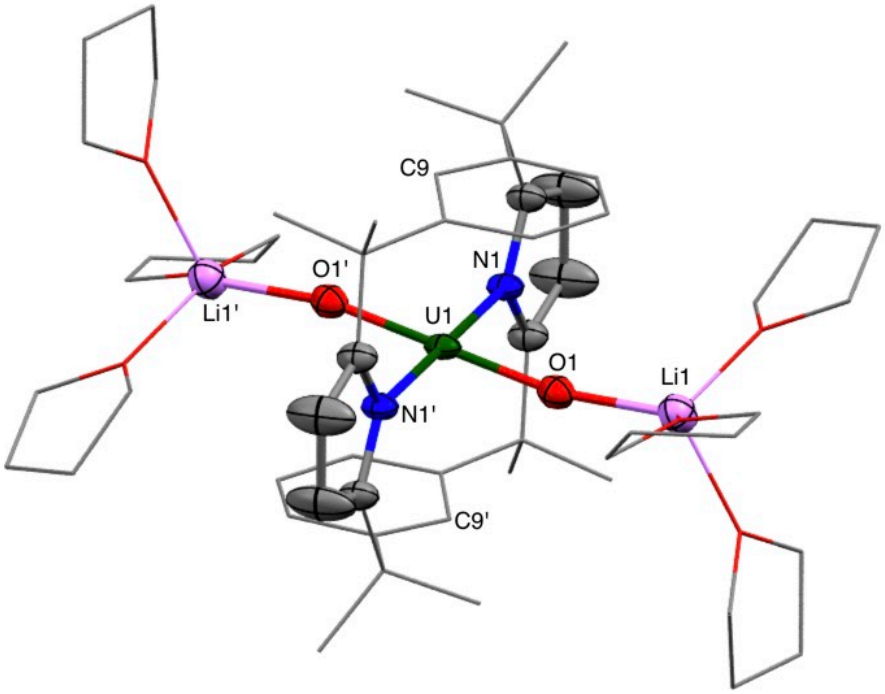

Figure 3.2 Solid-state structure of **26** (thermal ellipsoids set at 50 % probability level). Hydrogen atoms and iodide counterion are omitted, with the phenyl rings and alkyl linkers depicted as wire-frame for clarity. Selected bond lengths (Å) and angles (°) for **26**: U1–O1 1.862(2), U1–N1 2.385(3), O1–Li1 1.917(7), U1–C9 2.763(3), N1–U1–N1′ 180.00(13), C9–U1–C9′ 180.0, O1–U1–O1′ 180.0, N1–U1–O1 90.00(10), O1–U1–C9 74.72(10), O1–U1–C9′ 105.28(10).

The highly-symmetric solid-state structure of **26** (Figure 3.2) shows a new binding mode for $(L)^{2-}$. Here, the uranium is κ^1-bound to the pyrrolic nitrogens with a N1–U1–N1′ angle of 180.00(13)°. Carbon atoms C9 and C9′ are located on a mirror-plane above and below the uranium with a C9–U1–C9′ angle of 180.0°. The O1–U1–O1′ angle is also perfectly linear and located on a mirror plane. The N1–U1–O1 angle is 90.00(10)°, however the U1–C9 and U1–C9′ bonds are not perfectly perpendicular to the U1–O1/O1′ bonds with O1–U1–C9 and O1–U1–C9′ angles of 74.72(10)° and 105.28(10)°, respectively. Further examination of the crystal shows that the arene rings of the macrocycle are not planar, with C9 located 0.12 Å above the plane of the arene. The slight twisting of the macrocycle indicates that the U^V centre is η^2-coordinated to the arene rings. The arene distortion from planar symmetry might suggest some degree of π-backbonding from the uranium to the arenes, however there appears to be no significant elongation of any of the arene carbon-carbon bonds. The U1–O1 bond length in **26** is 1.862(2) Å, which is slightly longer than that found in the U^V coordination polymer $\{[UO_2(py)_5][KI_2(py)_2]\}_n$ (U–O bond average: 1.835(2) Å).[1] The U1–O1 bond length in **26** is

comparable to those observed in U^{V}-dioxo complexes $[\{UO_2(py)_5\}_2LnI_4]I$ (Ln = Sm, Dy) and a range of Pacman-supported U^{V}-dioxo complexes reported by Arnold and Love. [8-17] Hayton's silylated U^{V}-dioxo complexes supported by β-ketoiminate and β-ketonate ligands display longer U1–O1 (1.986(5)-2.044(2) Å) bonds than **26**.[18-20]

3.3 Uranium(IV)-μ-Oxo Complex

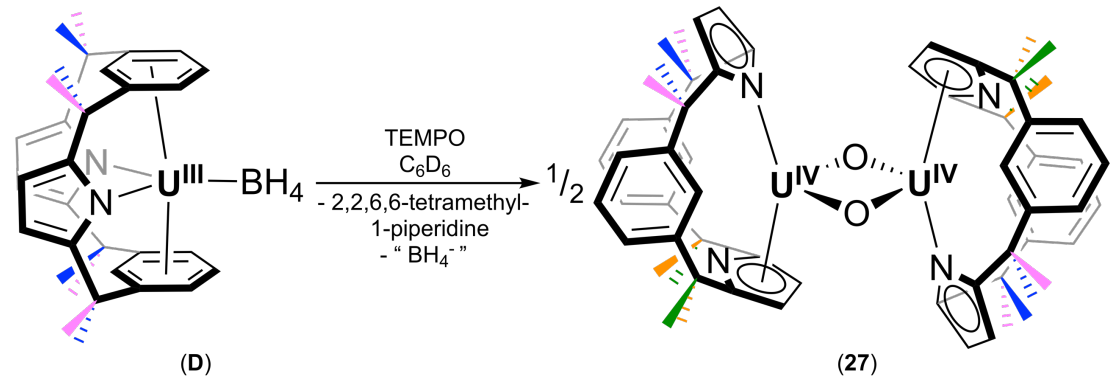

(**D**) (**27**)

two methyl-H environments: *endo* and *exo* four methyl-H environments: *endo*, *exo* and *endo*, *exo*

Scheme 3.4 Oxidation of $[(L)U(BH_4)]$ (**D**) to $[(L)U(O)]_2$ (**27**). Symmetrically inequivalent methyl groups are shown in blue, pink, orange and green.

A group member, Dr Rianne M. Lord, added one equivalent of oxygen-atom transfer agent TEMPO to U^{III} bis-arene complex $[(L)U(BH_4)]$ (**D** in Scheme 3.4), reported previously by our group,[21] which afforded pale orange X-ray quality crystals of a U^{IV}-μ-oxo complex $[(L)U(O)]_2$ (**27**) (Figure 3.3), isolated from a saturated C_6D_6 solution, in poor yield. The solid-state structure of **27** shows that the macrocyclic ligand rearranges from the $\kappa^1{:}\eta^6{:}\kappa^1{:}\eta^6$ binding mode in **D** to afford a new binding mode for $(L)^{2-}$. Here, the macrocycle is desymmetrised with one pyrrolide κ^1-bound and the second pyrrolide η^5-bound to uranium. In complexes **1**-**16**, **18**-**25** and **D**,[21] two resonances for the methyl groups of the macrocycle (*endo* and *exo*: shown in blue and pink on **D** in Scheme 3.4), integrating to 12H each, are characteristic of C_{2v} symmetry. Although the ^{1}H NMR spectroscopic resonances of **27** are shifted and broadened due to the paramagnetism of the U^{IV} f^2 ion, four new resonances for the methyl groups of the macrocycle can be identified, integrating to 6H each (two sets of *endo* and *exo* resonances: shown in blue, pink, orange and green in Scheme 3.4). This indicates that the desymmetrisation of the macrocycle from C_{2v} to C_{2h} symmetry in **27** is also seen in solution.

The flexibility of the macrocycle allows for the two uranium centres in **27** to come close to each other (3.418(1) Å) by adopting the new $\kappa^1{:}\eta^5$ coordination mode. The arenes of the macrocycle in **1** and **15** are oriented away from the uranium centre, whereas the arenes in **27** are oriented towards the uranium centre, once again demonstrating the adaptability of this

ligand system to a range of substituents. A handful of U^{IV}-μ-oxo complexes have been reported in the literature,[22-24] such as the U^{IV} metallocene $[(Cp'')U(O)]_2$ (U1–O1, U1–O1′: 2.096(6), 2.129(5) Å),[25] with U1–O1 and U1–O1′ bond lengths similar to those in **27** (2.112(5) Å and 2.141(5) Å). The distance between the uranium centres in **27** (3.418(1) Å) is also comparable to literature distances (avg. 3.422 Å).[22-25]

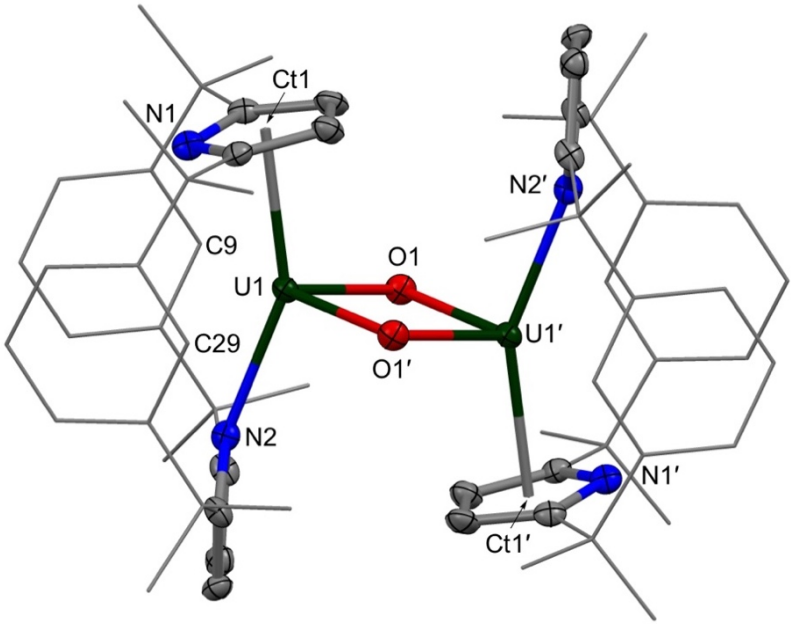

Figure 3.3 Solid-state structure of **27** (thermal ellipsoids set at 50 % probability level). Hydrogen atoms and iodide counterion are omitted, with the phenyl rings and alkyl linkers depicted as wire-frame for clarity. Selected bond lengths (Å) and angles (°) for **27**: U1–O1 2.112(5), U1–O1′ 2.141(5), U1–N2 2.471(6), U1–Ct1 2.535(4), U1–U1′ 3.418(1), N2–U1–Ct1 151.87, U1–O1–U1′ 106.96(19), O1–U1–O1′ 73.0(2), C9–U1–C29 125.00.

3.4 Synthesis of Uranium(IV)-Oxo Complexes

3.4.1 D_2O

Based on the postulated synthetic route to **26** (Scheme 3.2), two equivalents of D_2O were added to $[Li(L^{-2H})U(Me)]$ (**8**) in THF *via* syringe. The solution discoloured immediately and dark precipitate formed. The ^1H NMR and ^2H NMR spectra showed the presence of D_4L and trace DCH_3 with no paramagnetic resonances remaining. This reaction was repeated with one equivalent of D_2O, however the same products were obtained. This reaction was then repeated with a lower concentration of D_2O in solution by adding one equivalent of a 0.1 M solution of D_2O in THF to **8** in THF. The resulting solution discoloured over 5 minutes, D_4L and trace DCH_3 were once again observed with no paramagnetic resonances remaining. Addition of LiI, or performing reactions at -20 °C had no effect on the outcomes of the reactions. Attempts were also made to access U^V- or U^{VI}-oxo complexes from the oxidation of

[(L)U(C≡CSiMe$_3$)$_2$] (**14**), however addition of D_2O using the methods described above resulted in the formation of D_2L and dark precipitate. These observations indicate that U^{VI}-oxo products, such as clusters, may be precipitating and ligand deuteration and abstraction occurs simultaneously.

3.4.2 Oxygen-Atom Transfer Reagents

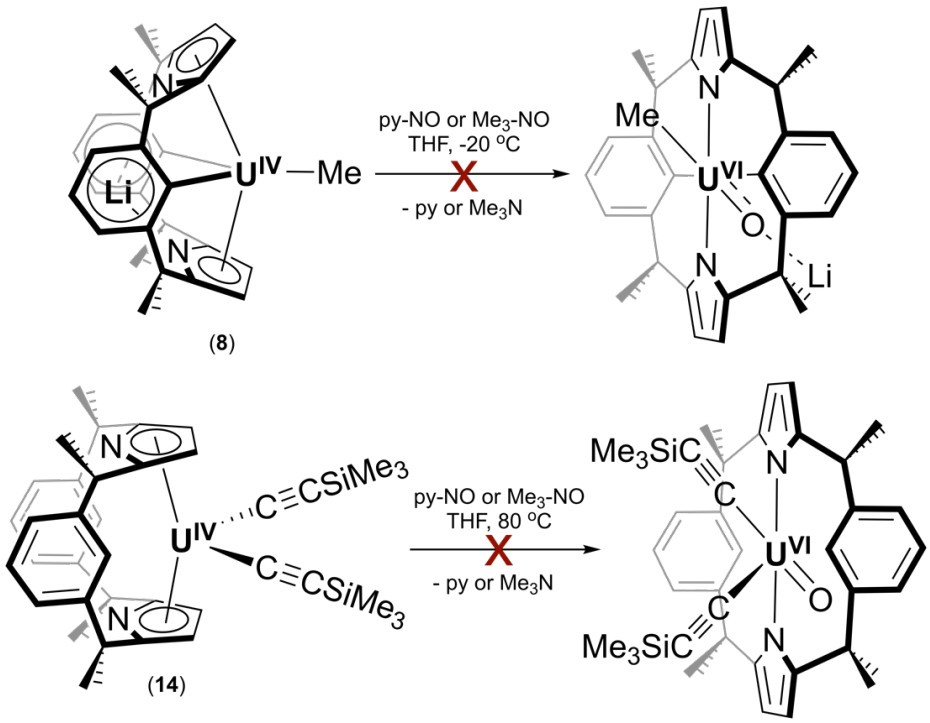

Scheme 3.5 Attempted synthesis of U^{VI}-monooxo complexes from **8** and **14**.

The U^{VI}-monooxo complexes [OU(R)(N(SiMe$_3$)$_2$)$_3$] (R = Me (**3.3a**), C≡CPh (**3.3b**) in Figure 3.1) were synthesised *via* the addition of *N*-methylmorpholine-*N*-oxide to U^{IV} alkyl complexes [U(R)(N(SiMe$_3$)$_2$)$_3$].[5] Due to the ligand deuteration to D_4L when using D_2O, U^{IV} oxidation reactions were carried out in the absence of a proton source to ascertain whether U^{VI}-monooxo complexes of this ligand system would form. One equivalent of pyridine-*N*-oxide was added to **8** to determine whether a two-electron oxidation would yield a U^{VI}-monooxo complex cleanly (Scheme 3.5). An inseparable mixture of diamagnetic products formed, indicating that U^{VI} had been synthesised, though not cleanly. Slow addition of a pyridine-*N*-oxide solution in THF to **8** at -20 °C also resulted in the formation of a mixture of inseparable diamagnetic products. No reaction occurred upon the addition of one equivalent of pyridine-*N*-oxide to **14** at room temperature (Scheme 3.5). Heating at 80 °C for 10 minutes showed oxidation of approximately 20 % of material to a mixture of diamagnetic products. Oxidation using the stronger oxidant trimethylamine-*N*-oxide gave analogous results.

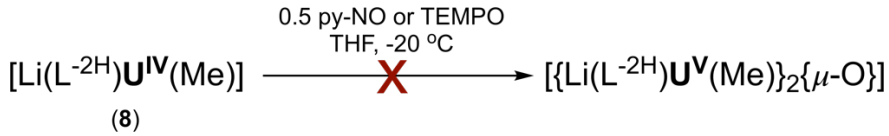

Scheme 3.6 Attempted synthesis of a bridging U^{V}-μ-oxo complex.

Similarly to the synthesis of **27** (Scheme 3.4), attempts were made to synthesise a bridging U^{V}-μ-oxo complex via the addition 0.5 equivalents of pyridine-*N*-oxide or TEMPO to **8** in THF at -20 °C (Scheme 3.6). This resulted in incomplete conversion to mixture of inseparable diamagnetic products using pyridine-*N*-oxide. An inseparable mixture of diamagnetic products formed immediately when using TEMPO instead.

These results suggest that the oxidation of **8** to U^{VI}-oxo products occurs, however this reactivity cannot be easily controlled. It was therefore concluded that the oxidation of **8** to a U^{V}-oxo complex was unlikely to occur in a controlled manner without a proton source to reprotonate the methyl substituent or the arene rings of the macrocycle. It is interesting that **14** is remarkably stable against oxidation, perhaps due to the strength and rigidity of the U–alkynyl bonds, resulting in insufficient flexibility to accommodate an oxo-group.[26]

3.4.3 Hydroxides

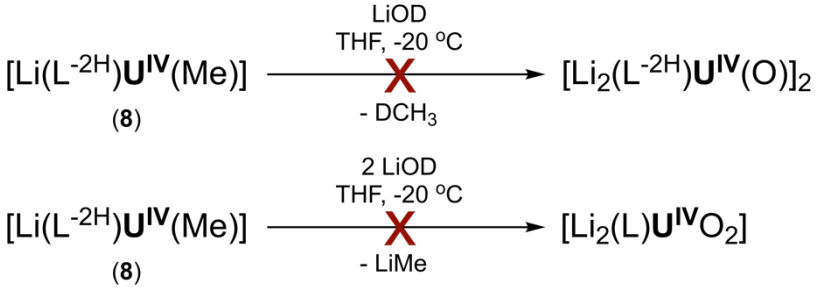

Scheme 3.7 Attempted synthesis of U^{IV}-μ-oxo and U^{IV}-dioxo complexes.

In order to achieve controlled reprotonation of the macrocycle without oxidising the metal centre, LiOD was used in an effort to synthesise U^{IV}-μ-oxo and U^{IV}-dioxo complexes (Scheme 3.7). One equivalent of LiOD was added to a solution of **8** in THF at -20 °C. There was no indication of DCH_3 liberation in the ^{1}H NMR spectrum of the crude mixture. After work-up, the ^{1}H NMR spectrum showed that approximately 16 % of the reaction mixture had converted to at least two paramagnetic products with resonances located from 84.2 to 33.73 ppm, 16 % to D_4L and 67 % to Li_4L. The ^{2}H NMR spectrum however showed only the fully deuterated D_4L, suggesting that the paramagnetic product had not been deuterated. Unfortunately, the paramagnetic products could not be isolated cleanly, however the addition of D_2O to the products resulted in their decomposition, liberation of DCH_3 and an increased

concentration of D_4L in solution. These observations suggest that methyl-containing U^{IV}- or U^{V}-oxo complexes had likely been synthesised (Figure 3.4) and were supported by the macrocycle in its $(L^{-2H})^{4-}$ form. As the formation of these products is not stoichiometric, the presence of excess Li^+ in solution could stabilise various oxidation states of uranium. Interestingly, the addition of two equivalents of LiOD to **8** resulted in the same ratio of products and unreacted LiOD.

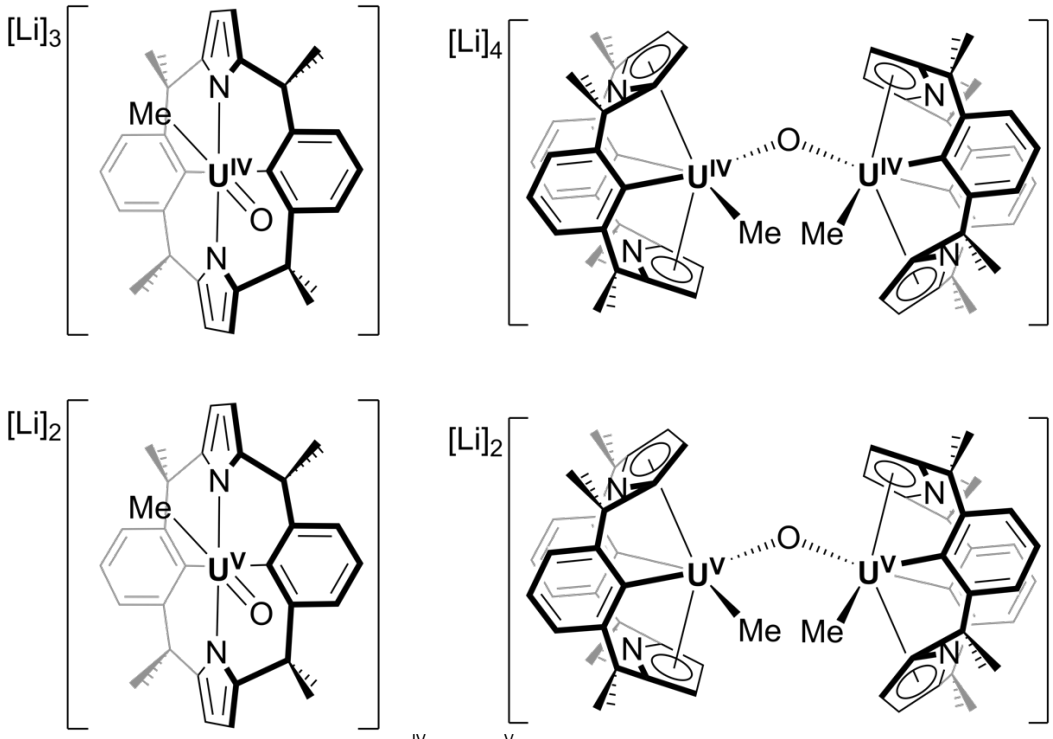

Figure 3.4 Possible paramagnetic U^{IV}- and U^{V}-oxo products from the reaction of **8** with LiOD.

The formation of Hayton's U^{IV}-monooxo complex $[OU(N(SiMe_3)_2)_3][K(18\text{-c-}6)]$ from the reaction of the U^{IV} alkoxide $[(Ph_3CO)U(N(SiMe_3)_2)_3]$ with KC_8 in the presence of 18-crown-6,[3] inspired the use of triphenylmethanol in this work. It was postulated that triphenylmethanol would allow for the synthesis of a U–O bond and the reprotonation of the aryls of the macrocycle in **8**, without a change in oxidation state and without introducing excess Li^+ (Scheme 3.8). Two or three equivalents of Ph_3COH were added to a solution of **8** in THF at -20 °C: a mixture of at least two paramagnetic products and inseparable diamagnetic products formed. No reaction occurred upon the addition of two equivalents of Ph_3COH to **14**, which is likely to result from the strength of the uranium-alkynyl bonds. Addition of two or three equivalents of Me_3SiOH to **8** in THF at -20 °C resulted in a mixture of diamagnetic products.

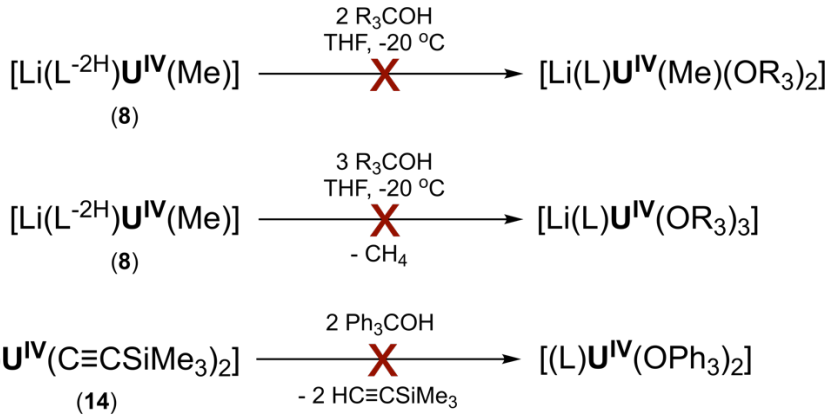

Scheme 3.8 Attempted aryl and methyl reprotonation in **8** and **14** using ROH (R = CPh_3, $SiMe_3$).

These results show that although uranium-oxo products form, in most cases mixtures of products are obtained. Although the flexibility of the macrocyclic ligand can be advantageous to the accommodation of a range of substituents, it is likely that it can also result in the formation of multiple coordination complexes from a single reaction. Additionally, when targeting U^{V}-oxo complexes, it is perhaps unsurprising that oxidation to thermodynamically stable diamagnetic uranyl(VI) occurs preferentially.

3.4.4 Air

Mazzanti reported that the oxidation of $[UI_3(THF)_4]$ to coordination polymer $\{[UO_2(py)_5][KI_2(py)_2]\}_n$ was also observed when air was allowed to slowly diffuse into a pyridine solution of $[UI_3(THF)_4]$.[1] Slow diffusion of air into a solution of **8** or **14** in C_6D_6 resulted in the formation of H_2L and dark precipitate. Once again this indicated that oxidation of U^{IV} had occurred, however ligand protonation and demetallation occurred simultaneously.

3.4.5 Salt Metathesis Routes

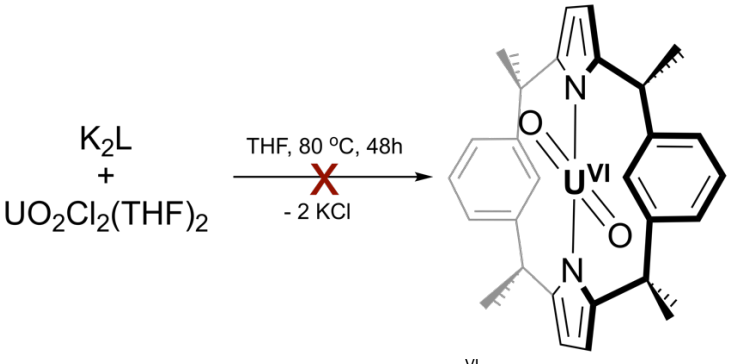

Scheme 3.9 Attempted synthesis of U^{VI} complex $[(L)UO_2]$.

Mazzanti and co-workers showed that the coordination polymer $\{[UO_2(py)_5][KI_2(py)_2]\}_n$ could be used to access other U^{V}-oxo complexes via salt metathesis

with ligand salts such as salenK_2.[27] Reaction of $\{[UO_2(py)_5][KI_2(py)_2]\}_n$ with K_2L in THF was attempted to synthesise the potassium analogue of **26**, however this resulted in the formation of an inseparable paramagnetic and diamagnetic product mixture. In order to establish whether a uranyl(VI) complex $[(L)UO_2]$ could be synthesised by salt metathesis, uranyl(VI) chloride, $[UO_2Cl_2(THF)_2]$, and K_2L were heated at 80 °C for 48 hours (Scheme 3.9). Surprisingly, no reaction occurred. This suggests that although a rogue crystal of **26** was obtained, the uranium-dioxo moiety is perhaps insufficiently stabilised by the macrocyclic ligand system $(L)^{2-}$, meaning that uranium-oxo complexes or clusters form preferentially outside of the ligand framework.

3.5 Summary and Conclusions for Chapter Three

Two new oxidation products, the U^V complex $[(L)U(OLi\{THF\}_3)_2]I$ (**26**) and the U^{IV} complex $[(L)U(O)]_2$ (**27**), supported by *trans*-calix[2]benzene[2]pyrrolide, $(L)^{2-}$, have been isolated from the oxidation of the U^{IV} complex $[Li(L^{-2H})U(Me)]$ (**8**) and the U^{III} complex $[(L)U(BH_4)]$ (**D**), respectively. **26** is a rare example of U^{IV} oxidation to a U^V-dioxo. Unfortunately, a reproducible oxidation route to the synthesis of **26** could not be established. Although complex **27** is isolated in low yields, it is also one of a small number of U^{IV}-μ-oxo complexes.

Attempts were made to establish reproducible oxidation routes to a range of U^V- and U^{VI}-oxo complexes supported by $(L)^{2-}$ and $(L^{-2H})^{4-}$ from the U^{IV} complexes $[Li(L^{-2H})U(Me)]$ (**8**) and $[(L)U(C{\equiv}CSiMe_3)_2]$ (**14**). Although oxidation was successful in many cases, inseparable mixtures of products, with uranium in various oxidation states, were obtained. It is possible that in addition to oxidation state disproportionation, the flexibility of this ligand system led to the formation of multiple products as a result of varying ligand coordination. Additionally, the salt metathesis reaction of the U^V coordination polymer $\{[UO_2(py)_5][KI_2(py)_2]\}_n$ with K_2L did not proceed cleanly and the reaction of uranyl(VI) chloride $[UO_2Cl_2(THF)_2]$ with K_2L did not occur.

These observations suggest that despite the isolation of the rogue complex **26**, the *trans*-calix[2]benzene[2]pyrrolide ligand is not well suited to supporting the uranium-dioxo dication. As the oxidation state of uranium increases, it becomes 'harder' as its ionic radius decreases,[28] resulting in an increased preference for ionic bonding. Perhaps the macrocyclic ligand system used in this work, containing only two N-donors, provides poor electronic stabilisation around the equatorial plane of the uranium-dioxo dication resulting in its demetallation in reactions presented herein.

3.6 References for Chapter Three

1. L. Natrajan, F. Burdet, J. Pécaut and M. Mazzanti, *J. Am. Chem. Soc.*, 2006, **128**, 7152-7153.
2. S. Fortier, J. L. Brown, N. Kaltsoyannis, G. Wu and T. W. Hayton, *Inorg. Chem.*, 2012, **51**, 1625-1633.
3. D. E. Smiles, G. Wu and T. W. Hayton, *J. Am. Chem. Soc.*, 2014, **136**, 96-99.
4. A. J. Lewis, P. J. Carroll and E. J. Schelter, *J. Am. Chem. Soc.*, 2013, **135**, 511-518.
5. A. J. Lewis, P. J. Carroll and E. J. Schelter, *J. Am. Chem. Soc.*, 2013, **135**, 13185-13192.
6. S. Fortier, N. Kaltsoyannis, G. Wu and T. W. Hayton, *J. Am. Chem. Soc.*, 2011, **133**, 14224-14227.
7. D. P. Halter, F. W. Heinemann, J. Bachmann and K. Meyer, *Nature*, 2016, **530**, 317-321.
8. P. L. Arnold, E. Hollis, F. J. White, N. Magnani, R. Caciuffo and J. B. Love, *Angew. Chem., Int. Ed. Engl.*, 2011, **50**, 887-890.
9. P. L. Arnold, E. Hollis, G. S. Nichol, J. B. Love, J.-C. Griveau, R. Caciuffo, N. Magnani, L. Maron, L. Castro, A. Yahia, S. O. Odoh and G. Schreckenbach, *J. Am. Chem. Soc.*, 2013, **135**, 3841-3854.
10. P. L. Arnold, B. Cowie, M. Suvova, M. Zegke, N. Magnani, E. Colineau, J.-C. Griveau, R. Caciuffo and J. Love, *Angew. Chem., Int. Ed. Engl.*, 2017, **56**, 10775-10779.
11. P. L. Arnold, M. S. Dutkiewicz, M. Zegke, O. Walter, C. Apostolidis, E. Hollis, A.-F. Pécharman, N. Magnani, J.-C. Griveau, E. Colineau, R. Caciuffo, X. Zhang, G. Schreckenbach and J. B. Love, *Angew. Chem., Int. Ed. Engl.*, 2016, **55**, 12797-12801.
12. G. M. Jones, P. L. Arnold and J. B. Love, *Chem. Eur. J.*, 2013, **19**, 10287-10293.
13. M. Zegke, G. S. Nichol, P. L. Arnold and J. B. Love, *Chem. Commun.*, 2015, **51**, 5876-5879.
14. P. L. Arnold, A.-F. Pecharman, E. Hollis, A. Yahia, L. Maron, S. Parsons and J. B. Love, *Nat. Chem.*, 2010, **2**, 1056-1061.
15. G. M. Jones, P. L. Arnold and J. B. Love, *Angew. Chem., Int. Ed.*, 2012, **51**, 12584-12587.
16. P. L. Arnold, D. Patel, C. Wilson and J. B. Love, *Nature*, 2008, **451**, 315-317.
17. P. L. Arnold, G. M. Jones, S. O. Odoh, G. Schreckenbach, N. Magnani and J. B. Love, *Nat Chem*, 2012, **4**, 221-227.
18. J. L. Brown, G. Wu and T. W. Hayton, *J. Am. Chem. Soc.*, 2010, **132**, 7248-7249.
19. D. D. Schnaars, G. Wu and T. W. Hayton, *Inorg. Chem.*, 2011, **50**, 4695-4697.
20. E. A. Pedrick, G. Wu and T. W. Hayton, *Inorg. Chem.*, 2014, **53**, 12237-12239.
21. P. L. Arnold, C. J. Stevens, J. H. Farnaby, M. G. Gardiner, G. S. Nichol and J. B. Love, *J. Am. Chem. Soc.*, 2014, **136**, 10218-10221.
22. T. Le Borgne, P. Thuery and M. Ephritikhine, *Acta Crystallogr., Sect. C*, 2002, **58**, m8-m9.
23. J. G. Reynolds, A. Zalkin, D. H. Templeton and N. M. Edelstein, *Inorg. Chem.*, 1977, **16**, 1090-1096.
24. W. W. Lukens, P. G. Allen, J. J. Bucher, N. M. Edelstein, E. A. Hudson, D. K. Shuh, T. Reich and R. A. Andersen, *Organometallics*, 1999, **18**, 1253-1258.
25. A. Zalkin and S. M. Beshouri, *Acta Crystallogr., Sect. C*, 1988, **44**, 1826-1827.
26. J. W. Bruno, T. J. Marks and L. R. Morss, *J. Am. Chem. Soc.*, 1983, **105**, 6824-6832.
27. V. Mougel, P. Horeglad, G. Nocton, J. Pécaut and M. Mazzanti, *Angew. Chem.*, 2009, **121**, 8629-8632.
28. L. H. Ahrens, *Geochim. Cosmochim. Acta*, 1952, **2**, 155-169.

Chapter Four: Experimental Details

4.1 General Procedures and Techniques

Standard high-vacuum Schlenk-line techniques and Vac and MBraun glove boxes were used to manipulate and store air- and moisture-sensitive compounds under an atmosphere of dried and deoxygenated dinitrogen. All gases were supplied by BOC gases UK. All glassware was dried in an oven at 160 °C, cooled under 10^{-3} mbar vacuum and then purged with nitrogen. Prior to use, all Fisherbrand® 1.2 μm retention glass microfiber filters and cannulae were dried in an oven at 160 °C.

All solvents for use with air- and moisture-sensitive compounds were stored in teflon-valved ampoules containing pre-dried 4 Å molecular sieves from the Vac Atmospheres solvent tower drying system, where they had been passed over a column of molecular sieves for 24 hours prior to collection. They were then degassed prior to use and subsequent storage. The solvents benzene-d_6, toluene-d_8, THF-d_8 and pyridine-d_5 were heated under reflux over the appropriate drying agent for 24 hours, vacuum transferred into ampoules and stored under an atmosphere of nitrogen prior to use. All solvents were purchased from Sigma-Aldrich or Fisher Scientific.

All NMR spectroscopic analyses were recorded at 298 K using Bruker Avance III 500.12 MHz spectrometers with ^{1}H NMR spectra run at 500.12 MHz, ^{13}C NMR spectra at 125.77 MHz, ^{7}Li NMR spectra run at 194.41 MHz, ^{11}B NMR spectra at 160.49 MHz and ^{29}Si NMR spectra at 99.37 MHz. $SiMe_4$, $BF_3{\cdot}(OEt_2)$ and LiCl were used to externally reference the relevant spectra. The ^{1}H NMR and $^{13}C\{^{1}H\}$ NMR spectra were referenced internally to residual protio solvent (^{1}H) or solvent (^{13}C) and are reported to tetramethylsilane (δ = 0 ppm). Chemical shifts are quoted in δ (ppm) and coupling constants in Hz.

Elemental analyses were performed by Mr. Stephen Boyer at the London Metropolitan University. All FTIR were recorded using JASCO 410 or JASCO 460 plus spectrometers.

4.2 Preparation of Reagents

Potassium metal, $NaBH_4$, $NaNH_2$, LiMe, NH_2Dipp, NH_2Ph, Ph_3SnH, Et_3SiH, $PhSiH_3$, $[Re_2(CO)_{10}]$, $[Co_2(CO)_8]$, Ph_3COH, Me_3SiOH, 1,1-diphenyl ethylene, styrene, pyridine-*N*-oxide, trimethylamine-*N*-oxide, TEMPO, 1-hexene, cyclohexene, 1-methyl-1-cyclohexene, *cis*-stilbene, Cs_2CO_3, CS_2, ^{t}BuNC, $HCCSiMe_3$ and $HCCSi^iPr_3$ were purchased from Sigma-Aldrich and where appropriate, stored over pre-dried 4 Å molecular sieves. $[Ni(COD)_2]$, P_4 and LiOD were kindly donated by Dr Johann A. Hlina Dr Jamie McKinven and Dr Nicola L. Bell, respectively. KNHDipp,[1] KNHPh,[1] KCH_2Ph,[2] $LiCH_2SiMe_3$,[3] $KN(SiMe_3)_2$,[4] $ThCl_4(DME)_2$,[5] *trans*-calix[2]benzene[2]pyrrole (H_2L),[6] K_2L,[7] $[(L)ThCl_2]$ (**A**),[8] $KCH(SiMe_3)_2$,[9] $\{[UO_2(py)_5][KI_2(py)_2]\}_n$,[10] $[UO_2Cl_2(THF)_2]$,[11] $[K(L^{-2H})Th(N(SiMe_3)_2)]$ (**C**),[8] and $[(L)U(BH_4)]$ (**D**),[12] were synthesised according to literature procedures, in some cases with slight modifications. [Ni(dppf)(COD)] and [Pt(dppf)(nb)] were synthesised via the addition of dppf to $[Ni(COD)_2]$ and $[Pt(nb)_3]$ solutions in toluene.

4.3 General Procedure for Gas Reactions

A Young's tube was charged with a desired solution and the volume of the head-space in the Young's tube measured. The solution was then freeze-pump-thaw degassed three times and kept at -40 °C. Given the volume of the head-space, the pressure on the regulator was adjusted to give the desired number of equivalents of gas. The gas was then passed through a de-gassed line and de-gassed column packed with pre-dried $MgSO_4$ into the Young's tube. The Young's tube and gas cylinder were then sealed and the solution in the Young's tube allowed to warm to room temperature.

For high pressure reactions, an autoclave, allowing for pressures up to 10 bar, was preloaded in an inert-atmosphere glovebox. The autoclave was then gently degassed on the Schlenk line. The gas cylinder was connected directly to the autoclave using Swagelok connections. Although high purity gases were used, they could not be further dried prior to reaction, due to the high pressures required, which the drying column could not withstand.

4.4 Synthetic Procedures for Chapter Two

4.4.1 Synthesis of $[(L)UCl_2]$ (1)

A Teflon-valved ampoule with a magnetic stirrer-bar was charged with $UCl_4(THF)_{0.75}$ (0.601 g, 1.38 mmol) and K_2L (0.730 g, 1.38 mmol). THF (40 ml) was added, and the reaction was then stirred and heated at 80 °C for 48 hours. The resulting dark orange solution was

cannula-filtered to remove KCl and the volatiles were subsequently removed under reduced pressure. The solids were washed with hexane (3 x 10 ml) and dried under vacuum to yield **1** as an orange solid. Single crystals suitable for X-ray were grown by vapour diffusion of hexane into a saturated solution of **1** in THF at ambient temperature.

Yield: 0.772 g (1.02 mmol), 74 %.

^{1}H NMR (benzene-d_6): δ 101.07 (s, 4H, pyrrolide C<u>H</u>, width: 31.40 Hz), 25.93 (s, 12H, C<u>H</u>$_3$, width: 2.42 Hz), -5.56 (s, 12H, C<u>H</u>$_3$, width: 3.63 Hz), -10.23 (s, 4H, *meta*-C_6H_4, width: 6.56 Hz), -14.62 (s, 2H, *para*-C_6H_4, width: 6.54 Hz). 2H on *ipso*-C_6H_4 were not observed.

Analysis (%) calc. for $C_{32}H_{36}N_2Cl_2U$: C 50.73; H 4.79; N 3.70, found C 50.86; H 4.74; N 3.83.

4.4.2 Synthesis of [(L)Th(BH$_4$)$_2$] (2)

A Teflon-valved ampoule with a magnetic stirrer-bar was charged with **A** (0.200 g, 0.266 mmol) and $NaBH_4$ (2 eq, 0.020 g, 0.532 mmol). THF (10 ml) was added, and the reaction was then stirred and heated at 80 °C for 24 hours. The resulting colourless solution was cannula-filtered to remove NaCl and the volatiles were subsequently removed under reduced pressure. The solids were washed with hexane (3 x 2 ml) and dried under vacuum to yield **2** as an off-white solid. Single crystals suitable for X-ray were grown by vapour diffusion of hexane into a saturated solution of **2** in THF at ambient temperature.

Yield: 0.119 g (0.168 mmol), 63 %.

^{1}H NMR (benzene-d_6): δ 9.64 (s, 2H, *ipso*-C_6H_4), 7.32 (m, 2H, *para*-C_6H_4), 6.16 (s, 4H, pyrrolide C<u>H</u>), 2.10 (br m, 8H, B<u>H</u>$_4$), 1.89 (s, 12H, C<u>H</u>$_3$), 1.50 (s, 12H, C<u>H</u>$_3$) ppm. The resonance for *meta*-C_6H_4 could not be definitely assigned.

^{1}H{^{11}B} NMR (benzene-d_6): δ 2.10 (s, 8H, B<u>H</u>$_4$).

^{13}C{^{1}H} NMR (benzene-d_6): δ 157.0 (quaternary aromatic), 152.0 (quaternary aromatic), 134.4 (pyrrolide <u>C</u>H), 123.7 (*meta*-C_6H_4), 121.4 (*para*-C_6H_4), 116.8 (*ipso*-C_6H_4), 40.9 (quaternary), 32.4 (<u>C</u>H$_3$), 27.5 (<u>C</u>H$_3$).

^{11}B{^{1}H} NMR (benzene-d_6): δ -11.19 (<u>B</u>H$_4$).

Analysis (%) calc. for $C_{32}H_{44}N_2B_2Th$: C 54.11; H 6.24; N 3.94, found C 54.26; H 6.31; N 3.83.

FTIR (cm^{-1}): 2478 [terminal B-H stretch], 2230 and 2147 [bridging B-H stretches], 1083 [strong B-H bridge deformation]. All other absorption bands (cm^{-1}): 2965-2866, 1600, 1467, 1383, 1260, 1148, 1045, 940, 824-796, 727-710.

4.4.3 Synthesis of [(L)U(BH_4)$_2$] (3)

A Teflon-valved ampoule with a magnetic stirrer-bar was charged with **1** (0.200 g, 0.264 mmol) and $NaBH_4$ (2 eq, 0.020 g, 0.528 mmol). THF (10 ml) was added, and the reaction was then stirred and heated at 80 °C for 24 hours. The resulting dark-orange solution was cannula-filtered to remove NaCl and the volatiles were subsequently removed under reduced pressure. The solids were washed with hexane (3 x 2 ml) and dried under vacuum to yield **3** as an orange solid. Single crystals suitable for X-ray were grown by vapour diffusion of hexane into a saturated solution of **3** in THF at ambient temperature.

Yield: 0.108 g (0.150 mmol), 57 %.

^{1}H NMR (benzene-d_6): δ 23.9 (s, 2H, *ipso*-C_6H_4, width: 17.22 Hz), 20.3 (s, 4H, *meta*-C_6H_4, width: 18.38 Hz), 17.0 (m, 2H, *para*-C_6H_4, width: 22.62 Hz), 10.3 (s, 12H, C$\underline{H}_3$, width: 6.62 Hz), 9.63 (s, 12H, C$\underline{H}_3$, width: 6.01 Hz), -28.7 (s, 4H, pyrrolide C$\underline{H}$, width: 24.87 Hz), -36.7 (br d, 6H, η^3-$\underline{H}_3$BH, width: 200.52 Hz), -57.9 (s, 2H, η^3-$H_3B\underline{H}$, width: 21.35 Hz).

^{13}C{^{1}H} NMR (benzene-d_6): δ 216.3 (aromatic, width: 9.86 Hz), 202.6 (aromatic, width: 6.93 Hz), 197.9 (aromatic, width: 12.55 Hz), 189.2 (aromatic, width: 9.02 Hz), 189.0 (aromatic, width: 9.21 Hz), 186.6 (aromatic, width: 7.85 Hz), 100.1 (quaternary aliphatic, width: 6.15 Hz), 44.2 (C$\underline{H}_3$, width: 11.63 Hz), 38.0 (C$\underline{H}_3$, width: 10.23 Hz).

^{11}B{^{1}H} NMR (benzene-d_6): δ 85.79 ($\underline{B}H_4$, width: 2808.48 Hz).

Analysis (%) calc. for $C_{32}H_{44}N_2B_2U$: C 53.65; H 6.19; N 3.91, found C 53.54; H 6.13; N 4.01.

FTIR (cm^{-1}): 2471 [terminal B-H stretch], 2210 and 2147 [bridging B-H stretches], 1077 [strong B-H bridge deformation]. All other absorption bands (cm^{-1}): 3468, 2962-2869, 1599-1577, 1486-1330, 1260, 1176, 961, 905, 812.

4.4.4 Synthesis of [K(L^{-2H})Th(N($SiMe_3$)$_2$)] (C)

In a modification of the procedure reported by Arnold,[8] a Teflon-valved ampoule with a magnetic stirrer-bar was charged with **1** (0.500 g, 0.665 mmol) and KN($SiMe_3$)$_2$ (3 eq, 0.398 g, 2.00 mmol). Toluene was added (150 ml) and the reaction was heated at 80 °C with stirring for 16 hours. This reaction was found to also proceed without heating. The resulting

purple solution was cannula-filtered to remove KCl and the volatiles were removed under reduced pressure. The solids were washed with hexane (3 x 20 ml) and dried under vacuum to yield **C** as a purple solid.

Yield: 0.434 g (0.495 mmol), 74%.

^{1}H NMR and ^{13}C{^{1}H} NMR spectroscopic data agree with literature values.[8]

4.4.5 Synthesis of [K(L^{-2H})U(N($SiMe_3$)$_2$)] (4)

A Teflon-valved ampoule with a magnetic stirrer-bar was charged with **1** (0.100 g, 0.132 mmol) and KN($SiMe_3$)$_2$ (3eq, 0.079 g, 0.396 mmol). Toluene was added (20 ml) and the reaction sonicated for 15 minutes and stirred for 16 hours. The resulting dark brown solution was cannula-filtered to remove KCl and the volatiles were removed under reduced pressure. The solids were washed with hexane (3 x 5 ml) and then dried under vacuum to yield **8** as a dark orange solid.

Yield: 0.067 g (0.075 mmol), 57 %.

^{1}H NMR (benzene-d_6): δ 94.3 (s, 4H, pyrrolide C<u>H</u>, width: 47.40 Hz), 24.1 (s, 12H, C<u>H</u>$_3$, width: 34.48 Hz), 14.5 (s, 4H, *meta*-C_6H_3, width: 10.19 Hz), 9.25 (s, 18H, Si(C<u>H</u>$_3$)$_3$, width: 10.30 Hz), -27.2 (s, 2H, *para*-C_6H_3, width: 2.00 Hz), -42.0 (br s, 12H, C<u>H</u>$_3$, width: 228.69 Hz).

^{13}C{^{1}H} NMR (benzene-d_6): δ 238.9 (quaternary aromatic, width: 9.75 Hz), 153.4 (aromatic, width: 5.82 Hz), 152.6 (aromatic, width: 3.43 Hz), 148.0 (aromatic, width: 4.24 Hz), 121.4 (aromatic, width: 8.56 Hz), 113.2 (aromatic, width: 12.51 Hz), 67.5 (quaternary aliphatic, width: 15.13 Hz), 40.5 (<u>C</u>H$_3$, width: 6.23 Hz), 30.3 (<u>C</u>H$_3$, width: 10.18 Hz), 1.43 (Si-<u>C</u>H$_3$, width: 1.73 Hz).

^{29}Si{^{1}H} NMR, INEPT sequence, (benzene-d_6): δ -131.1 (width: 9.35 Hz).

Analysis (%) calc. for $C_{38}H_{52}N_3Si_2KU$: C 51.62; H 5.93; N 4.75, found C 51.63; H 5.95; N 4.60.

4.4.6 Synthesis of [Li(L^{-2H})Th(Me)] (5)

A Teflon-valved ampoule with a magnetic stirrer-bar was charged with **A** (1.50 g, 2.00 mmol) and LiMe (3eq, 0.132 g, 6.00 mmol). THF was added (20 ml), the reaction sonicated for 15 minutes and stirred for 16 hours. The resulting yellow solution was cannula-filtered to remove LiCl. The volatiles were then removed under reduced pressure and the solids

dried under vacuum to yield **5** as a pale yellow solid. Single crystals suitable for X-ray were grown by vapour diffusion of hexane into a saturated THF solution of **5** at ambient temperature.

Yield: 1.30 g (1.86 mmol), 93 %.

^{1}H NMR (THF-d_8): δ 6.96 (d, $|^{3}J_{HH}|$ = 7.65 Hz, 4H, *meta*-C_6H_3), 6.84 (t, $|^{3}J_{HH}|$ = 7.69 Hz, 2H, *para*-C_6H_3), 6.44 (s, 4H, pyrrolide C<u>H</u>), 1.58 (s, 12H, *exo*-C<u>H</u>$_3$), 1.41 (s, 12H, *endo*-C<u>H</u>$_3$), -0.73 (s, 3H, Th–C<u>H</u>$_3$).

^{13}C{^{1}H} NMR (THF-d_8): δ 217.6 (Th–<u>C</u>), 167.2 (quaternary aromatic), 159.2 (quaternary aromatic), 125.7 (*para*-C_6H_3), 121.7 (*meta*-C_6H_3), 115.7 (pyrrolide <u>C</u>H), 54.1 (Th–<u>C</u>H$_3$), 45.3 (quaternary), 35.2 (<u>C</u>H$_3$), 31.7 (<u>C</u>H$_3$).

^{7}Li{^{1}H} NMR (THF-d_8): δ 0.15.

Analysis (%) calc. for $C_{41}H_{53}N_2O_2LiTh$ (Li[(L^{-2H})Th(Me)]·2THF): C 58.29; H 6.32; N 3.32, found C 58.45; H 6.46; N 3.22.

4.4.7 Synthesis of [Li(L^{-2H})Th(CH$_2$SiMe$_3$)](6)

A Teflon-valved ampoule with a magnetic stirrer-bar was charged with **A** (1.28 g, 1.70 mmol) and $LiCH_2SiMe_3$ (3eq, 0.481 g, 5.11 mmol). Toluene was added (20 ml), the reaction sonicated for 15 minutes and then stirred for 16 hours. The resulting yellow solution was cannula-filtered to remove LiCl and the volatiles were removed under reduced pressure. The solids were washed with hexane (3 x 5 ml) and then dried under vacuum to yield **6** as a pale yellow solid. Single crystals suitable for X-ray were grown in the presence of LiCl by vapour diffusion of hexane into a saturated THF solution of **6** at ambient temperature.

Yield: 0.958 g (1.24 mmol), 73 %.

^{1}H NMR (benzene-d_6): δ 7.31 (t, $|^{3}J_{HH}|$ = 6.77 Hz, 2H, *para*-C_6H_3), 7.22 (d, $|^{3}J_{HH}|$ = 7.58 Hz, 4H, *meta*-C_6H_3), 6.81 (s, 4H, pyrrolide C<u>H</u>), 1.59 (s, 12H, *exo*-C<u>H</u>$_3$), 1.54 (s, 12H, *endo*-C<u>H</u>$_3$), 0.33 (s, 9H, Si(C<u>H</u>$_3$)$_3$), -0.17 (s, 2H, Th–C<u>H</u>$_2$).

^{13}C{^{1}H} NMR (benzene-d_6): δ 213.3 (Th–<u>C</u>), 165.4 (quaternary aromatic), 159.3 (quaternary aromatic), 123.6 (*meta*-C_6H_3), 122.9 (*para*-C_6H_3), 115.5 (pyrrolide <u>C</u>H), 44.6 (quaternary), 35.4 (<u>C</u>H$_3$), 31.1 (<u>C</u>H$_3$), 25.2 (Th–<u>C</u>H$_2$), 4.9 (Si(<u>C</u>H$_3$)$_3$).

^{29}Si{^{1}H} NMR, INEPT sequence, (benzene-d_6): δ -0.52 (<u>Si</u>(CH$_3$)$_3$).

$^{7}Li\{^{1}H\}$ NMR (benzene-d_6): δ -0.24.

Analysis (%) calc. for $C_{41}H_{53}N_2O_2LiTh$ (Li[(L^{-2H})Th(CH_2SiMe_3)]·2THF): C 58.29; H 6.32; N 3.32, found C 58.45; H 6.46; N 3.22.

4.4.8 Synthesis of [K(L^{-2H})Th(CH_2Ph)] (7)

A Teflon-valved ampoule with a magnetic stirrer-bar was charged with **A** (0.200 g, 0.266 mmol) and KCH_2Ph (3eq, 0.104 g, 0.798 mmol). Toluene was added (20 ml) and the reaction sonicated for 15 minutes and stirred for 16 hours. The resulting orange solution was cannula-filtered to remove KCl and the volatiles were removed under reduced pressure. The solids were washed with hexane (3 x 5 ml) and then dried under vacuum to yield **7** as a pale orange solid. Single crystals suitable for X-ray were grown by vapour diffusion of hexane into a saturated THF solution of **7** at ambient temperature.

Yield: 0.152 g (0.188 mmol), 71 %.

^{1}H NMR (benzene-d_6): δ 7.30 (m, 4H, *meta*-C_6H_3), 7.15-6.99 (m, 4H, *para*-C_6H_3 and *meta*-C_6H_5), 6.94 (d, $|^{3}J_{HH}|$ = 7.32 Hz, 2H, *ortho*-C_6H_5), 6.84 (t, $|^{3}J_{HH}|$ = 6.90 Hz, 1H, *para*-C_6H_5), 6.38 (s, 4H, pyrrolide C<u>H</u>), 1.91 (s, 2H, Th–C<u>H_2</u>), 1.63 (s, 12H, *exo*-C<u>H_3</u>), 1.49 (s, 12H, *endo*-C<u>H_3</u>).

$^{13}C\{^{1}H\}$ NMR (benzene-d_6): δ 215.8 (Th–<u>C</u>), 166.8 (quaternary aromatic), 160.4 (quaternary aromatic), 151.5 (quaternary aromatic), 128.6 (*meta*-C_6H_3), 126.1, 125.7 (*para*-C_6H_3 and *meta*-C_6H_5), 125.0 (*ortho*-C_6H_5), 119.0 (*para*-C_6H_5), 115.7 (pyrrolide <u>C</u>H), 67.4 (Th–<u>C</u>H_2) 45.3 (quaternary), 34.5 (<u>C</u>H_3), 30.5 (<u>C</u>H_3).

Analysis (%) calc. for $C_{39}H_{41}N_2KTh$: C 57.91; H 5.11; N 3.46, found C 58.08; H 5.23; N 3.32.

4.4.9 Synthesis of [Li(L^{-2H})U(Me)] (8)

A Teflon-valved ampoule with a magnetic stirrer-bar was charged with **1** (0.900 g, 0.957 mmol) and LiMe (3eq, 0.063 g, 2.87 mmol). THF was added (20 ml), the reaction sonicated for 15 minutes and stirred for 16 hours. The resulting dark brown solution was cannula-filtered to remove LiCl. The volatiles were then removed under reduced pressure and the solids dried under vacuum to yield **8** as a dark orange solid.

Yield: 0.653 g (0.924 mmol), 97 %.

^{1}H NMR (THF-d_8): δ 84.4 (s, 4H, pyrrolide C<u>H</u>, width: 114.05 Hz), 12.8 (s, 12H, C<u>H</u>$_3$, width: 143.63 Hz), 5.18 (s, 12H, C<u>H</u>$_3$, width: 76.13 Hz), -2.68 (s, 5H, U–C<u>H</u>$_3$ and C_6H_3, width: 15.62 Hz), -3.84 (s, 4H, C_6H_3, width: 14.13 Hz).

^{13}C{^{1}H} NMR (benzene-d_6): δ 150.1 (aromatic, width: 5.68 Hz), 129.3 (aromatic, width: 1.44 Hz), 128.6 (aromatic, width: 2.11 Hz), 125.7 (aromatic, width: 1.63 Hz), 104.2 (aromatic, width: 19.70 Hz), 67.9 (quaternary aliphatic, width: 30.15 Hz), 55.9 (U–<u>C</u>H$_3$, width: 28.16 Hz), 24.8 (<u>C</u>H$_3$, width: 19.19 Hz), 19.7 (<u>C</u>H$_3$, width: 11.36 Hz). *Ipso*-<u>C</u>$_6$H$_3$ could not be assigned.

^{7}Li{^{1}H} NMR (benzene-d_6): δ -36.0 (width: 457.36 Hz).

Analysis (%) calc. for $C_{33}H_{37}N_2LiU$: C 56.09; H 5.28; N 3.96, found C 56.22; H 5.37; N 3.74.

4.4.10 Synthesis of [Li(L^{-2H})U(CH$_2$SiMe$_3$)] (9)

A Teflon-valved ampoule with a magnetic stirrer-bar was charged with **1** (0.030 g, 0.039 mmol) and $LiCH_2SiMe_3$ (3eq, 0.011 g, 0.180 mmol). Benzene-d_6 was added (1 ml), the reaction sonicated for 20 minutes and left to react for 16h. The resulting dark brown solution was centrifuged and glass-filtered to remove LiCl and the volatiles were removed under reduced pressure. The solids were dried under vacuum to yield **9** as a dark orange solid. Single crystals suitable for X-ray were grown in the presence of LiCl by vapour diffusion of hexane into a saturated THF solution of **9** at ambient temperature.

Yield: 0.020 g (0.026 mmol), 65 %.

^{1}H NMR (benzene-d_6): δ 88.7 (s, 4H, pyrrolide C<u>H</u>, width: 285.75 Hz), 18.5 (s, 12H, C<u>H</u>$_3$, width: 338.15 Hz), -2.69 (s, 12H, C<u>H</u>$_3$, width: 158.19 Hz), -3.93 - -8.17 (m, 6H, *meta*-C_6H_3 and *para*-C_6H_3), -12.9 (s, 2H, U–C<u>H</u>$_2$, width: 47.61 Hz), -27.9 (s, 9H, Si(C<u>H</u>$_3$)$_3$, width: 74.93 Hz).

^{13}C{^{1}H} NMR (benzene-d_6): δ 151.1 (aromatic, width: 3.49 Hz), 147.5 (aromatic, width: 5.98 Hz), 124.2 (aromatic, width: 3.49 Hz), 122.5 (aromatic, width: 4.49 Hz), 102.4 (aromatic, width: 3.99 Hz), 68.2 (quaternary aliphatic, width: 4.99 Hz), 40.5 (<u>C</u>H$_3$, width: 14.91 Hz), 31.7 (<u>C</u>H$_3$, width: 3.99 Hz), 25.5 (U–<u>C</u>H$_2$, width: 29.84 Hz), 1.43 (Si-<u>C</u>H$_3$, width: 3.19 Hz). *Ipso*-<u>C</u>$_6$H$_3$ could not be assigned.

^{29}Si{^{1}H} NMR (benzene-d_6): Resonance could not be found.

^{7}Li{^{1}H} NMR (benzene-d_6): δ -52.7 (width: 530.67 Hz).

Analysis (%) calc. for $C_{36}H_{45}N_2LiSiU$: C 55.52; H 5.82; N 3.60, found C 55.48; H 5.63; N 3.71.

4.4.11 Synthesis of [K(L^{-2H})U(CH_2Ph)] (10)

A Teflon-valved ampoule with a magnetic stirrer-bar was charged with **1** (0.100 g, 0.132 mmol) and KCH_2Ph (3eq, 0.052 g, 0.396 mmol). Toluene was added (20 ml) and the reaction sonicated for 15 minutes and stirred for 16 hours. The resulting dark brown solution was cannula-filtered to remove KCl and the volatiles were removed under reduced pressure. The solids were washed with hexane (3 x 5 ml) and then dried under vacuum to yield **10** as a dark orange solid.

Yield: 0.050 g (0.061 mmol), 46 %.

^{1}H NMR (benzene-d_6): δ 97.8 (s, 4H, pyrrolide C<u>H</u>, width: 203.39 Hz), 28.6 (s, 12H, C<u>H</u>$_3$, width: 155.88 Hz), 11.2 (s, 2H, *para*-C_6H_3, width: 2.29 Hz), -4.42 (s, 4H, *meta*-C_6H_3, width: 53.68 Hz), -4.76 (s, 2H, *para*-C_6H_5, width: 15.26 Hz), -5.62 (m, 4H, *ortho*-C_6H_5 and *meta*-C_6H_5, width: 34.00 Hz), -6.58 (s, 12H, C<u>H</u>$_3$, width: 130.07 Hz), -57.8 (v br s, 2H, U–C<u>H</u>$_2$, width: 104.00 Hz).

^{13}C{^{1}H} NMR (benzene-d_6): δ 225.8 (quaternary aromatic, width: 4.21 Hz), 144.6 (aromatic, width: 4.99 Hz), 142.0 (aromatic, width: 2.30 Hz), 128.8 (aromatic, width: 1.91 Hz), 128.6 (aromatic, width: 1.96 Hz), 126.2 (aromatic, width: 1.86 Hz), 122.7 (aromatic, width: 3.49 Hz), 121.2 (aromatic, width: 3.90 Hz), 113.3 (aromatic, width: 5.49 Hz), 67.1 (quaternary aliphatic, width: 4.49 Hz), 38.2 (<u>C</u>H$_3$, width: 2.12 Hz), 30.0 (<u>C</u>H$_3$, width: 5.87 Hz), 25.5 (U–<u>C</u>H$_2$, width: 40.21 Hz). One aromatic resonance is obscured by the solvent peak and could not be assigned.

Analysis (%) calc. for $C_{39}H_{41}N_2KU$: C 57.48; H 5.07; N 3.44, found C 57.60; H 5.00; N 3.34.

4.4.12 Synthesis of [MgCl(L^{-2H})Th(CH_2Ph)] (11)

A Teflon-valved ampoule with a magnetic stirrer-bar was charged with **A** (0.200 g, 0.266 mmol) and $MgClCH_2Ph$ (3eq, 0.120 g, 0.798 mmol). Toluene was added (20 ml) and the reaction sonicated for 15 minutes and stirred for 16 hours. The resulting yellow solution was cannula-filtered to remove $MgCl_2$ and the volatiles were removed under reduced pressure. The solids were washed with hexane (3 x 5 ml) and then dried under vacuum to yield **11** as an off-white solid.

Yield: 0.095 g (0.115 mmol), 43 %.

^{1}H NMR (benzene-d_6): δ 7.21 (m, 4H, *meta*-C_6H_3), 7.14-6.99 (m, 7H, *para*-C_6H_3, *meta*-C_6H_5, *ortho*-C_6H_5 and *para*-C_6H_5), 6.59 (s, 4H, pyrrolide C<u>H</u>), 1.80 (s, 2H, Th–C<u>H</u>$_2$), 1.78 (s, 12H, *exo*-C<u>H</u>$_3$), 1.75 (s, 12H, *endo*-C<u>H</u>$_3$).

^{13}C{^{1}H} NMR (benzene-d_6): δ 216.1 (Th–<u>C</u>), 151.7 (quaternary aromatic), 147.9 (quaternary aromatic), 142.0 (quaternary aromatic), 129.5 (*meta*-C_6H_3), 127.6, 126.2, 124.7, 122.7 (*para*-C_6H_3, *meta*-C_6H_5, *ortho*-C_6H_5 and *para*-C_6H_5), 104.7 (pyrrolide <u>C</u>H), 69.9 (Th–<u>C</u>H$_2$) 41.1 (quaternary), 35.8 (<u>C</u>H$_3$), 29.9 (<u>C</u>H$_3$).

Analysis (%) calc. for $C_{39}H_{41}N_2MgClTh$: C 56.47; H 4.98; N 3.38, found C 56.28; H 5.20; N 3.43.

4.4.13 Synthesis of [(L)Th(C≡CSiMe$_3$)$_2$] (12)

A Teflon-valved ampoule with a magnetic stirrer-bar was charged with **5** (1.00 g, 1.43 mmol) and HC≡CSiMe$_3$ (2eq, 0.280 g, 2.86 mmol). Hexane was added (30 ml) and the reaction was stirred for 3 hours. The hexane solution of **12** was filtered away from the solids, the volatiles were removed under reduced pressure and the solids were then dried under vacuum to yield **12** as yellow solid. Single crystals suitable for X-ray were grown from a saturated solution of benzene at ambient temperature.

Yield: 0.544 g (0.622 mmol), 44 %.

^{1}H NMR (benzene-d_6): δ 7.96 (s, 2H, *ipso*-C_6H_4), 7.51 (s, 4H, pyrrolide C<u>H</u>), 7.09 (d, $|^{3}J_{HH}|$ = 7.01 Hz, 4H, *meta*-C_6H_4), 7.02 (t, $|^{3}J_{HH}|$ = 8.00 Hz, 2H, *para*-C_6H_4), 1.92 (s, 12H, C<u>H</u>$_3$), 1.51 (s, 12H, C<u>H</u>$_3$), 0.28 (s, 18H, Si(C<u>H</u>$_3$)$_3$).

^{13}C{^{1}H} NMR (benzene-d_6): δ 188.7 (Th–<u>C</u>), 155.4 (quaternary aromatic), 152.9 (quaternary aromatic), 133.7 (*para*-C_6H_4), 123.9 (*ipso*-C_6H_4), 123.7 (*meta*-C_6H_4), 119.4 (pyrrolide <u>C</u>H), 41.9 (quaternary), 30.3 (<u>C</u>H$_3$), 27.8 (<u>C</u>H$_3$), 0.58 (Si(<u>C</u>H$_3$)$_3$).

^{29}Si{^{1}H} NMR, INEPT sequence, (benzene-d_6): δ -24.7.

Analysis (%) calc. for $C_{42}H_{54}N_2Si_2Th$: C 57.65; H 6.22; N 3.20, found C 57.51; H 6.33; N 2.98.

FTIR (cm^{-1}): 2140 [C≡C stretch]. All other absorption bands (cm^{-1}): 3480, 3340, 2964-2876, 1996, 1920, 1584, 1486-1358, 1246, 1072-1048, 846-802, 758, 670.

4.4.14 Synthesis of [(L)Th(C≡CSi^{i}Pr$_3$)$_2$] (13)

A Teflon-valved ampoule with a magnetic stirrer-bar was charged with **5** (0.100 g, 0.143 mmol) and HC≡CSi^{i}Pr$_3$ (2eq, 0.052 g, 0.286 mmol). Hexane was added (10 ml) and the reaction was stirred for 3 hours. The hexane solution of **13** was filtered away from the solids, the volatiles were removed under reduced pressure and the solids were then dried under vacuum to yield **13** as yellow solid. Single crystals suitable for X-ray were grown from a saturated solution of benzene at ambient temperature.

Yield: 0.080 g (0.077 mmol), 54 %.

^{1}H NMR (benzene-d_6): δ 7.90 (s, 2H, *ipso*-C$_6$H$_4$), 7.53 (s, 4H, pyrrolide C<u>H</u>), 7.10 (d, $|^{3}J_{HH}|$ = 7.70 Hz, 4H, *meta*-C$_6$H$_4$), 7.02 (t, $|^{3}J_{HH}|$ = 7.70 Hz, 2H, *para*-C$_6$H$_4$), 1.97 (s, 12H, C<u>H</u>$_3$), 1.52 (s, 12H, C<u>H</u>$_3$), 1.35 (d, $|^{3}J_{HH}|$ = 7.20 Hz, 36H, SiCH(C<u>H</u>$_3$)$_2$, 1.22 (septet, $|^{3}J_{HH}|$ = 7.20 Hz, 6H, SiC<u>H</u>).

^{13}C{^{1}H} NMR (benzene-d_6): δ 190.04 (Th–<u>C</u>), 155.4 (quaternary aromatic), 152.9 (quaternary aromatic), 133.6 (*para*-C$_6$H$_4$), 123.7 (*ipso*-C$_6$H$_4$ and *meta*-C$_6$H$_4$), 119.0 (pyrrolide <u>C</u>H), 41.9 (quaternary), 30.3 (<u>C</u>H$_3$), 28.0 (<u>C</u>H$_3$), 19.4 (SiCH(<u>C</u>H$_3$)$_2$), 12.3 (Si<u>C</u>H).

^{29}Si{^{1}H} NMR, INEPT sequence, (benzene-d_6): δ -6.83.

Analysis (%) calc. for C$_{54}$H$_{78}$N$_2$Si$_2$Th: C 62.16; H 7.54; N 2.68, found C 62.33; H 7.62; N 2.46.

FTIR (cm^{-1}): 2032 [C≡C stretch]. All other absorption bands (cm^{-1}): 3480, 3294, 2948-2886, 1990, 1598-1582, 1464, 1384-1364, 1244-1218, 1074-966, 918-884, 800, 674.

4.4.15 Synthesis of [(L)U(C≡CSiMe$_3$)$_2$] (14)

A Teflon-valved ampoule with a magnetic stirrer-bar was charged with **8** (0.050 g, 0.071 mmol) and HC≡CSiMe$_3$ (2eq, 0.014 g, 0.142 mmol). Hexane was added (3 ml) and the reaction was stirred for 3 hours. The hexane solution of **14** was filtered away from the solids, the volatiles were removed under reduced pressure and the solids were then dried under vacuum to yield **14** as orange solid.

Yield: 0.031 g (0.035 mmol), 50 %.

^{1}H NMR (THF-d_6): δ 92.8 (s, 4H, pyrrolide C<u>H</u>, width: 105.18 Hz), 26.6 (s, 12H, C<u>H</u>$_3$, width: 83.26 Hz), -6.11 (s, 12H, C<u>H</u>$_3$, width: 75.19 Hz), -10.2 (s, 4H, *meta*-C$_6$H$_4$, width: 23.42 Hz),

-12.7 (m, 2H, C_6H_4, width: 35.42 Hz), -13.9 (s, 18H, $Si(C\underline{H}_3)_3$, width: 16.57 Hz), -14.4 (s, 2H, C_6H_4, width: 25.08 Hz).

$^{29}Si\{^1H\}$ NMR, INEPT sequence, (benzene-d_6): δ 34.5 (width: 12.67 Hz).

Analysis (%) calc. for $C_{42}H_{54}N_2Si_2U$: C 57.25; H 6.18; N 3.18, found C 57.32; H 6.05; N 3.11.

4.4.16 Synthesis of [(L)U(C≡CSi^{i}Pr$_3$)$_2$] (15)

A Teflon-valved ampoule with a magnetic stirrer-bar was charged with **8** (0.100 g, 0.142 mmol) and HC≡CSi^{i}Pr$_3$ (2eq, 0.052 g, 0.284 mmol). Hexane was added (10 ml) and the reaction was stirred for 3 hours. The hexane solution of **15** was filtered away from the solids, the volatiles were removed under reduced pressure and the solids were then dried under vacuum to yield **15** as orange solid. Single crystals suitable for X-ray were grown from a saturated solution of benzene at ambient temperature.

Yield: 0.074 g (0.071 mmol), 50 %.

^1H NMR (benzene-d_6): δ 92.5 (s, 4H, pyrrolide C$\underline{H}$, width: 50.45 Hz), 26.3 (s, 12H, $C\underline{H}_3$, width: 25.94 Hz), -6.00 (s, 12H, $C\underline{H}_3$, width: 57.39 Hz), -9.50 (m, 38H, ^{i}Pr-$C\underline{H}_3$ and C_6H_4, width: 9.53 Hz), -10.2 (s, 4H, *meta*-C_6H_4, width: 16.93 Hz), -12.7 (septet, $|^3J_{HH}|$ = 7.25 Hz, 6H, ^{i}Pr-C$\underline{H}$, width: 23.75 Hz), -14.1 (s, 2H, C_6H_4, width: 12.21 Hz).

$^{29}Si\{^1H\}$ NMR, INEPT sequence, (benzene-d_6): δ -21.9 (width: 5.11 Hz).

Analysis (%) calc. for $C_{54}H_{78}N_2Si_2U$: C 61.80; H 7.49; N 2.67, found C 62.07; H 7.34; N 2.83.

FTIR (cm^{-1}): 2032 [C≡C stretch]. All other absorption bands (cm^{-1}): 3472-3442, 2965-2865, 2280, 2117, 1600-1583, 1483-1359, 1261, 1207, 1080-998, 961, 883.

4.4.17 Attempted Syntheses of Thorium(IV) Imido Complexes from 5

In a vial charged with a magnetic stirrer-bar, in an N_2-atmosphere glove box, **5** (0.030 g, 0.043 mmol) was dissolved in THF-d_8 (1 ml) and NH_2Dipp (1eq, 0.007 g, 0.043 mmol) or NH_2Ph (1eq, 0.004 g, 0.043 mmol) was added and the reaction mixture stirred for 4 hours. The solution was then filtered. ^1H and $^{13}C\{^1H\}$ NMR spectroscopy indicated that a mixture of products had formed. The reaction mixtures stored at room temperature for 24 hours after which time the products had decomposed to H_2L. This procedure was repeated with **5** (0.030 g, 0.043 mmol) and $NaNH_2$ (1eq, 0.002 g, 0.043 mmol). Na_2L was isolated from this reaction.

4.4.18 Attempted Syntheses of Thorium(IV) Imido Complexes from C

The procedure described in Section 4.4.17 was repeated for **C** (0.030 g, 0.034 mmol) in C_6D_6 (1 ml) and NH_2Dipp (1eq, 0.006 g, 0.034 mmol), KNHDipp (1eq, 0.007 g, 0.034 mmol) or KNHPh (1eq, 0.004 g, 0.034 mmol). Slow decomposition to H_2L, K_2L and other decomposition products was observed.

4.4.19 Attempted 1,2-insertion into Th–C Bond of 5

A Young's tube was charged with **5** (0.030 g, 0.043 mmol) in THF-d_8 (1 ml). An excess of 1,1-diphenyl ethylene (0.018 g, 0.100 mmol) was added and the reaction mixture heated at 80 °C for 48 hours. No reaction occurred. This reaction was repeated for styrene (0.010 g, 0.100 mmol), 1-hexene (0.008 g, 0.100 mmol), cyclohexene (0.008 g, 0.100 mmol) and 1-methyl-1-cyclohexene (0.010 g, 0.100 mmol). No reaction occurred with styrene or 1-hexene. Cyclohexene and 1-methyl-1-cyclohexene displayed some reactivity but products could not be isolated.

4.4.20 Attempted [2+2+2] Cycloaddition Reactions with 12

A Young's tube was charged with **12** (0.030 g, 0.034 mmol) in C_6D_6 (1 ml). An excess of *cis*-stilbene (0.018 g, 0.100 mmol) was added and the reaction mixture heated at 80 °C for 16 hours. No reaction occurred.

4.4.21 Attempted Th^{IV} Hydride Synthesis with Silanes

A Young's tube was charged with **5** (0.030 g, 0.043 mmol) in THF-d_8 (1 ml). Et_3SiH (1 eq, 0.005 g, 0.043 mmol) or $PhSiH_3$ (1 eq, 0.004 g, 0.043 mmol) was added. ^1H and $^{13}C\{^1H\}$ NMR spectroscopy indicated that a mixture of products and H_2L had formed. This procedure was repeated with **12** (0.030 g, 0.034 mmol) in C_6D_6 (1 ml) and Et_3SiH (1 eq, 0.004 g, 0.034 mmol) or $PhSiH_3$ (1 eq, 0.004 g, 0.034 mmol). No reaction occurred. The reaction mixture was then heated at 80 °C for 2 hours. A mixture of inseparable products formed.

4.4.22 Attempted Th^{IV} Hydride Synthesis with Tin Hydride

In a vial charged with a magnetic stirrer-bar, in an N_2-atmosphere glove box, **5** (0.030 g, 0.043 mmol) was dissolved in THF-d_8 (1 ml) and cooled to -20 °C. Frozen Ph_3SnH (1 eq, 0.015 g, 0.043 mmol) was added and the reaction stirred at -20 °C for 2 hours. ^1H, ^7Li and $^{119}Sn\{^1H\}$ NMR spectroscopy indicated that a mixture of at least three products formed. Fractional crystallisation from a saturated THF solution at -20 °C afforded crystals of $(Ph_3Sn)_2$.

4.4.23 Synthesis of [(L^{-2H})U(η^2-O_2SiMe_2)(Li{THF})$_2$] (16)

A saturated solution of **8** (0.051 g, 0.072 mmol) in THF, containing an excess of silicone grease, was prepared in a N_2-atmosphere drybox. After two weeks, orange single crystals of **16** suitable for X-ray were isolated from the saturated solution.

Yield: 0.009 g (0.010 mmol), 13 %.

^{1}H NMR (THF-d_8): δ 40.3 (s, 12H, C$\underline{H}_3$, width: 17,64 Hz), 30.5 (s, 2H, *para*-C_6H_3, width: 12.40 Hz), 30.3 (s, 6H, Si(C$\underline{H}_3$)$_2$, width: 20.30 Hz), 9.87 (s, 4H, *meta*-C_6H_3, width: 6.79 Hz), -4.55 (s, 4H, pyrrolide C$\underline{H}$, width: 13.40 Hz), -13.49 (s, 16H, bound THF-H, width: 7.09 Hz), -45.6 (s, 12H, C$\underline{H}_3$, width: 24.62 Hz).

^{13}C{^{1}H} NMR (THF-d_8): δ 128.9 (width: 6.80 Hz), 128.5 (width: 7.85 Hz), 95.4 (width: 4.99 Hz), 94.4 (width: 8.79 Hz), 68.4 (width: 1.49 Hz), 48.9 (width: 3.31 Hz), 27.8 (width: 9.86 Hz), 26.6 (width: 1.49 Hz). Four quaternary carbon resonances were too weak to observe.

^{7}Li{^{1}H} NMR (THF-d_8): no signals observed, likely due to paramagnetism.

^{29}Si{^{1}H} NMR (THF-d_8): no signals observed, likely due to paramagnetism.

Analysis (%) calc. for $C_{42}H_{54}N_2O_4Li_2SiU$: C 54.19; H 5.85; N 3.01, found C 54.18; H 6.02; N 2.99.

4.4.24 Attempted Small Molecule Activation by Complexes 5-10

Reactions of 1, 2 or 3 equivalents or an excess of CO, CO_2 and H_2 with complex **5** (0.020 g, 0.029 mmol) in THF-d_8 or complexes **6** (0.020 g, 0.026 mmol), **7** (0.020 g, 0.025 mmol), **8** (0.020 g, 0.028 mmol), **9** (0.020 g, 0.026 mmol) or **10** (0.020 g, 0.025 mmol) in benzene-d_6 were performed according to the procedure described in Section 4.3. 1, 2 or 3 equivalents of CS_2 or ^{t}BuNC were added *via* syringe. In all cases, inseparable mixtures of products were obtained immediately.

4.4.25 Attempted Small Molecule Activation by Complexes 12-15

Reactions of 2 bar CO or H_2 or 10 bar CO_2 with complexes **12** (0.030 g, 0.034 mmol), **13** (0.030 g, 0.029 mmol), **14** (0.030 g, 0.034 mmol) or **15** (0.030 g, 0.029 mmol) in C_6D_6 (1 ml) were performed according to the procedure described in Section 4.3. No reactions occurred. Reaction mixtures containing 2 bar of CO or H_2 were heated at 80 °C for 16 hours. No reactions occurred.

4.4.26 Synthesis of [LCO] (17)

A Young's tube was charged with **12** (0.050 g, 0.057 mmol) or **13** (0.050 g, 0.049 mmol) in C_6D_6 (1 ml), 1 bar of CO_2 added and the reaction vessel heated at 80 °C for 16 hours. Off-white solids formed and were filtered away from the solution containing **17**. The volatiles were removed under reduced pressure and the solids then dried under vacuum to yield **17** as a colourless solid. Single crystals suitable for X-ray were grown from a saturated solution of **17** in hexane at -20 °C.

Yield: 0.019 g (0.040 mmol), 70 %.

^{1}H NMR (benzene-d_6): δ 7.41 (m, 1H, arene-H), 7.32-7.25 (m, 3H, arene-H), 7.08 (m, 1H, arene-H), 6.98 (m, 1H, arene-H), 6.90 (m, 1H, arene-H), 6.34 (m, 1H, pyr-C<u>H</u>), 5.92 (m, 2H, pyr-C<u>H</u>), 5.23 (m, 1H, pyr-C<u>H</u>), 3.86 (br. s, 1H, pyr-N<u>H</u>), 1.75 (br. s, 12H, C<u>H</u>$_3$), 1.60 (s, 6H, C<u>H</u>$_3$), 1.34 (s, 6H, C<u>H</u>$_3$).

^{13}C{^{1}H} NMR (benzene-d_6): δ 159.4 (<u>C</u>=O), 156.5 (quaternary arene), 149.4 (quaternary arene), 149.0 (quaternary arene), 148.7 (quaternary arene), 143.3 (quaternary arene), 143.0 (quaternary arene), 142.6 (quaternary arene), 138.7 (quaternary arene), 131.1 (arene-<u>C</u>H), 129.1 (arene-<u>C</u>H), 129.0 (quaternary arene), 126.5 (arene-<u>C</u>H), 124.8 (arene-<u>C</u>H), 123.7 (arene-<u>C</u>H), 123.2 (arene-<u>C</u>H), 121.0 (arene-<u>C</u>H), 115.7 (pyr-<u>C</u>H), 106.3 (pyr-<u>C</u>H), 104.9 (pyr-<u>C</u>H), 103.4 (pyr-<u>C</u>H), 44.5 (<u>C</u>H$_3$), 41.6 (<u>C</u>H$_3$), 39.5 (<u>C</u>H$_3$), 37.4 (<u>C</u>H$_3$), 30.4 (quaternary), 29.6 (quaternary), 25.8 (quaternary).

Analysis (%) calc. for $C_{33}H_{36}N_2O$: C 83.15; H 7.61; N 5.88, found C 83.06; H 7.69; N 5.93.

4.4.27 Attempted Reaction of 12 with [$Co_2(CO)_8$] or [$Re_2(CO)_{10}$]

A Young's tube was charged with **12** (0.030 g, 0.034 mmol) in THF (1 ml) and [$Co_2(CO)_8$] (0.5 eq, 0.006 g, 0.017 mmol) or [$Re_2(CO)_{10}$] (0.5 eq, 0.011 g, 0.017 mmol) was added. No reaction occurred. No reaction occurred upon the exposure of the reaction mixtures to UV radiation (λ = 351 nm) over 10 hours in a Quartz tube.

4.4.28 Attempted Reaction of 12 with P_4

A Young's tube was charged with **12** (0.030 g, 0.034 mmol) in THF (1 ml) and P_4 (0.5 eq, 0.002 g, 0.017 mmol or 1 eq, 0.004 g, 0.034 mmol) was added. No reaction occurred. No reaction occurred upon the exposure of the reaction mixtures to UV radiation (λ = 351 nm)

over 10 hours in a Quartz tube. The reaction mixture was then heated at 80 °C for 20 minutes. A mixture of inseparable products H_2L was obtained.

4.4.29 Synthesis of [Li(L^{-2H})Th(N")] (18)

A Teflon-valved ampoule with a magnetic stirrer-bar was charged with **1** (0.500 g, 0.665 mmol) and $LiN(SiMe_3)_2$ (3 eq, 0.334 g, 2.00 mmol). Toluene was added (150 ml) and the reaction was heated at 80 °C with stirring for 48 hours. The resulting blue solution was cannula-filtered to remove LiCl and the volatiles were removed under reduced pressure. The solids were washed with hexane (3 x 20 ml) and then dried under vacuum to yield **18** as an off-white solid.

Yield: 0.253 g (0.299 mmol), 45%.

^{1}H NMR (benzene-d_6): δ 7.36 (m, 2H, *para*-C_6H_3), 7.26 (d, $|^3J_{HH}|$ = 7.47 Hz, 4H, *meta*-C_6H_3), 6.96 (s, 4H, pyrrolide C<u>H</u>), 1.71 (s, 12H, C<u>H</u>$_3$), 1.68 (s, 12H, C<u>H</u>$_3$), 0.43 (s, 18H, Si(C<u>H</u>$_3$)$_3$).

Analysis (%) calc. for $C_{38}H_{52}N_3Si_2LiTh$: C 53.95; H 6.20; N 4.97, found C 54.10; H 6.13; N 5.01.

4.4.30 Synthesis of [Na(L^{-2H})Th(N")] (19)

A Teflon-valved ampoule with a magnetic stirrer-bar was charged with **1** (0.500 g, 0.665 mmol) and $NaN(SiMe_3)_2$ (3 eq, 0.365 g, 2.00 mmol). Toluene was added (150 ml) and the reaction was heated at 80 °C with stirring for 16 hours. The resulting purple solution was cannula-filtered to remove NaCl and the volatiles were removed under reduced pressure. The solids were washed with hexane (3 x 20 ml) and then dried under vacuum to yield **19** as a pink solid.

Yield: 0.320 g (0.372 mmol), 56%.

^{1}H NMR (benzene-d_6): δ 7.35 (t, $|^3J_{HH}|$ = 4.09 Hz, 2H, *para*-C_6H_3), 7.26 (d, $|^3J_{HH}|$ = 7.37 Hz, 4H, *meta*-C_6H_3), 6.72 (s, 4H, pyrrolide C<u>H</u>), 1.67 (s, 12H, C<u>H</u>$_3$), 1.65 (s, 12H, C<u>H</u>$_3$), 0.36 (s, 18H, Si(C<u>H</u>$_3$)$_3$).

Analysis (%) calc. for $C_{38}H_{52}N_3Si_2NaTh$: C 52.95; H 6.08; N 4.87, found C 52.82; H 6.00; N 4.76.

4.4.31 Synthesis of [Cs(L^{-2H})Th(N")] (20)

A Teflon-valved ampoule with a magnetic stirrer-bar was charged with **2** (0.020 g, 0.023 mmol) and Cs_2CO_3 (1.2 eq, 0.005 g, 0.014 mmol). THF was added (5 ml) and the reaction was heated to 80 °C with stirring for 16 hours. The solution was cannula-filtered to remove K_2CO_3 and excess Cs_2CO_3. The volatiles were then removed under reduced pressure and the solids dried under vacuum to yield **20** as an off-white solid.

Yield: 0.016 g (0.016 mmol), 69%.

^{1}H NMR (THF-d_8): δ 7.17 (m, 2H, *para*-C_6H_3), 7.14 (d, $|^3J_{HH}|$ = 7.55 Hz, 4H, *meta*-C_6H_3), 6.51 (s, 4H, pyrrolide C<u>H</u>), 1.54 (s, 12H, C<u>H</u>$_3$), 1.51 (s, 12H, C<u>H</u>$_3$), 0.15 (s, 18H, Si(C<u>H</u>$_3$)$_3$).

Analysis (%) calc. for $C_{38}H_{52}N_3Si_2LiTh$: C 46.96; H 5.39; N 4.32, found C 47.12; H 5.63; N 4.31.

4.4.32 Attempted Exchange of Group 1 Cations for *f*-Elements

In a Young's tube, an excess of SmI_3 (0.053 g, 0.100 mmol), $EuI_2(THF)_2$ (0.055 g, 0.100 mmol), $UI_3(dioxane)_{1.5}$ (0.075 g, 0.100 mmol), $UCl_4(THF)_{0.75}$ (0.043 g, 0.100 mmol) or $ThCl_4(DME)_2$ (0.047 g, 0.100 mmol) was added to a solution of **C** (0.030 g, 0.034 mmol) in THF (1 ml). The reaction mixtures were sonicated for 15 minutes and then stirred for 18 hours at 80 °C. No reaction occurred.

4.4.33 Synthesis of [(L)Th(CH_2Ph)][BPh_4] (21)

A Teflon-valved ampoule with a magnetic stirrer-bar was charged with **7** (0.040 g, 0.050 mmol) and [Et_3NH][BPh_4] (2eq, 0.042 g, 0.100 mmol). THF was added (2 ml) and the resulting suspension was stirred for 2 hours. The pale yellow solution was then cannula-filtered to remove $KBPh_4$. The volatiles were removed under reduced pressure and the solids were then dried under vacuum to yield **21** as off-white solid. Material sufficiently pure for elemental analysis could not be obtained.

Yield: 0.017 g (0.016 mmol), 31 %.

^{1}H NMR (THF-d_8): δ 7.72 (s, 2H, *ipso*-C_6H_4), 7.40-7.08 (m, 19H, aromatic-H), 7.00 (s, 4H, pyrrolide C<u>H</u>), 6.85 (t, $|^3J_{HH}|$ = 7.28 Hz, 8H, *meta*-C_6H_5), 6.71 (t, $|^3J_{HH}|$ = 6.92 Hz, 4H, *para*-C_6H_5), 2.89 (s, 2H, Th–C<u>H</u>$_2$), 1.79 (s, 12H, C<u>H</u>$_3$), 1.47 (s, 12H, C<u>H</u>$_3$).

$^{13}C\{^{1}H\}$ NMR (THF-d_8): δ 158.3 (quaternary aromatic), 153.9 (aromatic-C_6H_5), 153.2 (aromatic-C_6H_5), 137.3 (tetraphenyl borate *meta*-$\underline{C}_6H_5$), 134.9 (quaternary aromatic), 129.1 (*ipso*-C_6H_4), 128.8 (aromatic-C_6H_5), 128.4 (aromatic-C_6H_5), 126.7 (*para*-C_6H_4), 125.8 (tetraphenyl borate *ortho*-$\underline{C}_6H_5$), 123.9 (pyrrolide $\underline{C}$H), 123.3 (*meta*-C_6H_4), 121.9 (tetraphenyl borate *para*-$\underline{C}_6H_5$), 42.6 (quaternary), 30.9 ($\underline{C}H_3$), 30.8 (Th–$\underline{C}H_2$) 28.0 ($\underline{C}H_3$).

$^{11}B\{^{1}H\}$ NMR (THF-d_8): δ -6.56.

4.4.34 Synthesis of [(L)Th(N(SiMe$_3$)$_2$)][BPh$_4$] (22)

A Teflon-valved ampoule with a magnetic stirrer-bar was charged with **C** (0.500 g, 0.570 mmol) and [Et_3NH][BPh_4] (2eq, 0.480 g, 1.140 mmol). THF was added (30 ml) and the resulting suspension was stirred for 2 hours. The grey solution was then cannula-filtered to remove $KBPh_4$. The volatiles were removed under reduced pressure and the solids were then dried under vacuum to yield **22** as a grey solid. Single crystals suitable for X-ray were grown by vapour diffusion of hexane into a saturated THF solution of **22** at ambient temperature.

Yield: 0.449 g (0.387 mmol), 68 %.

^{1}H NMR (THF-d_8): δ 8.23 (s, 2H, *ipso*-C_6H_4), 8.04 (d, $|^3J_{HH}|$ = 1.54 Hz, 4H, *meta*-C_6H_4), 7.26 (m, 8H, *ortho*-C_6H_5), 7.15 (m, 2H, *para*-C_6H_4), 6.85 (t, $|^3J_{HH}|$ = 7.47 Hz, 8H, *meta*-C_6H_5), 6.70 (t, $|^3J_{HH}|$ = 7.19 Hz, 4H, *para*-C_6H_5), 6.15 (s, 4H, pyrrolide C$\underline{H}$), 1.78 (s, 12H, C$\underline{H}_3$), 1.63 (s, 12H, C$\underline{H}_3$), 0.14 (s, 18H, Si(C$\underline{H}_3$)$_3$).

$^{13}C\{^{1}H\}$ NMR (THF-d_8): δ 158.3 (quaternary aromatic), 157.2 (quaternary aromatic), 137.3 (tetraphenyl borate *meta*-$\underline{C}_6H_5$), 132.4 (*ipso*-C_6H_4), 127.8 (*para*-C_6H_4), 126.0 (tetraphenyl borate *ortho*-$\underline{C}_6H_5$), 122.4 (*meta*-C_6H_4), 122.1 (tetraphenyl borate *para*-$\underline{C}_6H_5$), 107.4 (pyrrolide $\underline{C}$H), 42.7 (quaternary), 33.4 ($\underline{C}H_3$), 29.3 ($\underline{C}H_3$), 4.1 (Si($\underline{C}H_3$)$_3$).

$^{29}Si\{^{1}H\}$ NMR, INEPT sequence, (THF-d_8): δ -12.4.

$^{11}B\{^{1}H\}$ NMR (THF-d_8): δ -6.57.

Analysis (%) calc. for $C_{62}H_{74}BN_3Si_2Th$: C 64.18; H 6.43; N 3.62, found C 64.26; H 6.34; N 3.55.

4.4.35 Attempted Small Molecule Activation by 22

Reactions of 1 bar of CO or CO_2 with complex **22** (0.030 g, 0.026 mmol) in THF-d_8 were performed according to the procedure described in Section 4.3. In both cases, inseparable mixtures of products and H_2L were obtained immediately.

4.4.36 Attempted Reduction of 22

In a vial charged with a magnetic stirrer-bar, in an N_2-atmosphere glove box, **22** (0.050 g, 0.043 mmol) was dissolved in THF (2 ml) and cooled to -20 °C. KC_8 (1 eq, 0.006 g, 0.043 mmol) was added and the reaction stirred at -20 °C for 5 minutes, after which time colourless precipitate formed. The reaction mixture was then filtered to remove the solids. The ^{1}H NMR and $^{13}C\{^{1}H\}$ NMR spectra indicated that a mixture of diamagnetic products formed.

4.4.37 Alternative Synthesis of C

In a vial charged with a magnetic stirrer-bar, in an N_2-atmosphere glove box, **22** (0.050 g, 0.043 mmol) was dissolved in THF (2 ml) and $KN(SiMe_3)_2$ (2 eq, 0.017 g, 0.086 mmol) or KCH_2Ph (2 eq, 0.011 g, 0.086 mmol) added. The reaction was stirred for 20 minutes and then filtered to remove solids. The volatiles were removed under reduced pressure and the solids were then dried under vacuum to yield **C** as a purple solid. ^{1}H NMR and $^{13}C\{^{1}H\}$ NMR spectroscopic data agree with literature values.[8]

4.4.38 Synthesis of [(L)Th(C≡CSiMe$_3$)$_2$·Ni] (23)

A Teflon-valved ampoule with a magnetic stirrer-bar was charged with **12** (0.050 g, 0.057 mmol) and $[Ni(COD)_2]$ (1eq, 0.016 g, 0.057 mmol). Hexane was added (2 ml) and the reaction was stirred for 2 hours. The volatiles were removed under reduced pressure and the solids were then dried under vacuum to yield **23** as an orange solid.

Yield: 0.010 g (0.010 mmol), 15 %.

^{1}H NMR (benzene-d_6): δ 9.43 (s, 2H, *ipso*-C_6H_4), 7.24 (d, $|^{3}J_{HH}|$ = 8.57 Hz, 4H, *meta*-C_6H_4), 7.12 (t, $|^{3}J_{HH}|$ = 8.11 Hz, 2H, *para*-C_6H_4), 6.11 (s, 4H, pyrrolide C<u>H</u>), 1.91 (s, 12H, *exo*-C<u>H</u>$_3$), 1.62 (s, 12H, *endo*-C<u>H</u>$_3$), 0.67 (s, 18H, Si(C<u>H</u>$_3$)$_3$).

$^{13}C\{^{1}H\}$ NMR (benzene-d_6): δ 217.0 (Th–<u>C</u>), 151.6 (quaternary aromatic), 151.0 (quaternary aromatic), 128.2 (*ipso*-C_6H_4 and *meta*-C_6H_4), 122.2 (*para*-C_6H_4), 112.5 (pyrrolide <u>C</u>H), 40.4 (quaternary), 32.1 (<u>C</u>H$_3$), 29.5 (<u>C</u>H$_3$), 27.87 (Si(CH$_3$)$_3$).

$^{29}Si\{^{1}H\}$ NMR, INEPT sequence, (benzene-d_6): δ -15.39.

Analysis (%) calc. for $C_{42}H_{54}N_2Si_2NiTh$: C 54.02; H 5.83; N 3.00, found C 53.98; H 6.02; N 2.79.

FTIR (cm^{-1}): 2143 [C≡C stretch]. All other absorption bands (cm^{-1}): 3475, 2963-2873, 2280, 1965, 1811, 1748, 1600-1583, 1486-1357, 1330, 1246-1220,1083, 1045, 994, 960, 844.

4.4.39 Synthesis of [(L)Th(C≡CSiMe$_3$)$_2$·NiPPh$_3$] (24)

A Teflon-valved ampoule with a magnetic stirrer-bar was charged with **12** (0.100 g, 0.114 mmol), [Ni(COD)$_2$] (1eq, 0.031 g, 0.114 mmol) and PPh_3 (1eq, 0.030 g, 0.114 mmol). Hexane was added (5 ml) and the reaction was stirred for 3 hours. The volatiles were removed under reduced pressure and the solids were then dried under vacuum to yield **24** as dark orange solid. Single crystals suitable for X-ray were grown by vapour diffusion of hexane into a saturated THF solution of **24** at ambient temperature.

Yield: 0.025 g (0.021 mmol), 18 %.

^{1}H NMR (298 K, benzene-d_6): δ 9.09 (s, 2H, *ipso*-C_6H_4), 7.94 (m, 6H, *ortho*-P-C_6H_5), 7.22-7.16 (m, 10H, *meta*-C_6H_4 and *meta*-P-C_6H_5), 7.12 (m, 3H, *para*-P-C_6H_5), 7.04 (m, 2H, *para*-C_6H_4), 6.68 (s, 4H, pyrrolide C$\underline{H}$), 1.90 (s, 12H, *exo*-C$\underline{H}_3$), 1.58 (s, 12H, *endo*-C$\underline{H}_3$), 0.00 (s, 18H, Si(C$\underline{H}_3$)$_3$).

^{1}H NMR (298 K, toluene-d_8): δ 9.03 (s, 2H, *ipso*-C_6H_4), 7.89 (m, 6H, *ortho*-P-C_6H_5), 7.13 (m, 6H, *meta*-P-C_6H_5), 7.06-7.01 (m, 9H, *para*-P-C_6H_5, *meta*-C_6H_4 and *para*-C_6H_4), 6.60 (s, 4H, pyrrolide C$\underline{H}$), 1.87 (s, 12H, *exo*-C$\underline{H}_3$), 1.55 (s, 12H, *endo*-C$\underline{H}_3$), 0.05 (s, 18H, Si(C$\underline{H}_3$)$_3$).

^{1}H NMR (210 K, toluene-d_8): δ 9.77 (s, 1H, *ipso*-C_6H_4), 8.60 (s, 1H, *ipso*-C_6H_4), 7.93 (m, 6H, *ortho*-P-C_6H_5), 7.19-7.04 (m, 15H, *meta*-P-C_6H_5, *para*-P-C_6H_5, *meta*-C_6H_4 and *para*-C_6H_4), 6.77 (br m, 4H, pyrrolide C$\underline{H}$), 1.96-1.81 (very br d, 12H, *exo*-C$\underline{H}_3$), 1.61 (s, 12H, *endo*-C$\underline{H}_3$), 0.04 (br s, 18H, Si(C$\underline{H}_3$)$_3$).

^{1}H NMR (298 K, THF-d_8): δ 8.85 (s, 2H, *ipso*-C_6H_4), 7.72 (m, 6H, *ortho*-P-C_6H_5), 7.36-7.06 (m, 15H, *meta*-C_6H_4, *meta*-P-C_6H_5, *para*-P-C_6H_5 and *para*-C_6H_4), 6.39 (s, 4H, pyrrolide C$\underline{H}$), 1.79 (s, 12H, *exo*-C$\underline{H}_3$), 1.45 (s, 12H, *endo*-C$\underline{H}_3$), -0.27 (s, 18H, Si(C$\underline{H}_3$)$_3$).

^{1}H NMR (193 K, THF-d_8): δ 9.48 (s, 1H, *ipso*-C_6H_4), 8.35 (s, 1H, *ipso*-C_6H_4), 7.80-7.51 (br m, 6H, *ortho*-P-C_6H_5), 7.39-6.98 (br m, 15H, *meta*-C_6H_4, *meta*-P-C_6H_5, *para*-P-C_6H_5 and

para-C_6H_4), 6.54 (d, 2H, pyrrolide C<u>H</u>), 6.26 (d, 2H, pyrrolide C<u>H</u>), 1.82 (br s, 12H, *exo*-C<u>H</u>$_3$), 1.45 (br s, 12H, *endo*-C<u>H</u>$_3$), -0.27 (s, 9H, Si(C<u>H</u>$_3$)$_3$), -0.36 (s, 9H, Si(C<u>H</u>$_3$)$_3$).

$^{13}C\{^1H\}$ NMR (benzene-d_6): δ 157.2 (quaternary aromatic), 153.8 (quaternary aromatic), 139.5 (d, $|^1J_{PC}| = 30.7$ Hz, *ipso*-P-C_6H_5), 135.0 (d, $|^2J_{PC}| = 13.7$ Hz, *ortho*-P-C_6H_5), 132.4 (*para*-C_6H_4), 129.3 (d, $|^4J_{PC}| = 1.29$ Hz, *para*-P-C_6H_5), 128.0 (*meta*-P-C_6H_5), 123.4 (*ipso*-C_6H_4), 123.4 (*meta*-C_6H_4), 114.8 (pyrrolide <u>C</u>H), 42.2 (quaternary), 30.8 (<u>C</u>H$_3$), 28.9 (<u>C</u>H$_3$), 23.1 (C≡C), 14.4 (C≡C), 2.53 (Si(<u>C</u>H$_3$)$_3$).

$^{29}Si\{^1H\}$ NMR, INEPT sequence, (benzene-d_6): δ -16.0.

$^{31}P\{^1H\}$ NMR (benzene-d_6): δ 37.0.

Analysis (%) calc. for $C_{60}H_{69}N_2Si_2PNiTh$: C 60.25; H 5.81; N 2.34, found C 60.49; H 5.73; N 2.30.

FTIR (cm^{-1}): 2120 [C≡C stretch], 2071 [C≡C stretch]. All other absorption bands (cm^{-1}): 3056, 2962-2873, 2365-2323, 1592, 1486-1458, 1437, 1417, 1382, 1359, 1308, 1244-1240, 1152-1093, 981, 940, 842.

4.4.40 Synthesis of [(L)Th(C≡CSiMe$_3$)$_2$·NiPCy$_3$] (25a and 25b)

A Teflon-valved ampoule with a magnetic stirrer-bar was charged with **12** (0.100 g, 0.114 mmol), [Ni(COD)$_2$] (1eq, 0.031 g, 0.114 mmol) and PCy$_3$ (1eq, 0.032 g, 0.114 mmol). Hexane was added (5 ml) and the reaction was stirred for 3 hours. The volatiles were removed under reduced pressure and the solids were then dried under vacuum to yield **25** as dark orange solid. Single crystals suitable for X-ray were grown by two different methods: slow evaporation of hexane from a saturated solution of **25** in hexane to yield **25a** and vapour diffusion of hexane into a saturated THF solution of **25** at ambient temperature to yield **25b**.

Yield of **25a**: 0.010 g (0.008 mmol), 7 %.

Yield of **25b**: 0.006 g (0.005 mmol), 4 %.

^1H NMR (benzene-d_6): δ 8.22 (s, 2H, *ipso*-C_6H_4), 7.29 (m, 2H, *para*-C_6H_4), 7.22 (m, 4H, *meta*-C_6H_4), 6.39 (s, 4H, pyrrolide C<u>H</u>), 2.46-2.11 (m, 33H, Cy-H), 1.79 (s, 12H, *exo*-C<u>H</u>$_3$), 1.64 (s, 12H, *endo*-C<u>H</u>$_3$), 0.28 (s, 18H, Si(C<u>H</u>$_3$)$_3$).

$^{13}C\{^1H\}$ NMR (benzene-d_6): δ 158.0 (quaternary aromatic), 152.9 (quaternary aromatic), 134.0 (*para*-C_6H_4), 132.0 (*ipso*-C_6H_4), 131.5 (*meta*-C_6H_4), 114.1 (pyrrolide <u>C</u>H), 68.2 (C≡C),

42.2 ($\underline{C}H_3$), 42.0 (quaternary), 36.6 (d, $|^1J_{PC}|$ = 12.7 Hz, P-C_6H_{11}), 33.8 (C≡C), 30.8 (d, $|^2J_{PC}|$ = 1.34 Hz, P-C_6H_{11}), 29.3 ($\underline{C}H_3$), 28.0 (P-C_6H_{11}), 27.3 (P-C_6H_{11}), 25.6 (Si($\underline{C}H_3$)$_3$).

$^{29}Si\{^1H\}$ NMR, INEPT sequence, (benzene-d_6): δ -17.6.

$^{31}P\{^1H\}$ NMR (benzene-d_6): δ 49.2.

Analysis (%) calc. for $C_{60}H_{87}N_2Si_2PNiTh$: C 59.35; H 7.22; N 2.31, found C 59.15; H 7.05; N 2.39.

4.4.41 Attempted Synthesis of [(L)Th(C≡CSiMe$_3$)$_2$·TM(dppf)] (TM = Ni, Pt)

The procedure in Section 4.4.38 was repeated in THF with [Ni(dppf)(COD)] (1eq, 0.041 g, 0.057 mmol) and [Pt(dppf)(nb)] (1eq, 0.048 g, 0.057 mmol). No reaction occurred.

4.5 Synthetic Procedures for Chapter Three

4.5.1 Synthesis of [(L)U(OLi{THF}$_3$)$_2$]I (26)

A saturated solution of **8** (0.030 g, 0.042 mmol) in THF, containing trace amounts of H_2O, was prepared in a N_2-atmosphere drybox in the presence of LiI (residual, from the preparation of **8**). After two weeks at -20 °C, red single crystals of **26** suitable for X-ray were isolated from the saturated solution.

Yield: 0.011 g (0.009 mmol), 20 %.

NMR data could not be obtained because crystals of **26** did not dissolve.

Analysis (%) calc. for $C_{56}H_{78}N_2O_8Li_2UI$: C 52.30; H 6.11; N 2.18, found C 52.28; H 6.10; N 2.15.

4.5.2 Synthesis of [(L)U(O)]$_2$ (27)

A Young's tube was charged with **D** (0.030 g, 0.043 mmol) in C_6D_6 (1 ml) and TEMPO (1 eq, 0.006 g, 0.043 mmol). The reaction mixture was left to react for 4 hours. The volatiles were removed under reduced pressure and the solids then dried under vacuum to yield **27** as an orange solid. Single crystals suitable for X-ray were grown from a saturated solution of **27** in C_6D_6 at room temperature.

Yield was poor and exact amounts were not recorded.

^{1}H NMR (benzene-d_6): δ 101.08 (br. s, 4H, pyrrole C<u>H</u>), 25.76 (br. s, 6H, 2 x C<u>H</u>$_3$ methyl), 9.52 (s, 6H, 2 x C<u>H</u>$_3$ methyl), 3.57 (s, 6H, 2 x C<u>H</u>$_3$ methyl), -5.55 (br. s, 6H, 2 x C<u>H</u>$_3$ methyl), -10.18 (s, 4H, *ortho* arene C<u>H</u>), -14.50 (s, 2H, *meta* arene C<u>H</u>).

EI MS (*m/z*): 703.3 $[U(L)\text{-}O]^+ + H^+$

Analysis (%) calc. for C 54.70, H 5.16, N 3.99 EA found: C 54.84, H 5.22, N 4.18.

4.5.3 Oxidation of 8 or 14 with D_2O

Method 1: A Teflon-valved ampoule with a magnetic stirrer-bar was charged with **8** (0.100 g, 0.142 mmol) or **14** (0.100 g, 0.113 mmol) in THF (5 ml) and cooled to -20 °C. One equivalent of freeze-pump-thaw degassed D_2O (1 eq, 2.8 μl, 0.142 mmol or 2.2 μl, 0.113 mmol) was added *via* syringe. The orange solution discoloured immediately and dark precipitate formed. The ^{1}H NMR and ^{2}H NMR spectra showed the presence of D_4L and trace DCH_3 with no paramagnetic resonances remaining.

Method 2: A Teflon-valved ampoule with a magnetic stirrer-bar was charged with **8** (0.100 g, 0.142 mmol) or **14** (0.100 g, 0.113 mmol) in THF (10 ml) and cooled to -20 °C. A 0.1M solution of D_2O in THF (1 eq, 1.42 ml or 1.13 ml) was added *via* syringe. The orange solution discoloured over 5 minutes and dark precipitate formed. The ^{1}H NMR and ^{2}H NMR spectra showed the presence of D_4L and trace DCH_3 with no paramagnetic resonances remaining.

4.5.4 Attempted Oxidation of 8 or 14 with O-Atom Transfer Agents

In a vial charged with a magnetic stirrer-bar, in an N_2-atmosphere glove box, **8** (0.030 g, 0.042 mmol) was dissolved in THF (1 ml) and cooled to -20 °C. A solution of pyridine-*N*-oxide (1 eq, 0.004 g, 0.042 mmol) or trimethylamine-*N*-oxide (1 eq, 0.003 g, 0.042 mmol) in THF (1 ml) was added dropwise over 10 minutes. The reaction mixture was stirred for 4 hours. An inseparable mixture of diamagnetic products formed.

This procedure was repeated with **14** (0.030 g, 0.034 mmol) and pyridine-*N*-oxide (1 eq, 0.003 g, 0.034 mmol) or trimethylamine-*N*-oxide (1 eq, 0.002 g, 0.034 mmol). No reaction occurred. The reaction mixture was then heated at 80 °C for 10 minutes, resulting in partial oxidation to a mixture of diamagnetic products.

This procedure was also repeated with **8** (0.030 g, 0.042 mmol) and TEMPO (0.5 eq, 0.003 g, 0.021 mmol) or pyridine-*N*-oxide (0.5 eq, 0.002 g, 0.021 mmol). Incomplete

conversion to mixture of inseparable diamagnetic products occurred using pyridine-*N*-oxide. An inseparable mixture of diamagnetic products formed when using TEMPO.

4.5.5 Attempted U^{IV}-oxo syntheses from 8 with LiOD

In a vial charged with a magnetic stirrer-bar, in an N_2-atmosphere glove box, **8** (0.030 g, 0.042 mmol) was dissolved in THF (1 ml) and cooled to -20 °C. LiOD (1eq, 0.001 g, 0.042 mmol or 2eq, 0.002 g, 0.084 mmol) was added and the reaction mixture stirred for 4 hours. The solution was then filtered. The ^{1}H NMR spectrum showed that approximately 16 % of the reaction mixture had converted to at least two paramagnetic products with resonances located from 84.2-33.73 ppm, 16 % to D_4L and 67 % to Li_4L. The ^{2}H NMR spectrum however showed only the fully deuterated D_4L, suggesting that the paramagnetic product had not been deuterated. Addition of excess D_2O to the products resulted in their decomposition, liberation of DCH_3 and an increased concentration of D_4L in solution.

4.5.6 Attempted U^{IV}-oxo syntheses from 8 or 14 with ROH (R = CPh_3, $SiMe_3$)

The procedure in Section 4.5.5 was repeated with **8** (0.030 g, 0.042 mmol) and Ph_3COH (2eq, 0.022 g, 0.084 mmol or 3eq, 0.033 g, 0.126 mmol) or Me_3SiOH (2eq, 0.007 g, 0.084 mmol or 3eq, 0.011 g, 0.126 mmol). A mixture of at least two paramagnetic products and a mixture of inseparable diamagnetic products formed. Repeating the reactions gives the same products in varying ratios.

This procedure was repeated with **14** (0.030 g, 0.034 mmol) and Ph_3COH (2eq, 0.017 g, 0.068 mmol). No reaction occurred.

4.5.7 Oxidation of 8 or 14 in Air

A Young's tube was charged with **8** (0.030 g, 0.042 mmol) or **14** (0.030 g, 0.034 mmol) in C_6D_6 (1 ml) and the Teflon seal loosened, allowing for slow diffusion of air into the tube. Dark precipitate formed after 8 hours and the ^{1}H NMR spectrum of the solution showed only H_2L.

4.5.8 Attempted synthesis of U^V and U^{VI} Complexes by Salt Metathesis

A Young's tube was charged with $\{[UO_2(py)_5][KI_2(py)_2]\}_n$ (0.030 g, 0.027 mmol) with and K_2L (1eq, 0.014 g, 0.027 mmol) in THF-d_8 (1 ml). The reaction mixture was sonicated for 10 minutes and then allowed to react for 2 hours. The ^{1}H NMR spectrum showed an inseparable paramagnetic and diamagnetic product mixture. This procedure was repeated with

$[UO_2Cl_2(THF)_2]$ (0.030 g, 0.062 mmol) and K_2L (1eq, 0.033 g, 0.062 mmol). No reaction occurred. The solution was then heated at 80 °C for 48 hours. No reaction occurred.

4.6 Crystallographic Details

X-ray crystallography on compounds **1**, **2**, **4**, **5**, **6·LiCl**, **7·THF**, **9·LiCl·THF**, **12**, **13**, **15**-**17**, **22**, **24**, **25a**, **25b**, **26** and **27** was completed using an Oxford Diffraction Excalibur Eos diffractometer with Mo Kα radiation at 170(2) K or an Agilent Technologies Supernova dual source Atlas diffractometer using a Mo Kα source at 120(10) K. All structures were solved using SHELXT and least-square refined using SHELXL in Olex2.[13, 14] Absorption corrections were completed using *CrysAlis PRO* 1.171.38.42b (Rigaku Oxford Diffraction, 2015) or 1.171.37.34 (Agilent Technologies, 2014) software. Analytical numeric absorption corrections used a multifaceted crystal model based on expressions derived by Clark and Reid.[15] Numerical absorption correction was based on a Gaussian integration over a multifaceted crystal model. Empirical absorption correction using spherical harmonics, implemented in SCALE3 ABSPACK scaling algorithm.

No restraints were applied during the refinement of **12**, **15**, **16**, **24**, **25a**, **25b** and **27**. The anisotropic displacement parameters in the direction of the bonds and perpendicular to the planar groups in the arene and pyrrolide rings of the macrocycle in the unit cells of **4** and **7·THF** were restrained to be equal within effective standard deviation. Heavily disordered THF solvent molecules in the unit cells of **5**, **7·THF** and **22** were restrained. Disordered benzene solvent molecules in the unit cells of **6·LiCl** and **26** were heavily restrained. Disordered THF and benzene solvent molecules in the unit cell of **9·LiCl·THF** were restrained. The PLATON SQUEEZE[16] function was used to remove residual electron density of $16e^-$ from a solvent accessible void in **24**, which corresponded to approximately one third of a molecule of lattice benzene per unit cell.

Table 4.1 Crystallographic data summary for complexes **1**, **2** and **4**.

Complex	[(L)UCl_2] (**1**)	[(L)$Th(BH_4)_2$] (**2**)	[K(L)$U(N(SiMe_3)_2)$] (**4**)
Local code	po4029_refinalized3	p14099monoclinicref	p15114b
Chemical formula	$C_{36}H_{36}Cl_2N_2U$	$C_{32}H_{44}B_2N_2Th$	$C_{38}H_{52}KN_3Si_2U$
M_r	757.56	710.35	884.13
Crystal system, space group	monoclinic, $P2_1/n$	monoclinic, $P2_1/n$	Orthorhombic, $P2_12_12_1$
Temperature (K)	120	170	170
a, *b*, *c* (Å)	10.1067 (1), 15.3885 (2), 18.1667 (2)	13.8898 (4), 10.2311 (2), 21.5733 (6)	12.2561 (2), 12.9086 (2), 23.3522 (4)
β (°)	90.028 (1)	103.493 (3)	-
V (Å^3)	2825.41 (6)	2981.11 (14)	3694.52 (11)
Z	4	4	4
Radiation type	Mo *K*a	Mo *K*a	Mo *K*a
μ (mm^{-1})	18.08	5.03	4.60
Crystal size (mm)	0.57 × 0.04 × 0.04	0.31 × 0.18 × 0.04	0.30 × 0.17 × 0.10
Diffractometer	SuperNova, Dual, Cu at zero, Atlas	Xcalibur, Eos	Xcalibur, Eos
Absorption correction	Gaussian	Analytical	Multi-scan
T_{min}, T_{max}	0.985, 0.999	0.608, 0.898	0.503, 1.000
No. of measured, independent and observed [$I > 2\sigma(I)$] reflections	46449, 5895, 5765	32977, 6748, 5551	60438, 7551, 6310
R_{int}	0.061	0.037	0.122
$(\sin\theta/\lambda)_{max}$ (Å^{-1})	0.630	0.649	0.625
$R[F^2 > 2\sigma(F^2)]$, $wR(F^2)$, *S*	0.028, 0.080, 1.12	0.028, 0.057, 1.06	0.050, 0.129, 1.07
No. of reflections	5895	6748	7551
No. of parameters	330	366	420
No. of restraints	42	8	136
$\Delta\rho_{max}$, $\Delta\rho_{min}$ (e Å^{-3})	1.61, -2.79	1.11, -0.97	4.57, -1.82
H-atom treatment	Mixture of independent and constrained refinement	Mixture of independent and constrained refinement	Constrained refinement
CCDC number	1565454	-	-

Table 4.2 Crystallographic data summary for complexes **5**, **6·LiCl** and **7·THF**.

Complex	[Li(L)Th(Me)] (**5**)	[Li(L)Th(CH_2SiMe_3)·LiCl] (**6·LiCl**)	[K(L)Th(CH_2Ph)·THF] (**7·THF**)
Local code	p15111-peakpicking	p15054	p14096h_peakhunting_87
Chemical formula	$C_{33}H_{37}N_2Th{\cdot}Li{\cdot}2(C_4H_8O)$	$C_{72}H_{90}Cl_2Li_4N_4Si_2Th_2{\cdot}5(C_6H_6)$	$C_{172}H_{196}K_4N_8O_4Th_4$
M_r	844.83	2020.93	3523.92
Crystal system, space group	Triclinic, *P*-1	Triclinic, *P*-1	Monoclinic, $P2_1/c$
Temperature (K)	170	170	170
a, *b*, *c* (Å)	11.1822 (9), 12.8647 (5), 15.6401 (6)	13.0979 (2), 19.0344 (4), 19.8212 (4)	22.6444 (5), 20.1790 (6), 34.2439 (8)
α, β, γ (°)	71.151 (3), 71.068 (5), 66.050 (5)	95.2189 (17), 106.5357 (17), 93.9698 (15)	97.325 (2)
V (Å^3)	1896.7 (2)	4694.14 (16)	15519.7 (7)
Z	2	2	4
Radiation type	Mo *K*a	Mo *K*a	Mo *K*a
μ (mm^{-1})	3.97	3.29	3.98
Crystal size (mm)	0.48 × 0.14 × 0.09	0.49 × 0.37 × 0.13	0.46 × 0.17 × 0.11
Diffractometer	Xcalibur, Eos	Xcalibur, Eos	Xcalibur, Eos
Absorption correction	Multi-scan	Analytical	Analytical
T_{min}, T_{max}	0.719, 1.000	0.051, 0.581	0.720, 0.904
No. of measured, independent and observed [$I > 2\sigma(I)$] reflections	28682, 5667, 4022	116828, 19176, 15590	271761, 24607, 12940
R_{int}	0.087	0.078	0.160
$(\sin\theta/\lambda)_{max}$ (Å^{-1})	0.603	0.625	0.575
$R[F^2 > 2\sigma(F^2)]$, $wR(F^2)$, *S*	0.061, 0.163, 1.01	0.040, 0.109, 1.04	0.088, 0.179, 1.11
No. of reflections	5667	19176	24607
No. of parameters	418	1043	1713
No. of restraints	65	621	48
$\Delta\rho_{max}$, $\Delta\rho_{min}$ (e Å^{-3})	2.32, -1.43	2.69, -2.23	4.76, -2.77
H-atom treatment	Constrained refinement	Constrained refinement	Constrained refinement
CCDC number	1565442	1565443	1565444

Table 4.3 Crystallographic data summary for complexes **9·LiCl·THF**, **12** and **13**.

Complex	[Li(L)U(CH_2SiMe_3)·LiCl(THF)] (**9·LiCl·THF**)	[(L)Th(C≡C$SiMe_3$)$_2$] (**12**)	[(L)Th(C≡CSi^iPr_3)$_2$] (**13**)
Local code	p15099monoclinic	p15146_ortho	p15167-peakhunting
Chemical formula	$C_{40}H_{53}ClLi_2N_2OSiU·C_6H_6$	$C_{21}H_{27}NSiTh_{0.5}·C_6H_6$	$2(C_{54}H_{78}N_2Si_2Th)$
M_r	971.40	515.65	2086.80
Crystal system, space group	Monoclinic, *C*2/*c*	Orthorhombic, *Pnma*	Triclinic, *P*-1
Temperature (K)	170	170	170
a, *b*, *c* (Å)	28.5640 (5), 16.0900 (2), 19.5678 (3)	12.5399 (2), 20.5585 (4), 19.7595 (3)	12.89171 (16), 18.7076 (2), 22.4490 (3)
α, β, γ (°)	100.5761 (15)	-	74.8672 (10), 89.4904 (10), 89.2130 (9)
V (Å^3)	8840.5 (2)	5094.03 (15)	5225.77 (11)
Z	8	8	2
Radiation type	Mo *K*a	Mo *K*a	Mo *K*a
μ (mm^{-1})	3.79	3.01	2.93
Crystal size (mm)	0.45 × 0.25 × 0.11	0.19 × 0.16 × 0.13	0.40 × 0.19 × 0.06
Diffractometer	Xcalibur, Eos	Xcalibur, Eos	Xcalibur, Eos
Absorption correction	Analytical	Multi-scan	Analytical
T_{min}, T_{max}	0.739, 0.909	0.780, 1.000	0.465, 0.846
No. of measured, independent and observed [$I > 2\sigma(I)$] reflections	77412, 9730, 7751	79498, 5358, 4540	99402, 19126, 9282
R_{int}	0.056	0.075	0.033
$(\sin\theta/\lambda)_{max}$ (Å^{-1})	0.641	0.648	0.607
$R[F^2 > 2\sigma(F^2)]$, $wR(F^2)$, *S*	0.030, 0.078, 1.08	0.031, 0.063, 1.07	0.020, 0.059, 1.01
No. of reflections	9730	5358	19126
No. of parameters	498	296	1121
No. of restraints	66	0	2
$\Delta\rho_{max}$, $\Delta\rho_{min}$ (e Å^{-3})	1.73, -0.92	0.78, -0.65	1.06, -0.41
H-atom treatment	Constrained refinement	Constrained refinement	Mixture of independent and constrained refinement
CCDC number	1565445	1565446	1565447

Table 4.4 Crystallographic data summary for complexes **15**-**17**.

Complex	[(L)U(C≡CSi^{i}Pr$_3$)$_2$] (**15**)	[(L^{-2H})U(η^2-O$_2$SiMe$_2$)(Li{THF})$_2$] (**16**)	[LCO] (**17**)
Local code	p16006_peakhunting	p15058	p16098_mono
Chemical formula	$C_{54}H_{78}N_2Si_2U$	$C_{42}H_{56}Li_2N_2O_4SiU$	$4(C_{33}H_{36}N_2O)$
M_r	1049.39	932.88	1906.54
Crystal system, space group	Triclinic, *P*-1	Triclinic, *P*-1	Monoclinic, $P2_1$
Temperature (K)	170	170	170
a, *b*, *c* (Å)	12.6749 (8), 13.1326 (7), 18.6834 (12)	11.4726 (2), 13.0726 (2), 14.0684 (3)	17.5798 (6), 11.9781 (4), 25.3364 (11)
α, β, γ (°)	92.222 (5), 109.317 (6), 113.959 (6)	83.4821 (16), 75.9093 (17), 77.3279 (14)	90.018 (3)
V (Å^3)	2627.4 (3)	1992.57 (7)	5335.1 (4)
Z	2	2	2
Radiation type	Mo *K*a	Mo *K*a	Mo *K*a
μ (mm^{-1})	3.17	4.15	0.07
Crystal size (mm)	0.38 × 0.19 × 0.03	2.00 × 0.48 × 0.28	0.30 × 0.17 × 0.06
Diffractometer	Xcalibur, Eos	Xcalibur, Eos	Xcalibur, Eos
Absorption correction	Multi-scan	Analytical	Analytical
T_{min}, T_{max}	0.916, 1.000	0.848, 0.973	0.572, 0.858
No. of measured, independent and observed [$I > 2\sigma(I)$] reflections	44025, 12323, 6530	41201, 8136, 7279	51089, 11106, 7659
R_{int}	0.137	0.038	0.107
$(\sin\theta/\lambda)_{max}$ (Å^{-1})	0.688	0.625	0.500
$R[F^2 > 2\sigma(F^2)]$, $wR(F^2)$, *S*	0.075, 0.150, 0.91	0.029, 0.070, 1.10	0.057, 0.093, 1.01
No. of reflections	12323	8136	11106
No. of parameters	552	479	1329
No. of restraints	0	0	1
$\Delta\rho_{max}$, $\Delta\rho_{min}$ (e Å^{-3})	3.56, -1.95	2.91, -0.93	0.16, -0.16
H-atom treatment	Constrained refinement	Constrained refinement	Constrained refinement
CCDC number	1565448	-	1565450

Table 4.5 Crystallographic data summary for complexes **22**, **24** and **25a**.

Complex	[(L)Th(N(SiMe$_3$)$_2$)][BPh$_4$] (**22**)	[(L)Th(C≡CSiMe$_3$)$_2$·NiPPh$_3$] (**24**)	[(L)Th(C≡CSiMe$_3$)$_2$·NiPCy$_3$] (**25a**)
Local code	p14052	p16128-sr	p16197
Chemical formula	$C_{38}H_{54}N_3Si_2Th·C_{24}H_{20}B·C_4H_8O$	$C_{60}H_{69}N_2NiPSi_2Th$	$C_{60}H_{87}N_2NiPSi_2Th$
M_r	1232.37	1196.07	1214.21
Crystal system, space group	Monoclinic, $P2_1/n$	Triclinic, P-1	Triclinic, P-1
Temperature (K)	170	170	170
a, b, c (Å)	12.2283 (3), 23.6198 (5), 20.7851 (4)	12.5896 (3), 14.9229 (3), 17.0361 (4)	12.9869 (5), 13.7304 (6), 18.9562 (8)
α, β, γ (°)	96.1100 (18)	81.0245 (17), 72.535 (2), 70.462 (2)	106.943 (4), 93.828 (3), 113.591 (4)
V (Å^3)	5969.3 (2)	2871.78 (12)	2897.6 (2)
Z	4	2	2
Radiation type	Mo Ka	Mo Ka	Mo Ka
μ (mm^{-1})	2.58	3.02	2.99
Crystal size (mm)	0.76 × 0.28 × 0.19	0.55 × 0.18 × 0.15	0.34 × 0.18 × 0.06
Diffractometer	Xcalibur, Eos	Xcalibur, Eos	Xcalibur, Eos
Absorption correction	Multi-scan	Multi-scan	Analytical
T_{min}, T_{max}	0.531, 1.000	0.731, 1.000	0.716, 0.922
No. of measured, independent and observed [I > 2σ(I)] reflections	49499, 12193, 9486	14130, 14130, 11928	59325, 11834, 10287
R_{int}	0.039	0.053	0.086
(sin θ/λ)$_{max}$ (Å^{-1})	0.625	0.691	0.625
R[F^2 > 2σ(F^2)], wR(F^2), S	0.031, 0.077, 1.01	0.031, 0.071, 1.08	0.050, 0.127, 1.11
No. of reflections	12193	14130	11834
No. of parameters	667	618	618
No. of restraints	30	0	0
Δρ$_{max}$, Δρ$_{min}$ (e Å^{-3})	0.93, -0.48	0.95, -0.63	2.46, -1.75
H-atom treatment	Constrained refinement	Constrained refinement	Constrained refinement
CCDC number	1565449	1565453	1565451

Table 4.6 Crystallographic data summary for complexes **25b**, **26** and **27**.

Complex	$[(L)Th(C{\equiv}CSiMe_3)_2{\cdot}NiPCy_3]$ (**25b**)	$[Li(L)UO_2{\cdot}LiI(THF)_6]$ (**26**)	$[(L)U(O)]_2$ (**27**)
Local code	p16072	p16007	EDPA2
Chemical formula	$C_{60}H_{87}N_2NiPSi_2Th{\cdot}C_4H_8O$	$C_{28}H_{42}LiNO_4U_{0.5}{\cdot}0.5(I){\cdot}C_6H_6$	$C_{32}H_{36}N_2OU$
M_r	1286.31	724.14	702.66
Crystal system, space group	Triclinic, *P*-1	Triclinic, *P*-1	Triclinic, *P*-1
Temperature (K)	170	170	170
a, *b*, *c* (Å)	12.5364 (3), 13.3351 (2), 18.5853 (4)	10.27744 (17), 12.4041 (2), 13.6234 (2)	10.297 (4), 11.095 (4), 13.052 (5)
α, β, γ (°)	85.9847 (15), 80.0243 (17), 76.3860 (16)	73.4164 (14), 89.4859 (13), 74.6630 (15)	108.057 (5), 100.187 (6), 107.158 (2)
V (Å^3)	2972.64 (10)	1601.06 (5)	1294.2 (8)
Z	2	2	2
Radiation type	Mo *K*a	Mo *K*a	Mo *K*a
μ (mm^{-1})	2.92	3.07	6.30
Crystal size (mm)	0.20 × 0.14 × 0.08	0.36 × 0.18 × 0.10	0.08 × 0.08 × 0.08
Diffractometer	Xcalibur, Eos	Xcalibur, Eos	Xcalibur, Eos
Absorption correction	Analytical	Analytical	Multi-scan
T_{min}, T_{max}	0.942, 0.978	0.552, 0.804	0.383, 1.000
No. of measured, independent and observed [$I > 2\sigma(I)$] reflections	49292, 12153, 11146	24847, 6074, 6072	18716, 4763, 4435
R_{int}	0.042	0.027	0.064
$(\sin\theta/\lambda)_{max}$ (Å^{-1})	0.625	0.610	0.604
$R[F^2 > 2\sigma(F^2)]$, $wR(F^2)$, *S*	0.025, 0.054, 1.10	0.029, 0.081, 1.10	0.029, 0.122, 1.23
No. of reflections	12153	6074	4763
No. of parameters	663	365	333
No. of restraints	0	36	0
$\Delta\rho_{max}$, $\Delta\rho_{min}$ (e Å^{-3})	1.16, -0.54	1.40, -0.99	1.53, -1.29
H-atom treatment	Constrained refinement	Constrained refinement	Constrained refinement
CCDC number	1565452	-	-

4.7 References for Chapter Four

1. N. L. Bell, L. Maron and P. L. Arnold, *J. Am. Chem. Soc.*, 2015, **137**, 10492-10495.
2. P. J. Bailey, R. A. Coxall, C. M. Dick, S. Fabre, L. C. Henderson, C. Herber, S. T. Liddle, D. Loroño-González, A. Parkin and S. Parsons, *Chem. Eur. J.*, 2003, **9**, 4820-4828.
3. M. G. Assadi, M. Mahkam and Z. Tajrezaiy, *Heteroat. Chem.*, 2007, **18**, 414-420.
4. S. M. Mansell, B. F. Perandones and P. L. Arnold, *J. Organomet. Chem.*, **695**, 2814-2821.
5. T. Cantat, B. L. Scott and J. L. Kiplinger, *Chem. Commun.*, 2010, **46**, 919-921.
6. J. L. Sessler, W.-S. Cho, V. Lynch and V. Kral, *Chem. - Eur. J.*, 2002, **8**, 1134-1143.
7. S. Ilango, B. Vidjayacoumar and S. Gambarotta, *Dalton Trans.*, 2010, **39**, 6853-6857.
8. P. L. Arnold, J. H. Farnaby, R. C. White, N. Kaltsoyannis, M. G. Gardiner and J. B. Love, *Chem. Sci.*, 2014, **5**, 756-765.
9. P. B. Hitchcock, A. V. Khvostov and M. F. Lappert, *J. Organomet. Chem.*, 2002, **663**, 263-268.
10. L. Natrajan, F. Burdet, J. Pécaut and M. Mazzanti, *J. Am. Chem. Soc.*, 2006, **128**, 7152-7153.
11. M. P. Wilkerson, C. J. Burns, R. T. Paine and B. L. Scott, *Inorg. Chem.*, 1999, **38**, 4156-4158.
12. P. L. Arnold, C. J. Stevens, J. H. Farnaby, M. G. Gardiner, G. S. Nichol and J. B. Love, *J. Am. Chem. Soc.*, 2014, **136**, 10218-10221.
13. G. Sheldrick, *Acta Crystallogr., Sect. A:*, 2015, **71**, 3-8.
14. O. V. Dolomanov, L. J. Bourhis, R. J. Gildea, J. A. K. Howard and H. Puschmann, *J. Appl. Crystallogr.*, 2009, **42**, 339-341.
15. R. C. Clark and J. S. Reid, *Acta Crystallogr., Sect. A:*, 1995, **51**, 887-897.
16. A. Spek, *Acta Crystallogr., Sect. C*, 2015, **71**, 9-18.